Redéfinir le flux d'enfouissement de la silice biogène et son rôle dans le cycle global du silicium marin

Dongdong Zhu

COLLEGE SCIENCES DOCTORAL DE LA MER BRETAGNE ET DU LITTORAL

Université de Bretagne Occidentale

THESE DE DOCTORAT EN COTUTELLE INTERNATIONALE DE

L'UNIVERSITE
DE BRETAGNE OCCIDENTALE
ECOLE DOCTORALE N° 598
Sciences de la Mer et du Littoral
Spécialité : *Chimie marine*

AVEC

OCEAN UNIVERSITY OF CHINA
ECOLE DOCTORALE N°10423
Ocean University of China
Spécialité : Marine Chemistry

Par

Dongdong ZHU

Redefining the burial flux of biogenic silica and its role in the global marine silicon cycle

Thèse présentée et soutenue à Qingdao, Chine, le 11.10.2023
Unité de recherche : Institut Universitaire Européen de la Mer, Laboratoire des sciences de l'environnement marin

Rapporteurs avant soutenance :

Wei-Li HONG	Professeur assistant	Université de Stockholm
Rahman SHAILY	Professeur assistant	Université du Colorado Boulder

Composition du Jury :

Président :	Paul TREGUER	Professeur émérite des universités	Univ. De Bretagne Occidentale
Examinateurs :	Wei-Li HONG	Professeur assistant	Université de Stockholm
	Aude LEYNAERT	Directrice de recherche	Univ. De Bretagne Occidentale
	Rahman SHAILY	Professeur assistant	Université du Colorado Boulder
	Xiangbin RAN	Directrice de recherche	First Institute of Océanographie
	Jingling REN	Professeur	Université Océanique de Chine
Dir. de thèse :	Sutton N. JILL	Professeur agrégé	Univ. De Bretagne Occidentale
Co-dir. de thèse :	Su Mei LIU	Professeur	Université Océanique de Chine
Invité(s) :			
	Dejiang FAN	Professeur	Université Océanique de Chine
	Qingzhen YAO	Professeur	Université Océanique de Chine

Dedicated to my family, my supervisors, friends and everyone who has supported me during the past four years.

——————————Dongdong Zhu

Redefining the Burial Flux of Biogenic Silica and its Role in the Global Marine Silicon Cycle

Date of thesis defense: 2023.10.11

Supervisors:

Jury members:

Redefining the Burial Flux of Biogenic Silica and its Role in the Global Marine Silicon Cycle

Abstract

The burial of biogenic silica (bSi) in sediments is an important aspect of the investigation and reconstruction of the present and past ocean productivity as well as understanding the biogeochemical cycles of silicon (Si) and the contemporary marine Si state. However, due to the lack of an internationally recognized and standardized bSi determining procedure taking into account of the different sediment types and compositions, large uncertainties of the determined bSi content ($bSiO_2$%) bias the evaluation of the global burial flux of bSi. The methodological bias of the estimated bSi burial flux brings out the question of whether the contemporary marine Si cycle is at steady state. To redefine the global burial flux of bSi, the different methods (e.g., wet chemical methods, X-ray diffraction, Infrared method) and the principal influencing factors (types of sediment and bSi, matrix and provenance) that affect bSi determinations were thoroughly evaluated. In addition, an optimum protocol to accurately measure bSi in sediments was proposed. The main results are listed below:

The accurate determination of $bSiO_2$% in sediment of coastal and continental margin zones (CCMZs) is particularly difficult due to mineral interferences. As a typical CCMZs, the east China seas (the Bohai Sea, Yellow Sea and the East China Sea) sediments are characterized by high silicate mineral and low $bSiO_2$% content. Therefore, it is challenging to quantify the $bSiO_2$% and the bSi burial flux of the east China seas. To evaluate the bSi burial flux of the east China seas and find out an appropriate procedure of determining the $bSiO_2$% of CCMZs sediments, this thesis determined the types and abundances of bSi in sediments and determined the $bSiO_2$% using several wet chemical methods, e.g., the continuous analysis method and conventional wet alkaline digestion. The results showed the major type of bSi in sediments of the Bohai Sea and Yellow Sea is diatom, and the major types of bSi in sediments of the East China Sea are diatoms and sponge spicules. Radiolarian tests were found mainly in sediments of the East China Sea slope. The abundance of radiolarians and sponge spicules outweigh that of diatoms in sediments of East China Sea slope which indicates that radiolarians and sponges are important Si sinks of this region. The results showed that alkaline digestions using stronger solutions (2.0 M Na_2CO_3) and sediments pretreatment steps (pretreating sediments using 1.0 M HCl and 10% H_2O_2, grinding) resulted in an overestimate of the $bSiO_2$% due to increased leaching of silica mainly from authigenic silicates and clays, whereas weak digestions (0.1 M and 0.2 M Na_2CO_3)

underestimated the $bSiO_2$% owing to incomplete digestion of sponge spicules. Alkaline extraction results showed that the use of the automated continuous analysis method (0.5 M NaOH, 1 h extraction) accurately corrects for the lithogenic silica (lSi) fraction in marine sediments, and thereby improves the determinations of $bSiO_2$% in the sediments of east China seas CCMZs. Ensuring full digestion of all bSi remains challenging, in particular for sponge spicules, motivating both verifications via microscopy and longer duration of extraction times.

Accurately evaluating the global marine bSi burial flux is particularly challenging due to the methodological biases since there is still a lack of internationally recognized procedure for measuring the opal content of various sediment types of the world ocean. In order to estimate the methodological biases of the global bSi burial flux, this study examined samples from different marine environments, e.g., sediment of coastal and continental marginal zones (East China Sea, the Congo deep-sea fan and Baffin Bay) and sediments of open oceans (the Southern Ocean, North Atlantic, Equatorial Pacific) using X-ray Diffraction (XRD) method and different wet chemical methods. This study also evaluated the Infrared method (IR: including Infrared method and Fourier Transform Infrared Spectrometer method). The results showed that the $bSiO_2$% determined by XRD method was about 0.5 ($bSiO_2$% > 10%) to 5.5 ($bSiO_2$% < 10%) times higher than that determined by wet chemical method, the $bSiO_2$% determined by IR method was about 10% ($bSiO_2$% > 30%) to 35% ($bSiO_2$% < 30%) lower than that determined by wet chemical method. There are also variations between different wet chemical methods. For example, the $bSiO_2$% determined following the direct wet alkaline digestion (no mineral correction) was significantly higher ($p < 0.05$) than other wet chemical methods, e.g., continuous analysis method and conventional wet alkaline digestion. The $bSiO_2$% determined following an intercept of the Si vs Al plot was significantly lower than that determined by the continuous analysis method and conventional wet alkaline digestion. There is no significant difference between the continuous analysis method and conventional wet alkaline digestion.

In order to emphasize the influence of these methodological differences, this thesis revised the bSi burial flux in the east China seas and the global ocean. The new estimate of the bSi burial flux in east China seas is 253 (± 286) Gmol-SiO_2 yr^{-1}, which is one third of the previous estimates which applied a pretreatment procedure prior to alkaline extractions. This estimate under-evaluates the sponge bSi due to incomplete digestion of sponge spicules. Based on this study and previously published data, this thesis re-evaluated the global bSi burial flux to 6.7 ± 2.7 Tmol-SiO_2 yr^{-1} which is about 30% lower than previous studies, showing the needs of a better understanding the bSi burial flux determinations in order to know either there is an overestimation by previous study or there is a missing Si sink. To minimize the methodological

biases, this thesis proposed a new general wet alkaline extraction procedure for determining the bSi content in sediments both CCMZs and open oceans.

The dissolution of silicate minerals on seafloor releases an important amount of dSi which is necessary for maintaining high diatom productions of the CCMZs, although silicate minerals dissolution is incongruent along the continental shelves. Here, we investigated surface sediments of a typical CCMZs of the Chinese marginal Seas (Bohai Sea, Yellow Sea, East China Sea and the South China Sea) using a continuous alkaline extraction technique, grain-size and chemical (organic carbon, inorganic carbon and total nitrogen) analysis as well as a qualitive measurement of clay mineral compositions by X-ray Diffraction for understanding the discrepancy of silicon (Si) dissolution in different sediment matrix and its potential controlling factor. The results showed 2 times higher amount of Si and aluminum (Al) were leached from muddy sediments as compared to sandy sediments. High dissolution rate (> 0.20 mg-SiO_2 g^{-1} min^{-1}) of silicate minerals is positively correlated to large sediment specific surface area. Further, our modeling data showed the high Al contents (Si:Al < 40) of biogenic silica (bSi) reduces opal reactivity. And the source of Al incorporated with bSi structure is mostly due to the silicate minerals dissolution. We show that although the reactivity of silicate minerals is less active than bSi, it still potentially releases more bio-available Si and Al to seawater due to its dominant content (70.3% − 99.0%wt) on seafloor. The results highlight silicate minerals dissolution as an important potential marine Si source and emphasize a broad application of the continuous alkaline extraction technique for understanding the dissolution kinetics of silica of marine sediments.

Keywords: **Biogenic Silica, Burial Flux, Global Ocean, Silicon Cycle, Analytical Method**

Redéfinir le flux d'enfouissement de la silice biogène et son rôle dans le cycle global du silicium marin

Résumé

L'enfouissement de la silice biogénique (bSi) dans les sédiments est un aspect important de l'étude et de la reconstruction de la productivité océanique actuelle et passée ainsi que de la compréhension des cycles biogéochimiques du silicium (Si) et de l'état contemporain du Si marin. Cependant, en raison de l'absence d'une procédure de détermination du bSi reconnue et standardisée au niveau international prenant en compte les différents types et compositions de sédiments, de grandes variabilités de la teneur en bSi déterminée ($bSiO_2$%) biaisent l'évaluation du flux d'enfouissement global de bSi. Le biais méthodologique du flux d'enfouissement estimé de la bSi soulève la question de savoir si le cycle contemporain du Si marin est à l'état d'équilibre. Pour redéfinir le flux d'enfouissement global de bSi, j'ai évalué les les différentes méthodes (par exemple, méthodes chimiques humides, diffraction des rayons X (XRD), méthode infrarouge) utilisées pour la détermination de bSi et des biais associés aux rendements de bSi mesurés. J'ai aussi établi un protocole optimal pour analyser la bSi dans les sédiments avec une évaluation approfondie des principaux facteurs d'influence (types de sédiments et de bSi, matrice et provenance). Les principaux résultats sont listés ci-dessous :

Pour évaluer le flux d'enfouissement de bSi dans les mers de Chine orientale et mettre au point une procédure appropriée pour déterminer le $bSiO_2$% des sédiments des CCMZ (Coastal and Continental Marginal Zones), cette thèse a déterminé les différents types de bSi dans les sédiments et leur abondance (diatomées, radiolaires, éponges) en microscopie. Elle a déterminé le $bSiO_2$% en utilisant plusieurs méthodes chimiques humides, comme par exemple la méthode Si/Al et la méthode Si/temps.

Les résultats ont montré que le principal type de bSi dans les sédiments de la mer de Bohai et de la mer Jaune est la diatomée, et que les principaux types de bSi dans les sédiments de la mer de Chine orientale sont les diatomées et les spicules d'éponges. Les tests radiolaires ont été trouvés principalement dans les sédiments du talus de la mer de Chine orientale. L'abondance des radiolaires et des spicules d'éponges dépasse celle des diatomées dans les sédiments du talus de la mer de Chine orientale. Ceci indique que les radiolaires et les éponges sont d'importants puits de Si de cette région, sous-estimés jusqu'à présents en raison de leur résistance à la digestion alcaline lors de l'analyse.

Les résultats ont montré que les digestions alcalines utilisant des solutions plus fortes (2.0 M Na_2CO_3) et des étapes de prétraitement des sédiments (1.0 M HCl et 10% H_2O_2) entraînaient une surestimation du % de $bSiO_2$ en raison d'une lixiviation accrue de la silice provenant principalement des silicates et des argiles authigènes, alors que les digestions (0.1 M et 0.2 M Na_2CO_3) ont sous-estimé le % de $bSiO_2$ en raison d'une digestion incomplète des spicules d'éponges. Les résultats de l'extraction alcaline ont montré que l'utilisation de la méthode Si/Al (0.5 M NaOH, extraction 1 h) corrige avec précision la fraction de silice lithogène (lSi) dans les sédiments marins, et améliore ainsi les déterminations de $bSiO_2$% dans les sédiments de l'Est de la Chine.

Assurer une digestion complète de tous les bSi reste un défi, en particulier pour les spicules d'éponges, ce qui justifie à la fois des vérifications par microscopie et des durées d'extraction plus longues. Afin de souligner l'influence de ces différences méthodologiques, ce chapitre a révisé le flux d'enfouissement de bSi dans les mers de Chine orientale et fournit une nouvelle estimation de 253 (± 286) Gmol-SiO_2 an^{-1}, soit un tiers des estimations précédentes qui appliquaient une procédure de prétraitement avant les extractions alcalines. La contribution potentielle des radiolaires et des éponges à l'enfouissement de la bSi a été discutée et un nouveau protocole général pour la détermination de la bSi dans les sédiments minimisant le biais méthodologique dans la détermination du bSi a été proposé.

Afin d'estimer les biais méthodologiques du flux mondial d'enfouissement du bSi, cette étude a examiné des échantillons provenant de différents environnements marins, par exemple les sédiments des zones marginales côtières et continentales et des océans ouverts, à l'aide de la méthode XRD et de différentes méthodes chimiques humides. Nous avons également évalué la méthode infrarouge (IR: incluant la méthode infrarouge et la méthode du spectromètre infrarouge à transformée de Fourier). Nos résultats ont montré que le $bSiO_2$% déterminé par la méthode XRD était environ 0.5 ($bSiO_2$% > 10%) à 5.5 ($bSiO_2$% < 10%) fois supérieur à celui déterminé par la méthode chimique humide, et le bSiO2% déterminé par la méthode IR était d'environ 10 % ($bSiO_2$% > 30%) à 35% ($bSiO_2$% < 30%) inférieur à celui déterminé par méthode chimique humide. Le % de $bSiO_2$ déterminé selon la méthode de Mortlock et Froelich (1989) était significativement plus élevé ($p < 0.05$) que d'autres méthodes chimiques humides, par exemple DeMaster (1981), Koning et al. (2002) et Kamatani et Oku (2000). Le % de $bSiO_2$ déterminé d'après Kamatani et Oku (2000) était significativement inférieur à celui déterminé par DeMaster (1981). Il n'y a pas de différence significative entre les résultats de Koning et al. (2002) et DeMaster (1981). Sur la base de cette étude et des données publiées précédemment, cette thèse a réévalué le flux d'enfouissement global du bSi à 6.7 ± 2.7 Tmol-SiO_2 an^{-1}, ce qui

est environ 30 % inférieur aux études précédentes, montrant la nécessité de mieux comprendre les déterminations du flux d'enfouissement du bSi pour savoir s'il y a une surestimation par les études précédentes ou s'il y a un puits de Si manquant. De plus, nos résultats ont montré que la procédure de prétraitement, par exemple le broyage et le prétraitement des sédiments à l'aide de HCl et de H_2O_2, peut entraîner une surestimation du $bSiO_2$%. En outre, une procédure générale de digestion alcaline humide a été proposée pour déterminer le % de $bSiO_2$ dans les sédiments de divers environnements de dépôt.

Cette thèse a étudié les sédiments de surface d'une CCMZ typique des mers marginales chinoises (mer de Bohai, mer Jaune, mer de Chine orientale et mer de Chine méridionale) en utilisant une technique d'extraction alcaline continue, granulométrique et chimique (carbone organique, carbone inorganique et total). azote) ainsi qu'une mesure qualitative des compositions minérales argileuses pour comprendre l'écart de dissolution du silicium (Si) dans différentes matrices sédimentaires et son facteur de contrôle potentiel. Les résultats ont montré qu'une quantité 2 fois plus élevée de Si et d'aluminium (Al) était lessivée des sédiments boueux par rapport aux sédiments sableux. Un taux de dissolution élevé (> 0.20 mg-SiO_2 g^{-1} min^{-1}) des minéraux silicatés est positivement corrélé à une grande surface spécifique des sédiments. De plus, nos données de modélisation ont montré que la teneur élevée en Al (Si: Al < 40) de la silice biogénique (bSi) réduit la réactivité de l'opale. Et la source d'Al incorporée à la structure bSi est principalement due à la dissolution des minéraux silicatés. Les résultats ont montré que, bien que la réactivité des minéraux silicatés soit moins active que celle de la bSi, ils libèrent néanmoins potentiellement plus de Si et d'Al biodisponibles dans l'eau de mer en raison de leur teneur dominante (70.3 % - 99.0 % en poids) sur le fond marin. Les résultats mettent en évidence la dissolution des minéraux silicatés comme une source importante de Si marin et mettent l'accent sur une large application de la technique d'extraction alcaline continue pour comprendre la cinétique de dissolution de la silice des sédiments marins.

Mots clés : Silice Biogénique, Flux d'enfouissement, Océan Mondial, Cycle du Silicium, Méthode Analytique

重新评估生物硅埋藏通量及其在全球海洋硅循环中的意义

摘　要

沉积物中生物硅的埋藏是调查和重建现在和过去海洋生产力、以及了解硅的生物地球化学循环和现代海洋硅收支状态的一个重要参数。然而，由于缺乏依据不同沉积物组成和生物硅类型而建立的国际公认的标准化的生物硅测定方法，现有沉积物中生物硅含量的测定存在较大的差异。导致全球海洋生物硅埋藏通量的评估仍存在大的偏差，进而造成了目前对当代海洋硅循环处于稳定状态的疑问。为了重新估算全球海洋生物硅埋藏通量，本论文对多种碱液化学提取法、X 射线衍射法和红外光谱分析法及其测定生物硅含量结果的差异进行了分析。测定了全球不同海域（渤海、黄海、东海、南海、 巴芬湾，刚果深海沉积扇、 北太平洋、赤道太平洋和南大洋）的表层沉积物，对影响海洋沉积物中生物硅含量测定的主要因素（如沉积物组成、生物硅类型和沉积环境）进行了全面评估，提出了准确测定不同类型沉积物中生物硅含量的方法，并研究了生物硅测定方法差异对边缘海（中国海域）及全球海洋生物硅埋藏通量的影响。本论文取得的主要认识如下：

由于沉积物中粘土等硅酸盐矿物的干扰，陆架边缘海沉积物中生物硅含量的准确测定尤为困难。作为典型的陆架边缘海，中国东部海域（渤海、黄海和东海）沉积物中的硅酸盐矿物含量高而生物硅含量低。因此，定量评估中国东部海域的生物硅含量和生物硅埋藏通量具有挑战性。为了准确估算中国东部海域的生物硅埋藏通量并找出适合测定陆架边缘海沉积物中生物硅含量的方法。本研究采用自动连续碱液提取法和传统碱液化学提取法，测定了中国东部海域表层沉积物中生物硅含量。利用显微镜技术鉴定了沉积物中生物硅的类型（如硅藻、放射虫和海绵骨针）及其丰度。显微观察结果表明，渤海和黄海沉积物中生物硅的主要类型是硅藻，东海沉积物中生物硅主要类型是硅藻和海绵骨针，放射虫壳体主要出现在东海陆陂沉积物中。东海陆陂沉积物中放射虫和海绵骨针的丰度超过了硅藻丰度，表明放射虫和海绵骨针是该区域沉积物中重要的硅汇。碱液提取实验结果表明，使用较强的碱性溶液（2.0 M Na_2CO_3）提取沉积物和沉积物预处理（1.0 M HCl 和 10% H_2O_2 预处理，研磨沉积物）过程会导致测定的生物硅含量被高估，这主要由于自生硅酸盐和粘土中的二氧化硅被过量提取所致；而弱碱液（0.1 M 和 0.2 M Na_2CO_3）由于无法完全提取海绵骨针，则会低估生物硅含量。

使用自动连续碱液提取法（0.5 M NaOH，提取时长 1 小时）通过 Si:Al 可准确校正从沉积物中提取出的成岩硅，从而提高中国东部海域沉积物生物硅含量的测定准确度。确保完全提取沉积物中所有类型的生物硅仍具有挑战性，尤其是沉积物中的海绵骨针，因此需要通过显微镜观察验证生物硅的提取，并延长提取时间。

生物硅测定中的方法学偏差造成全球海洋生物硅埋藏通量的定量评估存在较大不确定性。为了评估生物硅测定的方法不同导致的偏差，本研究使用 XRD 法和多种碱液化学提取法测定了不同海洋沉积物样本，如陆架边缘海（中国东部海域、刚果深海沉积扇和巴芬湾）以及开阔大洋（南大洋、北大西洋、赤道太平洋）的沉积物。分析了红外光谱分析法（IR:包括红外光谱分析法和傅立叶变换红外光谱分析法）测定的生物硅数据。结果表明，XRD 法测定的生物硅含量（$bSiO_2$%）约为碱液化学提取法测定生物硅含量的 0.5 倍（$bSiO_2$% > 10%）至 5.5 倍（$bSiO_2$% < 10%），IR 法测定的 $bSiO_2$%比碱液化学提取法测定值低 10%（$bSiO_2$% > 30%）至 35%（$bSiO_2$% < 30%）。因此，相对于 XRD 和 IR 法，碱液化学提取法更适用于测定海洋沉积物中生物硅的含量。不同碱液化学提取法测定的生物硅含量仍存在差异，直接碱液提取法由于缺乏对成岩硅校正，测定的 $bSiO_2$% 明显偏高（$p < 0.05$）。基于碱液提取硅、铝浓度的截距法测定的 $bSiO_2$%低于连续碱液提取法（5 h）和自动连续提取法（1 h）测定的测定值。此外，连续碱液提取法（5 h）和自动连续碱液提取法（1 h）测定的 $bSiO_2$%没有显著差异。

为了强调这些生物硅测定方法差异的影响，本论文重新评估了中国东部海域以及全球海洋生物硅埋藏通量。新评估的中国东部海域生物硅埋藏通量（253 ± 286 Gmol-SiO_2 yr^{-1}）是前人使用碱液化学提取法测定的预处理后沉积物中生物硅含量的估算值的三分之一。结合本论文结果和校正后的前人已发表数据，重新评估后的全球生物硅埋藏通量（6.7 ± 2.7 Tmol-SiO_2 yr^{-1}）比已有的研究低 30%。因此，为了确认前人对于生物硅埋藏通量的计算是否被高估或仍存在遗失的生物硅的汇存在，进一步研究和评估海洋生物硅的埋藏通量是海洋硅循环研究亟需开展的工作之一。为最大限度地减少生物硅测定中的方法学偏差，本论文提出了适用于测定陆架边缘海及开阔大洋沉积物中生物硅含量的标准碱液化学提取步骤。

沉积物中硅酸盐矿物溶解释放出的溶解硅是维持陆架边缘海硅藻高生产力的必要条件。然而，陆架边缘海不同类型沉积物中硅酸盐矿物的溶解能力并不一致。本论文采用自动连续碱液提取法、粒度分析和化学（有机碳、无机碳和总氮）分析以及粘土矿物成成份分析（X 射线衍射分析法：XRD），对中国边缘海（渤海、黄海、东海和南海）

这一典型陆架边缘海域的表层沉积物进行了分析，研究了硅在不同类型沉积物中溶解能力的差异及其潜在的控制因素。结果表明，泥质沉积物中提取的硅和铝是砂质沉积物的 2 倍。硅酸盐矿物的高溶解速率（> 0.20 mg-SiO_2 g^{-1} min^{-1}）与沉积物大的比表面积呈正相关。此外，溶解动力学模型数据显示，生物硅中高的铝含量（Si:Al < 40）降低了其反应活性。与生物硅结合的铝重要来源为硅酸盐矿物的溶解。另外，尽管硅酸盐矿物的反应活性低于生物硅反应活性，但由于其在沉积物中的含量（70.3% − 99.0%wt）远高于生物硅含量（< 3%wt），硅酸盐矿物向海水释放更多生物可利用的硅和铝。本研究认为陆架边缘海沉积物中硅酸盐矿物溶解是重要的海洋硅源，并强调了自动连续提取技术在沉积物硅溶解动力学研究中广泛的应用前景。

关键词：生物硅；埋藏通量；全球海洋；硅循环；分析方法

Contents

1. Introduction and research background

1.1. General introduction

Silicon (Si) is the second most abundant element in the Earth's crust and the seventh most abundant element in the universe. It is a key element for the maintenance of a stable climate on planet Earth over the geological time scales (Harrison, 2000; Isson and Planavsky, 2018) and is also a required nutrient element by many terrestrial and marine organisms. In the marine realm, the cycling of Si is of particular interest owning to its interplay with other biogeochemical cycles, such as Carbon (C) and Nitrogen (N) (Tréguer and De La Rocha, 2013; Blattmann et al., 2019) as well as other elements (e.g., Al, Ge and Zn) (Sutton et al., 2018). Therefore, understanding the processes that control the Si cycle is critical for understanding the functioning of marine biogeochemical cycles (Leynaert et al., 1993; Ragueneau et al., 2002, 2006; Liu et al., 2003, 2005; Brzezinski et al., 2017; Tréguer et al., 2018, 2021; DeMaster, 2019).

Marine dissolved silicon (dSi) is a necessary nutrient for the growth and production of diatoms which contribute about 40% of the primary production of the world ocean and 70% of the primary production for coastal oceans (Nelson et al., 1995; Van Cappellen et al., 2002). Marine silicifiers (i.e., diatoms, radiolarians, siliceous sponges) utilize dSi to build their frustules/skeletons, these silicified bio-structures are called biogenic silica (bSi) by aquatic scientists or opal by geologists. Recent studies demonstrated that the bSi production will decrease in future oceans due to the dSi decline in surface waters, and the bSi burial rate will be enhanced because of the reduced dissolution rate of silica in acidified seawater (Tréguer et al., 2018; Taucher et al., 2022). The changes in riverine dSi input into oceans and the bSi production as well as bSi removal from the oceans raised concerns about whether the state of marine silicon cycle is at equilibrium, therefore, further studies for minimizing the uncertainties from both marine Si input and output fluxes are necessary (Tréguer et al., 2021).

The cycling of Si in the modern ocean and marine Si budget has been evaluated for several times over the past four decades (DeMaster, 1981, 2002, 2019; Nelson et al., 1995; Tréguer et al., 1995, 2021; Tréguer and De La Rocha, 2013). However, large uncertainties of the marine Si burial flux still exist (Figure 1.1). The reason for the large uncertainty is partly attributed to errors of determined bSi content ($bSiO_2$%) (Conley, 1998; DeMaster, 2002; Tréguer et al., 2021), since there is still a lack of a standardized determination method and internationally recognized standard sample for measuring and calibrating the $bSiO_2$% in sediments of various marine depositional environments (Zhu et al., 2022, 2023). Therefore, evaluating the methodological

biases of bSi burial flux is essential and would shed light to a better understanding of global marine Si cycle (DeMaster, 2019; Tréguer et al., 2021). So far, numerous techniques are used for measuring $bSiO_2$% in marine sediments. Generally, they can be divided into five groups: (1) the wet alkaline methods, including Si/time method and Si/Al method (DeMaster, 1981; Mortlock and Froelich, 1989; Müller and Schneider, 1993; Schlüter and Rickert, 1998; Kamatani and Oku, 2000; Koning et al., 2002; Liu et al., 2002; Lyle and Lyle, 2002), (2) X-ray diffraction method (XRD) (Goldberg, 1958; Eisma and van der Gaast, 1971; Leinen, 1985), (3) infrared analysis (including the infrared analysis and Fourier Transform Infrared Spectrometry, e.g., IR and FTIR) (Frohlich, 1989; Vogel et al., 2016; Melucci et al., 2019), (4) microfossil counts (Pudsey, 1993; Varkouhi et al., 2020b) and (5) the normative calculation of bSi based on sediment bulk elemental contents (Leinen, 1977). Among them, wet chemical methods, XRD and IR method can quantitatively determine the $bSiO_2$%, whereas microfossil counts method and Normative calculation method can only qualitatively determine the $bSiO_2$%. Previous research had shown that XRD (Goldberg, 1958; Hurd, 1983; Leinen, 1985) and IR (Vogel et al., 2016; Melucci et al., 2019) methods are capable of determining the $bSiO_2$% efficiently but loose accuracy in determining samples that contain < 10% $bSiO_2$%. Wet chemical methods are the most popular general class of methods used, however, there are considerable variations of alkaline digestion protocols and large variabilities of the determined $bSiO_2$% exist among different protocols (DeMaster, 1991; Conley, 1998; Michalopoulos and Aller, 2004). Moreover, the biases of the $bSiO_2$% determined by the wet chemical methods, XRD and IR method and the subsequent effect on the bSi burial flux evaluation were not clear. To accurately determine the $bSiO_2$%, a complete measurement of the different types of bSi and minimizing the interference of non-bSi is a necessary condition. However, these two conditions are difficult to achieve simultaneously. Marine sediments consist of several types of bSi (mainly diatoms, radiolarians, sponge spicules) and lithogenic silica (lSi: clay minerals, authigenic alumino-silicates, feldspar and quartz) which are characterized by different physical (morphology, crystallinity, dissolution rate/reactivity) and chemical properties (Si/Al ratio, Si isotopic composition). Groups of investigators had applied sequential extractions to determine bSi, the Si isotope signals of the alkaline solutions have shown distinct imprints of a variety of Si sources (bSi, authigenic alumino-silicates and clays) at separate digestion steps (Rahman et al., 2016, 2017; Pickering et al., 2020). Quantitatively defining different Si phases (bSi, authigenic aluminosilicate, clay minerals) using Si isotopic techniques ($\delta^{30}Si$, ^{32}Si) is challenging, because of the overlaps of $\delta^{30}Si$ signal of bSi and lSi (Sutton et al., 2018) and protentional contamination source of ^{32}Si from terrestrial soils (DeMaster, 2019).

Recent study found the burial of bSi in sediments contributes about 60% of the global marine Si sink (Tréguer et al., 2021), thus any effort to better evaluate the bSi burial flux must take into account the (1) accurate quantification of opal contents in sediments of variety oceanic regions (estuary, costal seas and open ocean) and (2) defining the influences of physical (physical structure, mineral content), chemical (Si, Al composition) and biological (types and abundances of bSi) properties of marine sediments on bSi determinations. To redefine the burial flux of bSi of the world ocean, this thesis thoroughly examined the physical (grain size, specific surface area) and chemical (organic carbon, inorganic carbon, total nitrogen, clay mineral content) properties of sediments that were obtained from varieties of marine depositional environments (Baffin Bay, Arctic, the Western Antarctic Peninsula, North Atlantic, Equatorial Pacific, Southern Ocean, coastal and continental margin zones (CCMZs) of the east China seas and the Congo deep-sea fan). The factors (sediment types, types of bSi, concentration and types of alkaline solutions, period of extraction time and method of calculations) that influence bSi determinations were evaluated by using multiple methods (physical methods: XRD and IR; chemical methods: different wet chemical methods). Based on the wet alkaline extractions and microscopic observation of different types of bSi in sediments, a general protocol for accurate quantification of bSi in CCMZs was proposed and a re-estimated bSi burial flux of the east China seas (Bohai Sea, Yellow Sea, East China Sea) CCMZs was presented (see chapter 3). Incongruent dissolution of silica from different sediment types was studied by applying continuous analysis of Si and Al of alkaline solutions (e.g., the Si/Al method), and detailed explanations of the modeling parameters from Si/Al method and their relationship with sediment composition ($bSiO_2$%, organic carbon, inorganic carbon, grain size, specific surface area, clay mineral compositions) were presented (see chapter 4). Further, this thesis thoroughly evaluated the bSi methodological biases, and determined the effect of pretreatment procedures on bSi determinations. Eventually, a general wet alkaline extraction procedure proposed for measuring bSi of CCMZs sediments was tested using sediments of different marine regions and the effect of methodological biases on bSi burial determinations were examined (see chapter 5). This thesis provides insights of appropriate measurement of the $bSiO_2$% in marine sediments and provides a better understanding of the bSi determination, the dissolution kinetics of various silicates as well as the state of the modern marine Si cycle.

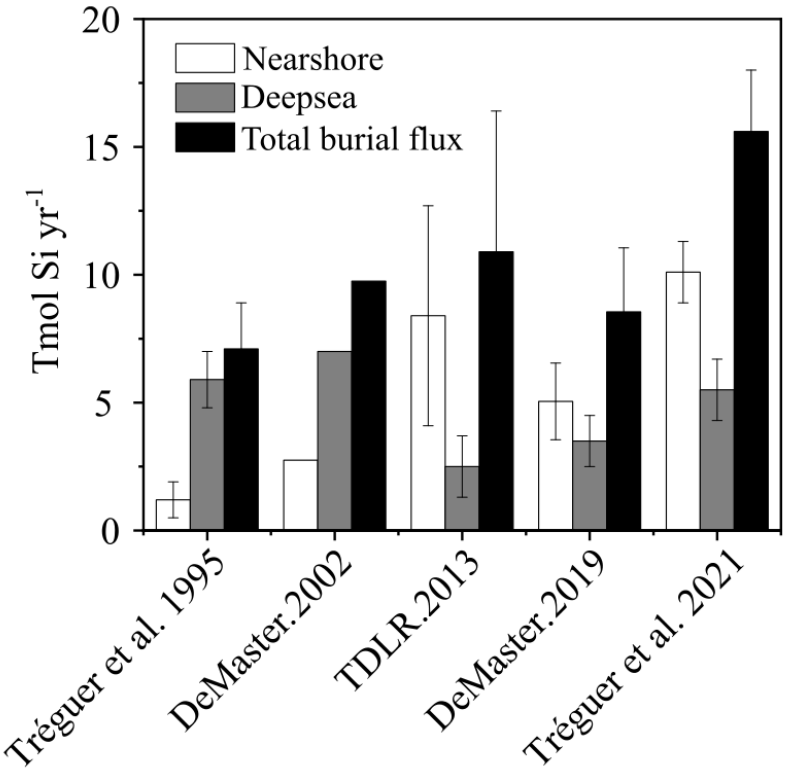

Figure 1.1. The burial flux of Si in nearshore (< 1000 m), deep-sea (> 1000 m) and the total bSi burial flux of the global ocean. TDLR 2013 represents Tréguer and de La Rocha (2013). T mol-Si yr^{-1} equals to 10^{12} mol-Si yr^{-1}.

1.2. Research background

The Marine Si cycle is tightly intertwined with the marine carbon and nitrogen cycles through the biological Si pump, thus, understanding the marine Si cycle is essential for knowing the functioning of marine food webs, biogeochemical cycles, and the biological carbon pump (Tréguer et al., 2021). Marine dSi is a required nutrient for the growth of marine silicified organisms throughout the geological time (Figure 1.2) of planet Earth (Siever, 1991; Conley et al., 2017). Marine silicifiers, such as diatoms, silicious sponges, radiolarians, silico-flagellates, and some cyanobacteria, utilize dSi to build their physical structures (Armstrong and Brasier, 2013; Tréguer and De La Rocha, 2013). These bio-silicious frustules/skeletons, in the form of amorphous silica combined with water molecules, are called biogenic silica by aquatic scientists or opal/opal-A by geologists. The biological processes of oceanic dSi date back to the Archean (Conley et al., 2017) with eukaryotic silicon metabolism occurring in the Neoproterozoic (Maliva et al., 1989). Subsequently, a direct fossil evidence proved that Si biomineralization appeared since the late Precambrian (Siever, 1992) accompanied by a secular decrease of dSi in the seawater (Conley et al., 2017). Eventually, the marine dSi concentration decreased approximately thirteen times (from 1000 μM to 75 μM) during the past 3000 million years

(Siever, 1991; Conley et al., 2017). The drop of oceanic dSi concentrations has caused continuous competition and evolution of oceanic silicifiers and non-silicifiers through geological time (Finkel et al., 2010; van Tol et al., 2012; Hendry et al., 2018) which indicates the importance of understanding the state of Si budget and the marine Si cycle. In addition, the trend of the continuous decrease of dSi concentrations and the enhanced diatom burial relative to other silicified organisms in the past possibly remain unchanged in future oceans (Figure 1.2), because of the (1) decreased riverine dSi input to the world ocean (Phillips, 2020) and (2) enhanced bSi burial on the seafloor in future acidified ocean (Tréguer et al., 2018; Taucher et al., 2022).

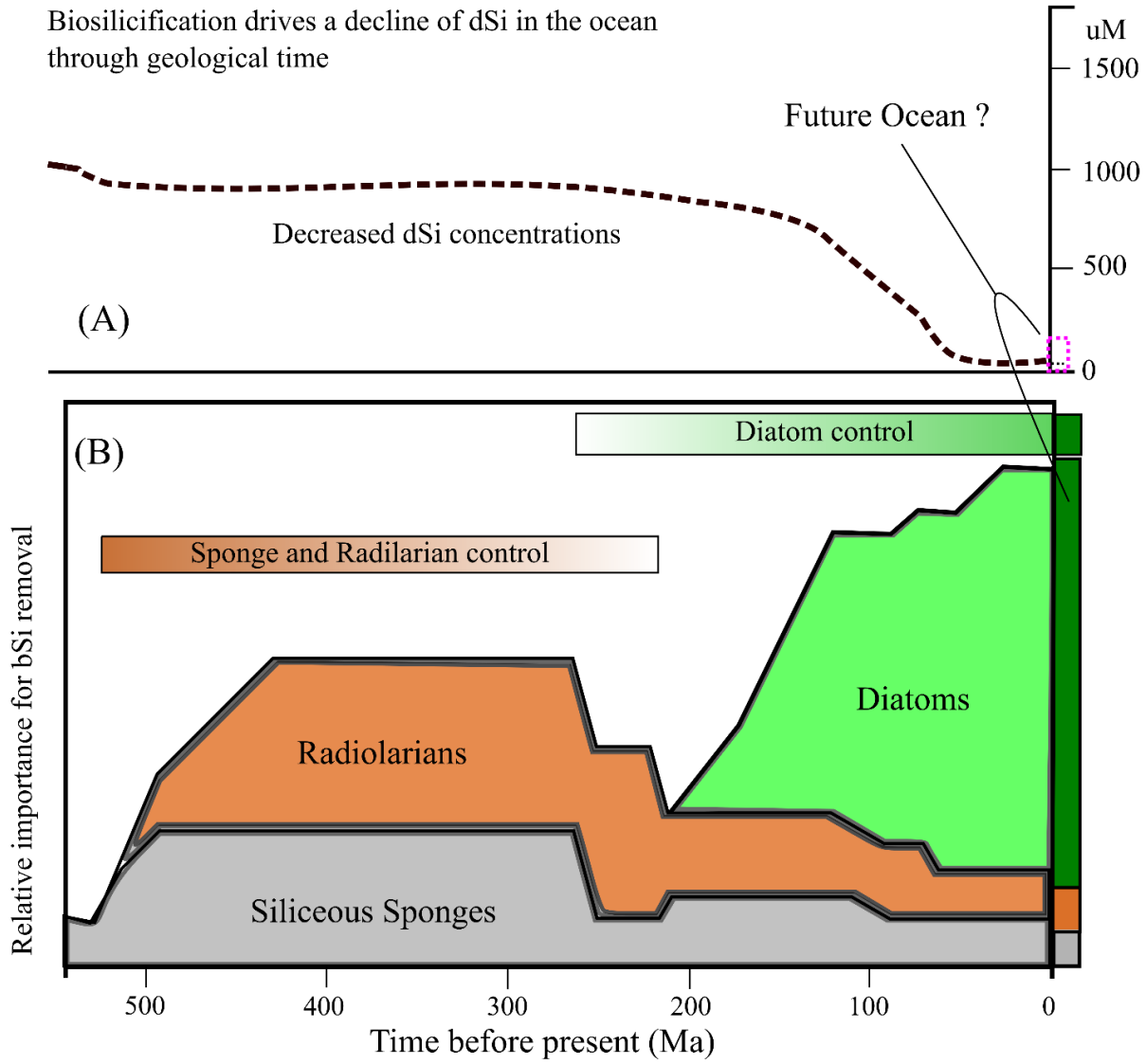

Figure 1.2. The diagram shows the marine Si cycle through geological time. Figure plotted after Siever (1991) and Conley et al. (2017). (A): A continuous decrease of marine dSi concentrations since 500 Ma. (B): The relative importance of bSi removal due to siliceous sponges, radiolarians and diatoms. According to recent study by Tréguer et al. (2018) and

Taucher et al. (2022), the marine dSi in surface water will decrease and the bSi burial will be enhanced in future acidified oceans. Thus, possibly the relative importance for bSi removal of radiolarians and sponges will continue to decrease in future oceans.

The marine Si cycle consists of biological, physical, and chemical processes (Kamatani et al., 1980; Kamatani, 1982; Tréguer et al., 1995, 2018; Rahman, 2019; Ma et al., 2022; Zhu et al., 2022). Current study demonstrated that three bSi producers contribute most of the bSi in the modern ocean, i.e., diatoms (phytoplankton), radiolarians (zooplankton), and silicious sponges (animal) (Maldonado et al., 2019). Among them, diatoms play a major role in global marine bSi production. Pelagic diatoms contribute 40% of the global oceanic primary production (Tréguer et al., 2018) and 70% of the primary production at the coastal seas (Nelson et al., 1995). However, most of the bSi produced in the photic zone dissolve in the water column and at the sediment-water interface, only ~ 3.6% of total diatom production has been buried on the seafloor (Tréguer et al., 2021). Recent studies found the deposition of bSi in sediments is mainly due to diatoms and siliceous sponge spicules (Maldonado et al., 2019; Tréguer et al., 2021). Besides biological processes and physical dissolutions, bSi also participates in chemical reactions, i.e., reverse weathering (a relatively rapid chemical reaction in estuaries and tropical regions as reported by Mackenzie and Garrels (1966) and Michalopoulos and Aller (1995)). Once deposited on the seafloor, bSi starts reacting with the major cations (Al, Fe, K) in seawater/porewater and subsequently generates authigenic alumino-silicates surrounding the bio-siliceous structures (Michalopoulos and Aller, 1995, 2004). Reverse weathering process removes large quantity of Si from ocean through 1) the formation of authigenic clays at the sediment-water interface which prevents the escape of dSi from seabed and 2) a rapid transformation of bSi to alumino-silicates (Rahman et al., 2016, 2017). These three pathways (e.g., the burial of diatom bSi, sponge spicules and the reverse weathering process) remove 15.6 ± 2.4 Tmol-Si yr^{-1} from seawater which is approximately equals to the total Si input fluxes (14.8 ± 2.6 Tmol-Si yr^{-1}), showing a relatively equilibrium state of the modern marine Si cycle (a balance between the marine Si input flux and the marine Si output flux) (Tréguer et al., 2021). Nevertheless, the Si budget and the biological fluxes within the water column are strongly influenced by climate change (e.g., ocean acidification and global warming) and anthropogenic activities (Tréguer et al., 2018, 2021; Cael et al., 2021; Taucher et al., 2022). Seawater acidification (a decrease of seawater pH values) can induce a decreased bSi dissolution rate and therefore enhance the exportation of bSi from the water column to sediment, thus, cause a decrease in the dSi concentrations of seawater which subsequently limit the production of

diatoms in future oceans (Tréguer et al., 2018; Taucher et al., 2022). In addition, the trend of global warming and the anthropogenic activities also cause a decrease dSi discharge from the global rivers (an increase only in the Arctic region) (Phillips, 2020), therefore, cause a decrease of ocean dSi concentrations of surface water layer. Those impacts will inadequately influence the marine Si cycles on both regional (such as CCMZs) and global scales (Tréguer et al., 2021; Taucher et al., 2022).

1.2.1. The biogeochemical cycle of Si in modern ocean

DeMaster (2019) and Tréguer et al. (2021) reviewed the up-to-date knowledge about the biogeochemical cycle of Si in the modern ocean and estimated the marine Si budgets. Both studies demonstrated that the marine Si budget of modern ocean is at a relatively steady state. However, both anthropogenic activities and natural climate change can cause an imbalanced state of the marine Si budget (Tréguer et al., 2021). Detailed descriptions of the modern Si cycle are presented below:

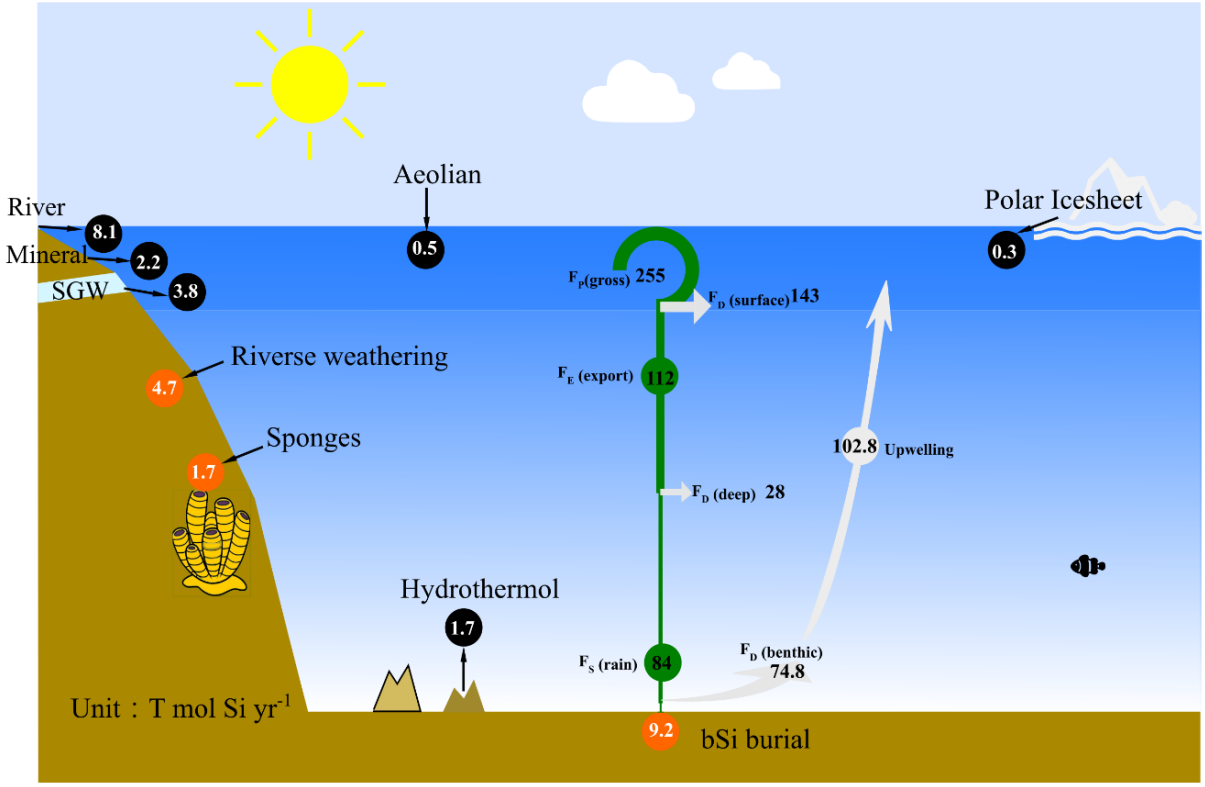

Figure 1.3. The biogeochemical cycle of Si in the modern ocean and the marine Si budget (Tréguer et al., 2021; Zhu et al., 2022). F_P(gross) represents the annual gross production of diatom Si, F_D(surface) represents the Si dissolved in surface water, F_E(export) represents Si exported to deep water, F_S(rain) represents the Si deposited to seabed, F_D(benthic) represent the Si dissolved at sediment/sediment-water interface, “Upwelling” means annual flux of dSi

transported from deepwater to surface, SGW represent submarine ground water. The unit 1 Tmol-Si yr^{-1} equals to 10^{12} mol-Si yr^{-1}. The values marked within black symbols represent marine input fluxes, and the values presented in orange symbols represent output fluxes. The green arrow represents bSi transportation from photic zone to deep-water, the white arrows represent bSi dissolution fluxes and transportation of dSi from deep-water to the surface through upwelling.

1.2.1.1. Marine Si input fluxes

There are six pathways of the marine Si input flux, including (1) rivers (8.1 ± 2.0 Tmol-Si yr^{-1}), (2) mineral dissolution (2.2 ± 1.0 Tmol-Si yr^{-1}), 3) submarine groundwater (3.8 Tmol-Si yr^{-1}; Cho et al. (2018)), (4) atmospheric deposition (0.5 ± 0.5 Tmol-Si yr^{-1}), (5) polar and subpolar glacier (0.33 ± 0.26 Tmol-Si yr^{-1}), and (6) hydrothermal activity (1.7 ± 0.8 Tmol-Si yr^{-1}) (Tréguer et al., 2021). These six Si input sources (Figure 1.3) are ultimately derived from the weathering of the Earth's crust (Tréguer and De La Rocha, 2013). Compared with the previous estimates by Tréguer and De La Rocha (2013), the Si input from the subpolar glaciers is defined as a new source of Si to marine environments (Hawkings et al., 2017, 2018).

1.2.1.2. Marine Si output fluxes

Marine dSi is removed from seawater by (1) the burial of diatoms on the seafloor at a depth of > 10 − 20 centimeters (cm) (9.2 ± 1.6 Tmol-Si yr^{-1}, Hayes et al., 2021; Tréguer et al., 2021), (2) deposition of sponge spicules (1.7 ± 1.6 Tmol-Si yr^{-1}; Maldonado et al. (2019)) and (3) the formation of authigenic silicates due to reverse weathering (4.7 Tmol-Si yr^{-1}; Rahman et al. (2017)) (see Figure 1.3). The burial of bSi in open ocean is approximately 5.5 Tmol-Si yr^{-1} (Hayes et al., 2021) and is larger than the bSi burial at CCMZs (3.7 Tmol-Si yr^{-1}, Tréguer et al., 2021).Which suggests CCMZs are important marine Si sinks because areas of CCMZs only represent 10% of global marine seafloor. Siliceous sponges play a significant role in removing Si from the ocean because of their long lives and specifically low dissolution rate (Maldonado et al., 2012, 2022). Reverse weathering process was considered to react slowly (> $10^4 - 10^5$ yr^{-1}), but direct evidence (SEM image of incubated diatom frustules) and the ^{32}Si activities in reactive Si pools have shown a rapid formation of authigenic alumino-silicates at large river estuaries, such as the Amazon River estuary, Yangtze River estuary, Mississippi River and Congo River estuary (Michalopoulos and Aller, 1995; Rahman et al., 2016, 2017; Zhao et al., 2017). In addition, several geochemical tools (^{32}Si, $\delta^{30}Si$, Ge/Al) have shown that authigenic clays may form ubiquitously in all the depositional environments of the global ocean (Ehlert et al., 2016; Baronas et al., 2017; Geilert et al., 2020; Pickering et al., 2020). However, there is

still an argument of whether authigenic silicates should be defined as marine Si sinks (DeMaster, 2019). Rahman et al. (2016, 2017) measured the natural ^{32}Si of alkaline solutions to quantify the authigenic Si formed through reverse weathering reactions and concluded that nearly all bSi produced in the photic zone were transformed as authigenic clay minerals. DeMaster (2019) argued that Rahman et al. (2016, 2017) overestimated the quantity of marine authigenic clays because he considered reverse weathering as a process that transforms solid (diatoms) to solid (authigenic silicates) materials, thus the formation of authigenic clay minerals could not be defined as a sink of dSi because the dSi in seawater is already removed from the ocean.

1.2.1.3. Biological fluxes of Si

Tréguer et al. (2021) re-estimated the annual global marine planktonic diatom production (255 ± 52 Tmol-Si yr^{-1}) using both the field data and modeling results, the estimate is not significantly different from the previously reported value by Nelson et al. (1995). Besides planktonic diatoms, other siliceous organisms also contribute to bSi production. For example, picocyanobacterial (such as Synechococcus, Brzezinski et al. (2017)) contribute < 20 Tmol-Si yr^{-1}, radiolaria contribute to 2 – 58 Tmol-Si yr^{-1} (Llopis Monferrer et al., 2020), siliceous sponges contribute > 6.15 ± 5.86 Tmol-Si yr^{-1} to the world ocean (Tréguer et al., 2021). Nonetheless, these bSi productions (picocyanobacterial, radiolaria and siliceous sponges: 51.2 Tmol-Si yr^{-1}) are within the uncertainty of the global diatom bSi production at the photic zone.

Recycling of Si in the water column is important for maintaining marine primary productions. Due to the low dSi levels in seawater (~75 µM), bio-siliceous frustules produced in the photic zone continuously dissolve in the water column and at the sediment-water boundary. According to recent estimates, about 56% of the diatom bSi dissolved in the photic zone (< 200 m depth), and 40% dissolved in deep water and sediment-water interface. Eventually, only less than 4% of bSi is buried on the seafloor (Tréguer et al., 2021). Unlike diatoms, radiolarians and sponge spicules are more resistant to dissolve. Thus, the burial efficiency of radiolarians and sponge spicules (27.6%) are much higher than diatoms (Maldonado et al., 2019). The dissolution rate of bSi are effected by several factors, such as temperature, pH and cations (Al^{3+}) combined with bSi (Kamatani et al., 1980; Van Cappellen and Qiu, 1997, 1997; Pondaven et al., 2000; DeMaster, 2002; Gallinari et al., 2002; Van Cappellen et al., 2002b; Gallinari et al., 2008; Liu et al., 2002; Rickert et al., 2002; Wu and Liu, 2020; Ma et al., 2022, 2023).

Based on the OCIM grid results using annual mean dSi concentration from the World Ocean Atlas (2018), Tréguer et al, (2021) calculated the total dSi inventory value (120000 Tmol Si) of modern ocean. Thus, the overall geological residence time for Si (dSi inventory value divided

by the dSi input flux) reduces to 8000 years. Therefore, the residence of Si in the ocean is closer to the residence time of N (< 3000 yr^{-1}). The updated estimate of the Si residence time is about 60% shorter than the previous value (18000 yr^{-1}, Tréguer and De La Rocha, (2013)), which suggests that the Si cycle may fluctuate over the glacial-interglacial timescales (Tréguer et al., 2021).

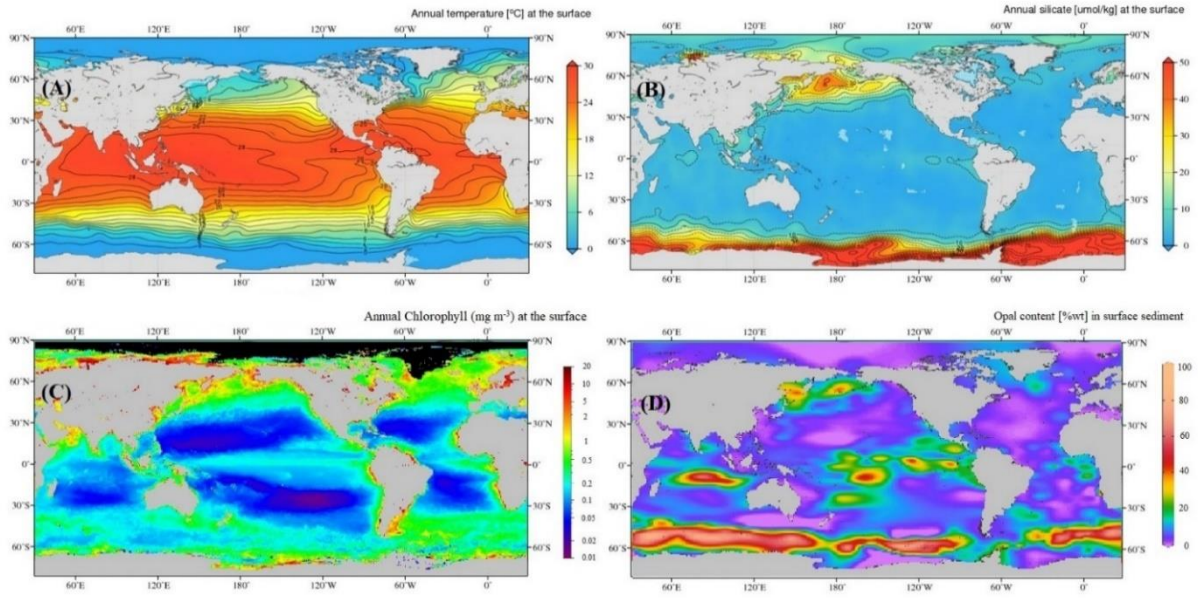

Figure 1.4. Map of the sea surface temperature, dSi concentration, chlorophyll α and $bSiO_2$% in surface sediment. (A) sea surface temperature (SST/°C, from the World Ocean Atlas (2018)): high SST in tropical and sub-tropical regions; (B) silicate concentration in surface water (World Ocean Atlas, 2018), high dSi concentration in polar area (North Pacific and the Southern Ocean) and intermediate dSi concentration at Equatorial Pacific; (C) chlorophyll α concentration (data from the Ocean Color Webmaster: https://oceancolor.gsfc.nasa.gov/l3/): high chlorophyll α concentrations were observed in high latitude and the equatorial regions; and (D) $bSiO_2$% in surface sediment (plotted using raw data from Hayes et al. (2021)): the Southern Ocean, Equatorial Pacific, Central Indian Ocean and North Pacific are regions enriched in bSi.

1.2.2. Physical property, types and distributions of biogenic silica in global ocean

Biogenic silica is a term which represents all types of biogenic siliceous structures. There are several types of bSi in marine sediment, and each bSi type consists of several hundreds of species that are characterized by different shapes and physical properties (such as water content and dissolution rate). Among them, diatoms, sponge spicules and radiolarians play major role in bSi burial in the ocean. There are other types of bSi found in marine sediment, such as phytolith (transported from land to coastal seas) (Meunier et al., 2014; Ran et al., 2017) and silico-flagellate (Wang et al., 2016), but their contribution to the global marine bSi burial are

less important (Maldonado et al., 2019). The introduction of diatom, radiolaria, sponge spicules and other types of bSi and their distributions in the world ocean are briefly described in the following sub-sections.

1.2.2.1. Physical property of biogenic silica

Biogenic silica ($SiO_2 \cdot nH_2O$) is amorphous silica that contains a certain amount of combined water molecule (Hurd, 1983). The content of combined water content of bSi is dependent on the bSi types (Table 1.1), age (living bSi or bSi obtained in deep sediments, Mortlock and Froelich, (1989) and Dodd et al. (2017)) and the living environment of bSi (Leynaert et al., 2018). Normally, bSi goes through diagenesis process and loses its combined waters. Thus, aged bSi contains less water molecules than fresh bSi. The average water content of bSi (only consider diatoms, radiolarians and sponge spicules) is ca. 10% ($SiO_2 \cdot 0.4H_2O$, see Table 1.1 and reference therein). To systematically standardize the problem of water content and formula of bSi, the opal content is preferably reported as SiO_2 (molecular mass: 60 g mol^{-1}) (Mortlock and Froelich, 1989).

The dissolution rate of various types of bSi varied significantly. Sponge spicules and radiolarians are more resistant to dissolution in both seawater and alkaline solutions than diatoms (Mortlock and Froelich, 1989; Müller and Schneider, 1993; Kamatani and Oku, 2000; Maldonado et al., 2019). This information has important implication for bSi determinations because the commonly used wet alkaline extraction technique needs to be adjusted to different bSi types when measuring the $bSiO_2$% of sediment from the different marine regions (DeMaster, 1981, 1991). The bSi structures undergoes the physical dissolution and diagenesis process in marine environments. Once the diatom died, the aging of the frustule begins and the bSi starts losing the silanols (Si-OH), this dihydroxylation process is dependent on surrounding temperature and diagenetic reactions (Dodd et al., 2017). A combination of selective dissolution of Si and precipitation of Al dissolved from minerals in sediment cause an elevated Al content in diatom frustules, and X-ray diffraction spectra have shown that Al substituted the Si throughout the entire diatom test (van Bennekom et al., 1989). The dihydroxylation of bSi and incorporation of Al in silica tetrahedral unit have prevented the dissolution of amorphous silica, therefore, enhance its preservation in marine sediments (Dixit et al., 2001; Dodd et al., 2017). Note, additional subsection (section 1.2.2.3) is presented for describing the dissolution kinetics of different types of bSi and lithogenic silicates.

Table 1.1 Combined water content (%wt.) of various types of biogenic silica. The average combined water content for diatoms, radiolarians and sponge spicules are 7.1%, 12.0% and 11.1%, respectively.

Types	Age	Region	Numbers	H_2O%	References
Diatoms	0−12ka	Guaymas Basin	3	4.1	Wang and Yeh (1985)
	0−12ka	Southern Ocean	6	12.1	Shemesh et al. (1988)
	12ka−2.6Ma	Guaymas Basin	72	3.9	Wang and Yeh (1985)
	12ka−2.6Ma	Southern Ocean	3	8.1	Mortlock and Froelich (1989)
Radiolarian	0−12ka	Central Equatorial Pacific	2	15.9	Hurd and Theyer (1977)
		Southern Ocean	6	7.9	Shemesh et al. (1988)
	2−40Ma	Central Equatorial Pacific	26	12.1	Hurd and Theyer (1977)
Sponge spicules	0	−	6	12.3	Sandford (2003)
		−	−	9.5	Schwab and Shore (1971)
		−	3	11.5	Levi et al. (1989)
	0−12ka	Kuannel Channel, Hawaii	1	9.7	Hurd and Theyer (1977)
		Kaneohe Bay, Hawaii	3	10.2	
		Sagami Bay Hawaii	1	13.4	

1.2.2.2. Biogenic silica types and distributions

The distribution of bSi on seafloor is inhomogeneous. Generally, CCMZs are areas with low $bSiO_2$%, and certain ocean regions, such as the Southern Ocean, the Equatorial Pacific, the Central Indian Ocean and the North Pacific are areas enriched in opal (Figure 1.4 D) (DeMaster, 2002; Liu et al., 2002, 2016; Zhang et al., 2015; Wu et al., 2015, 2017; Wu and Liu, 2020b; Hayes et al., 2021; Tréguer et al., 2021; Ma et al., 2022, 2023; Zhu et al., 2023). As shown in Figure 1.4, the $bSiO_2$% distribution in surface sediments is controlled by both the diatom production and preservation. Thus, $bSiO_2$% in sediments are controlled by the nutrient concentrations in surface water, the bSi production and the physical parameters of seawater (e.g., SST, salinity, pH) (Ragueneau et al., 2000). The distributions of different types of bSi are described in subsections below.

1.2.2.2.1. Diatoms

Diatoms are unicellular algae with golden-brown photosynthetic pigments and are the dominant marine primary producers in the ocean (Nelson et al., 1995; Tréguer et al., 2018; Dutkiewicz et al., 2020). Diatoms require light to live and are therefore limited to live in the photic zone (< 200 m). The size of the diatom can reach up to 2000 µm, however, most of the diatom species are in the size range of 10 µm to 100 µm. As predominant bSi primary producer, diatoms are important opponents of phytoplankton biomass at the high latitudes (e.g., the Southern Ocean, Sea of Okhotsk) and in equatorial and coastal upwelling regions (Bracher et al., 2009). In addition, in areas of high nutrient supply (i.e., the equatorial and coastal upwelling zones and deep chlorophyll maximum; see Figure1.4B), the growth rate of diatoms reaches its maximum (Hamm et al., 2003). Diatoms live in both water columns and at the sediment-water interface of the coastal regions. The production of planktonic diatom in global oceans was evaluated, however, the production of benthic diatoms in global coastal zones were not clear (Leynaert et al., 2011; Tréguer et al., 2021).

1.2.2.2.2. Radiolarians

Radiolaria, also called Polycystina, Collodaria or Rhizaria, are protozoa distinguished by the segregation of their soft anatomy into the central capsule, containing the endoplasm, and the surrounding ectoplasm (or calymma), and by their siliceous (opaline) skeletons of most species. The scientific definition of radiolaria has varied through time, generally, they are a group of diverse unicellular eukaryotes bearing delicate and elegant mineral skeletons (Biard et al., 2017; Biard, 2022). Radiolarians are zooplankton that live in the water column (from the surface to the bottom waters) and they have existed since the beginning of the Paleozoic era (541 Ma), producing an astonishing diversity of intricate shapes during their ~ 600-million-year history. After the death of radiolaria, the siliceous skeletons are preserved in sediments for millennia and subsequently records the imprint of its living environments, providing excellent tools to reconstruct past environments (Wever et al., 2002). In the modern ocean, ca. 400 − 800 living species (and several thousand extinct forms whose maximum dimension varies from 30 µM to 2 mm) of radiolarians occupy almost all ecologic niches from shallow water to the deep ocean (Boltovskoy and Correa, 2016), most of living radiolarians live in water depth < 1000 m (Boltovskoy, 2017). Radiolarians distribute widely (70° N to 85° S) in the global ocean (Figure.1.5), however, most of the radiolarian species live in the sub-tropical to low latitude (30° N to 30° S) ocean regions where the sea surface temperature (SST/°C) is high (Boltovskoy and Correa, 2016; Boltovskoy et al., 2017). In addition, based on the plankton samples,

sediment trap and surface sediment data, Boltovskoy et al. (2010) found the radiolarian production is higher in the sub-tropical to low-latitude regions than in sub-polar and polar regions.

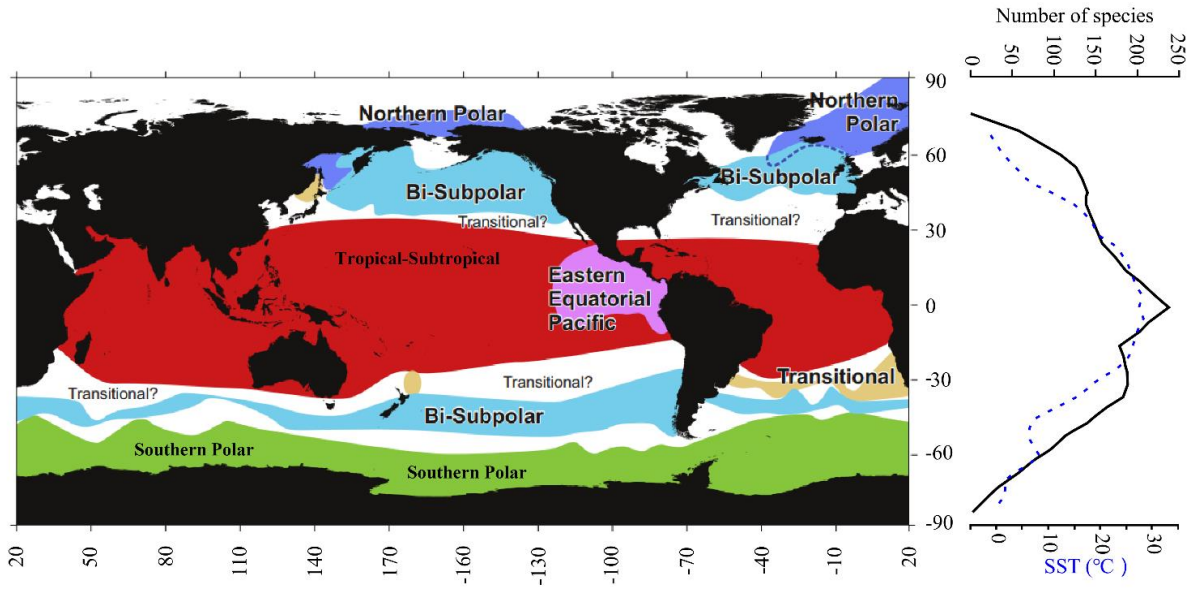

Figure 1.5. The different biogeographic domains marked in different colors (Northern Polar, Bi-Subpolar, Transitional, Tropical-Subtropical, Eastern Equatorial Pacific, Southern Polar) are defined by radiolarian species and parameters of sea water such as the mean annual temperature, salinity, chlorophyll α, silicate, nitrate, and phosphate concentrations. The figure is replotted following Boltovskoy and Correa (2016), detailed descriptions of the different domains are referred to the reference.

Individual radiolarian is thought to live for about one month (Armstrong and Brasier, 2013; Hori et al., 2021), due to their required specific living conditions and relatively short lives, radiolarians are used as a practical tool for biostratigraphy and paleo-oceanographical indicators (Chen and Tan, 1997; Wever et al., 2002; Rogers and De Deckker, 2007; Fontorbe et al., 2013, 2017; Chen et al., 2014; Cortese and Prebble, 2015; Boltovskoy and Correa, 2016; Boltovskoy et al., 2017). Thus, the radiolarian abundances, content (Leinen, 1985), species (De Wever et al., 2001) and their Si isotopic composition (Bole et al., 2022) were determined for re-constructing the paleo-environment. Radiolarian is also an important bSi producer and active marine C exporter. A recent study found radiolarians contain relatively large amounts of Si and C compared to diatom frustules (Llopis Monferrer et al., 2021) and they contribute 2 to 58 T mol-Si yr^{-1} (1% to 19%) of the global oceanic silica production (Llopis Monferrer et al., 2020).

Similar to the burial of diatoms, radiolarians carry both Si and C while sinking to the deep-water (Llopis Monferrer et al., 2021). However, compared to diatoms, radiolarian test carry

more Si in a single cell (Llopis Monferrer et al., 2020) and is more difficult to dissolve in seawater (Kamatani, 1971). A recent study demonstrates that the contribution of radiolarians to the global marine Si sink is negligible (Maldonado et al., 2019). However, this estimate was based on the results of 10 sediment cores of the world ocean and may underestimate the radiolarian bSi burial flux because a large amount (average 10% of the total bSi production) of bSi is produced by the slow dissolving radiolarians (Llopis Monferrer et al., 2020). In addition, there are areas enriched in radiolarian oozes, such as the Southern China Sea (Chen and Tan, 1997; Zhang et al., 2015), Equatorial Pacific and Southern Ocean (Boltovskoy et al., 2010; Dutkiewicz et al., 2015).

1.2.2.2.3. Siliceous sponges

Sponges are ubiquitous marine animals, occurring with moderate to high abundance on the seafloor (i.e., continental shelves, slopes, abyssal plains and hadal bottoms, Figure 1.6) (Chu et al., 2011; Maldonado et al., 2012; Van Soest et al., 2012; Gutt et al., 2013; Kou et al., 2018; Li et al., 2020; Morganti et al., 2022). Sponges utilize varieties of C, nitrogen (N), phosphorous (P) and dSi compounds, in addition to the particulate C, N, and P obtained by regular feeding (Maldonado et al., 2012). Among all the known marine sponge species, about 75% of species (most Demospongiae species and all the known Hexactinellida species) utilize dSi to build their siliceous skeletons. The quantity of siliceous skeletons represents up to 90% – 95% of the body dry weight (Maldonado et al., 2011, 2012). Siliceous sponges live in a variety of marine environments. Large sponge reefs were found in several spots of the ocean, such as the central Arctic seamounts (Morganti et al., 2022) and Antarctic (Gutt et al., 2013), which indicate silicious sponge are important marine Si reservoirs. Van Soest et al. (2012) summarized the recognized sponge species at 232 marine ecoregions (excluding open ocean; Figure 1.6) and further confirmed a wide adaptation of sponges in different marine environments of global ocean.

Large sponges can live for several hundred years. After their death, sponge spicules are released from the structures surrounded by organic matters. Sponge spicules are the skeletons to strengthen the mesohyl, assisting to support the growth of the soft sponge tissues and reinforcing the epithelia, and avoiding the collapse of aquiferous subectosomal spaces and cannals (Maldonado et al., 2012). The size of the spicules ranges from 1 μm to about $2 - 3$ meters (m), depending on the species. Spicules larger than 100 μm are called megascleres, and small spicules (< 100 μm) are called microscleres. In addition, spicules also show a large variety of shapes and ornamentation details (Boury-Esnault and Rutzler, 1997; Uriz et al., 2003) and

the formation of spicule is genetically controlled (Müller et al., 2006). Due to their low dissolution rate, sponge skeletons can be preserved in sediment over long term thus they become important Si sinks in the ocean (Chu et al., 2011; Maldonado et al., 2019, 2022). The information of the content and distribution of sedimentary sponge spicules is limited in several locations, such as the South China Sea (Chou et al., 2012), Baffin Bay (Murillo et al., 2018), Bay of Best (López-Acosta et al., 2022) and 17 cores of world ocean (Maldonado et al., 2019).

According to the alkaline extractions of different shapes of spicules and sponge spicules obtained from different species, Maldonado et al. (2019, 2022) found the dissolution of spicules is dependent on their size, types (Demospongiae, Hexactinellida, Homoscleromorpha) and organic compound incorporated within the silica layers of the spicules. Due to the complexity of the spicule dissolution rate, accurately quantification of the sponge bSi content in sediment is challenging (Conley and Schelske, 2001; Maldonado et al., 2022).

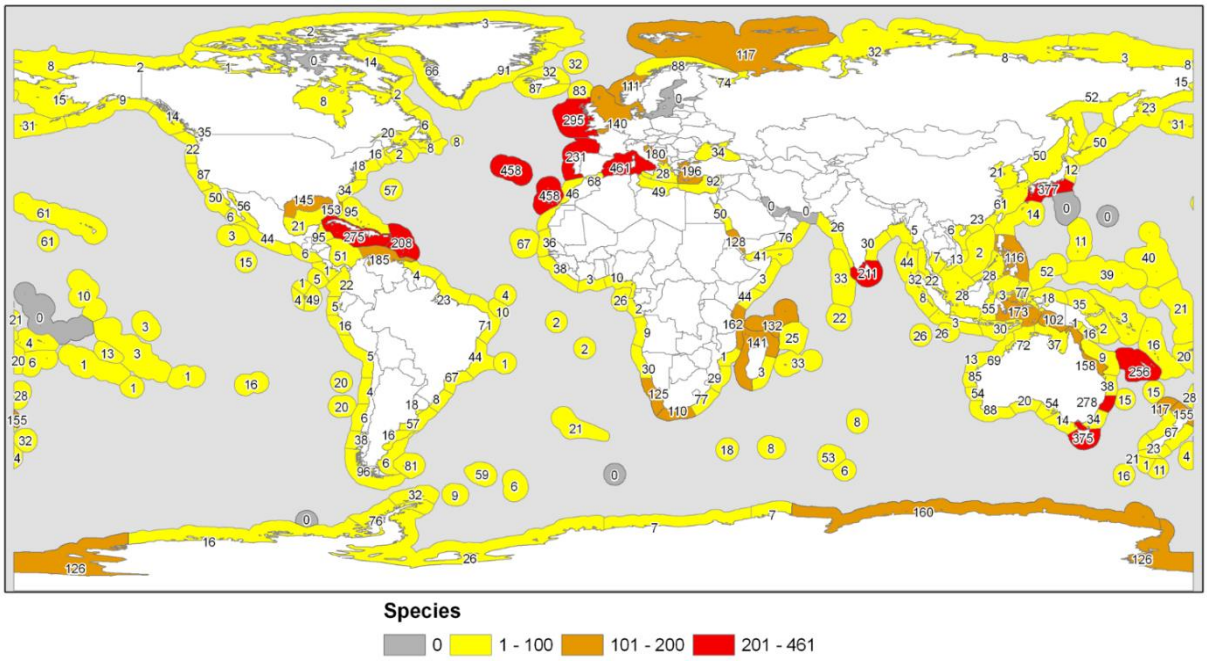

Figure 1.6. The global diversity of Porifera (sponges) at 232 marine eco-regions (Van Soest et al., 2012). The numbers within the map represent numbers of sponge species in each marine region. Information about marine sponges can be found on World Porifera Database webpage (https://www.marinespecies.org/porifera/). Additional knowledge about the sponge species and their distributions can be found in the weblink of NOAA Deep-Sea Coral & Sponge Map Portal (https://www.ncei.noaa.gov/maps/deep-sea-corals/mapSites.htm).

1.2.2.2.4. Other types of biogenic silica

As mentioned above, besides diatoms, radiolarians and sponge spicules, other types of bSi also contribute to the marine Si production and sinks. For example, phytoliths are produced by

terrestrial plants and are transported to the CCMZs by rivers (Struyf et al., 2005, 2006; Zang et al., 2016; Ran et al., 2018). Most phytoliths dissolve in estuary and river deltas, but the aged phytolith individuals are buried within sediments because of their low dissolution rate (Meunier et al., 2014). Additionally, unicellular silicoflagellate (size: 20 – 100 μm) also contributes to marine bSi production and bSi burial. Silicoflagellate is photoautotrophic phytoplankton live in the photic zone and thrive in silica-rich waters associated with current upwelling regions (i.e., equatorial and high latitude water along western margins of continents) (Armstrong and Brasier, 2013). Silicoflagellate frustules also exist in sediment of a variety of environments, such as the east China seas (Liu et al., 2015), Mediterranean Sea and Black Sea (Malinverno et al., 2019) and Santa Barbara Basin (Barron et al., 2015), and were used as an indicator to reconstruct the past marine environment and climate (Lipps, 1979).

1.2.2.3. Dissolution kinetics of biogenic silica and lithogenic silica

The dissolution of bSi and lSi provides necessary dSi nutrient for marine silicifiers (Frings, 2017; Tréguer et al., 2021). The controlling factors of solubility of the bSi in saline water, such as temperature, pH, specific surface area as well as the incorporated Al content of bio-siliceous materials, were evaluated previously by applying the flow through experiments (Van Cappellen and Qiu, 1997; Gallinari et al., 2008; Ma et al., 2023). Generally, the solubility of bSi is high under high pH, high temperature and large specific area conditions, and the solubility of bSi is reduced due to Al incorporation (Van Cappellen and Qiu, 1997, 1997; Rickert, 2000; Dixit et al., 2001), hinting asymmetrical dissolution kinetics/or solubilities of different silicates under different marine environments (Gallinari et al., 2002; Wu et al., 2015, 2017; Wu and Liu, 2020; Ma et al., 2023). In an alkaline solution, the dissolution of bSi is controlled by pH, extraction time, temperature and the pre-treatment of bio-siliceous structures (Müller and Schneider, 1993; Rickert, 2000; Maldonado et al., 2019, 2022). Normally, fresh diatoms and cleaned diatoms are more soluble (Maldonado et al., 2019), untreated diatoms (Kamatani and Oku, 2000) and aged diatoms are less soluble (Muller and Schneider, 1993). However, most diatoms can be extracted completely after 60 min of digestion in hot alkaline solutions (see Figure 1.7 A and references with the plot), except some altered bSi from river delta (Michalopoulos and Aller, 2004). The dissolution rate of radiolarian tests and sponge spicules are much less than diatoms, thus, are harder to digest completely. Muller and Schneider (1993) found 70% of radiolarian tests dissolved after 100 min in NaOH solution (Figure 1.7 B). Considering a 10% of water content of radiolarian skeletons (Table 1.1), there will be about 20% of the radiolarians escape dissolution. The dissolution of sponge spicules is particularly difficult, complete extraction of

sponge spicules requires about 1000 min (> 12 h) of alkaline digestion (Maldonado et al., 2022), bringing out challenges for bSi determination.

The dissolution of lSi releases large quantity of dSi to the ocean (Frings, 2017; Tréguer et al., 2021). Considering the even texture and the constant Si:Al ratio of clays (Koning et al., 2002), the dissolution of clays would also contribute tremendous dAl into the ocean. Direct measurements have shown an elevated dAl in the bottom waters of the Arctic Ocean, the western boundary undercurrent of the North Atlantic, the Mediterranean Sea and the core of the Equatorial Undercurrent, which suggest the dissolution of lSi as potential Si and Al sources. The relative enriched dSi and dAl at bottom waters provide conditions for a widely spread formation of reverse weathering product along continental margins (Measures and Hatta, 2021). Similar to bSi, the dissolution of clay minerals is dependent on pH, temperature, catalytic (Al effect) or inhibitor effect (organic matter), the deviation of equilibrium, surface area/surface reactivity and ionic strength effect (Cama and Ganor, 2015). Therefore, the release rate of Si and Al varied for different marine regions due to the physical and chemical characteristics of the seawater and sediment composition. In alkaline solutions, the proton-promoted reaction mechanism dominates the clay mineral dissolution process (Golubev et al., 2006) and the dissolution rate increases at high pH (Figure 1.7 D, E, F). Thus, the release of Si (also Al) from clay minerals varies under different extraction conditions. The information about dissolution of different clays has important implication for bSi determinations because about 1% to 50% of clays dissolve during alkaline extractions.

As shown in Figure 1.7, the dissolution of bSi and lSi in an alkaline solution varied significantly when applying different extraction techniques. This information has major implications for bSi determinations and the evaluation of the bSi burial flux on both the regional scale and a global scale, because most researchers select the wet alkaline methods to measure the $bSiO_2$% (Conley, 1998). These implications are listed below:

(1) The sources of Si released from sediment are bSi and lSi. Discriminating the different Si sources can help to understand the benthic Si cycle and to assist the accurate evaluation of bSi burial in the world ocean. Therefore, the key point for bSi determination is to accurately quantify bSi content and avoid the interference of lSi.

(2) The solubility of various types of bSi (diatoms, radiolarians and sponge spicules) and lSi (different clays and silicate minerals) is largely different. Thus, the types of bSi and sediment composition need to be considered when select the method for measuring the $bSiO_2$%.

(3) DeMaster (1991) found that previous studies underestimated the complexity of bSi types. The types of bSi and their size/shapes, organic matter content, age (fresh skeleton or fossil), and degree of silicification also affect their dissolution rate.

(4) The dissolution of lSi release dAl to bottom water (Measures and Hatta, 2021). Considering the differences of solubility in different clays, the efflux of Si and Al from sediments of different marine regions is incongruent. Further attempts aim to quantify the dSi and dAl dissolve from sediments need to deliberate the incongruent dissolution characteristics of various sediment types.

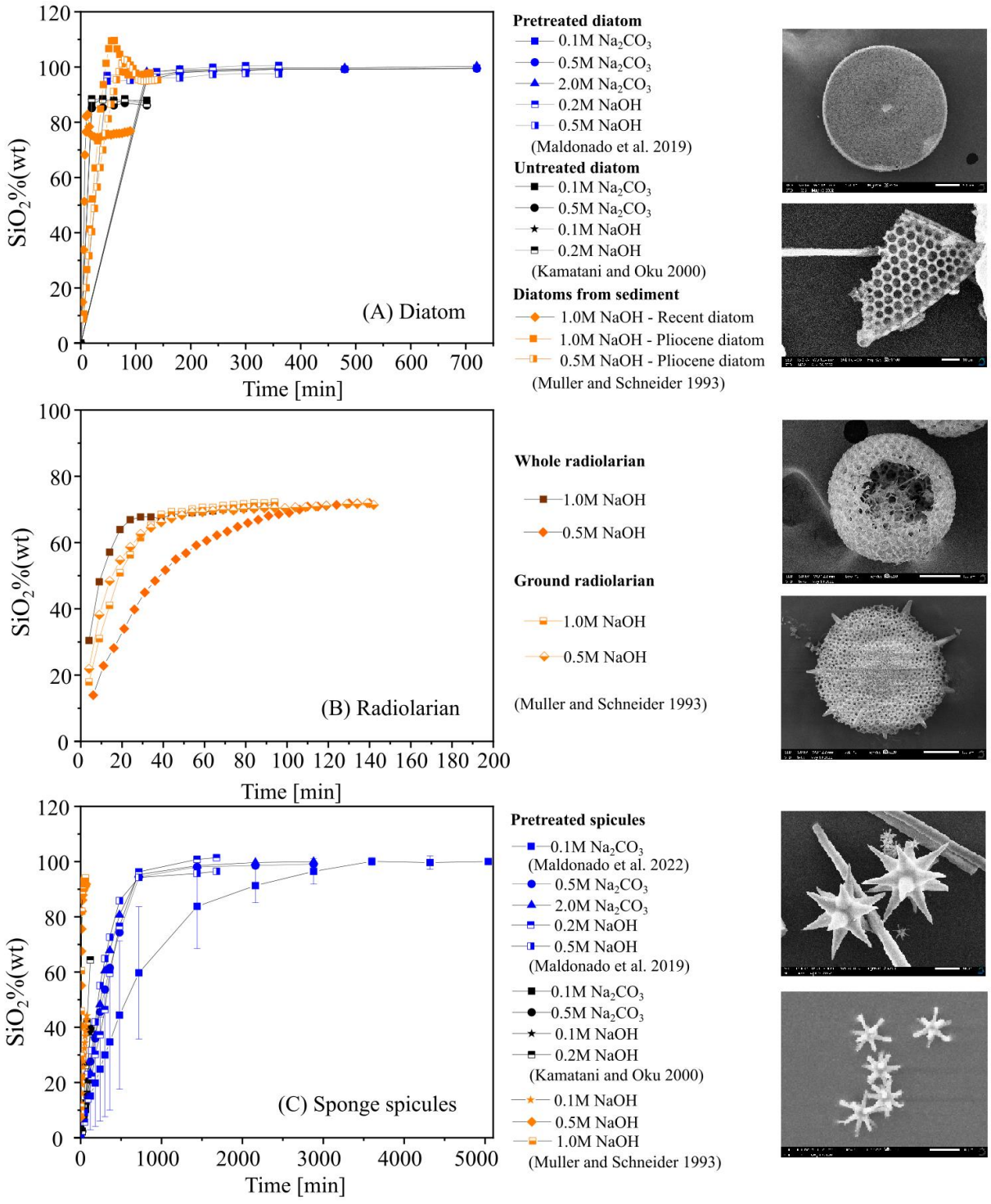
SiO2%(wt)
Time [min]
(A) Diatom
Pretreated diatom
0.1M Na2CO3
0.5M Na2CO3
2.0M Na2CO3
0.2M NaOH
0.5M NaOH
(Maldonado et al. 2019)
Untreated diatom
0.1M Na2CO3
0.5M Na2CO3
0.1M NaOH
0.2M NaOH
(Kamatani and Oku 2000)
Diatoms from sediment
1.0M NaOH - Recent diatom
1.0M NaOH - Pliocene diatom
0.5M NaOH - Pliocene diatom
(Muller and Schneider 1993)
(B) Radiolarian
Whole radiolarian
1.0M NaOH
0.5M NaOH
Ground radiolarian
1.0M NaOH
0.5M NaOH
(Muller and Schneider 1993)
(C) Sponge spicules
Pretreated spicules
0.1M Na2CO3
(Maldonado et al. 2022)
0.5M Na2CO3
2.0M Na2CO3
0.2M NaOH
0.5M NaOH
(Maldonado et al. 2019)
0.1M Na2CO3
0.5M Na2CO3
0.1M NaOH
0.2M NaOH
(Kamatani and Oku 2000)
0.1M NaOH
0.5M NaOH
1.0M NaOH
(Muller and Schneider 1993)

Figure 1.7.

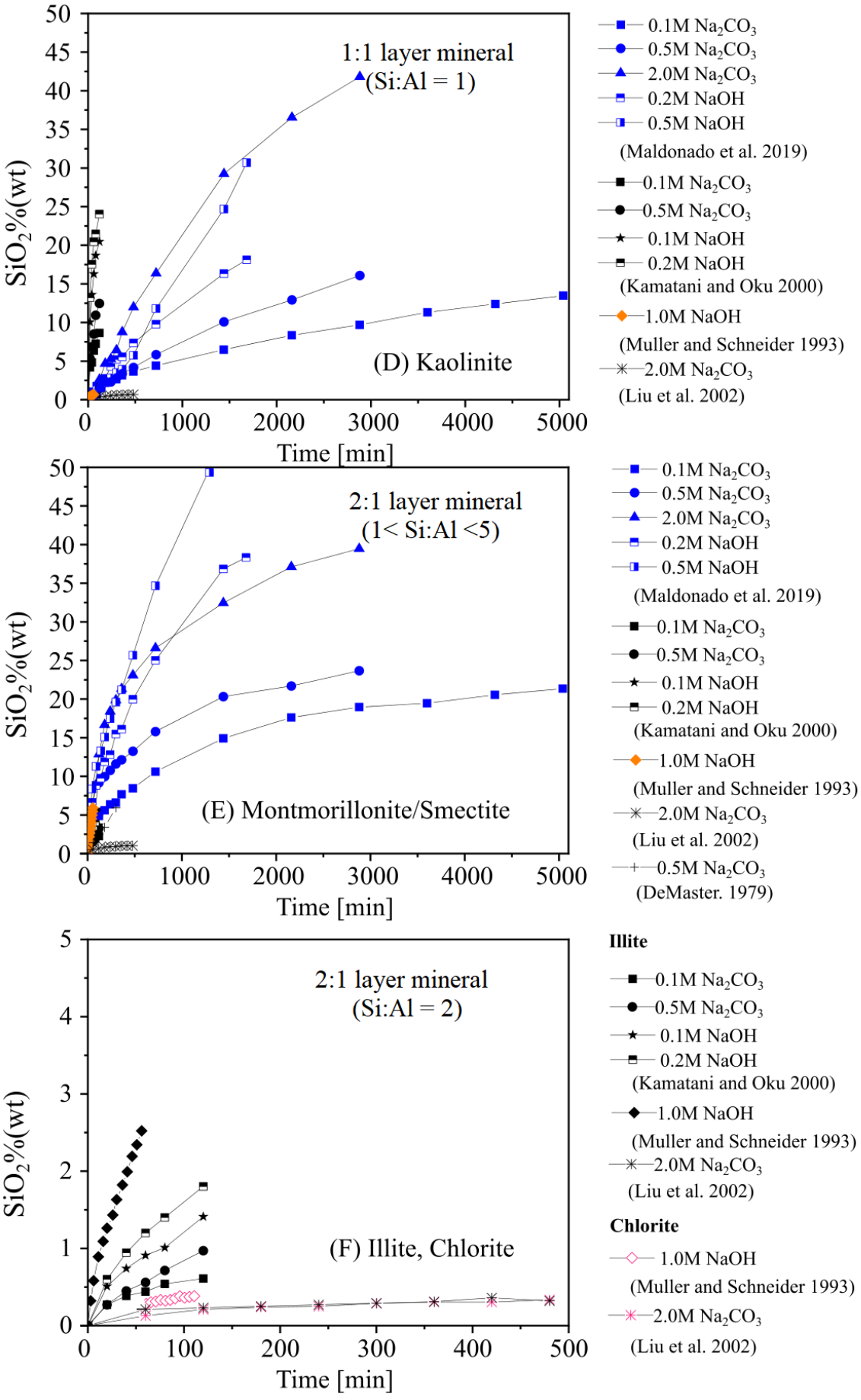
1:1 layer mineral
(Si:Al = 1)
(D) Kaolinite
SiO2%(wt)
Time [min]
0.1M Na2CO3
0.5M Na2CO3
2.0M Na2CO3
0.2M NaOH
0.5M NaOH
(Maldonado et al. 2019)
0.1M Na2CO3
0.5M Na2CO3
0.1M NaOH
0.2M NaOH
(Kamatani and Oku 2000)
1.0M NaOH
(Muller and Schneider 1993)
2.0M Na2CO3
(Liu et al. 2002)
2:1 layer mineral
(1< Si:Al <5)
(E) Montmorillonite/Smectite
SiO2%(wt)
Time [min]
0.1M Na2CO3
0.5M Na2CO3
2.0M Na2CO3
0.2M NaOH
0.5M NaOH
(Maldonado et al. 2019)
0.1M Na2CO3
0.5M Na2CO3
0.1M NaOH
0.2M NaOH
(Kamatani and Oku 2000)
1.0M NaOH
(Muller and Schneider 1993)
2.0M Na2CO3
(Liu et al. 2002)
0.5M Na2CO3
(DeMaster. 1979)
2:1 layer mineral
(Si:Al = 2)
(F) Illite, Chlorite
SiO2%(wt)
Time [min]
Illite
0.1M Na2CO3
0.5M Na2CO3
0.1M NaOH
0.2M NaOH
(Kamatani and Oku 2000)
1.0M NaOH
(Muller and Schneider 1993)
2.0M Na2CO3
(Liu et al. 2002)
Chlorite
1.0M NaOH
(Muller and Schneider 1993)
2.0M Na2CO3
(Liu et al. 2002)

Figure 1.7. Dissolution kinetics of different types of biogenic silica and clay minerals in hot alkaline solutions. The dissolution of silica is controlled by the pretreatment of bSi (acid and peroxide treatment, grinding), the concentration of alkaline solution and the duration of extraction. (A): Extraction of fresh, aged, cleaned and un-treated diatoms (see SEM pictures on the right): a complete digestion of diatoms takes < 120 min; (B): Extraction of radiolarians (see SEM pictures on the right): a complete digestion of radiolarians takes < 200 min; (C): Extraction of sponge spicules (see SEM pictures on the right): a complete digestion of sponge spicules takes > 3000 min (50 h); (D): Extraction of kaolinite (1:1 layer mineral): about 1% − 40% of silica dissolve from kaolinite in various alkaline solutions; (E): Extraction of montmorillonite (2:1 layer mineral): about 1% − 50% of silica dissolve from montmorillonite in various alkaline solutions; (F): Extraction of illite (2:1 layer mineral): about 1 − 3% of silica dissolve from illite and chlorite in various alkaline solutions. The order of bSi dissolution rate: diatoms > radiolarians > sponge spicules. The order of clay dissolution rate: montmorillonite > kaolinite > illite > chlorite. This figure is plotted based on previous published data (DeMaster, 1979; Muller and Schneider, 1993; Kamatani and Oku, 2000; Liu et al., 2002; Maldonado et a., 2019, 2022), detailed information about the data source was listed with the figure. Note the scales on X and Y axis are different for individual plot.

1.2.3. Methods used for biogenic silica determinations

Due to the positive relationship between diatom production and $bSiO_2$% in sediment (Nelson et al., 1995; Pondaven et al., 2000), the quantification of bSi in sediments is thus important for geologists, marine chemists, paleolimnologists and oceanographers who use $bSiO_2$% for understanding the past climate and environments (Conley, 1998). Previous studies developed numerous methods to quantify $bSiO_2$% in marine sediment. Generally, these methods are grouped as (1) X-ray diffraction (XRD) method (conversion of amorphous bSi to crystallized cristobalite (Goldberg, 1958); direct XRD measurement (Eisma and van der Gaast, 1971)); (2) Point counts of diatom frustules on a smear slide (Pokras and Molfino, 1986; Pudsey, 1993); (3) Infrared analysis (IR (Frohlich, 1989), Fourier transform infrared (FTIR) analysis (Vogel et al., 2008, 2010, 2016) and attenuated total reflection fourier transform infrared (ATR-FTIR) analysis (Melucci et al., 2019)); (4) Elemental partitioning of sediment chemistry (Leinen, 1977); (5) Microscope determination of sponge, radiolarian and silico-flagellate (Maldonado et al., 2019); (6) Wet chemical methods, also called wet alkaline method which include a single digestion without clay mineral calibration (Mortlock and Froelich, 1989), time sequential digestion with clay mineral calibration (DeMaster, 1981; Conley and Schelske, 1993, 2001; Liu

et al., 2002; Lyle and Lyle, 2002), clay mineral calibration using SiO_2/Al_2O_3 ratio (Kamatani and Oku, 2000) and continuous wet chemical method which requires a high resolution analysis of Si (Müller and Schneider, 1993) and Si & Al (Koning et al., 2002; Barão et al., 2015). Each of these procedures has certain inherent systematic problems or is analytically cumbersome (Mortlock and Froelich, 1989; DeMaster, 1991; Conley, 1998). General descriptions of these methods are presented below.

The XRD method described by Goldberg (1958) includes the combustion of sediment at 900 ℃ to 1050 ℃ for 4 hours in order to transform the X-ray amorphous bSi into crystallized cristobalite. XRD method gives a reproducibility of ± 10%$bSiO_2$ with a lower limit of detection about 2%$bSiO_2$ (Goldberg, 1958). Eisma and Van der Gaast (1971) recommended measuring the opal "bulge" without heating the samples to avoid the strong influence of cations (Na, K, Mg, Ca) and minerals on the cristobalite peak. The direct XRD measurement gives a precision of ± 3% for sediment samples with > 10% $bSiO_2$ and gives higher errors for $bSiO_2$% below 10% (Eisma and Van der Gaast, 1971). Based on an internationally calibration experiment, Conley (1998) reported a 0.5 to 5 times overestimation of $bSiO_2$% using the XRD method as compared to the opal content determined by several wet chemical methods. Hurd (1983) concluded two challenges that affect the XRD determination: (1) the unknown transformation efficiency of bSi into cristobalite and (2) the influence of silicate minerals on the calculation of amorphous silica spectra. So far, these two issues have not been resolved.

The microfossil counts of diatoms on a smear slide are used to semi-quantify the bSi content relative to other materials (Pudsey, 1993). Generally, the glued samples were placed under crossed-nicols illumination polarizing microscope, diatoms and clay particles appear the same as under plane-polarized light whereas quartz and silt grains appear yellow and gray on a light grey background. Pudsey (1993) calibrated the microfossil count method and found the disadvantages of this method are (1) the accuracy of measurement is dependent on the precision of balance or weighing, (2) the uneven sediment distribution on smear slide due to aggregation of sediment slurry, and (3) overestimation of diatoms due to the mounting medium used. The microfossil count method was proposed for a quick and shipboard use, thus a very precise estimate of the percent silica is not required. Varkouhi and Wells (2020) adopted the microfossil count results and convert the bSi volumetric content into mass percentage. However, whether this calculation is accurate is not clear due to a lack of comparation with other methods (such as the wet chemical method).

The infrared analysis method (IR, FTIR, ATR-FTIR) is a rapid and efficient method of determining bSi using a small amount of sediment (10 mg). Therefore, can be used as a cost-

effective method for paleolimnological research (Frohlich, 1989; Rosén et al., 2010; Meyer-Jacob et al., 2014; Vogel et al., 2016; Melucci et al., 2019). To quantify the bSi content, the absorbance of silica IR spectra (4000 cm^{-1} – 400 cm^{-1}) of processed sediments and reference samples (or standards) are analyzed, and the $bSiO_2$% is calculated based on the absorbance of sample and standards (Meyer-Jacob et al., 2014; Melucci et al., 2019). This method was applied for both marine and lacustrine sediments and showed a good co-relationship as compared with the $bSiO_2$% measured by wet alkaline methods. Variation between the bSi yield determined by the IR method and the wet alkaline method is still not clearly explained (Vogel et al., 2016). Previous study demonstrated that IR measurement is influenced by determining the environment (such as room moisture), homogeneity and granulometry of samples, and lSi content (Melucci et al., 2019).

Elemental partitioning of sediment chemistry method (or normative calculation method) was proposed to estimate the $bSiO_2$% based on an assumption that the SiO_2:Al_2O_3 of earth crust is a constant value (SiO_2:Al_2O_3 = 3), and the excess SiO_2 (equals to $SiO_2 - 3Al_2O_3$) is defined as the biogenic origin (Bostrom et al., 1972). However, the Si: Al ratios (2 − 11) are dependent on clay mineral compositions, and they change significantly (Leinen, 1977). To properly determine the $bSiO_2$% in sediments, Leinen (1977) suggests measuring the clay mineral composition for understanding the actual Si:Al ratio and then determining the bulk element composition (i.e., Si, Al, Mg, Mn, Fe) of the sample. However, the normative calculation method showed a high determination limit and large standard deviations. In addition, this method was used to determine sediments of open ocean and was not tested for nearshore sediments which contain low opal and high lSi content.

Microscope determination is used to measure the size (length, width) of individual bSi frustule/skeleton, and calculate the mass of bSi based on its volume and density (Maldonado et al., 2019). This method was applied specifically for determining the mass of sponge spicules and radiolarians (Maldonado et al., 2019). The microscope determination method is time-consuming and laborious, therefore, is not capable of determining large numbers of samples.

The wet chemical method is the most commonly used method for bSi determination so far (Kamatani and Oku, 2000; Koning et al., 2002). This method is based on the assumption of a fast-dissolving bSi (non-linear dissolution) phase and a slow-dissolving lSi phase (linear dissolution) during the hot alkaline extractions (DeMaster, 1981). Swann (2010) grouped the wet alkaline methods as (1) Si/time method (Hurd, 1973; Eggimann et al., 1980; DeMaster, 1981; Mortlock and Froelich, 1989; Gehlen and van Raaphorst, 1993; Müller and Schneider, 1993; Ragueneau and Tréguer, 1994; Conley and Schelske, 2001; Liu et al., 2002; Lyle and

Lyle, 2002; Michalopoulos and Aller, 2004) and (2) Si/Al method (Kamatani and Oku, 2000; Koning et al., 2002). The difference between the two methods is the way of $bSiO_2$% calculation. The Si/time method calculates $bSiO_2$% based on the dissolution Si through time, whereas the Si/Al method calculates the $bSiO_2$% based on the dissolution of Si, Al and the Si:Al ratios during the alkaline digestions. Barão et al. (2015) found the Si/Al method can accurately correct the lSi phases, especially when determining marine sediments. However, due to the needs of additional lab equipment and the time-consuming procedure, the Si/Al method (especially the continuous analysis of the Si and Al technique) is only applied in a few labs (such as the aquatic lab in University of Antwerp, Barão et al., 2014, 2015). Whereas most studies use the Si/time method to measure the $bSiO_2$% (DeMaster, 1981; Mortlock and Froelich, 1989; Conley and Schelske, 2001; Liu et al., 2002, 2005; Zhang et al., 2015; Ma et al., 2023; Ran et al., 2016, 2018; Maldonado et al., 2019). In addition, varieties of wet alkaline digestion procedures (Table 1.2) were applied by different investigators, such as (1) a sediment pretreatment process using HCl (Michalopoulos and Aller, 2004) or HCl and H_2O_2 (Mortlock and Froelich, 1989), (2) the use of different alkaline (NaOH, KOH and Na_2CO_3), (3) different concentrations of alkaline solutions (Conley, 1998) and (4) different sample to solution ratios (Landen et al., 1996; Liu et al., 2002; Rahman et al., 2016). Studies have found biases of the determined $bSiO_2$% among the different alkaline methods (Conley, 1998; Barão et al., 2015) which influences the evaluation of the bSi burial flux in both regional and global scale (Tréguer et al., 2021). Therefore, a generalized wet alkaline method adapted for sediment of varieties of marine environment and an international calibration is necessary (Tréguer et al., 2021).

In summary, although $bSiO_2$% determination methods have been developed for more than seven decades, there is still a lack of internationally recognized method and a standardized protocol for properly measuring the $bSiO_2$% in sediments (Goldberg, 1958; DeMaster, 1981; Mortlock and Froelich, 1989; Conley and Schelske, 1993; Liu et al., 2002; Kamatani and Oku, 2000; Koning et al., 2002; Muller and Schneider, 1993). As a result, the methodological biases would cause large uncertainties of the calculated bSi burial flux of the modern ocean. The current evaluation of the bSi burial flux of open ocean was based on previously published data determined by several methods (see Figure 1.8). Among ~ 3000 samples, more than 80% of samples were determined by wet chemical methods and XRD methods. In addition, different alkaline solutions (Na_2CO_3, NaOH, KOH) were used to determine the bSi in sediment, which lead to large uncertainties of the determined $bSiO_2$%.

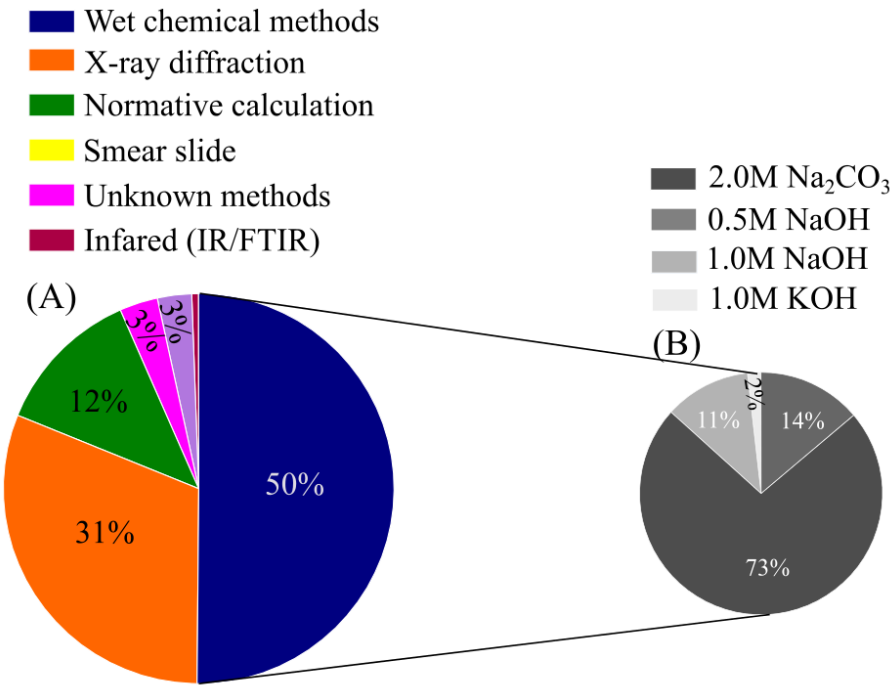

Figure 1.8. Pie charts show the proposition of different methods used for measuring $bSiO_2$% in sediments. The numbers represent percentage of data determined by different methods; the calculation was based on ~3000 raw data presented in Hayes et al. (2021).

1.2.4. Biogenic silica burial flux determinations

Robust evaluation of the bSi burial flux is necessary for understanding the state of the marine Si budget, marine Si cycles, and the sustainability of the marine ecosystem. The burial flux (F_b) of bSi in sediment is expressed as $F_b = C * w$ (Ingall and Jahnke, 1994), where C (mol g^{-1}) is the concentration of bSi, and w (g cm^{-2} yr^{-1}) is the mass accumulation rate. Therefore, any process that influences the bSi concentration in sediment and sediment mass accumulation rate will contribute uncertainties to the estimation of the bSi burial flux. From the $bSiO_2$% perspective, (1) physical and chemical processes can have an impact on bSi accumulation on the seafloor (such as temperature, pH of seawater (Tréguer et al., 2018; Taucher et al., 2022), salinity, and currents, these parameters influence the dissolution of bSi structures), (2) the errors and biases in bSi yield determined using different methods (incomplete extraction of resistant bSi can bring out underestimation and leach of lSi can bring out overestimation) can bring out uncertainties to the estimation of bSi burial flux. From the sediment mass accumulation rate perspective: (1) climate (flood, drought, and hurricane-driven eddies) impact and human activities (river damming and sand mining) can affect the sediment accumulation in CCMZs, (2) current induced sediment resuspension can also influence the measurement of sediment

accumulation rate. This thesis aims to re-evaluate the bSi burial flux by assessing the bSi methodologies biases.

1.2.5. Study importance and research objectives

Radiolarians, sponges and diatoms are key players in this evolution and, as such, have provided rich paleontological records for a multitude of palaeoceanographic studies (Racki and Cordey, 2000). These marine micro-organisms, which can produce intricate skeletons of silica, are very sensitive to changes in environmental conditions. The resistant silica-based skeletons of these organisms are particularly useful in regions of importance for studying climate change where carbonate-based archives are poorly preserved. The study of the biogeochemistry of these skeletons in the sediment layers allows us to obtain information on the environmental conditions and their variability over time.

The biological pump drives the transportation of both Si and C from photic zone to deep ocean, whereas the marine physical and chemical process effect the efficiency of cycling and recycling rate Si (Van Cappellen and Qiu, 1997a, 1997b; Van Cappellen et al., 2002; Rickert et al., 2002; Gallinari et al., 2008; Tréguer et al., 2021; Ma et al., 2023). To better understand the processes of silicification and the role of silicifiers in marine ecosystems and to improve our understanding of the marine silicon cycle, an internationally recognized method for accurately measuring bSi content in marine sediments is necessary. The only intercalibration exercises that have been performed dates backed to >20 years ago and have all highlighted that the disparity of the results for bSi analyses can vary by sample type, matrix, and provenance (Conley et al., 1998). To reassess the burial flux of opal in sediments as well as to better constrain the reverse weathering flux of the global marine silicon, this thesis will define the optimum protocol to analyze bSi in sediments of different depositional environments. To achieve the research objectives, this thesis conducted a thorough evaluation of the principal factors (already identified by the scientific community) that influence the accuracy the analysis of bSi in sediment including:

(1) the physical structure and trace element content of the bSi found within the sediment.

(2) the structural/mineral/chemical composition of the sediment samples (e.g., biogenic vs. lithogenic content; Si: Al ratio).

(3) the provenance (physicochemical environment) of the sediment samples.

This thesis thoroughly characterized the physical and chemical properties of sediments obtained from a variety marine region (e.g., the Chinese marginal seas, the Southern Ocean, the North Atlantic Ocean, Baffin Bay, Equatorial Pacific and the Congo deep-sea fan) using

multiple methods (see chapter 2. Materials and methods). This study will provide answers to the following important questions which still baffle marine chemists working on the early diagenesis of bSi and the modern marine Si cycles.

(1) What are the factors that control the accurate determination of biogenic silica (bSi) in the sediment of different marine regions and what are their associated impact on the estimation of bSi burial flux determination?

(2) What are the advantages and disadvantages of the different methods used for bSi determinations, and among the varieties of methods which one can be adopted as a standardized method for measuring bSi in sediments of all marine environments?

(3) How can lithogenic silica (clays, authigenic silicates), grain size, and carbon affect the reactivity/preservation of bSi?

(4) Is the previous evaluation of the bSi burial flux an over-estimation or under-estimation?

To answer these research questions, the necessary materials and methodologies (see chapter 2) were performed. The results and discussions were presented in chapter 3, 4 and 5, separately, focusing on (1) resolving the bSi burial flux determinations in the CCMZs of east China seas (see chapter 3), (2) uncovering the incongruent Si dissolution of CCMZs sediments and define the co-relationship between sediment compositions (i.e., clay minerals, organic matter, grain size) and opal content (see chapter 4) and (3) evaluating the bSi methodological biases and re-estimate the global marine bSi burial flux (chapter 5). Eventually, a general conclusion is presented in chapter 6.

Table 1.2 List of bSi determination methods which applied wet alkaline extractions. S/L represents the sample to alkaline solution ratio (unit: g/L).

Alkaline solution	$bSiO_2$%	S/L	Pretreatment	References
1% Na_2CO_3	4−20	0.2-0.6	No	DeMaster (1981)
1% Na_2CO_3	1.8	1.2	HCl	Michalopoulos and Aller (2004)
0.1M Na_2CO_3	< 0.2	2.5	No	Gehlen and van Raaphorst (1993)
2% Na_2CO_3	< 5	0.25−0.5	finely grind, HCl	Landen et al. (1996)
5% Na_2CO_3	0.42−1.65	0.16	finely grind	Hurd (1973)
2.0M Na_2CO_3	0.1−65	0.7−2.5	Grind	Eggimann et al. (1980)
2.0M Na_2CO_3	< 3	1−5	Grind, HCl, H_2O_2	Liu et al. (2002)
2.0M Na_2CO_3	< 0.2	2.5	No	Gehlen and van Raaphorst (1993)
2.0M Na_2CO_3	3−100	0.625−5	HCl, H_2O_2	Mortlock and Froelich (1989)
0.032M NaOH	< 50	0.2−1	Grind	Schluter and Rickert (1998)
0.2M NaOH	< 10	0.5−0.75	No	Kamatani and Oku (2000)
0.5−1.0M NaOH	55	0.2−0.6	No	DeMaster (1981)
0.5M NaOH	< 20	1	No	Koning et al. (2002)
1.0M NaOH	< 91	1	No	Muller and Schneider (1993)
2.0M KOH	< 60	0.2−1	Grind, HCl, H_2O_2	Lyle and Lyle (2002)
4.0M NaOH	<17	83	HCl	Rahman et al. (2016)

2. Materials and methods

2.1. General description

This study used surface sediments from different marine regions, such as the Baffin Bay (Arctic), the Equatorial Pacific, the east China seas (Bohai Sea, Yellow Sea, East China Sea and South China Sea), North Atlantic Ocean, Congo deep-sea fan, West Antarctic Peninsula, Southern Ocean and offshore Oceania (Eastern Australia and offshore New Zealand). Locations of the samples were shown in Figure 2.1. These samples represent different sediment types (high lSi content vs. high bSi content) and different bSi types (diatoms, radiolarians and sponge spicules).

The bSi types were determined using an inverted microscope. Sediment composition (total carbon, total inorganic carbon, total nitrogen) was determined using a Thermo Scientific FLASH 2000 CHN analyzer. Clay mineral types were determined using the X-ray Diffraction method. The $bSiO_2$% was determined using several wet alkaline methods (different Si/time and Si/Al method) and the XRD method. The methods used for characterizing the physical and chemical properties of sediments as well as for quantifying the bSi are presented in the following subsections.

2.2. Sediment location and sample descriptions

Sediment samples (n = 153) obtained at different ocean regions (see Figure 2.1) were freeze-dried and sealed in plastic bags before analysis. Surface sediments from the east China seas (Bohai Sea, Yellow Sea, East China Sea and Northern South China Sea, Figure 2.1 A) were obtained using box corer during the cruise between 2008 to 2013. The east China seas are known as opal depleted CCMZs and are recognized as a typical lSi rich sediment which is practically challenging for an accurate bSi determination (Koning et al., 2002; Tréguer et al., 2021). For example. the sediment contains high lSi content (70%, Wu and Liu, 2020) and low bSi content (< 3%, Liu et al., 2002; Liu et al., 2016; Wu et al., 2015, 2017; Wu and Liu, 2020; Ma et al., 2022). The sediment accumulation in the East China Sea is high due to terrigenous material delivered from large rivers (Yellow River, Yangtze River) and resuspension of sediment by currents (Qiao et al., 2017). In addition, the bSi types in sediments of the east China seas are complex. Previous research found diatoms and phytoliths (Ran et al., 2018), radiolarians (Zhang et al., 2015; Li et al., 2020a; Qu et al., 2020b) and siliceous sponges (Chou et al., 2012; Li et al., 2020a).

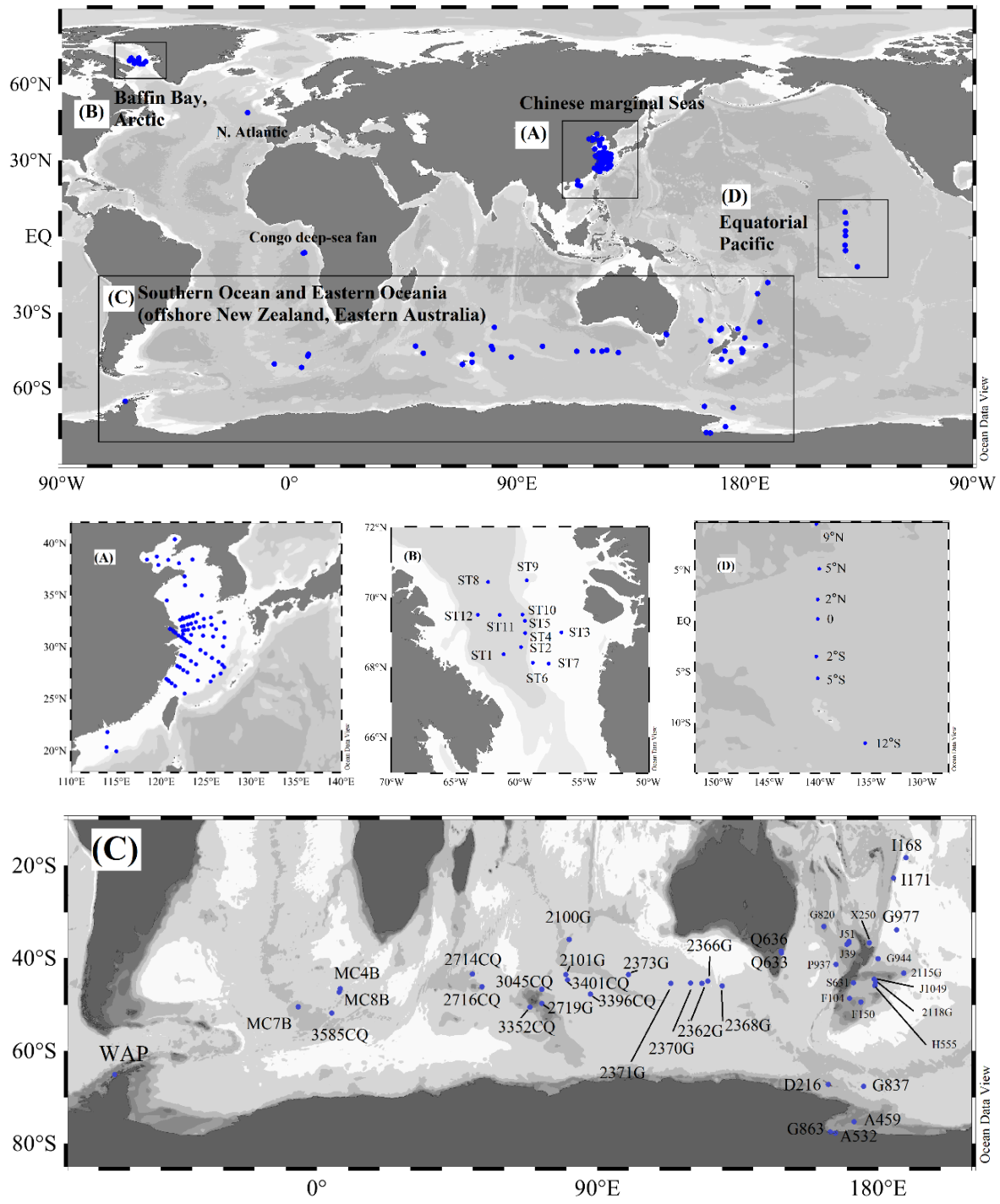

Figure 2.1. Map of Sample locations. Surface sediments (n = 153) from Coastal and Continental Margin Zones (CCMZs) and open ocean. (A) surface sediments from east China seas, sample locations were referred to Wu et al. (2017) and Wu and Liu (2020), (B) surface sediment from Baffin Bay, Arctic, (C) surface sediment from the Southern Ocean and Eastern Oceania (offshore New Zealand, Eastern Australia) (D) surface sediments from Equatorial Pacific. The BSi content of all sediment samples were measured using wet chemical method. Sample coordinates and water depth were listed in table S5.5.

The sediments from Baffin Bay (Figure 2.1 B) were obtained during the Green Edge Project (2016) research campaign (see weblink: http://greenedge-expeditions.com/about/) of which focuses on studying the Arctic marine ecosystem under phytoplankton spring bloom conditions. These samples were obtained from cold water (–0.3℃ to 3 ℃) environment at 200 to 2000 m water depth. The sampling area has an ice coverage of more than 330 days per year (Lafond et al., 2019; Randelhoff et al., 2019). The minerals in sediment of Baffin Bay are mainly from two sources, i.e., the West Greenland shelf and Baffin Island shelves (Andrews, 2019). In addition, diatoms (Lafond et al., 2019) and siliceous sponges (Baker et al., 2018) were found to be dominant bSi types in Baffin Bay.

The information (coordinates, sampling water depth and method, sediment type, SST, radiolarian species) of sediment of the Southern Ocean and Eastern Oceania (offshore Eastern Australia and offshore New Zealand) were described in Cortese and Prebble (2015). These samples (see Figure 2.1C, sampling water depth from 500 to 5000 m) were obtained using a piston core or gravity core, but only the surface sediments were used in this study. Even though the samples were obtained from surface seafloor, their ^{14}C age ranges from 400 years (before the present, BP) to 6000 years (BP) (Cortese and Prebble, 2015).

Sediment from three locations (Northern Atlantic Ocean, Congo deep-sea fan, and Western Antarctic Peninsula, see Figure 2.1) was specifically selected. Sample D226 was obtained at PAP site during the BENGAL program (Ragueneau et al., 2001; Gallinari et al., 2002, 2008). This sample is calcareous sediment containing low bSi and lSi. The bSi content and bulk Si dissolution rate were reported by Ragueneau et al, (2001). Samples from the Congo deep-sea fan (MTB2, MTB3, MTB6) were obtained in 2011 during the WACS cruise (Congo-lobe project), the samples were collected by multicores which minimize the disturbance of surface sediments (Rabouille et al., 2016). Sediments from the Congo deep-sea fan contains high Al (van Bennekom et al., 1989) and most of the materials (70%wt) were delivered through the Congo River (Garzanti et al., 2021). The surface sediment of WAP is composed of detrital material (70%wt) and biogenic siliceous remains (20%wt) (Gallinari et al., 2008), this site exhibits strong seasonal fluxes of biogenic particles following intense summer phytoplankton blooms accruing after the sea ice melting (Smith et al., 2006).

The samples from Equatorial Pacific (Figure 2.1D) were obtained during the JGOFS cruise (McManus et al., 1995). Generally, diatom and radiolarian are present in the sediments (Hurd, 1973) and the $bSiO_2$% of the samples were < 15% (McManus et al., 1995; Gallinari et al., 2002).

Further, two international calibration sediments (Still Pond, R-64) were used as international standards, and two types of clay minerals (kaolinite, provided by Prof. Oliver Ragueneau;

bentonite: Sigma Aldrich) were determined to examine the effect of different pretreatment procedures on clay dissolution.

2.3. Analytical methods

To characterize the sediments used in this thesis, the $bSiO_2$%, organic carbon content (OC%), total carbon (TC%), inorganic carbon (IC% = TC% − OC%, also calculated as $CaCO_3$%), total nitrogen (TN), the grain size of the sediment, clay mineral contents, types of major bSi and their abundances were determined. Detrital material content (detrital% = 100% − $bSiO_2$% − OC% − TN% − $CaCO_3$%) calculation follows Rickert (2002). The measurement of dSi and dAl concentrations in alkaline solutions were determined manually and automatically, the purpose of separating them is due to the differences in alkaline neutralization and the adjustment of the analysis due to sampling intervals. A detailed description of these methods is listed in the following sub-sections.

2.3.1. Biogenic silica

To find out an appropriate method of determining the $bSiO_2$% in marine sediments, both wet alkaline methods and the X-ray diffraction method were applied. Several wet alkaline extraction techniques (see table 1.2) were tested in this thesis, including manual alkaline digestions (Si/time method as described by DeMaster (1981) and Si/Al method as described by Kamatani and Oku (2000)) and the automated digestions (Si/Al method as described by Koning et al. (2002)). The calculation of the $bSiO_2$% follows the method described by DeMaster (1981), Mortlock and Froelich (1989), Conley et al. (2001), Liu et al. (2002), Kamatani and Oku (2000), Koning et al. (2002) and Barão et al. (2015).

2.3.1.1. Wet alkaline digestions

This study used both manual alkaline extractions (extraction procedures as described by DeMaster, 1981) and the continuous alkaline extractions (extraction procedures as described by Koning et al., 2002) to determine the $bSiO_2$%.

Manual digestions refer to the extraction of sediments in an alkaline solution (NaOH, Na_2CO_3, KOH) manually (DeMaster, 1981; Mortlock and Froelich, 1989; Kamatani and Oku, 2000; Conley and Schelske, 2001; Liu et al., 2002; Lyly and Lyly, 2002). The pretreated (pretreating sediments using 1.0 M HCl and 10% H_2O_2, and grinding sediments into powders) and untreated sediments were extracted in NaOH (0.5 M) and Na_2CO_3 (0.1 M, 0.2 M, 2.0 M) solutions. Before alkaline digestions, freeze-dried sediments were gently mixed using an agate pestle and agate mortar. The mixing process aims to homogenize the sediments without breaking the sediment

into fine powers (for not over-changing the bSi and lSi structures). Sediments (20 to 100 mg) were then weighed into a 50 mL polypropylene copolymer centrifuge tube (Nalgene no. 3119-0050; Caps no. DS3132-0024) or a 50 mL fluorinated ethylene propylene (FEP) centrifuge tube (Nalgene no. 3114-0050; Caps no. DS3131-0024). An alkaline solution (40 mL, Na_2CO_3 or NaOH) was added to the centrifuge tube using a calibrated 10 mL pipette (10 ± 0.01 mL, Eppendorf). The sample-to-liquid ratios (S/L) were ca. 2.5 g/L. The tubes were tightly capped after the addition of the alkaline solution. Sediment samples and alkaline solution were well mixed using a Vortex mixer. Then samples were immediately placed into a shaking water bath (Julabo SW22) pre-heated to 85 ℃ with an oscillation frequency of 100 rpm (as shown in the schematic diagram Figure 2.2). In addition, the sediment pretreatment procedure was applied following Mortlock and Froelich (1989). Freeze-dried sediment was weighted in plastic tube, 10 mL of 10% H_2O_2 was added to the tube for 30 min for removing organic matters. Then 10 mL of 1.0 M HCl was added to remove carbonate (for 30 min). Measurement of dSi of the mixture showed little amount of Si was leached (~0.1%SiO_2). After centrifugation and rinsing samples with Mili-Q water for 3 times, the HCl and H_2O_2 were removed from residual sediment. Residual sediment was dried for further analysis.

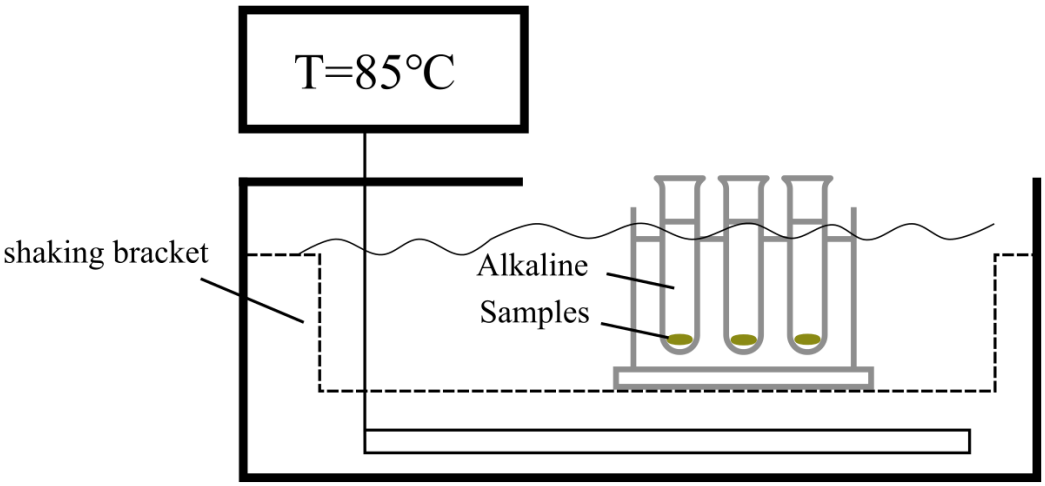

Figure 2.2. The schematic diagram shows the manual alkaline extractions. Sediments were added in plastic tubes filled with 40 mL of alkaline solutions (NaOH, Na_2CO_3). The duration of extraction ranges from 5 h to 60 h. The dashed line represents a shaking bracket, and the curved line represents water level.

An aliquot of 200 µL to 1000 µL clear centrifugation supernatant was taken from the extraction solution at each time interval (one hour) and neutralized using 1.0 M HCl solution. Prior to each sampling step, the sediment-solution mixture was centrifugated for 5 min at the

speed of 4000 rpm. Normally, it takes about 10 mins before next digestion step. This procedure does not affect the measurement of dSi and bSi (Liu et al., 2002). The period of digestion times was dependent on the purposes of the measurements and varied from 5 h to 60 h. Later, the neutralized samples were diluted by Milli-Q water (18.2 MΩ cm-1) to 10 mL, then the dSi was measured following the molybdate-blue method (Grasshoff et al., 1983) following a spectrometer as described in Mortlock and Froelich (1989) and Liu et al. (2002). The dAl concentration was measured following the lumogallion method (Hydes and Liss, 1976; Ragueneau et al., 2005). A detailed description of dSi and dAl measurement procedures was described in section 2.3.2. Additionally, to test the effect of pretreatment procedure on bSi determination, sediments were (1) ground into fine powders using agate mortar and pestle and (2) pretreated using 1.0 M HCl and 10% H_2O_2. Generally, about 40 mg of sediments were weighed in a tube, then 10 mL of H_2O_2 was added into the sample for removing the organic matters. After 30 min, 10 mL of 1.0 M HCl was added to remove inorganic carbon. After 30 min, the mixed solution was centrifugated at 4000 rpm for 5 min. The upper liquid was removed carefully using a pipette. Later, 10 mL of Mili-Q water was added to wash out the residual acid and peroxide. The washing procedure was repeated three times in order to remove residual acid and peroxide completely. The washing procedure does not leach Si from sediment as described by Pickering et al, (2020)). Then sediments were dried at 60 ℃ overnight.

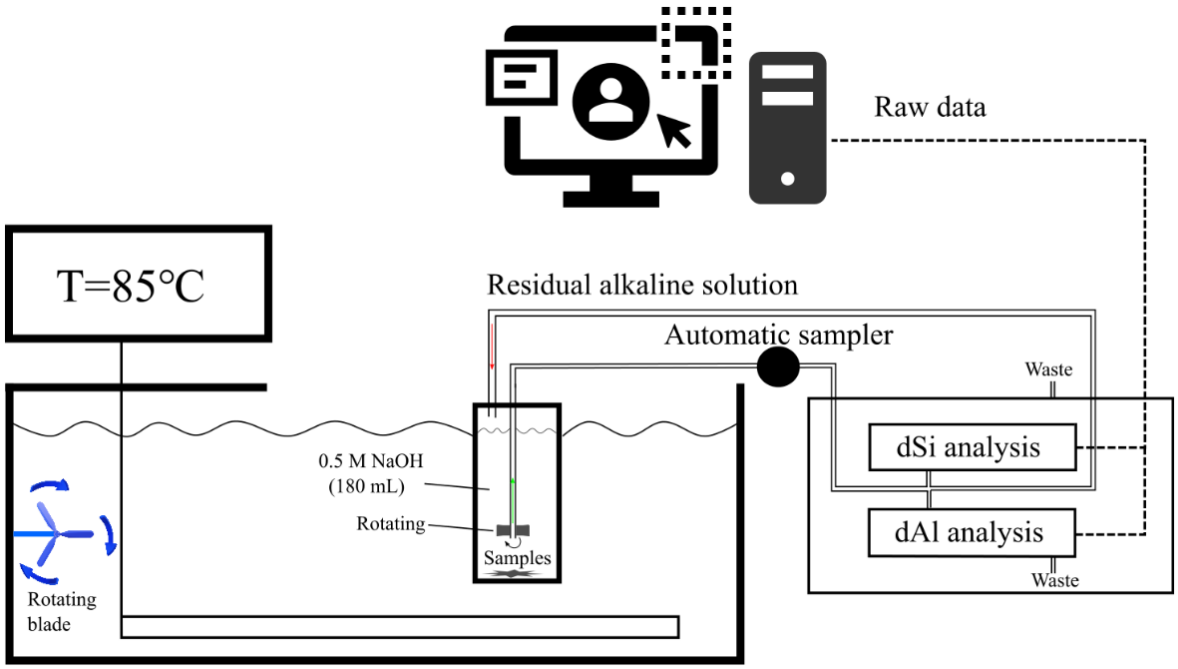

Figure 2.3. Schematic plot shows the extraction of sediments following continuous Si/Al method. Sediments were extracted in a stainless-steel vessel filled with 180 mL of 0.5 M NaOH solution. A rotating blade was placed inside the vessel to homogenize the sediment and alkaline

solution for generating a relative constant sample/liquid ratio. The water-bath was pre-heated at 85 ℃ before starting the experiment, and a rotating blade was equipped within the water-bath for keeping a homogenized temperature. The curved line represents water level, the dashed line represents connections between spectrometers and the signal processing system on computer. The dSi analysis and dAl analysis were further described in Figure 2.4 and Figure 2.5.

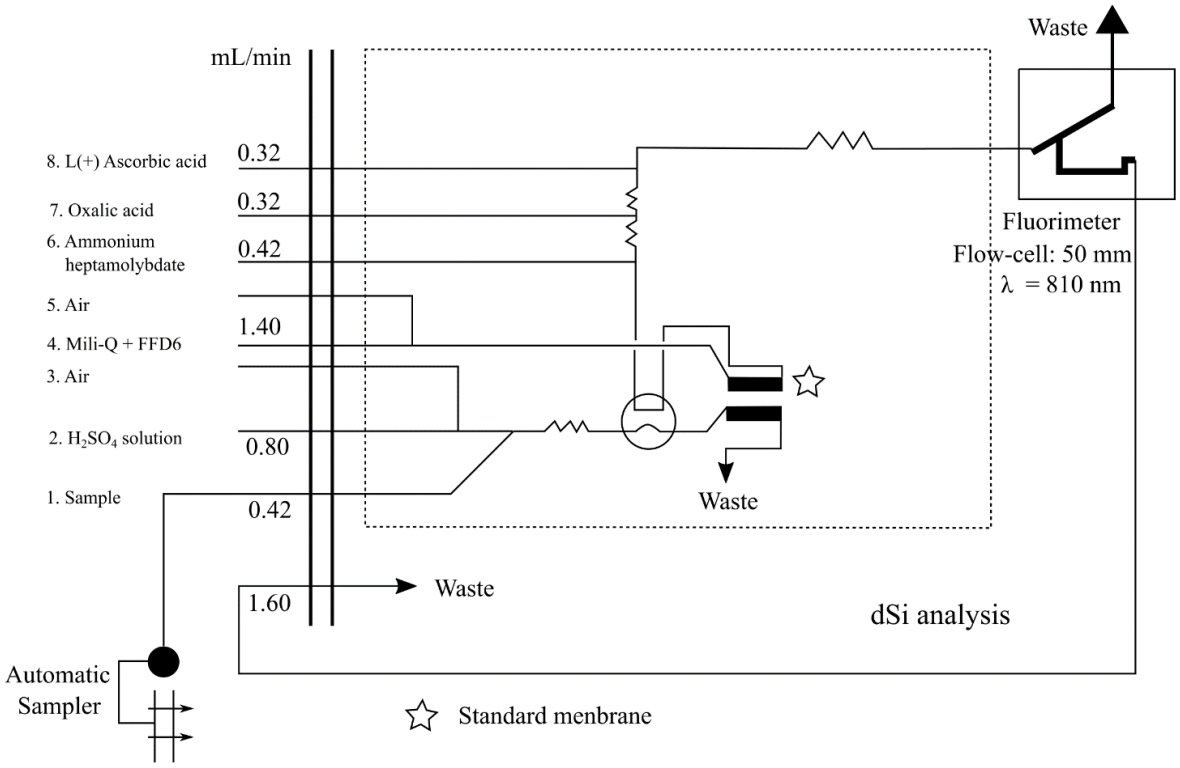

Figure 2.4. A schematic diagram shows the measurement of dissolved dSi by the automatic method. This system is connected to the reaction vessel through an automatic sampler for taking the samples continuously. Alkaline solution was neutralized and mixed with reagents. Then determined by a fluorimeter at the wavelength of 810 nm. The dashed line represents area that all reagents were mixed before dSi determination.

The continuous alkaline digestions refer to the digestion of sediments in 0.5 M NaOH solution with an automatic sampler and analytical system for determining the dSi and dAl concentration (Koning et al., 2002; Barão et al., 2015). This method allows a high-resolution (one second) record of the dissolution kinetics of both bSi and lSi. In this study, the $bSiO_2$% was measured following the continuous analysis method (Koning et al., 2002; Barão et al., 2015). The experiments were carried out at the University of Antwerp (Belgium). The dSi and dAl concentrations in 0.5 M NaOH solution were measured continuously at one second (s)

resolution (Müller and Schneider, 1993). In general, freeze-dried sediments (15 to 100 mg) were added into a stainless-steel vessel with an initial 180 mL of 0.5 M NaOH pre-heated to 85 ℃ (see Figure 2.3). The closed vessel (to avoid evaporation) is directly connected to a continuous analyzer (Skalar®, The Netherlands) and a rotating motor continuously homogenizes the sample in the extraction liquid, maintaining a constant S/L ratio. The dSi concentration is determined according to the molybdate-blue method (Grasshoff et al., 1983), while dAl is determined according to the fluorometric method (Hydes and Liss, 1976). Detailed descriptions of the dSi and dAl measurements can be found in section 2.3.2.

2.3.1.2. X-ray diffraction

The determination of bSi using the XRD followed the procedure described by Goldberg (1958) and Leinen (1985). Normally, the amorphous bSi was transformed into crystalized cristobalite under high temperatures, and the calculation of the $bSiO_2$% is based on the X-ray cristobalite spectra. In this thesis, a standard addition method was applied for quantifying the bSi in the sediment of the east China seas (sample: A1, F8, C12, DC). The aims of applying this method are to (1) evaluate whether the XRD method can be used for measuring the $bSiO_2$% in opal-depleted sediment, and (2) to test the precision of the XRD method. In general, about 25 g of freeze-dried sediments were pretreated using 1.0 M HCl to remove the calcium carbonate. This procedure does not change the amount of cristobalite in sediment (Goldberg, 1958). Then residual sediments were centrifugated at 4000 rpm for 5 min, and the upper clear solution was removed through pipetting. After washing the residual sediment three times using Mili-Q water, the sediments were dried (60 ℃) in an oven overnight. The dried sediments were ground into fine powers mechanically. Later, the weighted sediment was mixed with a known amount of decarbonated diatomite (0%, 0.5%, 1.0% and 1.5%SiO_2 dry weight) before combustion (1050 ℃, 4 hours). The area of the resultant 4.04 Å diffraction peak of cristobalite was determined on an X-ray Diffraction Spectrometer (Brucker AXS D8 Advance and Brucker AXS D2 Phaser) at 40 KV and 35 MA, using Cu - Kα radiation over 2θ ranging from 2° to 70° (Goldberg,1958). The $bSiO_2$% was then calculated based on the added $bSiO_2$% (X-axis) vs. cristobalite area (Y-axis) plot, the $bSiO_2$% of the sample equals the absolute value of the X-axis where Y is zero.

2.3.2. Dissolved Si and Al analysis

2.3.2.1. Dissolved Si analysis

The dSi analysis methods are different for manual extracted samples and automated extracted samples. The manual analysis of the dSi concentrations was performed for the samples extracted by manual alkaline digestions. The determination of dSi in Na_2CO_3 (0.1 M, 0.2 M, 2.0 M Na_2CO_3) and 0.5 M NaOH solution follows the molybdate-blue method as described by Mortlock and Froelich (1989), Liu et al. (2002) and Gallinari et al. (2002). Neutralized alkaline solutions were diluted 50 to 200 times using Mili-Q water, then mixed with acidified ammonium heptamolybdate solution. After 20 min, the reducing reagent (oxalic acid, H_2SO_4 solution and 4-Methylaminophenol sulfate) was added and well mixed. The solution is then placed within the lab for 1 h before analysis. Instead of determining the absorbance (Abs), the transmittance (T%) was measured using the UV spectrometer (Abs = − log T). The dSi standard solutions (the same matrix as alkaline solution) of 0 µM, 2.50 µM, 2.75 µM, 5.00 µM, 7.50 µM, 8.75 µM, 10.00 µM, 12.50 µM, 15.00 µM, 17.50 µM, 20.00 µM were measured for calculating dSi concentration.

The automated procedure for the measurement of the dSi concentration is based on the following reactions: the sample is acidified and mixed with an ammonium heptamolybdate solution forming molybdosilicic acid. The molybdosilicic acid is reduced with ascorbic acid to a blue dye, which is measured using a UV spectrophotometer. As shown in Figure 2.4, a sampler is connected with the reaction vessel for sampling the alkaline from the beginning of extraction. The alkaline solution is then mixed with acid solution (3% of H_2SO_4, percentage in volume, reagent number: Merck 100731) for neutralization. Subsequently, it is reacted with the ammonium heptamolybdate (2%wt, reagent number: Merck 101182), oxalic acid (4.2%wt, reagent number: Merck 100495) and ascorbic acid (3.8%wt, reagent number: Merck 100127). Then the solution was passed through a 50 mm flow-cell and the absorbance (Abs) is determined at the wavelength of 810 nm. Standard samples of dSi with concentrations of 1 mg L^{-1}, 2 mg L^{-1}, 4 mg L^{-1}, 6 mg L^{-1}, 8 mg L^{-1}, 10 mg L^{-1}, 20 mg L^{-1}, 30 mg L^{-1}, and 40 mg L^{-1} were used for calibration, and only the linear regression curves with correlation coefficients $R^2 \geq 0.9995$ were accepted according to previous studies (Barão et al., 2015). Two independent reference solutions (with concentrations of 3 mg L^{-1}, and 9 mg L^{-1} of dSi) were tested before and after the continuous alkaline extractions to guarantee an analytical error below 5%. The determination of the blanks during each extraction experiment showed the Si from both the reagent and tube was negligible. The stock standard solutions for Si were made using $Na_2SiO_3 \cdot 9H_2O$ (Sigma-Aldrich S4392).

2.3.2.2. Dissolved Al analysis

To measure the dAl in alkaline solutions, a lumogallion method was applied using a fluorimeter (Fluorimeter JASCO FP-920). This method was designed for measuring low concentrations of dAl in natural waters (Hydes and Liss, 1976; Ren et al., 2001) and adopted for determining the dAl in alkaline solutions by Koning et al. (2002) and Ragueneau et al. (2005).

Before measuring the dAl concentrations, the following reagents were prepared in advance. Including (1) buffer solution (24 mL of 2.0 M sodium acetate (GPR, VWR) mix with 10 mL of 2.0 M acetic acid (Sigma Aldrich)), (2) lumogallion ($C_{12}H_9ClN_2O_6S$, Brunschwig A5060) solution (200 mg/L), (3) 10 mg/L or 370.37 µM dAl stock solution (regent: $KAl(SO_4)_2 \cdot 12H_2O$, Merck 101047). After the preparation of the reagents, the alkaline solution (sub-samples obtained at each one-hour interval) was neutralized using 1.0 M HCl solution in a 15 mL plastic tube. For example, a 1 mL of 0.5 M NaOH solution is neutralized with 0.625 mL of 1.0 M HCl, or 0.5 mL- 0.5 M NaOH solution is neutralized with 0.313 mL of 1.0 M HCl. Then the neutralized solution was diluted to 10.0 mL with Mili-Q water (18.2 MΩ) using a pre-calibrated pipette. Later, 1.0 mL of buffer solution (sodium acetate and acetic acid mixture, pH = 5.05 − 5.10) was added into the plastic tube. After mixing the solution well, 0.5 mL of lumogallion solution (200 mg L^{-1}) was added and the tube was tightly closed. The tubes were put into a shaking (100 rpm) water bath (Julabo SW22) pre-heated at 80 ℃. After heating the solution for 90 minutes (min), the tubes were removed from the water bath and put in the lab for cooling down to an ambient temperature. The fluorimeter was then switched on and running for at least 30 min before analysis. Note that the working standard solutions were prepared in the same matrix as samples (using the same concentration/volume of alkaline solution, acid solution for neutralization and the same proportion of dilution). The concentrations of the standard dAl solution were: 0 µM, 0.125 µM, 0.25 µM, 0.50 µM, 0.75 µM, 1.00 µM, 2.50 µM, 5.00 µM, 10.00 µM, 15.00 µM. The parameter settings on the fluorimeter for dAl determinations are λ_{ex} = 498 nm, λ_{em} = 560 nm, Gain = 100 and ATTEN = 4. The plot of concentrations of standard solutions (µM) vs. Fluorescence value (constant) with an $R^2 > 0.9995$ was adopted for the calculation of the samples. The unit of the dAl concentrations (µM) was normalized to mg L^{-1} (1 µM = 2.7×10^{-2} mg L^{-1}).

The method of measuring the dAl using an automatic method originates from Hydes and Liss (1976) and is similar to the manual method as described above. However, the automatic method allows a rapid, high-resolution dAl analysis and continuously records the changes in dAl

concentration through time. This procedure was proposed by Koning et al. (1997, 2002) and was used for determining the alkaline extracted dAl from the soil, lacustrine and marine sediment (Barão et al., 2015). The automated procedure (Figure 2.5) for the determination of dAl in an alkaline solution (0.5M NaOH) is based on the following reactions: the alkaline solution was pimped by auto-sampler continuously, the sample was mixed with 0.05M HCl solution for neutralization. Hereafter, the buffer solution (sodium acetate and acetic acid solution, pH = 5.0) and the lumogallion solution (200 mg/L) were added. The mixture was then heated at 50 ℃ for a chromogenic reaction. Samples were measured by fluorimeter (flow-cell width: 2 mm) with λ_{ex} = 460 nm, λ_{em} = 550 nm (these parameters were adjusted for the rapid determination of dAl). Standard samples of dAl with concentrations of 1 mg L^{-1}, 2 mg L^{-1}, 4 mg L^{-1}, 6 mg L^{-1}, 8 mg L^{-1}, 10 mg L^{-1}, 20 mg L^{-1}, 30 mg L^{-1}, and 40 mg L^{-1} were used for calibration, and only the linear regression curves with correlation coefficients $R^2 \geq 0.9995$ were accepted according to previous studies (Barão et al., 2015). Two independent reference solutions (with concentrations of 3 mg L^{-1}, and 9 mg L^{-1} of dAl) were tested before and after the continuous alkaline extractions to guarantee an analytical error below 5%. The stock standard solutions for Al were made using $KAl(SO_4)_2 \cdot 12H_2O$ (Merck 101047). A detailed information of the reagents used for dAl analysis was listed below (1) NaOH and Brij 35 solution (mix 1000 mL of NaOH with 2 mL of 30% Brij 35 (Skalar SC 13900)); (2) HCl solution (dilute 45 mL of 32% HCl (Merck 100313) with Mili-Q water to 1000 mL and add 3 mL of Brij 35); 3) Buffer solution (dissolve 164.0 g of sodium acetate trihydrate (Merck 106267) into 400 mL then add 96% acetic acid (Merck 100062) continuously until the pH = 5.0, normally 70 to 75 mL of acetic acid is required); 4) Lumogallion stock solution (dilute 50 mg of lumogallion (Brunschwig A5060) into 250 mL); 5) Standard solution (1000 ppm dAl, dissolve 17.582 g aluminum potassium sulfate dodecahydrate (Merck 101047) into 1000 mL 0.5 M NaOH). Note that all pump tubes were rinsed for 20 min using 0.5 M NaOH solution after each digestion, and the reagent blank for dAl was determined continuously for 20 min for ensuring a stabilized signal.

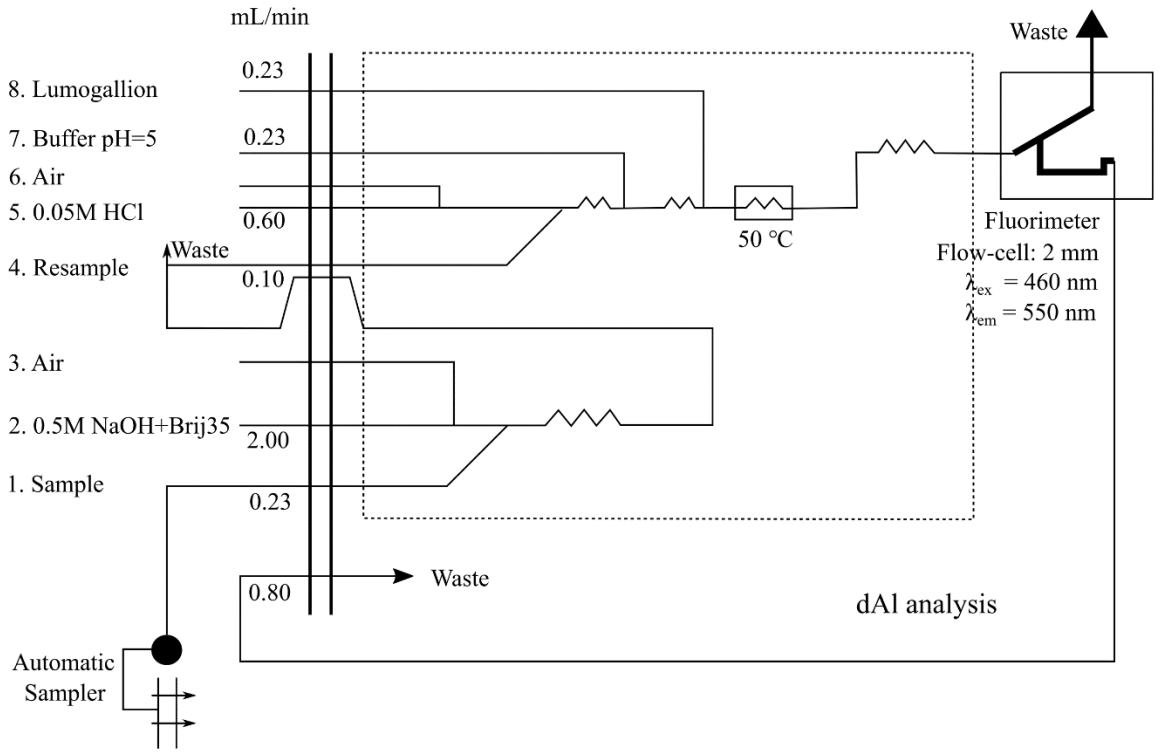

Figure 2.5. A schematic diagram shows the measurement of dAl by the automatic method. This system is connected to the reaction vessel through an automatic sampler for taking the samples continuously. The alkaline solution was neutralized and mixed with reagents (the system marked within dashed line), well mixed mixture was heated at 50 ℃ and then the dAl was determined by a spectrofluorometer.

2.3.3. Organic carbon (OC), total carbon (TC), inorganic carbon (IC), and total nitrogen (TN)

Freeze-dried sediments were homogenized and pulverized with an agate mortar and pestle. Approximately 10 mg sub-samples were thoroughly decarbonated using 1.0 M HCl. They were then subsequently dried overnight at 50 °C to evaporate HCl. The carbonate-free organic carbon (OC%), total carbon (TC%) and total nitrogen (TN%) were analyzed by flash combustion of precisely weighted sediments at 950 °C on a Thermo Scientific FLASH 2000 CHN at PACHIDERM, LEMAR (Brest, France). The IC content was calculated by TC content minus OC content. The R^2 of calibration curve for OC, TC and TN were 0.9999, 0.9998 and 0.9995, respectively.

2.3.4. Grain-size analysis

Grain-size distribution is a general characteristic of sediment. It is a widely used tool to classify and describe sedimentary environments (Blott and Pye, 2001). In this research, all the

grain size analysis were run triplicates using the Malvern Mastersizer 2000 grain size analyzer with a Hydro 2000S module. To remove the organic matter from the sediments and separate the small grains, several pretreatments were run before the analysis. The organic matter was removed by adding 30% H_2O_2 under room temperature. The addition of H_2O_2 was ceased until there was no reaction. The samples were then mixed by a Vortex mixer and put into an ultrasonic bath for 10 minutes. Before the grain size analysis, two drops of 2% Micro 90 detergent were added to the bath to clean the system. Two drops of a solution with dissolved calcite ('Calgon') were added during measurement as a disaggregate. The samples were then sonicated for 15 seconds, and the grain size distribution was determined using a Malvern Mastersizer 2000. The grain sizes of the sediments were measured between 0.02 μm to 2000 μm. The terminology (clay, silt, sand) of the sediment grain size descriptions follows Udden-Wentworth standards (Wentworth, 1922).

2.3.5. Relative clay mineral composition

To analyze clay mineralogy and the relative clay mineral (illite, kaolinite, chlorite and montmorillonite) contents, surface sediments obtained from various depositional environments were used. Clay minerals were identified by XRD using a Rigaku D-MAX 2500 X-ray diffractometer at the Qingdao Institute of Marine Geology, China Geological Survey. The bulk sediments were pretreated with 10% H_2O_2 and 15% acetic acid (CH_3COOH) to remove organic matter and inorganic carbonates, respectively. Then, the clay fractions (< 2 μM) were segregated from the bulk sediment solution based on conventional Stokes' settling velocity principles and centrifuged. Each sample was transmitted by moist smearing to slides and was kept for air-drying. XRD runs were then carried out three times following air-drying, ethylene–glycol solvation, and heating at 490 ◦C for 2 h. The identification of clay minerals was based primarily on the position of the (001) series of basal reflections on the three XRD diagrams. The ethylene glycolate XRD curves from different provinces were used to perform a qualitative analysis of clay minerals for comparison. The settings for XRD analysis were listed subsequently: voltage: 40KV/150 mA, scanning speed: 8°/min, sampling step: 0.024°. In addition, the chemical weathering index (CWI) and Illite crystallinity were calculated using the MacDiff software as described by (Warr, 2018).

2.3.6. Scanning electron microscopy coupled with energy dispersive spectrometer (SEM-EDS)

The observed siliceous organisms in the sediments were imaged using Scanning Electron Microscopy (SEM; FEI Quanta 200, and Hitachi TM4000). To chemically characterize the bSi and its associated authigenic aluminosilicate 'coating', the Scanning Electron Microscopy was coupled with an Energy Dispersive Spectrometer (SEM-EDS) analysis using FEI Quanta 200 and OXFORD X-MAX Silicon Drift Detector (detector size: 80 mm) at Ifremer-LCG (France). Typically, the bio-siliceous structures were handpicked under a stereomicroscope and mounted on an adhesive carbon tab (Leit) using a brush. The carbon tab was pasted on pin stubs and coated with gold (Cheize et al., 2019). The major elements were quantitatively determined under a high vacuum at 20 kV.

2.3.7. Microscopic observation

Microscopy observations were applied for determining the bSi types and abundances in sediments. The abundances (numbers per gram: 10^3 g^{-1} dry sediments) of different marine bSi organisms in samples A3, C4, C7, C12, and F2 were examined optically using an inverted microscope (Zeiss Axio Observer A1) at 10X magnification. The samples were selected based on their water depth and sediment type (A3, F2: silty-clay; C4, C7: sandy; C12: clay-silt). To prepare the samples for microscopic observation, ca. 5 to 10 mg of homogenized dry sediment was pretreated in 10 mL of 1.0 M HCl and 10 mL 10% H_2O_2 and heated at 60 °C for 2 h. The solution was subsequently discarded after centrifugation (4000 rpm, 5 min) and the residual sediment was rinsed three times using Milli-Q water (18.2 MΩ). The decarbonated sediments were homogenized in Milli-Q water (1 mL) and the samples were put on a glass microscope slide for optical observation. The abundance of individuals for different types of bSi (i.e., diatom frustules, radiolarian skeletons and siliceous sponge spicules) was counted and normalized as the number of individuals per gram of dry sediment (10^3 g^{-1}). In addition, all samples were observed under a microscope for determining the types of bSi and 14 samples (ST4, D226, Still Pond, R-64, Eq, MTB2, MC4-A, MC8-B, 3585CQ, 2714CQ, 2368G, F104, H555, A459) were selected as representative samples (representing different types of sediments of various marine environment).

2.3.8. Determination of pH

The pH of alkaline solutions (NaOH, Na_2CO_3) was determined using a Mettler Toledo-SG78-B pH meter. Before each measurement, the pH meter was calibrated at room temperature using three buffer solutions: pH 4.00, 6.86, 10.00. In order to know the effect of temperature on alkaline pH values, the pH values of the alkaline solutions were measured at both room temperature (~ 22 °C) and high temperature (> 70 °C).

2.3.9. Data analysis of Si/Al results

Each extraction of the continuous analysis procedure provides dSi and dAl concentrations through time at a one-second resolution (Figure S3.1), the unit of parameter t in the models (Eq. 2.1 – 2.3) was normalized into minutes (min). Determination of the $bSiO_2$% follows the procedure that assumes the presence of two discrete phases: (1) a linear phase indicating lSi dissolution and (2) a nonlinear phase indicating bSi and/or non-bSi dissolution (DeMaster, 1981; Koning et al., 2002). The $bSiO_2$% was calculated following the 4 models (Eq.2.1 = Model 1; Eq.2.2 and Eq. 2.3 = Model 2 and Model 3; Eq.2.3 = Model 4) described by Koning et al, (2002) using the Origin 2021b software.

Model 1 demonstrates the first-order dissolution of a single Si phase (Si_{extr}) as shown in Eq.1:

$$Si_{aq} = [Si_{extr}]_0\,(1 - e^{-kt}) + bt$$
$$Al_{aq} = \frac{1}{\beta_1}\,[Si_{extr}]_0\,(1 - e^{-kt}) + \frac{1}{\beta_{lin}}\,bt \qquad (2.1)$$

Here, Si_{aq} and Al_{aq} are the concentrations of silicic acid and aluminum in mg L^{-1}, in the reaction vessel at time t (min). $[Si_{extr}]_0$ is the initial extractable silica present in the vessel in mg L^{-1}, equivalent to the final concentration of Si_{aq} reached when all extractable silica (bSi and lSi) has dissolved, k is the reactivity constant (min^{-1}) and β_1 is the atomic ratio of Si and Al released during the dissolution of extractable silica fraction. b (mg L^{-1} min^{-1}) represents the constant dissolution rate of Si from clay minerals and β_{lin} is the Si/Al ratio in the lithogenic fraction.

Natural sediment samples may consist of several types of extractable bSi. For natural samples containing two Si_{extr} fractions ($Si_{extr}1 = ExtrSi_1$, $Si_{extr}2 = ExtrSi_2$; $n = 2$), the increases of the silicic acid concentration in the reaction vessel with time can be as the sum of two first-order dissolution processes (Model 2), using the same parameters as described in Eq.2.1. For natural samples containing three Si_{extr} fractions ($n = 3$), the increase in dSi concentration with time can be the sum of three first-order dissolution processes (described as Model 3). $[Si_{extr}]_{0,i}$ is the initial extractable silica present in the extractable silica fraction i, k_i is the reactivity constant and β_i is the Si/Al ratio for fraction i.

$$Si_{aq} = \sum_{i}^{n} [Si_{extr}]_{0,i}\,(1 - e^{-k_i t}) + bt$$
$$Al_{aq} = \sum_{i}^{n} \frac{1}{\beta_i}[Si_{extr}]_{0,i}\,(1 - e^{-k_i t}) + \frac{1}{\beta_{lin}}\,bt \qquad (2.2)$$

Model 4 demonstrates the reactive continuum dissolution of the infinite number of fractions (i) (Eq. 3) (Koning et al., 1997) and can be described as:

$$Si_{aq} = [Si_{extr}]_0 \left(1 - \left(\frac{\alpha}{\alpha + t}\right)^{v}\right) + bt$$

$$Al_{aq} = \frac{1}{\beta_1} [Si_{extr}]_0 \left(1 - \left(\frac{\alpha}{\alpha + t}\right)^{v}\right) + \frac{1}{\beta_{lin}} bt \quad (2.3)$$

Where the parameter α represents the average lifetime of the alkaline extractable components in sediment and v represents a non-dimensional parameter solely related to the shape of the distribution curve. Model 4 allows a continuum of reactivity of bSi and lSi and assumes one Si: Al ratio for all the bSi components, it is not justified by data fitting in this study. The highest number of bSi components justified by model fitting was model 2, in agreement with Barão et al. (2015) and Raimonet et al. (2015). The alkaline extractable Si (AlkExSi) may contain several non-linear fractions, based on the Si: Al ratio and reactivity constant (*k*). The origin of different extractable Si fractions (bSi, lSi) can be evaluated (Koning et al., 2002). The lSi fraction is normally characterized by low reactivity (Koning et al., 2002) and small Si:Al ratios (authigenic silicates: Si:Al < 2, Mackin (1989; Michalopoulos and Aller (1995); kaolinite: Si: Al = 1, illite: Si: Al = 2, montmorillonite, Si: Al < 5, Koning et al. (2002)), the bSi fraction is characterized by high reactivity (k > 0.1 min^{-1} and $\beta_i > \beta_{lin}$) and high Si: Al ratios (β_i > 5) (Koning et al., 2002; Barão et al., 2015). Moreover, chemically altered bSi structures were characterized by a nonlinear dissolution with low reactivity (k < 0.1 min^{-1}) and low Si: Al ratio (< 5) (Koning et al., 2002).

For the fitted results from the above-mentioned models, optimization was carried out by maximizing the likelihood statistic log(*L*) (Armstrong et al., 2002; Moriceau et al., 2009) as described as follows:

$$log(L) = -\frac{N}{2} log\left(\frac{\sum\left(log\left(\hat{C}_j\right) - log\left(C_j\right)\right)^2}{N}\right) \quad (2.4)$$

Where N is the total number of data points, C_j is the measured concentration (mg L^{-1}) for data point *j*. and the $\hat{C}_j$ is the corresponding model prediction. The difference in log(*L*) (Δ log(*L*)) between fits of different models to the same data gives the goodness of fit of one model compared to the other (Figure S1). As described in Moriceau et al. 2009, if the log(*L*) of one model is at least two points higher per added parameter than another, it is considered a better model (Hilborn and Mangel, 1997). In this study, the results from the fitted model were used for methodology comparison. A non-parametric Aligned Ranks Transformation (ART) Analysis of Variance (ANOVA) was performed using R. studio software to test for significant differences between methods.

3. Revisiting the biogenic silica burial flux determinations: A case study for the east China seas

Abstract

The Coastal and Continental Margin Zones (CCMZs) contribute to 40% of the total burial flux of biogenic silica (bSi) of the world ocean. However, the accurate determination of the bSi content ($bSiO_2$%) in marine sediments remains a challenge. The alkaline methods commonly used to quantitatively determine $bSiO_2$% can completely digest the amorphous silica of diatoms but are less effective at digesting radiolarians and sponge spicules. In addition, the lithogenic silica (lSi) found in sediments is partly digested during these alkaline extractions, which can bias the accuracy of the determined $bSiO_2$%. This is of importance in CCMZs where the lSi:bSi ratio is high. In this study, we examined sediments collected in the CCMZs of the east China seas, an environment of particular interest given the large amount of lSi deposited by the Yellow River and the Yangtze River. The results show that alkaline digestions using stronger solutions and pretreatment steps resulted in an overestimate of the $bSiO_2$% due to increased leaching of silica mainly from authigenic silicates and clays, whereas weak digestions underestimated the $bSiO_2$% owing to incomplete digestion of sponge spicules. We found that the use of the Si/Al method, which corrects for the lSi fraction in marine sediments, accurately determines the $bSiO_2$% in the sediments of east China seas CCMZs. To emphasize the influence of these methodological differences, we revised the bSi burial flux in the east China seas and provide a new estimate of 253 (± 286) Gmol-SiO_2 yr^{-1}, which is one-third of the previous estimates. We discuss the potential contribution from radiolarians and sponges, and we propose a new general protocol for the determination of bSi in sediments that minimizes the methodological bias in bSi determination.

3.1. Introduction

Coastal and Continental Margin Zones (CCMZs) are distinct settings for the interrogation of global marine biogeochemical cycling of silica (Si), climate change and marine ecological processes (Jeandel and Oelkers, 2015; Jeandel, 2016; Tréguer et al., 2018; Rahman et al., 2019). The CCMZs represent approximately 10% of the global marine surface area (3.61×10^8 km^2) (Costello et al., 2010), and account for 40% of the total bSi burial (~9.2 Tmol-Si yr^{-1}) in the global ocean (DeMaster, 2019; Tréguer et al., 2021). This estimate was based solely on the burial of diatom bSi. However, marine Si is also removed through reverse weathering in major tropical and subtropical deltas (Rahman et al., 2016, 2017), the burial of siliceous sponges spicules predominantly on the continental shelf and margins (DeMaster, 2019; Maldonado et al., 2019), and the burial of radiolarian tests (Maldonado et al., 2019). Recent work estimated that if all of these processes are taken into account, the burial flux of Si that occurs mainly within the CCMZs, removes 5.0 to 10.1 Tmol-Si yr^{-1} (DeMaster, 2019; Tréguer et al., 2021), which is equivalent to roughly one to two-thirds of the global Si output flux (15.6 Tmol-Si yr^{-1}) from the marine environment (DeMaster, 2019; Tréguer et al., 2021).

The calculation of the marine Si budget at the global or local level is dependent on the precision and accuracy of the bSi measurements (DeMaster, 1991). Within the CCMZs, the combination of lSi with bSi decreases the reactive surface area of biogenic opal and lowers its solubility (Dixit and Van Cappellen, 2003; Varkouhi and Wells, 2020; Varkouhi et al., 2020a), which enhances the bSi burial efficiency. However, high precipitation rates of terrestrial lSi dilutes the bSi and results in opal-depleted coastal sediment (DeMaster, 2002; Wu et al., 2017; Wu and Liu, 2020). Therefore, accurate determination of the bSi content ($bSiO_2$%) in the CCMZs sediment is particularly challenging owing to its characteristically low $bSiO_2$%, high lithogenic silica (lSi; clay mineral, authigenic aluminosilicate, quartz) content (DeMaster, 1991), and complexity of bSi types (e.g. diatoms, phytolith, radiolarians, sponge spicules; Figure 3.1A) (DeMaster, 1991; Maldonado et al., 2019). Among several different techniques (e.g., X-ray Diffraction (Goldberg, 1958; Eisma and van der Gaast, 1971), point counts of siliceous microfossil (Pudsey, 1993; Varkouhi et al., 2020a), infrared analysis (Frohlich, 1989), normative calculation technique (Leinen, 1977), wet chemical method (DeMaster, 1981; Muller and Schneider, 1993; Mortlock and Froelich, 1989)), wet chemical method is the most commonly used method for determining the $bSiO_2$% in marine sediments (Conley, 1998). Considering the complex sediment composition of CCMZs sediments, a mild alkaline leach (0.1 M Na_2CO_3) is recommended to minimize the interference of lSi in bSi determination when

using the wet chemical method (DeMaster, 1981). However, a mild alkaline leach underestimates the quantity of bSi due to an incomplete extraction of more resistant bSi (Figure 3.1A), such as radiolarians (Mortlock and Froelich, 1989; Müller and Schneider, 1993) and siliceous sponge spicules (Maldonado et al., 2019a). Nonetheless, complete digestion of resistant bSi using a strong alkaline solution can introduce additional bias due to the inevitable attack on lSi. To accurately determine $bSiO_2$% in sediment from different marine environments, various kinds of wet alkaline methods with different digestion conditions (i.e., alkaline solution, sample-to-solution ratio, extraction temperature, duration of extraction and pre-treatment of sediment by HCl and H_2O_2 before alkaline digestion) have been proposed and applied in the literature (DeMaster, 1981; Mortlock and Froelich, 1989; Müller and Schneider, 1993; Kamatani and Oku, 2000; Conley and Schelske, 2001; Koning et al., 2002; Liu et al., 2002; Olivarez Lyle and Lyle, 2002). These methods were grouped into two different types: (1) Si/time alkaline digestion and (2) Si/Al alkaline digestion (Swann, 2010). The Si/time method (Figure 3.1B), which is the conventional wet alkaline method, requires the measurement of alkaline extracted Si concentration and corrects the lSi fraction based on the assumption of the difference in dissolution kinetics between bSi (non-linear dissolution) and lSi (linear dissolution) (DeMaster, 1981). The Si/Al alkaline digestion method (Figure 3.1B) requires the measurement of alkaline extracted Si and Al concentrations, and corrects the lSi fraction based on the assumption that the Si:Al ratios of lSi is low (< 5, Figure 3.1A) and the extracted Al is mainly lSi origin (Kamatani and Oku, 2000; Koning et al., 2002). Previous studies found methodological differences in the $bSiO_2$% between Si/time and Si/Al methods in both lacustrine (Swann, 2010) and marine sediments (Barão et al., 2015). It has been noted that major biases in the $bSiO_2$% can be generated among different wet alkaline methods (DeMaster, 1991; Gehlen and van Raaphorst, 1993; Schlüter and Rickert, 1998; Kamatani and Oku, 2000; Barão et al., 2015), influencing the estimation of the bSi burial flux, especially in the opal-depleted ($bSiO_2$-poor) sediment of the CCMZs (DeMaster, 1991, 2002; Tréguer et al., 2021).

The east China seas, which consist of the Bohai Sea (BH), the Yellow Sea (YS), and the East China Sea (ECS), is one of the largest CCMZs in the Northwest Pacific Ocean. The east China seas are characterized by high sedimentation rates (Qiao et al., 2017), low $bSiO_2$% (< 3%) and high lithogenic material content (> 70%wt) (Liu et al., 2002; Wu et al., 2017; Wu and Liu, 2020). Previous studies demonstrated that the burial of bSi in the east China seas is 924 (± 693) Gmol-SiO_2 yr^{-1} (Liu et al., 2016; Wu et al., 2017; Wu and Liu, 2020a), accounting for ~5% of the bSi burial in the global ocean. These estimations were based on the $bSiO_2$% determined using several alkaline digestion techniques, such as using different concentrations of alkaline solution

(0.1 M Na_2CO_3, 2% Na_2CO_3, 2.0 M Na_2CO_3), duration of the alkaline digestion (5 h, 8 h) and pre-treatment process (with HCl and H_2O_2 prior to alkaline extraction) that may underestimate or overestimate the bSi content due to the incomplete digestion of bSi or the interference of lSi in bSi determination (Kamatani and Oku, 2000; Barão et al., 2015) and leaching of authigenic silicates activated by an acid treatment (Michalopoulos and Aller, 2004; Rahman et al., 2016; Pickering et al., 2020). Such an under- or overestimate of the bSi content will influence the magnitude of the burial flux of bSi determined for the CCMZs where sediment load is high and the bSi content is low. In addition, diatoms, radiolarians (Liu et al., 2017; Qu et al., 2020a, 2020b), sponge spicules (Chou et al., 2012) and living siliceous sponges (Zhang et al., 2003) were observed in the sediment of the east China seas. However, the influence of their presence on the determination of bSi content and consequent role in marine Si cycling for this region, is still not defined. The radiolarians and siliceous sponge spicules are more resistant to alkaline attacks than diatoms (DeMaster, 1981; Muller and Schneider, 1993), thus the types of bSi need to be considered when characterizing the bSi content of sediments (DeMaster, 1991).

This study aims to provide an accurate determination of the burial flux of the east China seas CCMZs by conducting a thorough evaluation of the potential methodological biases influencing the determination of bSi. To evaluate these methodological biases, multiple samples of characteristically diverse marine sediment from the east China seas were measured for $bSiO_2$% using different alkaline solution concentrations (0.1 M, 0.2 M, 2.0 M Na_2CO_3), with and without pre-treatment. In addition, the types of marine bio-siliceous structures (diatoms, radiolarian tests, and sponge spicules) and their abundances in the different sediment samples were quantified to select an appropriate wet alkaline method. Further, the $bSiO_2$% determined using the Si/time method (20 h digestion in 0.1 M Na_2CO_3) and the Si/Al method (1 h digestion in 0.5 M NaOH) were compared for an accurate evaluation of the alkaline extracted Si (bSi and lSi) from sediments of the CCMZs. The detailed evaluation of these methodological biases resulted in the production of a revised evaluation of the burial flux of biogenic silica for the east China seas CCMZ and a discussion on the implementation of a standardized method for the determination of $bSiO_2$% in similar depositional environments.

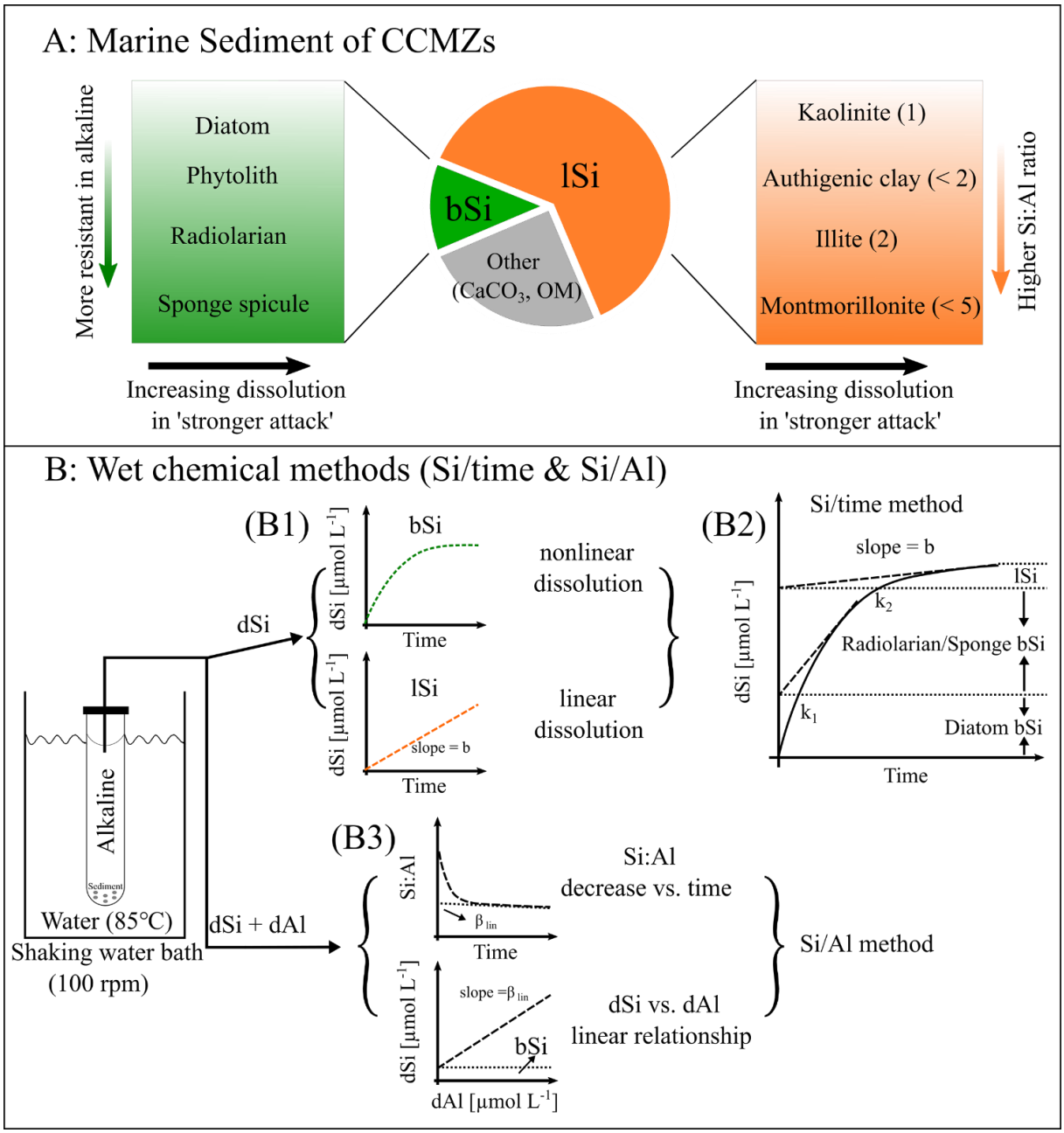

Figure 3.1. The schematic diagram shows the: (A) components in the sediment of CCMZs and (B) Wet chemical methods (B1: Si/time method; B2: Si/Al method). (A) shows the types of bSi (dissolution capability : diatom < phytolith < radiolarian < sponge spicule (Mortlock and Froelich, 1989; Müller and Schneider, 1993; Meunier et al., 2014) and types of lSi (Si:Al ratio: authigenic clay: Si:Al < 2 (Mackin, 1989; Michalopoulos and Aller, 1995); kaolinite: Si:Al = 1, illite: Si:Al = 2, montmorillonite: Si:Al < 5 (Koning et al. (2002)) in marine sediment. The 'stronger attack' represents high pH, longer extraction time and sample pre-treatment with acid (e.g., HCl) and/or oxidizing agents (e.g., H_2O_2). (B) shows the alkaline digestion (85°C) of bSi and correction of lSi using the Si/time method (B1) modified from DeMaster (1981), the Si/time method (B2) modified from Conley and Schelske (2001) and the Si/Al method (B3) modified

from Kamatani and Oku (2000). The Si/time method (B1 and B2) assumes the bSi dissolves non-linearly through time whereas the lSi dissolves linearly (the slope equals to dissolution rate '*b*') through time, the different types of bSi (diatom, radiolarian and sponge spicules) can be quantified based on their dissolution rate (B2: k_1, and k_2). The Si/Al alkaline digestion method (B3) assumes that the ratio of alkaline extractable Si vs. Al is constant, and the alkaline extractable Al is mainly lSi origin, the Si:Al ratio of bSi is higher (> 5) than lSi (< 5) (Koning et al.,2002). The Si: Al vs. time plot shows a decrease of Si:Al ratios to constant value after a complete digestion of bSi.

3.2. Materials and methods

3.2.1. Study area and sample locations

The east China seas (Figure 3.2) consist of the BH (surface area: 7.73×10^4 km^2), the YS (surface area: 38×10^4 km^2), and the ECS (surface area: 77×10^4 km^2) (Qiao et al., 2017). The semi-enclosed BH and YS are shallow water bodies with an average water depth of 18 m (maximum 85 m) and 44 m (maximum 140 m) respectively. About 21 large rivers (length of mainstream > 100 km) deliver 782.2×10^9 kg yr^{-1} of sediment to the BH, with more than 90% delivered by the Yellow River. Roughly 30 rivers discharge 13.0×10^9 kg yr^{-1} of sediment into the YS (Qiao et al., 2017). However, up to 90% of its total sediment burial flux (414.6×10^9 kg yr^{-1}) is transported from the BH and 5.7% is eroded sediment from the old Yellow River (Qiao et al., 2017). The ECS consists of a broad continental shelf and the Okinawa Trough, with an average water depth of 349 m (maximum 2700 m). About 18 rivers deliver 490.5×10^9 kg yr^{-1} of sediment into the ECS, of which approximately 80% is delivered from the Yangtze River (Qiao et al., 2017). The $bSiO_2$% in surface sediments of the BH, YS and ECS were 0.92 ± 0.24% (Liu et al., 2002), 2.20 ± 0.79% (Wu et al., 2017) and 1.97 ± 0.53% (Wu and Liu, 2020), respectively, and are considered to be relatively low values (< 3% is considered a threshold value for bSi concentrations) and requires an accurate determination (Koning et al., 2002; Liu et al., 2002; DeMaster, 2019; Tréguer et al., 2021).

Field observations were conducted in the east China seas from 2008 to 2013. The sampling sites are shown in Figure 3.2. At each sampling site, surface sediment samples (0 − 2 cm) were collected using a stainless-steel box sampler and subsequently packed in sealed plastic bags at -20 ℃ on board. Frozen samples were then freeze-dried in the laboratory and stored at room temperature (~20 ℃) until analysis. Two sediment samples for interlaboratory comparison (sample code: Still Pond, R-64) were also measured using the Si/time (0.1 M Na_2CO_3, 20 h digestion) and the Si/Al (0.5 M NaOH, 1 h digestion) alkaline digestion method. The location

of these sampled sediments and their descriptions are given in Conley (1998).

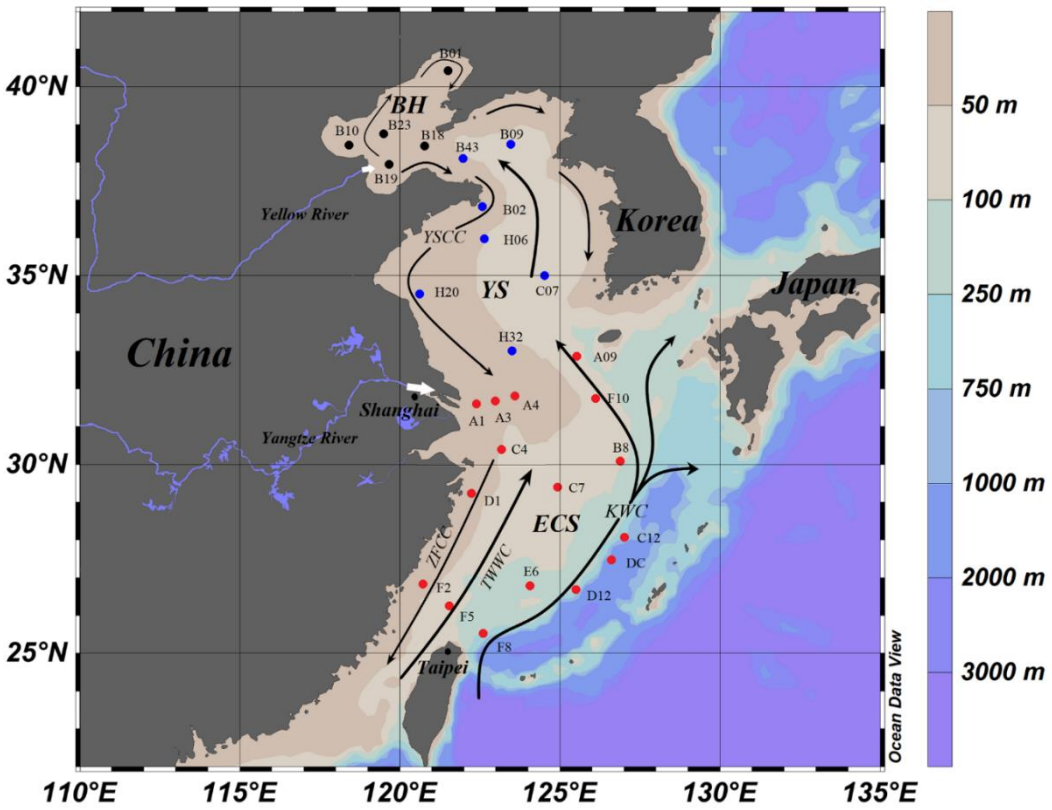

Figure 3.2. Map of the study area indicating the sampling stations. The location of samples is grouped in different colors at the Bohai Sea (black dots ●), Yellow Sea (blue dots ●), and the East China Sea (red dots ●). The surface sediment samples (0 − 2 cm) were obtained during several research cruises during 2008-2013. The distributions of currents are based on Liu et al, (2007) and Qin et al, (1996). White arrows represent the Yellow River and Yangtze River discharge. (YSCC: Yellow Sea Coastal Current; ZFCC: Zhejiang Fujian Coastal Current; TWWC: Taiwan Warm Current; KWC: Kuroshio Warm Current). The map is created using Ocean Data View (ODV) software (Schlitzer, Reiner, Ocean Data View, https://odv.awi.de, 2021).

3.2.2. Analytical methods

The content of bSi found in the sediments in this study is expressed as $bSiO_2$% (molar mass of $bSiO_2$: 60 g mol^{-1}) to avoid potential errors associated with the difference in bond water content of different types of bSi and/or ages of siliceous organisms. Two wet chemical methods were used to quantify the $bSiO_2$%: the Si/time method (DeMaster, 1981; Conley and Schelske, 1993, 2001; Liu et al., 2002) and the Si/Al method (Koning et al., 2002; Barão et al., 2014, 2015).

In this study, the $bSiO_2$% was determined following the calculation method described by Liu et al, (2002) where sediments undergo an 8 h digestion. In addition, the $bSiO_2$% was also calculated following the method described in DeMaster (1981), Liu et al, (2002) and Conley and Schelske, (1993, 2001) when sediment was digested in a 0.1 M Na_2CO_3 solution for 20 h. The method described in Conley and Schelske (1993, 2001) was applied for quantifying the diatom bSi, radiolarian and/or sponge bSi (Figure 3.1B). Moreover, the $bSiO_2$% analyzed according to the method described by Mortlock and Froelich (1989) was also performed.

To obtain high-resolution photos and to semi-quantify the elemental composition of bSi structures, a scanning microscope measurement was applied (see chapter 2). The types of bSi and abundances were determined using an inverted microscope. The evaluation of the bSi content was performed following the method described in chapter 2.

3.2.3. Burial flux of $bSiO_2$ in the CCMZs of east China seas

The burial flux (F_b) of $bSiO_2$ in sediment can be expressed as follows (Ingall and Jahnke, 1994):

$$F_b = C * w \tag{3.1}$$

Where C (mol g^{-1}) is the concentration of $bSiO_2$%, and is calculated from the $bSiO_2$% determined in dry sediment (in g of SiO_2 g^{-1}), and converted to mol g^{-1} by dividing it by the molecular weight of SiO_2 (6×10^{-3} g mol^{-1}), w (g cm^{-2} yr^{-1}) is the mass accumulation rate. The w used in this study is averaged sediment accumulation rate at BH (0.50 g cm^{-2} yr^{-1}), YS (0.37 g cm^{-2} yr^{-1}) and ECS (0.26 g cm^{-2} yr^{-1}) reported previously (Qiao et al., 2017). Note, a primary objective of this study was to determine the potential influence that methodological biases can have on the bSi burial flux. Therefore, an average sedimentation rate of the study area was applied. The F_b were then multiplied by the respective area of the BH, the YS and the ECS to calculate the burial flux of bSi of each region and the east China seas.

3.3. Results

3.3.1. Biogenic silica types and their abundances

Table 3.1 shows the abundance of the three types of marine bSi in sediment obtained from the east China seas (see Figure 3.2 for sample sites). All of the samples used in this study were examined under a microscope to determine the relative composition of different bSi types. Among the three major types of marine bSi (i.e., diatoms, radiolarians, sponge spicules), diatoms and sponge spicules were observed in the sediments of BH, YS, and ECS. Radiolarian

skeletons were only observed in the sediment of YS and ECS. The abundance of sponge spicules and their size (length) and the number of radiolarian tests varied between samples from the BH, the YS and the ECS. Microscopic observations indicated that radiolarian skeletons were rare in the sediment of the YS, whereas more radiolarian tests were found in the sediment samples of ECS. Although sponge spicules were found in all sediment samples (Table 3.1), the size of sponge spicules in the sediment of the BH (length: 10 − 40 μm), and YS (length: 50 − 300 μm) are smaller than that of the ECS (100 − 500 μm). The abundance of sponge spicules in the sediment of BH and YS is less than what was observed for diatoms. In contrast, the abundance of sponge spicules was greater than diatoms in ECS sediment samples (Table 3.1).

We found that radiolarians and sponge spicules were more abundant in the sediment of the ECS than the BH and the YS from the microscopic observations. Therefore, five samples (C4, C7, C12, F2, and A3) were selected from the ECS for determining the abundance of different types of bSi. The radiolarians and sponge spicules are more abundant in the offshore sediment (C7, C12) than in nearshore sediment (A3, F2, C4). The abundance of sponge spicules is greater than that of diatom tests in the 5 samples (C4, C7, C12, F2, A3) from ECS, especially in sample C12 where the abundance of sponge spicules (231.7×10^3 g^{-1}) is ca. 15 times greater than that of diatoms (14.8×10^3 g^{-1}). The abundance of diatoms is similar for the BH, YS and ECS, which is in agreement with previous research (Chen et al., 2014; Wang et al., 2016; Li et al., 2018, Li et al., 2020). However, radiolarians and sponge spicules are more abundant in the ECS, especially in the sediment of the outer shelf of the ECS.

3.3.2. Wet alkaline digestions

3.3.2.1. Evaluation of reference samples

Two interlaboratory comparison sediment samples (Still Pond, R-64) were measured using Si/time (Figure S3.2) and Si/Al (Figure S3.3) alkaline digestion to assess the accuracy of the biogenic silica measurement. Similar results were obtained to previous works (Table 3.2), but also showed dependence on the extraction method. The $bSiO_2$% applying a 0.5 M NaOH digestion (Still Pond: 2.74%; R-64: 7.23%) and a 0.1 M Na_2CO_3 digestion (Still Pond: 2.00 ± 0.05%; R-64: 5.50 ± 0.10%) are within the acceptable range of $bSiO_2$% values (Still Pond: 2.82 ± 1.17%; R-64: 6.49 ± 2.09%) reported in Conley (1998) (Table 3.2). The wide range of data presented in Conley (1998) is likely due to the influence of methodological differences applied (alkaline solution concentration and/or chemical pre-treatment), the act of crushing the sediment prior to the alkaline attack, and the existence of sponge spicules in Still Pond and R-64 which was not previously reported in Conley (1998), because siliceous sponge spicules were

observed in both reference samples. The coefficient of variability (i.e., relative standard deviation) for five parallel extractions was < 3%, indicating good reproducibility.

3.3.2.2. Comparation of the extraction methods

The results presented here compare the analysis of $bSiO_2$% determined using different Si/time methods. Triplicate digestion of the pre-treated (P) and non-pretreated (NP) sediment (Figure 3.3) was performed to determine the influence of the pre-treatment process on bSi determination. As expected, stronger solutions, and pretreatment of sediment led to greater release of silica (Table 3.3, Figure 3.3 and Figure 3.4). According to the different alkaline digestion and microscopic observation, this is mainly due to the extraction of lSi rather than bSi (e.g., sponge spicules). The pre-treatment of sediment using HCl (1.0 M) and H_2O_2 (10%) as described by Mortlock and Froelich (1989) will activate the authigenic silicate phases and the clay minerals, thus cause an overestimation of the $bSiO_2$%.

Figure 3.3 shows a continuous increase of the SiO_2% through time. The alkaline extracted silica (AlkExSi) content is higher for the pretreated sediments than the non-pretreated sediments. Similar result was obtained for the total amount of alkaline extracted silica (TAlkExSi) after the 8 h digestion (0.1 M Na_2CO_3, P > 0.1 M Na_2CO_3, NP; 0.2 M Na_2CO_3, P > 0.2 M Na_2CO_3, NP; 2.0 M Na_2CO_3, P > 2.0 M Na_2CO_3, NP; Figure 3.4). As shown in Figure S4 and Figure S5, most of SiO_2 was leached from sediments during the first 4 h ($AlkExSi_{(1-4)}$) and less SiO_2 was extracted during the 5 h to 8 h digestion ($AlkExSi_{(5-8)}$). The quantity of $AlkExSi_{(1-4)}$ and $AlkExSi_{(5-8)}$ correspond to 66% − 86% and 14% − 34% of total amount of silica (TAlkExSi; $TAlkExSi = AlkExSi_{(1-4)} + AlkExSi_{(5-8)}$) extracted during the 8 h alkaline digestion (Figure S5). In addition, the $AlkExSi_{(1-4)}$ leached from the pre-treated sediment was higher than from the non-pretreated sediment (Figure S4 and Figure S5), and the amount of the $AlkExSi_{(5-8)}$ was low (< 0.2%SiO_2) and showed small variations when digested under different alkaline solutions (0.1 M, 0.2 M and 2.0 M Na_2CO_3, P vs. NP). Moreover, more silica ($AlkExSi_{(1-4)}$ and $AlkExSi_{(5-8)}$) can be leached in stronger alkaline, but the proportion of $AlkExSi_{(1-4)}$ and $AlkExSi_{(5-8)}$ to TAlkExSi does not change much (Figure S3.5).

Table 3.1 Different types of marine bSi (diatoms, radiolarians, sponge spicules) and their abundances (10^3 g^{-1} dry sediments) in the surface sediment of east China seas. "+", "++", "+++": observation of bSi from low to high abundance; "–": not observed; a: observation of low abundance of small sponge spicules (length: 10 − 40 μm) of BH; b: observation of low abundance of sponge spicules with intermediate size (length: 50 − 300 μm) of YS; c: observation of high abundance of sponge spicules (length: 100 − 500 μm). Note that phytolith and siliceous dinoflagellate are not counted in this study.

Region		Biogenic silica types/abundance			References
		Diatom	Radiolarians	Sponge spicules	
Bohai Sea (n=5)		++	–	+[a]	This study
		13.0[1]	no data	no data	Other studies
Yellow Sea (n=7)		++	–	+[b]	This study
		17.0[2]	~0[5]	no data	Other studies
East China Sea (n=16)		++	+	+++[c]	This study
		11.3-19.9[3,4]	0.02-7.3[5,6]	no data	Other studies
	A3	3.8	0	5.2	This study
	F2	6.1	0.4	17.6	This study
	C4	2.2	0	3.3	This study
	C7	5.2	0.1	8.4	This study
	C12	14.8	12.4	231.7	This study

Note: the numbers in the table are references. 1: Li et al, 2020; 2: Wang et al, 2016; 3: Chen et al, 2014; 4: Li et al, 2018; 5: Qu et al, 2020; 6: Liu et al, 2017; n represents the number of samples used for evaluating the types of bSi of each region.

Table 3.2 The $bSiO_2$% of interlaboratory comparison sediment samples (Still Pond and R-64). The location of the two samples is described in Conley (1998). Note that sponge spicules were observed in the two sediment samples. NA represents not available.

Still Pond		R-64		Alkaline	Digestion time (h)	References
$bSiO_2$	std	$bSiO_2$	std			
2.00	0.05	5.50	0.10	0.1 M Na_2CO_3[a]	5	This study
2.74	-	7.23	-	0.5 M NaOH[a]	1	This study
1.84	-	7.80	-	0.5 M NaOH[a]	0.5	Barão et al. (2015)
2.68	0.06	-	-	2% Na_2CO_3[b]	8	Wu et al. (2015)
3.88	0.19	7.50	0.13	2.0 M Na_2CO_3[b]	8	Liu et al. (2002)
2.82	1.17	6.49	2.09	Na_2CO_3/NaOH	NA	Conley (1998)

a: no pre-treatment before the wet alkaline digestion; b: pre-treatment of sediment using HCl (1.0 M) and H_2O_2 (10%) before the alkaline digestion.

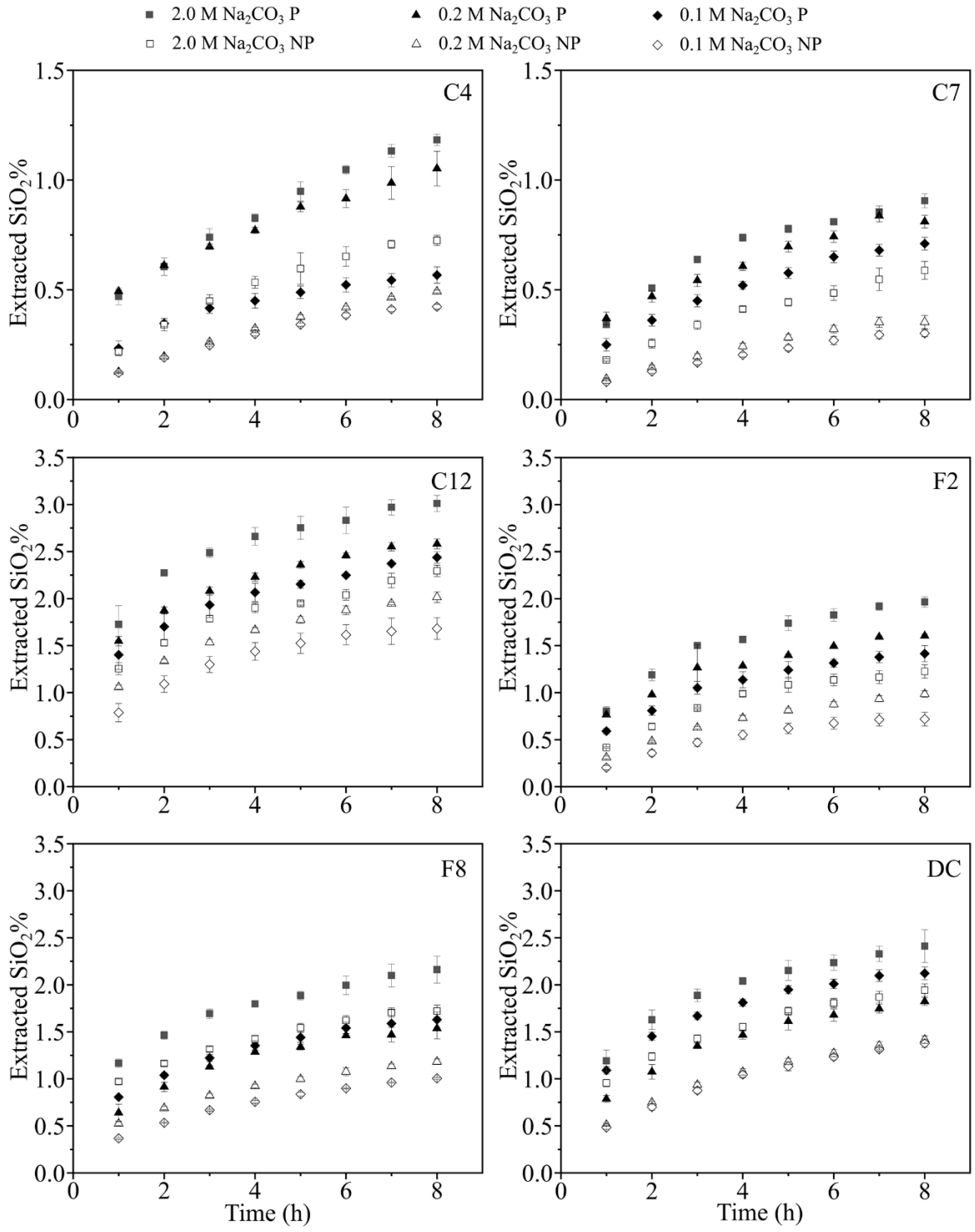

Figure 3.3. Conventional wet alkaline digestion using Na_2CO_3 (0.1 M, 0.2 M and 2.0 M; P vs. NP) solution. A subsample was removed at 1 each 1 h digestion with a total extraction of 8 h. The alkaline extracted silica content (SiO_2%) was normalized into the dry weight of the sediment. P represents pretreatment of sediment using HCl (1.0 M) and H_2O_2 (10%) before digestion; NP represents no pretreatment before alkaline digestion. The error bars were averaged from triplicate digestions. The locations of samples C4, C7, C12, F2, F8, and DC are shown in Figure 3.1.

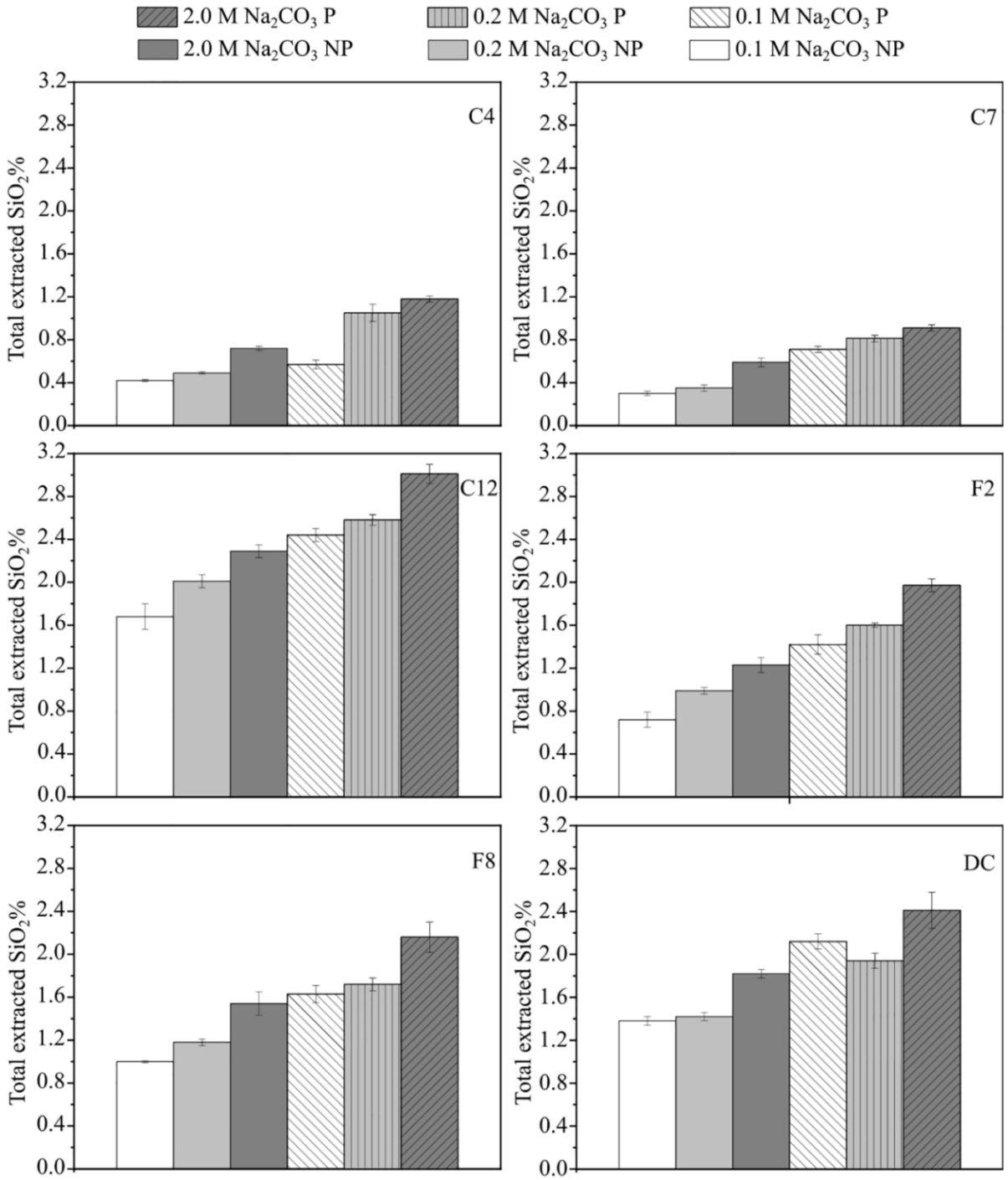

Figure 3.4. The total alkaline extracted silica content (SiO_2%) of sample C4, C7, C12, F2, F8, DC using 0.1 M, 0.2 M, 2.0 M Na_2CO_3 solution (P vs. NP). The results presented are the SiO_2% extracted after 8 h. More SiO_2% was extracted in a high concentration of the alkaline solution and after the pre-treatment process.

Table 3.3 and Figure S3.6 showed the $bSiO_2$% calculated from the 8 h digestion experiment. Through ART ANOVA analysis, a significant difference between different alkaline digestions was identified (Table S3.1). ART ANOVA analysis showed the increase of $bSiO_2$% between 0.1

M Na_2CO_3 (P vs. NP), 0.2 M Na_2CO_3 (P vs. NP) and 2.0 M Na_2CO_3 (P vs. NP) were significant ($p < 0.0001$; Noymer (2008)) (Table S3.1). The yield, expressed as $bSiO_2$%, between the P and the NP alkaline digestions are: 0.1 M Na_2CO_3 (P) = 194% 0.1 M Na_2CO_3 (NP), 0.2 M Na_2CO_3 (P) = 226% 0.2 M Na_2CO_3 (NP) and 2.0 M Na_2CO_3 (P) = 185% 2.0 M Na_2CO_3 (NP) in average (calculated from Table 3.3). Besides the pre-treatment process, a higher concentration of Na_2CO_3 can extract more silica significantly ($p < 0.0001$) than a lower concentration of Na_2CO_3 (C7, F2, F8 and DC; Figure S3.6), except for the $bSiO_2$% determined using a 0.2 M Na_2CO_3 (P) and the 2.0 M Na_2CO_3 (P) digestion ($p = 0.0726$). For the non-pretreated (NP) digestion experiment, the average $bSiO_2$% extracted using 2.0 M Na_2CO_3 solution is 49% and 69% higher than the 0.2 M Na_2CO_3 and 0.1 M Na_2CO_3 digestion, respectively. However, the $bSiO_2$% of sample C7 and C12 was approximately the same when the sample was digested using different concentrations of Na_2CO_3 (0.1, 0.2, 2.0 M), and the $bSiO_2$% of sample C4, F2, F8, and DC was higher when using higher concentration of Na_2CO_3 solution (Figure S3.6). Compared to the alkaline concentration, the pretreatment process has a more important influence on bSi determination. The $bSiO_2$% determined following the single-step alkaline digestion method proposed for abyssal deposits (Mortlock and Froelich, 1989) generated much higher $bSiO_2$% values ($p < 0.0001$) than all other digestions. Moreover, the $bSiO_2$% determined using 0.1 M Na_2CO_3 (NP; DeMaster, 1981) was not significantly different ($p = 0.0726$) compared to the $bSiO_2$% determined using 0.5 M NaOH (NP; Koning et al., 2002) (Table S3.1). The $bSiO_2$% determined by 2.0 M Na_2CO_3 (P) is about 2.6 times of the $bSiO_2$% determined by 0.1 M Na_2CO_3 (NP). The average $bSiO_2$% of sample C4, C7, C12, F2, F8 and DC determined using different methods (0.1 M, 0.2 M, 2.0 M Na_2CO_3, P vs. NP; Table 3.3) were 0.49 ± 0.25%, 0.40 ± 0.23%, 1.82 ± 0.56%, 1.00 ± 0.44%, 1.13 ± 0.49% and 1.34 ± 0.57% respectively, showed a large variation (31 − 57%) of the standard deviation. The proportion of standard deviation to the averaged $bSiO_2$% was larger for low $bSiO_2$% samples (C4: 51%, C7: 57%) than other samples. After the alkaline digestions (2.0 M Na_2CO_3, P), microscopic observations (10X; Zeiss Axio Observer A1) showed complete digestion of diatoms and radiolarians, whereas sponge spicules remain present.

Table 3.3 The $bSiO_2$% was determined using 0.1 M, 0.2 M and 2.0 M Na_2CO_3 (P vs. NP). The standard deviations were based on triplicate digestion. Detailed information on the digestion conditions (S/L, temperature, concentration of alkaline solution) and pretreatment process was described in section 3 (i.e., Materials and methods). The averaged $bSiO_2$% of C4 (0.49 ± 0.25%), C7 (0.40 ± 0.23%), C12 (1.82 ± 0.56%), F2 (1.00 ± 0.44%), F8 (1.13 ± 0.49%), DC (1.34 ± 0.57%) determined using different concentrations of alkaline solution (0.1 M, 0.2 M, 2.0 M Na_2CO_3, P vs. NP), showed large variation of standard deviation (30 − 60%), which was also reported previously in Conley (1998). ART ANOVA analysis showed a significant difference ($p < 0.0001$) of the $bSiO_2$% determined using different concentrations of Na_2CO_3 (P and NP). MF 1989 represents the $bSiO_2$% determined following the method described by Mortlock and Froelich (1989), this method (no mineral correction) is presented for comparing with the 2.0 M Na_2CO_3 digestion that applied a mineral correction.

Sample	0.1 M Na_2CO_3				0.2 M Na_2CO_3				2.0 M Na_2CO_3				2.0 M Na_2CO_3 MF 1989	
	NP		P		NP		P		NP		P		P	
	$bSiO_2$	std	$bSiO_2$	std	$bSiO_2$	std	$bSiO_2$	std	$bSiO_2$	std	$bSiO_2$	std	$bSiO_2$	std
C4	0.27	0.02	0.39	0.03	0.21	0.01	0.51	0.18	0.44	0.13	0.65	0.09	0.95	0.04
C7	0.17	0.03	0.47	0.03	0.14	0.05	0.56	0.02	0.18	0.03	0.52	0.10	0.78	0.02
C12	1.41	0.09	1.40	0.16	1.46	0.03	2.10	0.07	1.28	0.22	2.31	0.34	2.75	0.12
F2	0.55	0.04	0.72	0.13	0.55	0.03	1.18	0.07	0.86	0.05	1.42	0.23	1.74	0.08
F8	0.41	0.01	0.79	0.08	0.76	0.10	1.33	0.03	1.22	0.27	1.50	0.10	1.89	0.05
DC	0.80	0.04	1.35	0.07	0.84	0.04	1.39	0.07	1.24	0.34	1.71	0.29	2.15	0.11
Ave.	0.56	0.42	0.90	0.49	0.66	0.45	1.17	0.56	0.84	0.46	1.35	0.67	1.72	0.71

Table 3.4 The $bSiO_2$% in sediments of the east China seas (BH, YS, ECS) was determined using the Si/time alkaline digestion method (0.1 M Na_2CO_3; NP). The locations of the samples are shown in Figure 3.1. The different types of bSi determined (diatom, sponge and total $bSiO_2$) are specified according to the digestion time or method used. The "n" represents the total amount of samples used for bSi determination. ART ANOVA analysis showed a significant difference ($p < 0.0001$) between the $bSiO_2$% calculated at 5 h intervals (DeMaster, 1981; Diatom $bSiO_2$, Conley and Schelske, (2001)), 8 h intervals (Liu et al., 2002) and 20 h intervals (Conley and Schelske, 2001).

Region	Method	DeMaster (1981)		Conley and Schelske (2001)						Liu et al, (2002)	
		Total $bSiO_2$		Diatom $bSiO_2$		Sponge $bSiO_2$		Total $bSiO_2$		Total $bSiO_2$	
	digestion time (h)	5		5		20		20		8	
	Station	$bSiO_2$	std	$bSiO_2$	std	$bSiO_2$	std	$bSiO_2$	std	$bSiO_2$	std
Bohai Sea (n=5)	B01	0.22	0.02	0.25	0.02	0.27	0.01	0.52	0.01	0.43	0.01
	B10	0.24	0.02	0.27	0.03	0.27	0.01	0.54	0.03	0.43	0.04
	B19	0.25	0.005	0.28	0.02	0.26	0.02	0.54	0.03	0.42	0.02
	B23	0.37	0.01	0.42	0.01	0.39	0.01	0.80	0.03	0.67	0.03
	B18	0.13	0.02	0.15	0.003	0.11	0.01	0.26	0.01	0.21	0.03
	Ave.	0.24	0.08	0.27	0.09	0.26	0.09	0.53	0.18	0.43	0.15
Yellow Sea (n=7)	B43	0.51	0.03	0.60	0.02	0.37	0.02	0.97	0.03	0.79	0.07
	H20	0.13	0.03	0.15	0.00	0.25	0.03	0.40	0.03	0.28	0.03
	B09	0.11	0.04	0.11	0.01	0.05	0.04	0.15	0.01	0.12	0.04
	B02	0.29	0.01	0.34	0.02	0.38	0.01	0.72	0.03	0.57	0.03

	H06	0.20	0.05	0.21	0.08	0.50	0.01	0.71	0.07	0.47	0.07
	H32	0.19	0.02	0.22	0.02	0.30	0.01	0.51	0.03	0.33	0.02
	C07	0.19	0.01	0.23	0.01	0.34	0.02	0.57	0.01	0.40	0.02
	Ave.	0.23	0.13	0.26	0.16	0.31	0.14	0.58	0.25	0.41	0.11
East China Sea (n=12)	A09	0.09	0.01	0.09	0.01	0.16	0.002	0.26	0.01	0.13	0.01
	F10	0.13	0.05	0.17	0.02	0.39	0.02	0.57	0.04	0.34	0.02
	E6	0.02	0.01	0.003	0.01	0.03	0.01	0.04	0.01	0.01	0.02
	D1	0.20	0.02	0.27	0.02	0.41	0.01	0.68	0.01	0.41	0.01
	D12	0.51	0.03	0.59	0.03	0.48	0.02	1.07	0.03	0.73	0.05
	A3	0.12	0.01	0.13	0.01	0.17	0.01	0.29	0.02	0.24	0.02
	C4	0.09	0.01	0.11	0.01	0.20	0.01	0.31	0.01	0.27	0.02
	C7	0.06	0.01	0.07	0.01	0.11	0.01	0.18	0.01	0.17	0.03
	C12	0.83	0.07	0.97	0.06	0.52	0.03	1.49	0.09	1.41	0.09
	B8	0.04	0.01	0.05	0.01	0.11	0.00	0.16	0.01	0.14	0.01
	F2	0.20	0.03	0.25	0.03	0.33	0.02	0.58	0.05	0.55	0.04
	F5	0.06	0.02	0.06	0.02	0.06	0.01	0.12	0.02	0.13	0.04
	Ave.	0.19	0.23	0.23	0.27	0.25	0.17	0.48	0.42	0.38	0.37
East China seas	Ave.	0.22	0.18	0.25	0.22	0.27	0.15	0.52	0.34	0.40	0.29

(n=24)											
Reference	Still Pond	1.31	0.09	1.55	0.10	0.43	0.13	1.98	0.10	2.00	0.05
sample	R-64	4.06	0.07	4.30	0.03	1.57	0.43	5.87	0.44	5.50	0.10

Table 3.5 Parameters from the Si and Al continuous dissolution (Si/Al method) with 0.5 M NaOH (1 h digestion). $ExtrSi_i$ (mg-Si g^{-1}) is the concentration of each Si fraction dissolving nonlinearly, k_i (min^{-1}) is their respective reactivity and $Si: Al_i$ ratio. Parameter b refers to the slope of the fraction dissolving linearly. SP-1, SP-2 and R-64-1, R-64-2 represent duplicate digestions of sample Still Pond and R-64. TAlkExSi and TAlkExAl represent the total alkaline extracted Si and Al. The $bSiO_2$% presented here is the bSi content in dry weight. NA represents data that is not available.

Station	Model	$ExtrSi_1$	$ExtrSi_2$	TalkExSi	TalkExAl	k_1	k_2	β_1	β_2	b	β_{lin}	$bSiO_2$%
B01	Model 2	0.82	2.34	6.13	2.89	1.90	0.08	4.40	1.83	0.07	2.13	0.18
B10	Model 2	1.26	3.73	12.25	5.14	1.45	0.07	3.16	2.53	0.12	1.95	0.27
B19	Model 2	0.96	1.97	6.16	2.24	1.63	0.08	7.14	2.81	0.07	2.32	0.21
B23	Model 2	1.64	4.91	14.88	5.79	1.66	0.08	10.44	2.36	0.16	2.30	0.35
B18	Model 2	0.58	0.83	3.22	1.01	3.10	0.09	12.83	3.08	0.03	2.45	0.12
B43	Model 2	1.49	6.01	15.29	5.18	1.52	0.08	3.86	3.86	0.16	2.45	0.32
H20	Model 2	0.73	1.56	4.21	1.56	1.84	0.06	4.36	2.64	0.04	2.40	0.16
B09	Model 1	0.66	NA	1.58	0.36	0.69	NA	10.71	NA	0.03	3.23	0.14
B02	Model 2	1.40	3.80	10.83	3.77	2.46	0.10	7.83	3.06	0.17	2.38	1.11
H06	Model 2	1.46	4.50	12.21	4.26	1.64	0.08	11.89	2.81	0.16	2.45	0.31
H32	Model 2	1.10	1.69	5.83	1.94	2.23	0.09	12.15	2.13	0.07	2.82	0.24
C07	Model 2	1.04	2.48	7.00	2.29	2.79	0.08	9.01	2.88	0.08	2.65	0.22
A09	Model 2	0.46	0.68	2.19	0.65	2.46	0.09	8.05	3.44	0.02	2.66	0.10
F10	Model 2	0.88	1.74	7.50	2.72	2.17	0.11	6.75	2.81	0.11	2.45	0.56
A3	Model 2	0.66	0.64	2.92	1.02	2.50	0.10	13.83	1.83	0.03	2.74	0.28

D1	Model 2	0.89	4.08	10.59	4.95	0.99	0.07	2.00	2.29	0.09	2.07	0.19
D12	Model 2	2.47	2.63	23.31	3.73	1.89	0.12	8.94	7.84	0.08	5.07	1.09
DC	Model 2	4.99	5.88	17.82	3.72	1.32	0.05	7.91	5.44	0.15	3.60	2.33
E6	Model2	0.40	0.16	0.97	0.24	3.32	0.13	22.44	2.72	0.01	2.82	0.12
B8	Model 2	0.39	0.39	2.02	0.56	3.57	0.10	9.47	3.22	0.02	3.12	0.17
C4	Model 1	1.14	NA	2.97	1.20	0.06	NA	2.31	NA	0.03	2.71	0.24
C7	Model 2	0.25	0.39	2.25	0.68	4.50	0.09	9.21	3.35	0.02	2.98	0.05
C12	Model 2	5.29	5.67	17.10	3.54	1.17	0.06	7.86	4.79	0.10	3.80	1.13
F2	Model 2	0.90	3.52	9.15	3.93	1.52	0.07	4.80	2.09	0.09	2.27	0.19
F5	Model 2	0.39	0.44	1.68	0.51	2.56	0.08	6.92	3.26	0.02	2.69	0.08
F8	Model 2	2.50	4.62	10.69	2.77	1.06	0.05	7.35	4.15	0.08	2.70	0.54
A1	Model 2	0.81	2.72	6.35	2.84	1.46	0.08	3.44	2.22	0.06	2.09	0.17
A4	Model 1	0.21	NA	0.65	0.14	1.34	NA	25.02	NA	0.01	3.14	0.05
SP-1	Model 2	6.53	6.45	18.73	4.42	1.49	0.13	9.96	4.50	0.10	2.47	2.78
SP-2	Model 2	7.44	5.18	17.11	4.81	0.50	0.05	5.88	5.18	0.09	1.79	2.70
R-64-1	Model 2	19.20	15.32	46.09	7.97	0.64	0.15	20.39	6.37	0.19	2.49	7.40
R-64-2	Model 2	15.16	17.76	43.65	11.26	1.26	0.18	22.06	11.00	0.18	2.96	7.05

3.3.2.3. Separation of bSi from lSi using dissolution rates

A 20 h-alkaline digestion (Figure S3.7) was performed for separating different bSi (diatom, radiolarian and sponge) from lSi using Si dissolution rate (Conley and Schelske, 2001). Microscopic observations of the residual sediment indicated that diatoms and radiolarian skeletons were digested completely while sponge spicules were not fully extracted. The time dependent methods (e.g., 5 h, DeMaster (1981); 8 h, Liu et al. (2002); 20 h, Conley and Schelske (2001)) all showed variations which emphasize that the fixed duration approach (Mortlock and Froehlich, 1989) is insufficient in the study area. The time dependent methods yield different $bSiO_2$% estimates, that accord with the duration of digestion, i.e., the 5 h digestion with the shortest time showed the least $bSiO_2$% (0.22 ± 0.18%), the moderate duration (8 h) of attack gave an intermediate $bSiO_2$% (0.40 ± 0.29%), and the longest duration of digestion produce the highest $bSiO_2$% (0.52 ± 0.34%) (Table 3.4). The ART ANOVA analysis indicated a significant ($p < 0.0001$) difference of the $bSiO_2$% among the three different time intervals.

According to the method described in Conley and Schelske (2001), the diatom $bSiO_2$%, radiolarian and sponge $bSiO_2$% were calculated at a 5 h and 20 h digestion interval, respectively (Table 3.4, Figure S3.8). The diatom $bSiO_2$%, radiolarian and sponge $bSiO_2$% and total $bSiO_2$% in sediment used in this study averaged 0.25 ± 0.22% (0.003 – 0.97%), 0.27 ± 0.15% (0.03 – 0.52%) and 0.52 ± 0.34% (0.04 – 1.49%), respectively (see Table 3.4). The amount of diatom $bSiO_2$% is approximately equal to the amount of radiolarian and sponge $bSiO_2$% (Figure S3.8). ART ANOVA analysis showed significant difference ($p < 0.0001$) between diatom $bSiO_2$%, radiolarian and sponge $bSiO_2$% and the total $bSiO_2$%. Detailed calculations of the averaged $bSiO_2$% of the BH, YS and ECS were also presented (Table 3.4).

3.3.2.4. Separation of bSi form lSi using Si/Al ratios

The Si/Al method is proposed based on the assumption that Si is extracted continuously from bSi and lSi whereas the Al is extracted mainly from lSi (Koning et al., 1997, 2002; Kamatani and Oku, 2000), therefore the quantity of bSi and lSi can be corrected using the Si:Al ratio (Kamatani and Oku, 2000). The purpose of determining the $bSiO_2$% using the Si/Al method is to fully digest bSi and correct the lSi properly. It should be noted that after 1 h digestion using 0.5 M NaOH, diatoms were not observed whereas few radiolarian skeletons and some sponge spicules were observed within the residual sediment of ECS samples (Figure S3.9). Therefore, the Si/Al alkaline digestion method determines mostly diatom bSi and radiolarian bSi and partly sponge bSi, instead of the total $bSiO_2$%.

The measured dSi and dAl results and the best fit models were shown in Figure S3.3. After

the likelihood statistical analysis, we found most samples (27/30 samples including sample Still Pond and R-64) were fitted better with 2 components (Model 2) than 1 component (Model 1), and the time evolution of release rates and Si:Al ratios were never sufficient to justify higher component models (Models 3 or 4). Generally, Si and Al were released non-linearly during the first 20 minutes and followed by a linear dissolution, and the AlkExSi was always higher than the AlkExAl (Figure S3.3). The bulk Si:Al ratios ($2 < Si:Al < 20$) were high at the beginning of digestion and decreased to a relative constant value ($2< Si:Al < 5$ for most samples, except D12 and C12) after 30 min (Figure 3.5), showing a rapid bSi dissolution during the < 30 min and complete extraction of bSi after > 50 min. The TAlkExSi ranged from 0.65 mg-Si g^{-1} to 24.0 mg-Si g^{-1}, whereas the total alkaline extracted Al content (TAlkExAl) ranged from 0.14 mg-Si g^{-1} to 6.0 mg-Si g^{-1}, with a relative constant β_{lin} (2.71 ± 0.63, Table 3.5).

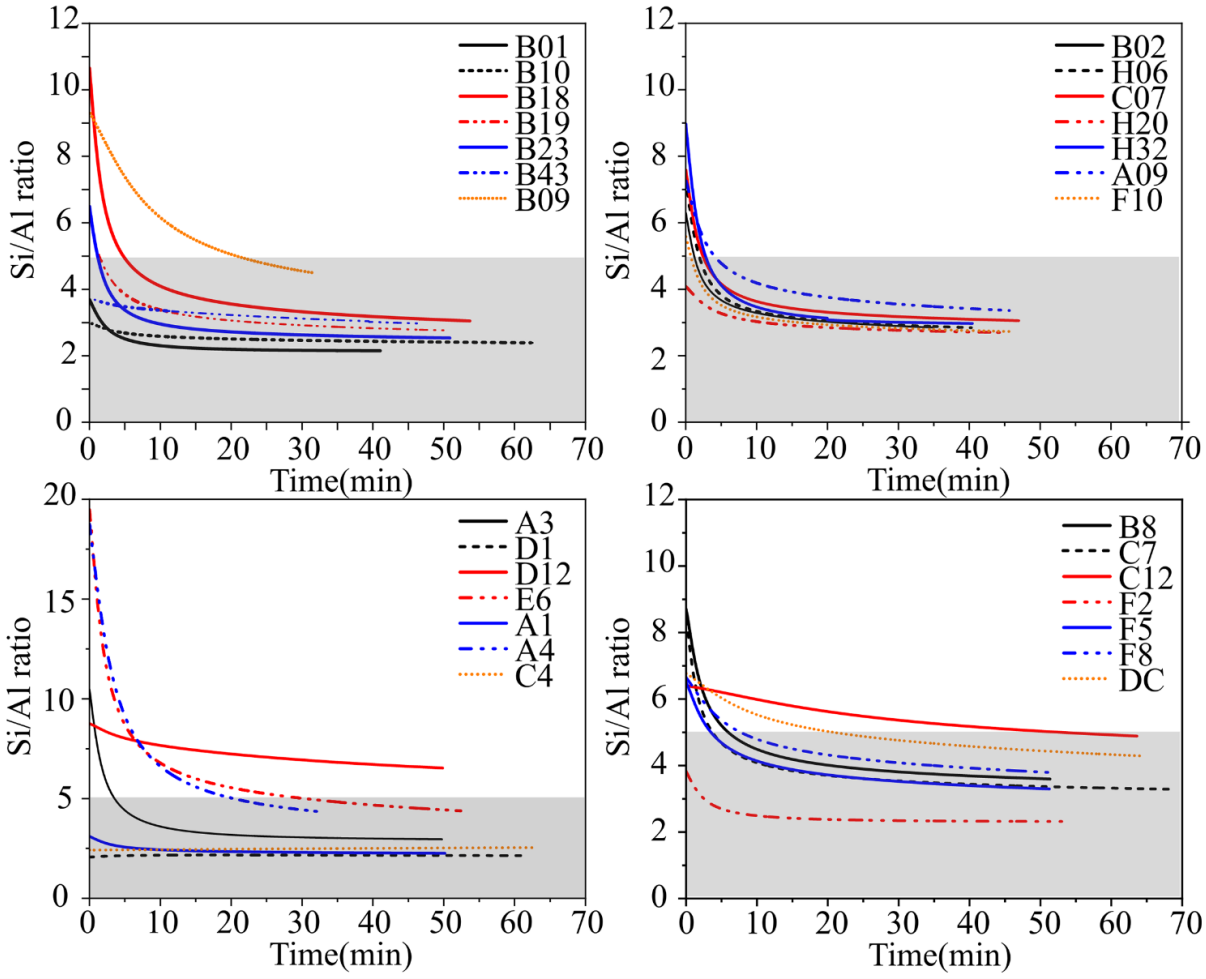

Figure 3.5. The Si/Al results show the Si:Al ratio through alkaline digestion (0.5 M NaOH). The grey area presents the Si:Al < 5.

The reactivity constant (k) of the first non-linear fraction (average $k_1 = 1.96$ min^{-1}) was greater than the second fraction (average $k_2 = 0.084$ min^{-1}) (Figure 3.6), and the β_1 is higher than the β_2

(except for D1, table 3.5). Figure 3.6 showed a wide range of Si:Al ratios for β_1 ($2 < \beta_1 < 25$) and k_1 ($0.5 < k_1 < 5$), and small ranges of β_2 ($2 < \beta_2 < 8$) and k_1 ($0 < k_2 < 0.2$). In addition, β_2 has similar Si:Al ratios compare to β_{lin}, and β_1 is always higher than the β_{lin} (Figure 3.6). The *ExtrSi*$_1$, *ExtrSi*$_2$ and the linear lSi fraction account for 19.3 ± 9.9%, 27.4 ± 12.6% and 53.3 ± 10.1% of the TAlkExSi, respectively (Table S3.2). Based on Si:Al ratio (β_i) and the reactivity (k_i), the calculated $bSiO_2$% (dry weight) and $lSiO_2$% (linear lSi fraction + non-linear lSi fraction) in sediments of east China seas were 1.82 ± 2.28 mg-Si g^{-1} (0.39 ± 0.49%$bSiO_2$) and 5.95 ± 4.69 mg-Si g^{-1} (1.28 ± 1.00% $bSiO_2$), respectively (calculated from Table 3.5). However, the definition of bSi ($\beta_i > 5$ or $\beta_{lin} < \beta_i < 5$ & $k > 0.1$ min^{-1}) and lSi ($1 < Si/Al < 4$) (Koning et al., 2002; Barão et al., 2015) based on Si/Al ratios and reactivity may limit our understanding of the different Si fractions. Our results showed that sometimes $\beta_2 < \beta_{lin}$ (B01, H32, A3, E6, F2; Table 3.5), suggest that the *ExtrSi*$_2$ is lSi origin. However, either this fraction is authigenic silicate is not clear, because the Si:Al ratio of authigenic silicates (< 2, Mackin (1989), Michalopoulos and Aller (1995)) and clay mineral (1- 4, Koning et al. (2002)) are both below 5. Barão et al, (2015) found the non-linear Si fractions (*ExtrSi*$_1$, *ExtrSi*$_2$) obtained using the Si/Al alkaline digestion method is higher than the $bSiO_2$% examined using the Si/time method (0.1 M Na_2CO_3). However, the *ExtrSi*$_1$ is approximately equal to diatom $bSiO_2$% (Barão et al., 2015). Implying the reactive non-linear fraction originates from the diatom bSi and the less reactive non-linear fraction originates from less soluble Si fractions (implicating resistant bSi, such as radiolarians, sponge spicules and/or altered diatoms, or lSi). So far, we cannot differentiate the less soluble Si fractions. A future study looking at the Si dissolution kinetics of diatoms, radiolarian skeletons, sponge spicules and synthesized sediment in alkaline digestion using both Si/Al method and Si/time method would improve our understanding on the definition of different Si fractions.

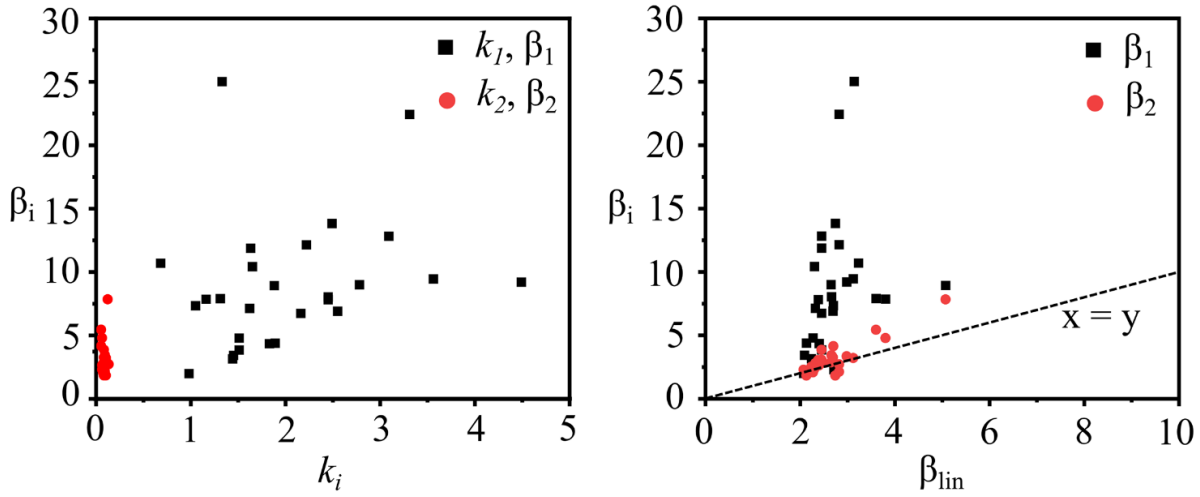

Figure 3.6. The Si:Al ratio (β_i, β_{lin}) and reactivity (k_i) of the east China seas sediment.

3.3.3. SEM and SEM-EDS analysis

The existence of a clay mineral "coating" on the surface of the siliceous organism was observed by SEM (Figure 3.7 and Figure S3.10) in samples before alkaline digestion. Generally, the diatoms and radiolarian tests were coated with more clay minerals than the siliceous sponge spicules. Diatom frustules in sample A1 were pre-treated using HCl (1.0 M) and H_2O_2 (10%), showing the partial removal of the coated clay minerals after the pre-treatment process. Additionally, Si, Al, K, Mg, Ca, Fe, Ti, S and As were detected from the diatom tests in sample A1 (Figure S10), indicating incomplete removal of clay materials (authigenic and/or allogenic clays) after pre-treatment. Besides Si and O, the major metal elements from reaction products of the reverse weathering process, such as Al, Mg, K and Fe (Michalopoulos and Aller, 2004), were commonly detected through EDS-SEM analysis (Figure S3.10).

In addition, diatoms and radiolarian tests were not observed in sediment residuals after the alkaline digestions (0.1 M, 0.2 M, 2.0 M Na_2CO_3, 8 h digestion, P vs. NP; 0.5 M NaOH, 1 h digestion, NP), whereas sponge spicules were found in the sediment residuals (post-digestion), especially in sediment from the outer shelf and slope of ECS. The digestion and destruction of the sponge spicule structures by the alkaline solution are visible from the SEM image (Figure 3.8). Different types of sponge spicules (i.e., *strongyle, acanthostyle, tignule*) were observed and picked from sediment residuals of sample C12, which was previously extracted in a 2.0 M Na_2CO_3 (P, 85 °C) solution for 8 h. Nevertheless, the degree of destruction of the different shapes/types of sponge spicules by alkaline solution is variable. For example, the *strongyle* sponge spicules (Figure 3.8 G, H, I) are more heavily digested than the *acanthostyle* sponge spicules (Figure 3.8 A, B, C) and the *tignule* sponge spicules (Figure 3.8 D, E, F).

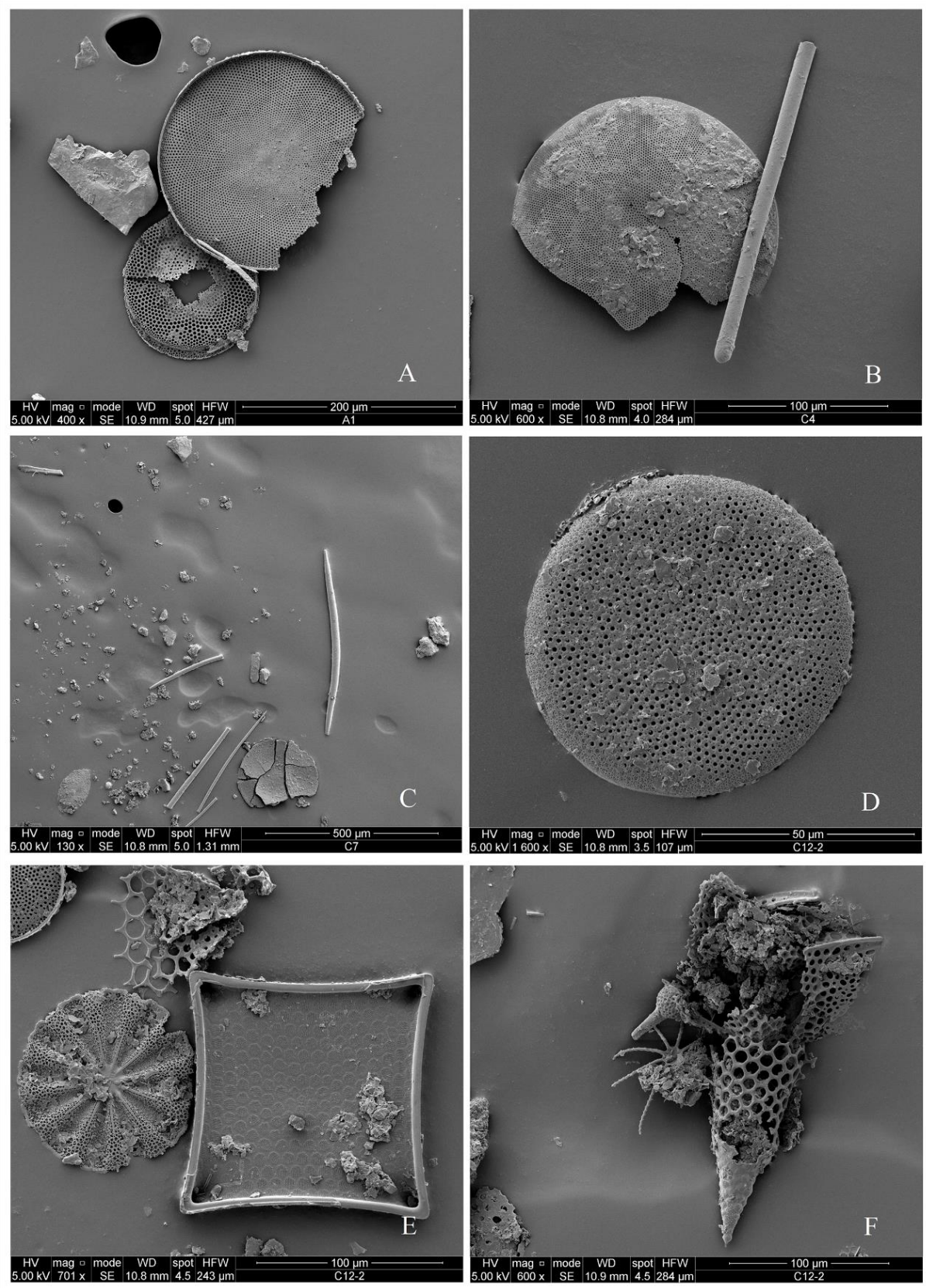

Figure 3.7. SEM images show different siliceous organisms found in sediment samples (A1, C4, C7, and C12) before alkaline digestion. A: diatom frustule in sample A1, B: diatom frustule and sponge spicule in sample C4, C: diatom frustule and sponge spicule in sample C7, D, E and

F: diatom frustules and radiolarian skeletons in sample C12. Sample A1 was pretreated using HCl (1.0 M) and H_2O_2 (10%) for 1 h, sample C4, C7, and C12 were not pretreated.

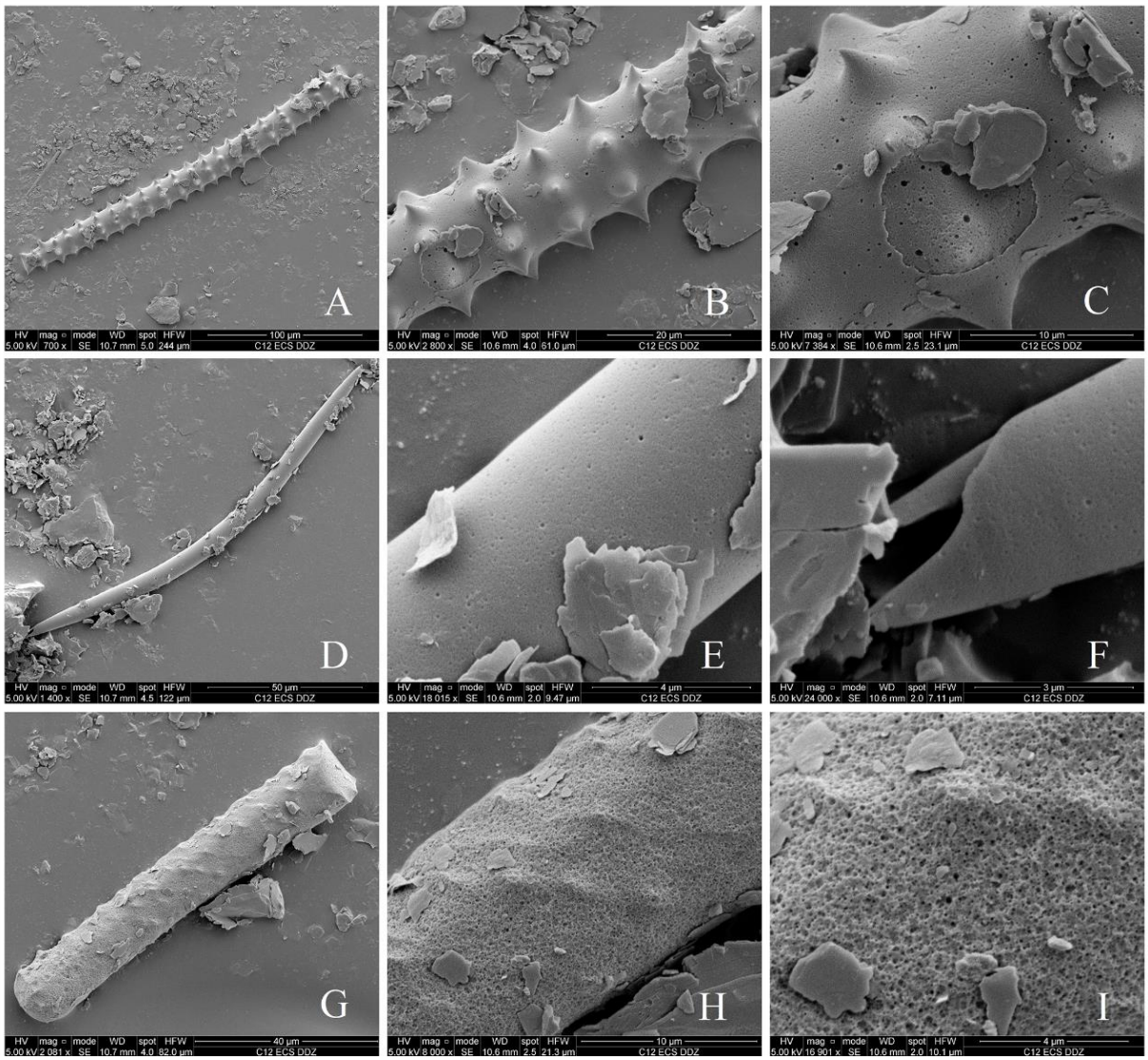

Figure 3.8. SEM images of three types of siliceous sponge spicule structures observed in the residual sediment of sample C12 after 8 h digestion using 2.0 M Na_2CO_3 (P). A-C: *acanthostyle* sponge spicule, D-F: *tignule* sponge spicule, G-I: *strongyle* sponge spicule. B and C, E and F, H and I are zoom-in views of images A, D and G, respectively.

3.4. Discussion

This study determined the $bSiO_2$% in sediment from the CCMZs of the east China seas using both the Si/time and the Si/Al methods and estimated the abundance of different types of bSi in sediment. The results show that the commonly used pretreatment step (Mortlock and Froelich, 1989) and different alkaline digestion methods (i.e., different concentrations of Na_2CO_3) inherently bias the accurate determination of $bSiO_2$%. For example, this study found that a

strong alkaline digestion can overestimate bSi content and does not completely digest sponge bSi, in agreement with Maldonado et al, (2019), which are important factors to consider when evaluating total bSi fluxes in the marine environment. These technical biases are important to understand since pretreatment procedures (e.g., HCl and H_2O_2) can overestimate the burial flux of bSi in CCMZs. To emphasize the influence of these methodological differences, we present a revised bSi burial flux for the east China seas. The causes of the methodological biases are discussed below (section 3.5.1) and the importance of resistant bSi in the east China seas is presented (section 3.5.2). Finally, a general procedure (section 3.5.3) is proposed to ensure that determination of bSi burial flux is supported by an accurate quantification of $bSiO_2$% in coastal sediments.

3.4.1. Re-evaluated burial flux of bSi in the CCMZs of east China seas

Considering the complex bSi types (diatoms, radiolarians and sponge spicules) (Table 3.1) and high AlkExSi from lSi from east China seas sediments (Table 3.5), an accurate determination of the bSi content is challenging due to the technical problems highted by Maldonado et al. (2019) and Koning et al. (2002) for coastal sediments. In this study, we assessed the Si/time and Si/Al methods in order to define the optimal method for the determination of the bSi content. This information is necessary to accurately evaluate bSi burial in the CCMZs of east China seas.

This study found two major limitations for the Si/time method: (1) insufficient correction of the lSi phase and (2) inadequate digestion of the resistant bSi (mainly sponge spicules). Applying a weak alkaline digestion completely digests the diatoms but cannot fully digest sponge spicules (Figure 3.8), whereas a strong alkaline digestion extracts more lSi from the sediment and resulting in an overestimation of the bSi content. In addition, the AlkExSi concentration continues to increase during an alkaline extraction (Figure 3.3, Figure S3.7, Figure S3.11) and a flat “plateau” as shown in Figure S3.2 is never reached, suggesting a continuous dissolution of resistant bSi (e.g., sponge spicules) and lSi. Therefore, a complete digestion of the bSi using the Si/time method cannot be defined for the sediment of east China seas, and the use of a simple tangent line to calculate bSi content (DeMaster, 1981) is insufficient.

Furthermore, authigenic silicates precipitate on the structure of bSi (Figure 3.7 and Figure S3.10) can decrease the reactive surface area of bSi and decrease its solubility (Williams et al., 1985; Varkouhi and Wells, 2020). Applying an acid and peroxide pretreatment procedure can remove the authigenic silicates and enhance the reactivity of bSi (Mortlock and Froelich, 1989).

However, our results showed the $bSiO_2$% increased more than 100% after the pre-treatment (Table 3.3, Figure S3.6), a significant ($p < 0.0001$) statistical increase (Table S3.1), which is not in agreement with our microscopic observations (Table 3.1, Figure 3.8). Ohlendorf and Sturm (2008) and Dai et al. (2017) found that using a pretreatment step increased the bSi yield and they suggested that more bSi was being digested after the removal of the mineral coating. We argue that this observed increase bSi yield is mainly due to an enlarged amount of Si extracted from authigenic silicate and clay minerals. This argument is supported by observations made by Michalopoulos and Aller (2004), who concluded that a mild acid pretreatment step (0.1 M HCl) can activate the authigenic silicate in the Amazon delta sediment, they also suggested that the mild acid pre-treatment can activate the neo-formed reverse weathering product (authigenic silicates) without changing the structure of crystallized clay minerals. However, applying a stronger acid (1.0 M HCl) and peroxide (10% H_2O_2) pretreatment can weaken the structure of clay minerals (Komadel and Madejová, 2006; Hu et al., 2022), therefore, enhance the solubility of the clay mineral. The chemical composition differences between bSi and authigenic silicates suggests that they are two different marine Si pools (Michalopoulos and Aller, 2004; Rahman et al., 2016; Pickering et al., 2020). Applying pre-treatment can cause an overestimation of the bSi pool, therefore, further studies on disentangling the different Si pools are required (DeMaster, 1991; Frings et al., 2021b) Frings et al., 2014, 2021a, 2021b; Ehlert et al., 2016; Pickering et al., 2020; Michalopoulos and Aller, 2004; Rahman et al., 2016).

Although the Si/time method determines the bSi content based on a simple Si vs. time tangent line, the mineral interference still needs to be corrected. This is typically done with the Si/Al method for CCMZs sediment (Koning et al., 2002; Barão et al., 2015). However, the quantification of the bSi content by Si/Al method is underestimated since the sponge bSi is not completely digested (Figure S3.9). Previous studies concluded that all sponge spicules and most (> 70%) of radiolarians were digested after 1 h continuous alkaline digestion using 0.5 M NaOH (Muller and Schneider, 1993). Maldonado et al, (2019) found that only 10% to 20% of fresh sponge spicules were dissolved after 1.5 h of alkaline digestion using 0.5 M NaOH. The sponge spicules used by Muller and Schneider, (1993) were treated in acid solution and 10% H_2O_2 for removing the organic matters and then ground, thus can be digested completely. However, the sponge spicules used by Maldonado et al, (2019) were not crushed, and were therefore harder to be digested completely. Thus, 30 to 90% of the sponge spicules may not be determined by the Si/Al method. Moreover, crushing the sediment or pre-treating the samples would enhance the digestion efficiency of the sponge bSi, but inevitably increase the surface area of lSi and bring out an overestimation of the bSi content. Therefore, a pretreatment of sediment should

be applied with caution, and we suggest applying a Si/Al method with an extension of extraction time to > 12 h (Maldonado et al. 2019). Unfortunately, this is not currently possible for the Si/Al method proposed by Koning et al, (2002).

The burial flux of bSi ($F_b = C * w$) in the CCMZs of the east China seas was re-evaluated, considering the sediment mass accumulation rate (w) from previously published studies and the concentration of $bSiO_2$ in sediments (C). The variations of the estimated bSi burial flux are dependent on the determination of the bSi content of the study area. The total bSi burial flux of the east China seas thus re-evaluated vary from 132 (± 112) Gmol-SiO_2 yr^{-1}, 249 (± 158) Gmol-SiO_2 yr^{-1} and 329 (± 209) Gmol-SiO_2 yr^{-1} using the $bSiO_2$% determined at 5 h, 8 h and 20 h digestion interval, respectively. And the estimated bSi burial flux is 253 (± 286) Gmol-SiO_2 yr^{-1} based on the Si/Al method (Table 3.6). Given the presence of high lSi content in the sediment samples of the east China seas, a well-known opal depleted CCMZs influenced by the terrestrial input delivered from the Yellow River and the Yangtze River, we opted the Si/Al (1 h digestion in 0.5 M NaOH) method as the optimal method for the determination of the bSi content in the east China seas. Our best estimate of the burial flux of $bSiO_2$ (253 ± 286 Gmol-SiO_2 yr^{-1}) in the east China seas is about one third of the previous studies (924 ± 693 Gmol-SiO_2 yr^{-1}; Wu et al., 2017, Wu and Liu, 2020).This is mainly due to the methodological bias, because the previous studies determined the $bSiO_2$% with a pre-treatment (with HCl and H_2O_2) process (Wu et al., 2017; Wu and Liu, 2020) that overestimate the $bSiO_2$%, subsequently, the bSi burial flux is over-estimated. The Si/Al method can correct the lSi properly, but still digest the sponge spicules insufficiently. Therefore, our estimation of the bSi burial flux is an underestimate.

Notably, the difference in bSi burial flux is also influenced by sampling technique (sampling at different locations and seasons) and the calculation of sediment mass accumulation rate. We adopted an average mass accumulation rate for the BH, YS and ECS and the potential factors (such as: riverine sediment input, resuspension of sediment by currents and primary production) that influence the sediment mass accumulation rate were not discussed in this study but are necessary for future works. The substantial decrease in the estimation of Si burial flux in the east China seas raises the question of whether it can have an impact at the global scale and on the balance of the silica cycle in the ocean.

Table 3.6 Burial flux of $bSiO_2$ (Gmol-SiO_2 yr^{-1}) of the BH, the YS, and the ECS. The total $bSiO_2$ burial flux of the east China seas equals the sum of the burial flux of the BH, YS, and ECS. The Si/time method (0.1 M Na_2CO_3, NP) and the Si/Al method (0.5 M NaOH, NP) was displayed for the determination of $bSiO_2$%. The Si/Al method was defined as an optimum method due to an accurate correction of lSi.

Methods	Time interval of digestion		BH	YS	ECS	Total burial flux (Gmol-SiO_2 yr^{-1})
Si/time (0.1 M Na_2CO_3)	5 h	$bSiO_2$%	0.24 ± 0.08	0.23 ± 0.13	0.19 ± 0.23	132 ± 112
		burial flux (Gmol-SiO_2 yr^{-1})	15.46 ± 5.15	54.03 ± 30.54	62.76 ± 75.98	
	8 h	$bSiO_2$%	0.43 ± 0.15	0.41 ± 0.11	0.38 ± 0.37	249 ± 158
		burial flux (Gmol-SiO_2 yr^{-1})	27.70 ± 9.66	96.31 ± 25.84	125.53 ± 122.22	
	20 h	$bSiO_2$%	0.53 ± 0.18	0.58 ± 0.25	0.48 ± 0.42	329 ± 209
		burial flux (Gmol-SiO_2 yr^{-1})	34.14 ± 11.60	136.24 ± 58.73	158.56 ± 138.74	
Si/Al (0.5 M NaOH)	1 h	$bSiO_2$%	0.23 ± 0.09	0.36 ± 0.34	0.46 ± 0.60	253 ± 286
		burial flux (Gmol-SiO_2 yr^{-1})	14.82 ± 5.80	84.36 ± 79.67	153.49 ± 200.20	

3.4.2. Contribution of radiolarian and sponge in bSi burial of the east China seas

Our findings emphasize that radiolarian and sponge bSi are important sinks of marine Si for the east China seas, especially the ECS. Microscopic observations indicate the sediment of BH is composed principally of diatoms (Li et al., 2020), YS is composed of diatoms (Wang et al., 2016), and the ECS is composed of diatoms (Chen et al., 2014; Li et al., 2018), radiolarians (Liu et al., 2017; Qu et al., 2020b) and sponge spicules (Table 4.1). No significant differences were observed in the average abundance of diatoms in surface sediment of BH, YS and ECS. However, the abundance of sponge spicules is of the same magnitude as diatoms in the sediment of ECS (Table 4.1), and the abundance of radiolarians is of the same magnitude as diatoms in the outer shelf and slope of ECS (Qu et al., 2020). Besides the observational data, our alkaline digestion results confirm the quantity of the less soluble bSi fraction (i.e., sponge spicules and radiolarians) is approximately equivalent to diatom bSiO2% (Table 4.4). Our data showed the abundance of radiolarians and sponge spicules was not as important as diatoms in the BH and YS (Table 4.1), thus the origin of the less soluble bSi in BH and YS may be partly due to phytolith discharged from rivers. Since phytoliths are less soluble than diatoms (Meunier et al., 2014) and can contribute 14% − 64% of bSi in estuaries and coastal sediment (Ran et al., 2017).

Although little is known about the quantity of radiolarian and sponge bSi in the east China seas (Zhang et al., 2003; Liang et al., 2021), the current results imply that the burial of "dark bSi" (radiolarian skeleton and sponge spicules, as defined by Maldonado et al. (2019)) is possibly as important as diatoms in east China seas. The burial of silicon associated with siliceous sponges was mainly found on continental slopes/margins (Maldonado et al., 2019), as one of the largest CCMZs in the Northwest Pacific, the Si burial through siliceous sponges would be more important than previously expected (Chou et al., 2012; Ran et al., 2017).

3.4.3. General protocol for the determination of bSi in coastal sediments

Our findings emphasize that besides diatoms, the less soluble types of bSi (i.e., radiolarians and sponge spicules) also act as an important marine Si sink in the CCMZs of the east China seas. However, the accurate determination of the magnitude of these marine Si sinks is complicated by different types of methods to determine the bSi content in sediments. The following is a brief summary of the different wet alkaline methods employed in this study and their technical limitations:

(1) The Si/time alkaline method (0.1 M Na_2CO_3, NP, 5 h digestion) (DeMaster, 1981), which is commonly used to quantitatively determine $bSiO_2$% in sediment of CCMZs, incompletely digests the skeletal structures of radiolarians and sponge spicules and partly digests lSi,

similar to the findings from Maldonado et al. (2019). A 20 h extraction in 0.1 M Na_2CO_3 solution can digest the diatom and radiolarian bSi and ca. 80% of sponge bSi. The determination of the $bSiO_2$% using a 2.0 M Na_2CO_3 solution overestimates the $bSiO_2$% because silica is digested from clay minerals, which bias the accuracy of the method.

(2) The one hour Si/Al method (0.5 M NaOH, NP) (Koning et al., 2002) underestimate the $bSiO_2$% due to incomplete digestion of radiolarian skeleton and sponge spicules. Therefore, an extension of the digestion time is necessary.

(3) The pre-treatment of sediment using HCl (1.0 M) and H_2O_2 (10%) prior to alkaline digestion can cause an overestimation of the $bSiO_2$% due to the digestion of authigenic silicates and/or clay minerals. Thus, a pre-treatment procedure should be avoided.

To resolve these technical problems, we propose the following general wet alkaline digestion procedure for the appropriate determination of bSi content in the sediments of CCMZs:

(1) Determining the types of bSi in sediment using a microscope.

(2) Selecting an appropriate alkaline solution according to the type of sediments.

−For sediment sample containing mainly diatoms, a 5 h alkaline digestion using 0.1 M Na_2CO_3 solution is capable of extracting bSi.

−For sediment sample from containing diatoms, sponge spicules and/or radiolarian skeletons, alkaline digestion > 2 h in 0.5 M − 1.0 M NaOH (Si/Al method) solution is suggested.

(3) Checking the residue sediment (post-digestion) using a microscope to observe if there are no more radiolarian tests and /or sponge spicules.

3.5. Conclusion

Our results showed that alkaline extractions of CCMZs sediments using 2.0 M Na_2CO_3 solution resulted in an overestimation of the $bSiO_2$% owing to silica being digested from clay minerals. Applying a 0.1 M Na_2CO_3 digestion (20 h) can minimize the lSi interference on bSi determination but can cause at least 20% of underestimation of the $bSiO_2$% owning to incomplete digestion of sponge spicules. Our results also show that alkaline extractions that apply a pretreatment procedure overestimate the determined $bSiO_2$% due to the digestion of the authigenic silicate phases and clays and subsequently overestimate the bSi burial flux. Consequently, we propose the general alkaline digestion protocol to accurately determine $bSiO_2$% in marine sediments of CCMZs using the Si/Al method by either applying the continuous analysis method (Koning et al., 2002) or the time-series digestion method (Kamatani and Oku, 2000). Based on these new results and the application of the Si/Al method in order to produce

accurate $bSiO_2$% results, we revised the current estimate of bSi burial flux to 253 ± 286 Gmol-SiO_2 yr^{-1}, which is one third of the previously reported (924 ± 693 Gmol-SiO_2 yr^{-1}). Our estimate still underestimates bSi burial flux of the east China seas, and further works on examining the resistant bSi (i.e., phytolith, radiolarian and sponge spicule) content are still required. We argue that the pre-treatment process (with HCl and H_2O_2) applied in previous estimates is the main reason that bSi burial flux was previously over-estimated. In order to ensure the accurate determination of bSi from different depositional settings in the future, we strongly suggest the development of an international intercalibration exercise.

4. Muddy sediments as an important silicon source of coastal and continental margin zones: Implications of continuous alkaline extractions

Abstract

The dissolution of silicate minerals on the seafloor releases an important amount of dissolved silicon (dSi) which is necessary for maintaining high diatom productions of the Coastal and Continental Margin Zones (CCMZs). However, the dissolution of silicate minerals along the continental shelves is incongruent which hinders our understanding of the marine Si cycle on both a regional and global scale. To understand the discrepancy of silicon (Si) dissolution in different sediment matrices and its potential controlling factors, we investigated surface sediments of typical CCMZs of the Chinese marginal Seas using a continuous alkaline extraction technique, grain-size and chemical (carbon and total nitrogen) analysis as well as a qualitative measurement of clay mineral compositions by X-ray diffraction. The results showed that Si and aluminum (Al) leached from muddy sediments were 2 times greater than sandy sediments. High dissolution rates (> 0.20 mg-SiO_2 g^{-1} min^{-1}) of silicate minerals are caused by a large sediment-specific surface area. Further, our data showed that high Al contents (Si:Al < 40) of biogenic silica (bSi) reduces opal reactivity, and that the source of Al incorporated in bSi is mostly due to silicate minerals dissolution. We show that although silicate minerals is less active than that of bSi, it still potentially releases more bio-available Si and Al to seawater due to its dominant presence on seafloor (70.3% − 99.0%wt). This study highlights silicate minerals dissolution as an important potential marine Si source and emphasizes the need for a better understanding of the roles of silicate minerals in the Si cycle of marginal seas in future studies.

Graphical Abstract:

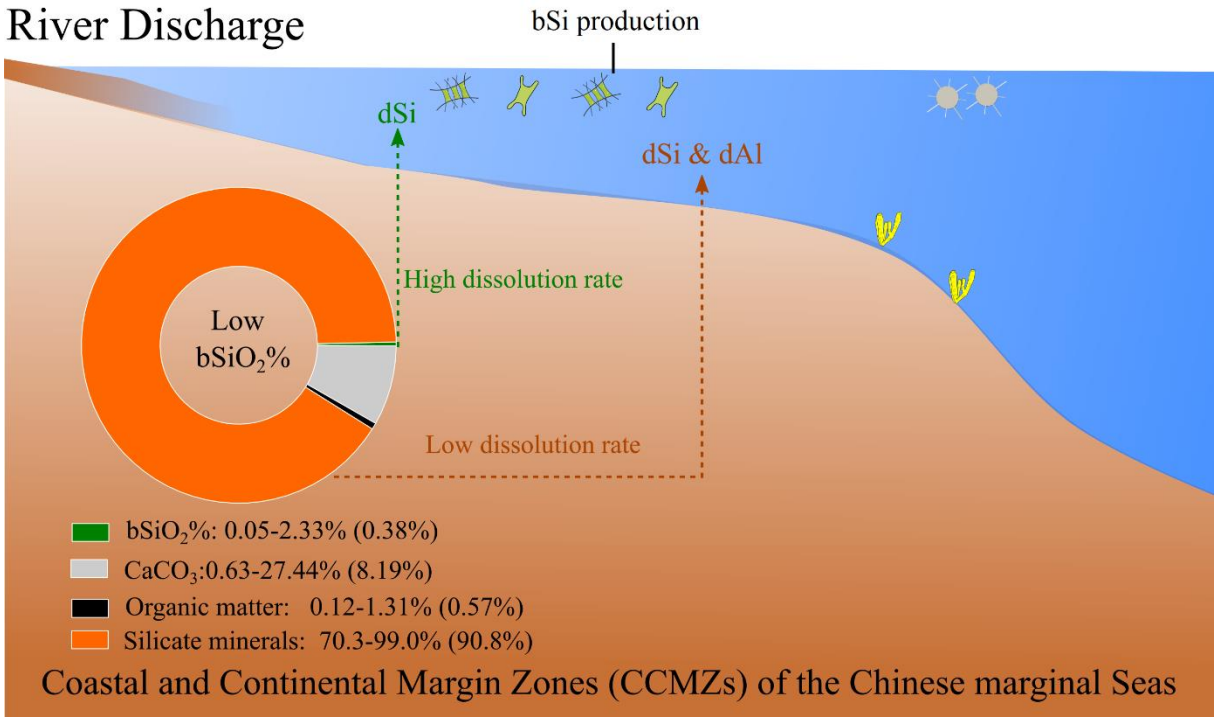

4.1. Introduction

The dissolution of silicate minerals (known as silicate weathering) in sediments of Coastal and Continental Margin Zones (CCMZs) contributes an important amount of dissolved silicon (dSi) (2 to 45 Tmol-Si yr^{-1}) to the global ocean (Jeandel et al., 2011; Jeandel and Oelkers, 2015; Frings, 2017; Tréguer et al., 2021) which fuels planktonic and benthic diatom productions (Tréguer et al., 1995; Leynaert et al., 2011). As a consequence of climate change, a decrease of riverine dSi discharge to the oceans is expected (Phillips, 2020) and less nutrients inputs from below in a warmer and more stratified ocean would cause less production of diatoms and a decline of biogenic silica (bSi) export to depth in mid and low latitude oceans (Tréguer et al., 2018), alternatively, Taucher et al. (2022) predicated that enhanced silica export in a future ocean might trigger global diatom decline. Jeandel et al. (2011) and Jeandel (2016) highlighted the importance of silicate minerals dissolutions in the silicate-rich CCMZs as necessary Si source of the oceans. Given the importance of silicate minerals dissolution for supplying Si to the ocean and sustaining oceanic productivity (Fabre et al., 2019; Zhang et al., 2020; Measures and Hatta, 2021; Ng et al., 2020, 2022; Ward et al., 2022), understanding the incongruent dissolution of silicate minerals along continental margins (Lerman et al., 1975; Jeandel et al., 2011; Jeandel and Oelkers, 2015) and evaluating its Si-release potential are necessary (Barão et al., 2015).

The interaction of silicate minerals with seawater contribute to the control of dSi concentration of seawater, with silicate minerals releasing Si to the silica-deficient seawater and precipitating Si from silicic acid enriched (> 25 ppm) seawater (Mackenzie et al., 1967; Siever, 1968). Based on theoretical and empirical studies of porewater dSi profiles, Frings (2017) concluded 45 Tmol-Si yr^{-1} is released from clay and calcareous seafloor. However, Tréguer et al. (2021) found that some of the non-biogenic-silica sediment classes described in Frings (2017) contain significant bSi which explains the overestimation of benthic Si efflux. The re-evaluated benthic Si efflux from opal-poor sediments is approximately 2 Tmol-Si yr^{-1} which still represents 13% of the total marine Si input (Tréguer et al., 2021). Quantitatively differentiating the Si outflux of silicate minerals from bSi is taxing due to the complex mineral composition (Jeandel et al., 2011; Tréguer et al., 2021). A flow-through experiment was established for evaluating the Si efflux from bulk sediment of various depositional environments (Open Ocean (Van Cappellen and Qiu, 1997; Rickert, 2000; Gallinari et al., 2002, 2008) and CCMZs (Wu et al., 2017; Wu and Liu, 2020; Ma et al., 2023)). However, the Si released during the flow-through experiment originates from both bSi and silicate minerals, and the relative contribution of either

Si sources was not distinguished according to the solely measurement of dSi concentrations (Ma et al., 2023). Applying a simultaneous measurement of dSi and dissolved aluminum (dAl) possibly resolves this issue (Kamatani and Oku, 2000; Koning et al., 2002), since the Al content in bio-siliceous frustules is far less than in mineral sediments (Ehlert et al., 2012).

The continuous alkaline extraction technique is an advanced wet chemical method that simultaneously analyzes dSi and dAl from extracting solution (Koning et al., 2002) and is widely applied for differentiating different sources of Si from soil (Barão et al., 2014, 2015) and marine sediments (Koning et al., 2002; Barão et al., 2015; Raimonet et al., 2015; Zhu et al., 2023). Through a high-resolution (one-second) alkaline extraction monitoring of the dSi and dAl contents and a first-order dissolution model, sources of Si are well defined based on the different dissolution kinetics and elemental compositions of bSi and silicate minerals (i.e., lithogenic silica) (Koning et al., 2002). This technique allows an accurate quantification of the bSi content (bSiO2%) and the lithogenic silica content particularly for sediments of CCMZs where silicate mineral content far exceeds the $bSiO_2$% (Barão et al., 2015; Zhu et al., 2023). Previous studies found that the amount of alkaline extracted Si from silicate minerals are significantly higher than bSi, hinting to the importance of non-biogenic silicate for marine ecosystem, although silicate mineral dissolution is significantly enhanced under a hot (85 °C) alkaline solution condition (Barão et al., 2015). Further, the dissolution rate of aluminosilicates in seawater was found to be comparable to the dissolution of bSi in oceanic sediments, particularly for silicates minerals of surface sediments which contain high active surface areas (Lerman et al., 1975; Köhler et al., 2005). This is probably due to 1) reduced dissolution rate of bSi caused by authigenic aluminosilicate coating surrounding the bio-siliceous structures (Michalopoulos and Aller, 1995, 2004; Michalopoulos et al., 2000; Amann et al., 2020) and 2) relative rapid dissolution of silicate minerals in surface sediments (Köhler et al., 2005). Therefore, simultaneous alkaline extractions can help to quantify different Si fractions that are more soluble than highly crystalized mineral and can be released back to seawater.

CCMZs are “boundary exchange zones” which play a major role in the land-to-ocean transfer of materials (Jeandel and Oelkers, 2015). As the largest CCMZs in western Pacific, the Chinese marginal Seas (i.e., the Bohai Sea (BH), Yellow Sea (YS), East China Sea (ECS) and South China Sea (SCS)) receive more than 1.4×10^9 tons yr^{-1} of terrestrial sediments from surrounding rivers (Milliman and Meade, 1983; Liu et al., 2009; Qiao et al., 2017; Ma et al., 2022). Even a lower limit of dissolution rate (0.5%-SiO_2 yr^{-1}, Jeandel et al., 2011; Jeandel and Oelkers, 2015) of the riverine transported solid phases would release 1.2×10^{11} mol-Si yr^{-1} to marine water column, which is still comparable to the dSi input from all surrounding rivers (6.4×10^{11} mol-

Si yr^{-1}, (Liu et al., 2003, 2005, 2009, 2011). In addition, both field observations and onboard/laboratory incubations have shown the Si efflux from the opal-poor sediments plays a major role in the diatom production of the BH (Liu et al., 2011), YS (Liu et al., 2003; Wu et al., 2017), ECS (Wu and Liu, 2020) and SCS (Ma et al., 2022; Zhu et al., 2023), as well as other CCMZs (i.e., the southern North Sea, Gehlen and van Raaphorst, 1993; Oehler et al., 2015). It is therefore necessary to understand the role of silicate minerals dissolution in the biogeochemical cycle of Si of the CCMZs.

In this context, we measured the sediment chemical compositions (i.e., total organic carbon, inorganic carbon, total nitrogen), physical properties (i.e., grain-size) and the clay mineral contents for understanding the sediment matrices. We conducted continuous alkaline extraction experiments to simultaneously determine the dissolution of bSi and silicate minerals in sediments, and further quantified the amount of different Si phases (bSi and silicate minerals) released from various types of sediments (muddy vs. sandy sediments) of the CCMZs of the Chinese marginal Seas.

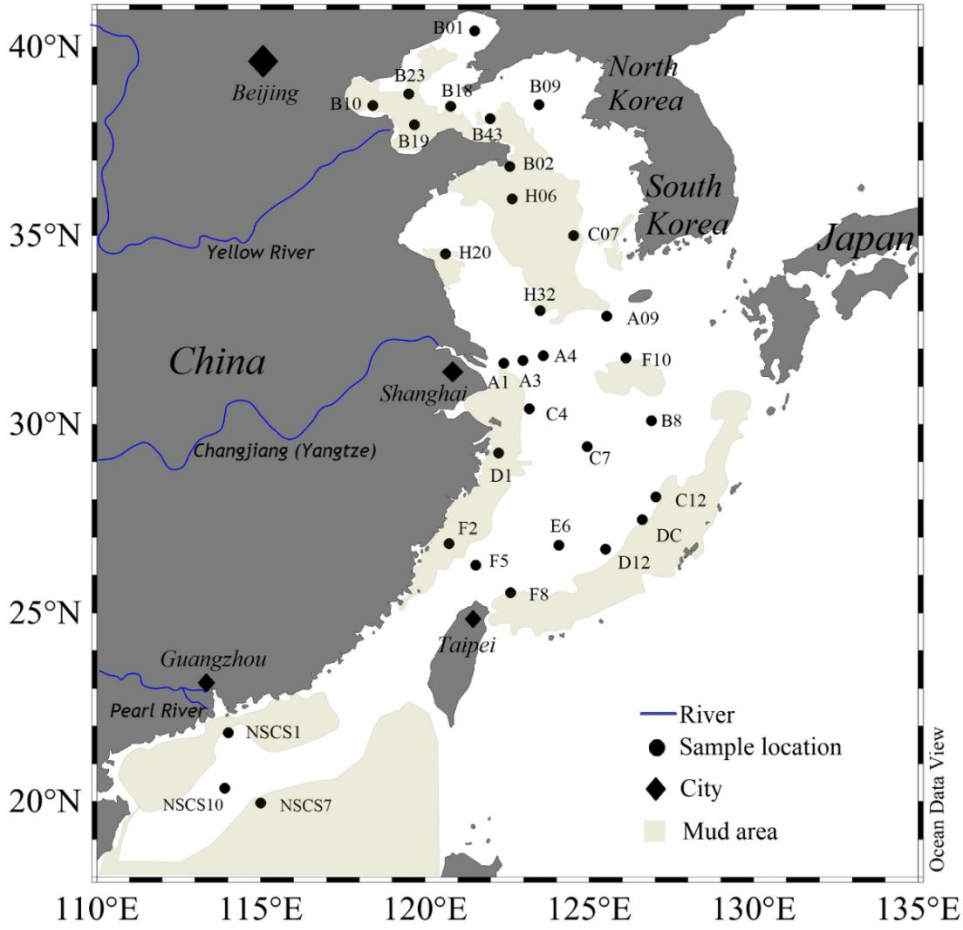

Figure 4.1. Map of the Chinese marginal seas showing sampling stations in the Bohai Sea, Yellow Sea, Eat China Sea and South China Sea. Mud sediment (< 62.5 μm) areas are also

indicated following Wu and Wen (2019) and Shi et al. (2021). Figure plotted using Ocean Data View (ODV) program (Schlitzer, 2023).

4.2. Materials and methods

4.2.1. Sampling of sediment samples

Surface sediments (0 − 2 cm) were collected from the BH, YS, ECS and SCS during August − September 2008, September − October 2010, May − June 2013 and March − April 2014, respectively (Figure 1). Information (research cruise, date, coordinates and water depth) of these samples is described in Wu et al, (2017), Ma et al, (2023) and Zhu et al, (2023). All samples were sealed in plastic bags and immediately stored on board at -20 ℃ and freeze-dried in the laboratory for further analysis.

4.2.2. Analytical methods

4.2.2.1. Continuous alkaline extractions

The simultaneous alkaline extraction of Si and Al was conducted following the wet chemical method described in previous studies (Koning et al., 2002; Barão et al., 2015; Zhu et al., 2023). The high-resolution analysis (one-second) of alkaline extracted dSi and dAl allows 1) an evaluation of the alkaline extracted Si fractions from bSi and silicate minerals, as Al content of diatoms in sediments is negligible (Ehlert et al., 2012), and 2) the determination of the dissolution kinetics of bSi and silicate minerals. In brief, freeze-dried sediments were added into a stainless-steel vessel filled with 180 mL of 0.5M NaOH pre-heated to 85℃. The alkaline extracted Si concentration was measured according to the molybdate-blue method (Grasshoff et al., 1983) and the Al concentration was determined according to the fluorometric method (Hydes and Liss, 1976). Standard samples of dSi and dAl with concentrations of 1 mg L^{-1}, 2 mg L^{-1}, 4 mg L^{-1}, 6 mg L^{-1}, 8 mg L^{-1}, 10 mg L^{-1}, 20 mg L^{-1}, 30 mg L^{-1}, and 40 mg L^{-1} were used for calibration, and only the linear regression curves with correlation coefficients ≥ 0.999 were accepted according to previous studies (Barão et al., 2015). Two independent reference solutions (with concentrations of 3 mg L^{-1}, and 9 mg L^{-1} of dSi and dAl) were tested before and after the continuous alkaline extractions to guarantee an analytical error below 5%. The concentrations of dSi and dAl of the reagents blank solutions were at the base-line of measurements. Samples from the BH, YS and ECS were determined previously, and the modeling parameters were reported in Zhu et al. (2023), three samples (NSCS1, NSCS7 and NSCS10) from the SCS were analyzed in this study.

4.2.2.2. Analytical procedure for Si and Al data

The alkaline extracted Si and Al concentrations were fitted (Eq. 4.1) using the first order dissolution models (model 1: i =1; model 2: i =2, model 3: i =3) as described in Koning et al. (2002), Barão et al. (2015) and Zhu et al. (2023). Here, Eq. 4.1 describes sediments contain less than three non-linear dissolving Si phases (*ExtrSi*$_1$, *ExtrSi*$_2$, *ExtrSi*$_3$):

$$Si_{aq} = \sum_{i}^{n} [ExtrSi_i]_0 \, (1 - e^{-k_i t}) + bt$$

$$Al_{aq} = \sum_{i}^{n} \frac{1}{\beta_i} [ExtrSi_i]_0 \, (1 - e^{-k_i t}) + \frac{1}{\beta_{lin}} \, bt \qquad (4.1)$$

Where Si_{aq} and Al_{aq} are the concentrations of leached dSi and dAl in mg L^{-1}, at time t (min). [ExtrSi_i]$_0$ is the initial extractable Si in mg L^{-1}, calculated under a condition when all alkaline extractable Si (bSi and silicate mineral) has dissolved, k_i is the reactivity constant (min^{-1}) of no-linear dissolving phases and β_i is the atomic ratio of Si and Al released during the dissolution of extractable silica fraction. b and β_{lin} represent the constant dissolution rate and the Si:Al ratios of silicate minerals, respectively. Normally, several alkaline extractable Si (*ExtrSi*$_i$) phases exist, the biogenic Si phases are distinguished with high Si:Al ratio (Si > 5) (Koning et al., 2002; Barão et al., 2015). Further, the total amount of alkaline extracted Si (TAlkExSi, mg-Si g^{-1}) and Al (TAlkExAl, mg-Al g^{-1}) were also presented. An optimum model (Eq.4.1) was selected by applying a likelihood statistical analysis (Armstrong et al., 2002; Moriceau et al., 2009; Zhu et al., 2023). The unit of *ExtrSi*$_i$, TAlkExSi, TAlkExAl, β and b were normalized as mg-Si g^{-1}, mg-Si g^{-1}, mg-Al g^{-1}, µmol:µmol and mg-SiO_2 g^{-1}, respectively.

4.2.2.3. Grain-size analysis

The grain-size measurement was conducted following an optimum−"PT2SD" protocol proposed by Jaijel et al. (2021). The freeze-dried sediments were added into a 15 mL plastic tube filled with 1 mL Mili-Q water (18 MΩ), then 2 mL of 30% H_2O_2 was mixed with samples for removing the organic matter (addition of the volume of H_2O_2 is dependent on organic matter content of sediment). Then 0.4 mL of Clagon solution was added to sample solution prior to measurement. Triplicate measurements were applied for grain-size analysis using Malvern Mastersizer 2000 grain-size analyzer with Hydro 2000S module, and an averaged value was calculated after measurements. The mean grain-size, specific surface area (SSA), D [3,2] surface area distribution weighted mean (D [3,2]) and fractions of clay (< 2 µm), silt (2 – 62.5 µm) and sand (> 62.5 µm) were also calculated. Definition of textural classification of clay, silt and sand follows the subdivisions introduced by Wentworth (1922). The specific surface area (SSA) of sediment is calculated by the total area of particles divided by the total weight of

sediment. The D [3,2] is most relevant where specific surface area is important, e.g., reactivity, dissolution and bioavailability, it is sensitive to the presence of fine particulates in the size distribution. Note that the definition of muddy (sand + silt >70%) and sandy (sand > 50%) sediment follows Flemming (2000).

4.2.2.4. Chemical analysis

The chemical analysis includes the measurement of total nitrogen (TN), organic carbon (OC) and total carbon (TC). TN, OC and TC contents were analyzed by flash combustion of precisely weighted sediment samples (about 10 mg) at 950 °C on a Thermo Scientific FLASH 2000 CHN. Measurement of OC was conducted using decarbonated (acidification with 1.0 M HCl) sediment. The calculation of inorganic carbon ($CaCO_3$) content is expressed as: $CaCO_3\%$ = 100*(TC% − OC%)/12. Detrital material content (detrital% = 100% − TN% − OC% − $CaCO_3\%$ − $bSiO_2\%$) was calculated following Rickert (2000). The calibration curve for TN, OC and TC measurement with $R^2 > 0.9997$ was created by using 9 standards, and the analytical precision of TN, OC and TC was < 5%.

4.2.2.5. Clay mineral analysis

The relative clay mineral (illite, kaolinite, chlorite and montmorillonite) contents were measured by X-ray diffraction (XRD) on oriented mounts of clay-size particles (< 2 μm). All samples were pretreated with 15 mL of 30% H_2O_2 for 24 h to remove the organic matter and then decarbonated using 0.5% HCl. The decarbonated suspensions were washed successively with distilled water to remove excess ions and to enhance deflocculation of clays. The clay-size particles were separated following Stokes' law and concentrated using a centrifuge. The resulting pastes were spread into calibrated recesses on glass slides. XRD analyses were conducted using a Rigaku D/max 2500 diffractometer with Cu kα radiation (40KV/150 mA; Speed: 8°/min; Step: 0.024°) at the Qingdao Institute of Marine Geology. Peak areas and illite crystallinity were calculated after manual baseline correction using MacDiff software version 4.2.6 (Petschick, 2002), following the semi-quantitative method of Biscaye (1965).

4.2.3. Statistical analysis

To show the distributions of the determined parameters in the studying area, data were plotted using ODV program which were interpolated in color employing the DIVA method (Schlitzer, 2023). Principal component analysis (PCA) was performed to identify the majority of the variance among the modeling parameters ($ExtrSi_1$, $ExtrSi_2$, TAlkSi, TAlkAl, b, β_{lin}, β_1, and k_1), sediment physical parameters (clay%, silt%, sand%, mean grainsize, D [3,2], sediment-specific

surface area and the relative clay mineral contents) and chemical compositions ($bSiO_2$%, TN%, TOC%, $CaCO_3$% and detrital%). Two–way Analysis of Variance (ANOVA) were used to test if there are significant differences among the determined parameters. Both PCA and two-way ANOVA tests were performed using origin 2021b software.

4.3. Results

4.3.1. Dissolution of Si and Al fractions

Our results showed heterogeneous distribution of alkaline extracted Si and Al in surface sediments of the Chinese marginal Seas. Figure 4.2 shows the distribution of non-linear dissolving Si phases ($ExtrSi_1$: 0.21 – 5.97 mg-Si g^{-1}, $ExtrSi_2$: 0.16 – 6.01 mg-Si g^{-1}), total alkaline extracted Si (TAlkSi: 0.65 – 23.31 mg-Si g^{-1}) and Al (TAlkAl: 0.14 – 5.79 mg-Si g^{-1}) as well as the dissolution rate of silicate minerals (b: 0.02 – 0.36 mg-SiO_2 g^{-1} min^{-1}). The distribution patterns of $ExtrSi_1$, $ExtrSi_2$, TAlkSi, TAlkAl and b values were similar with high values in sediments of the western BH, northern YS, Zhe-Min coast and the ECS continental slope. In addition, as shown in Figure S4.1, the reactivity and the Si:Al ratio of the first non-linear dissolving Si fraction (k_1: 0.06 – 4.50 min^{-1}; β_1: 2.00 – 36.07) were higher than the second non-linear dissolving Si fraction (k_2: 0.05 – 0.13 min^{-1}; β_2: 1.83 – 7.84), the Si:Al ratio of non-linear dissolving Si fractions (β_1 and β_2) were higher than silicate mineral (β_{lin}: 1.57 – 5.07).

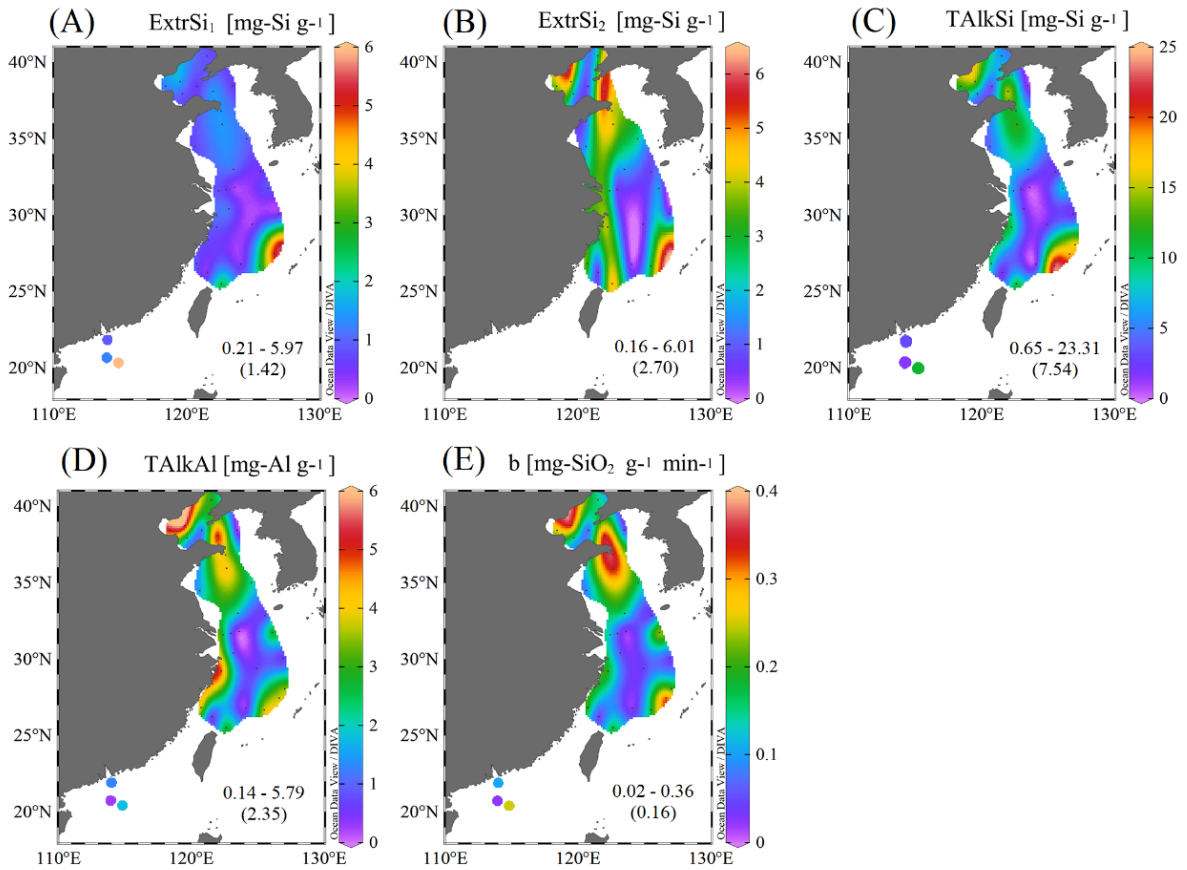

Figure 4.2. The paremeters (A: *ExtrSi*$_1$, first non-linear dissolving Si phase; B: *ExtrSi*$_2$, second non-linear dissolving Si phase; C: TAlkSi: total amount of Si; D: TAlkAl, total amount of Al; and E: *b*, silicate mineral dissolution rate) of the simultaneous alkaline extraction which were interpolated in colour employing the DIVA method (an in-built function in ODV). The values in each individual plot represent the ranges and average (shown in bracket) of data. The figure was generated using the ODV program (Schlitzer, 2023).

4.3.2. Grain-size distributions

Grain-size is a key physical parameter of marine sediments. Generally, the sediments used in this study contain mainly silt (54.1%) , sand (41.9%) and with minor amount of clay (3.9%) content. The mean grain-size distribution at the study area is similar to the sand distribution whereas the distribution of specific surface area of the sediments is similar to the distribution of clay and silt fractions (Figure 4.3). Further, areas characterized by fine grain-size fractions (clay and silt: grain-size < 62.5 µm) were found in the western BH, northern YS, Zhe-Min coast and ECS continental slope (Figure 4.3 A and B). The outer continental shelf of ECS is characterized by high sand content (Figure 4.3 C). The highest mean grain-size was found in a sample (NSCS10, Figure 4.3 D) from the NSCS. Our determined values are in agreement with the previous reported grain-size distribution patterns (Wu and Wen, 2019; Shi et al., 2021; Mei

et al., 2020; Ma et al., 2023).

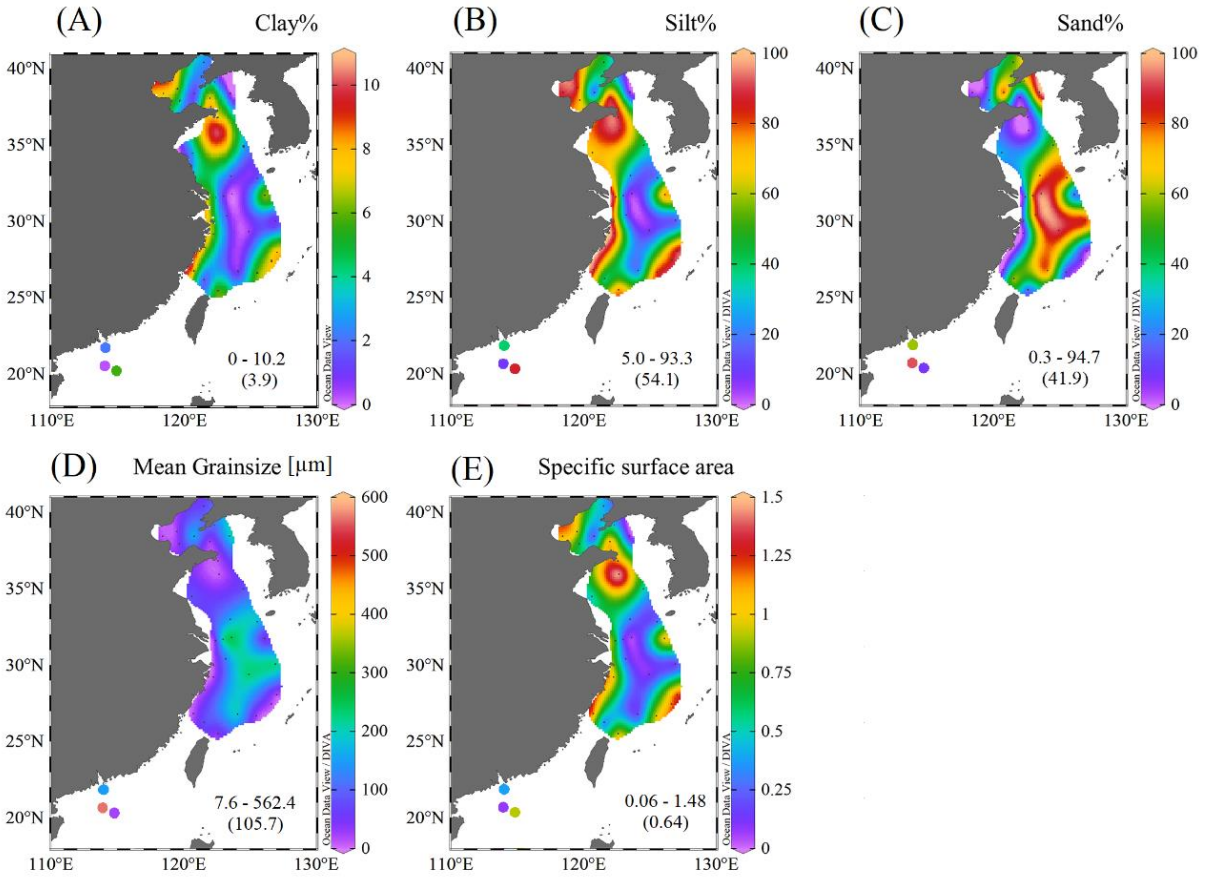

Figure 4.3. The clay% (A), silt% (B), sand% (C), mean grain-size (D) and specific surface area (E) of surface sediments. The values in each individual plot represent the ranges and average (shown in bracket) of data. The figure was generated using the ODV program (Schlitzer, 2023).

4.3.3. Chemical parameters

Figure 4.4 shows the distribution of detrital, bSi, $CaCO_3$, TN and TOC contents. Samples from the study area contain high detrital material (average: 90.8%, Figure 4.4 A) which confirm with previous studies (Wu and Liu, 2020; Ma et al., 2023). Higher detrital material content was found in near-shore sediments than sediments on the ECS continental shelf. The distribution of $bSiO_2$% and $CaCO_3$% (Figure 4.4 B, C) showed similar patterns with higher values in near-shore sediments and deep-water sediments (i.e., continental slope). Distributions of TN% and TOC% were similar (Figure 4.4 D, E) with high values in the central YS and the continental slope of ECS.

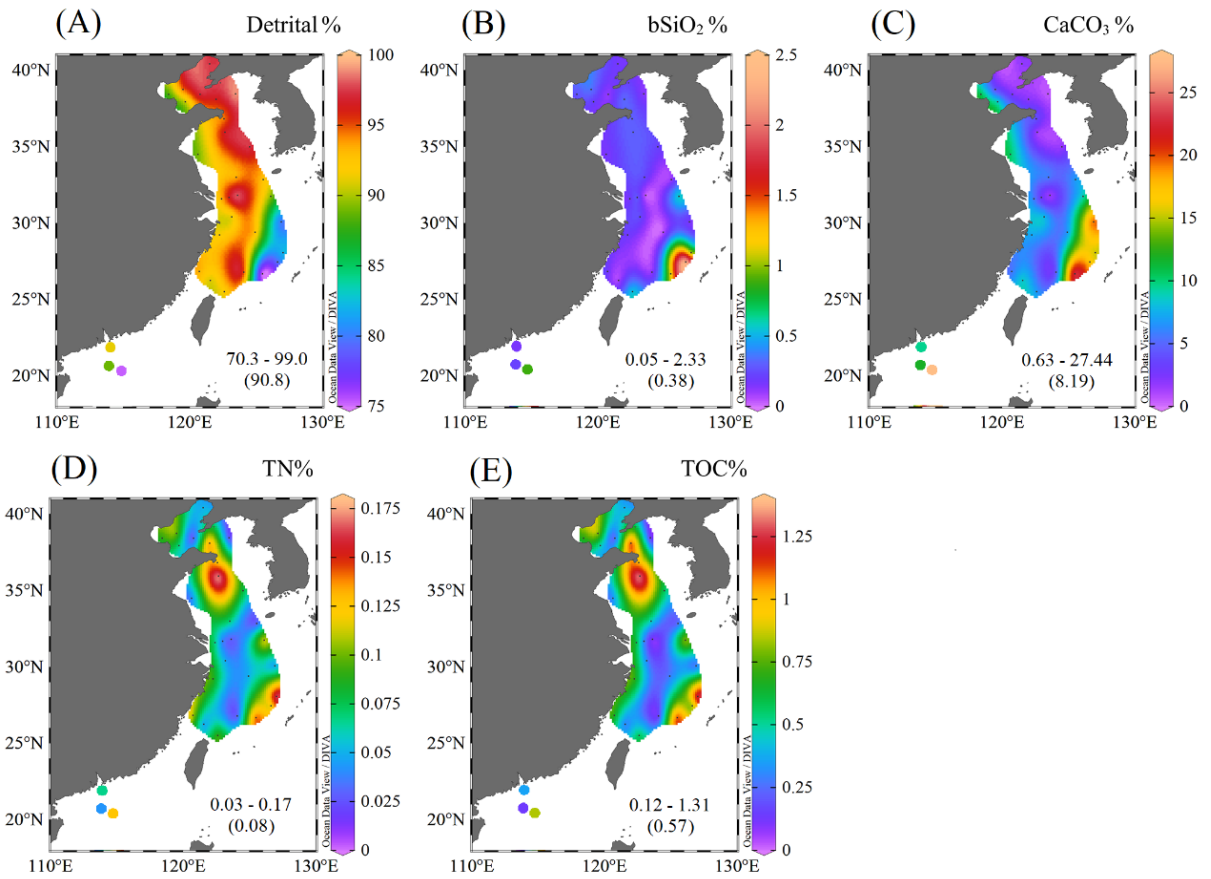

Figure 4.4. Detrital material content (A), $bSiO_2$% (B), $CaCO_3$% (C), TN% (D) and TOC% (E) of study area. The values in each individual plot represent the ranges and average (shown in bracket) of data. The figure was generated using the ODV program (Schlitzer, 2023).

4.3.4. Clay minerals

The relative clay mineral compositions of the study area were illite (63.5%), chlorite (20.4%), kaolinite (11.9%) and montmorillonite (4.3%). Generally, illite and chlorite content increases from the BH to ECS (Figure 4.5 A, B), whereas a reverse pattern was found for kaolinite (Figure 4.5 C). The sediments of BH contain higher montmorillonite content than sediments of other regions (YS, ECS and SCS) of this study (Figure 4.5 D). In addition, samples from BH and western YS and inner shelf of ECS is characterized by high illite crystallinity (> 0.28) than the other samples (Figure 4.5 E), which indicates a poor illite crystallinity of near-shore sediments.

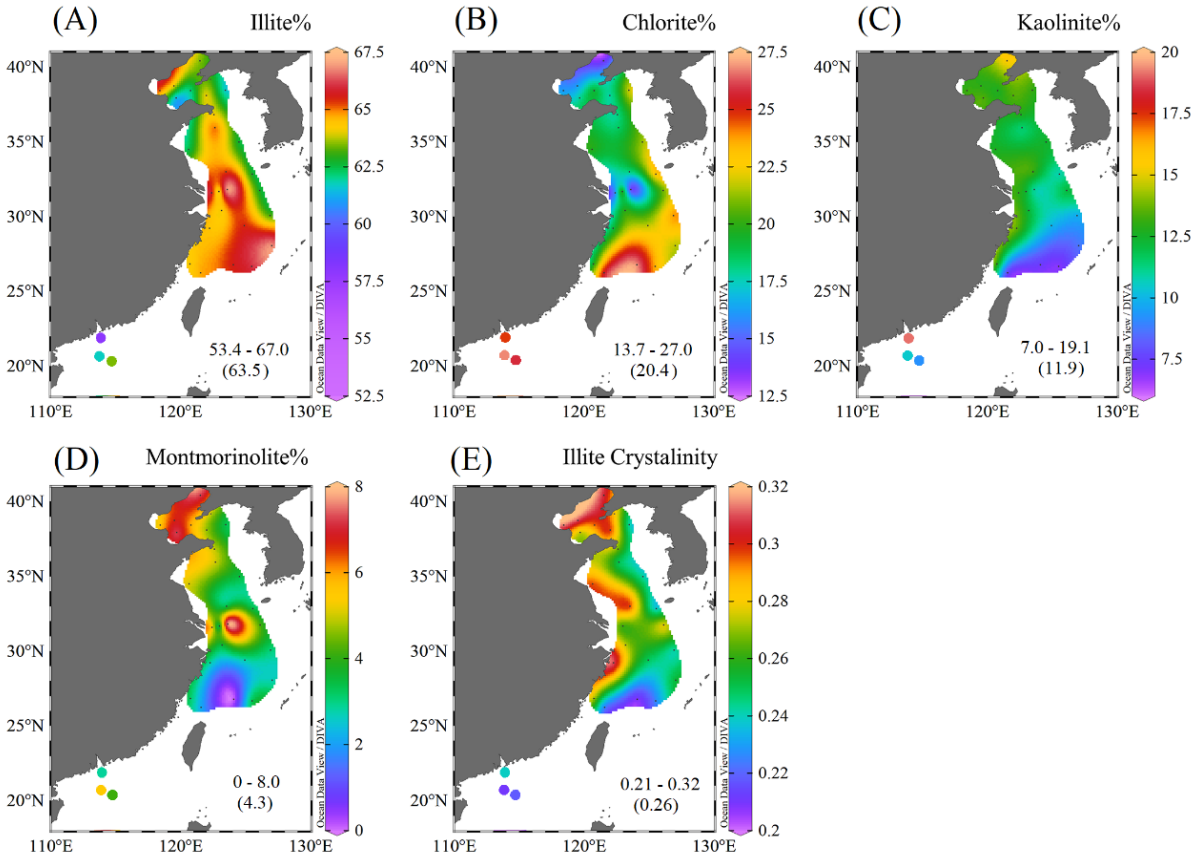

Figure 4.5. The illite% (A), chlorite% (B), kaolinite% (C), montmorillonite% (D) and illite crystaliinity (D) of the seidments. The values in each individual plot represent the ranges of data and the value within the bracket represents average value. The figure was generated using the ODV program (Schlitzer, 2023).

4.3.5. Principal component analysis

Through a PCA measurement, relationships between alkaline extraction parameters and sediment physical and chemical properities were displayed (Figure 4.6). Results showed that sandy sediments were positively related with high sand%, mean grainsize, D [3,2], β_1, detrital% and chlorite content, and muddy sediments were positively related with high clay%, silt%, sediment-specific surface area, *b*, TAlkSi, TAlkAl, TOC%, TN%, $ExtrSi_1$, $bSiO_2$% $CaCO_3$%, β_{lin}, illite crystalinity, illite, montmorillonite and kaolinite content. In addition, the Si:Al ratio of bSi (β_1) was neagtively related to clay mineral (illite, kaolinite and montmorillonite), fine size fractions (clay and silt) and TAlkAl content, whereas the Si:Al ratio of silicate minerals (β_{lin}) has positive relationship with these parameters.

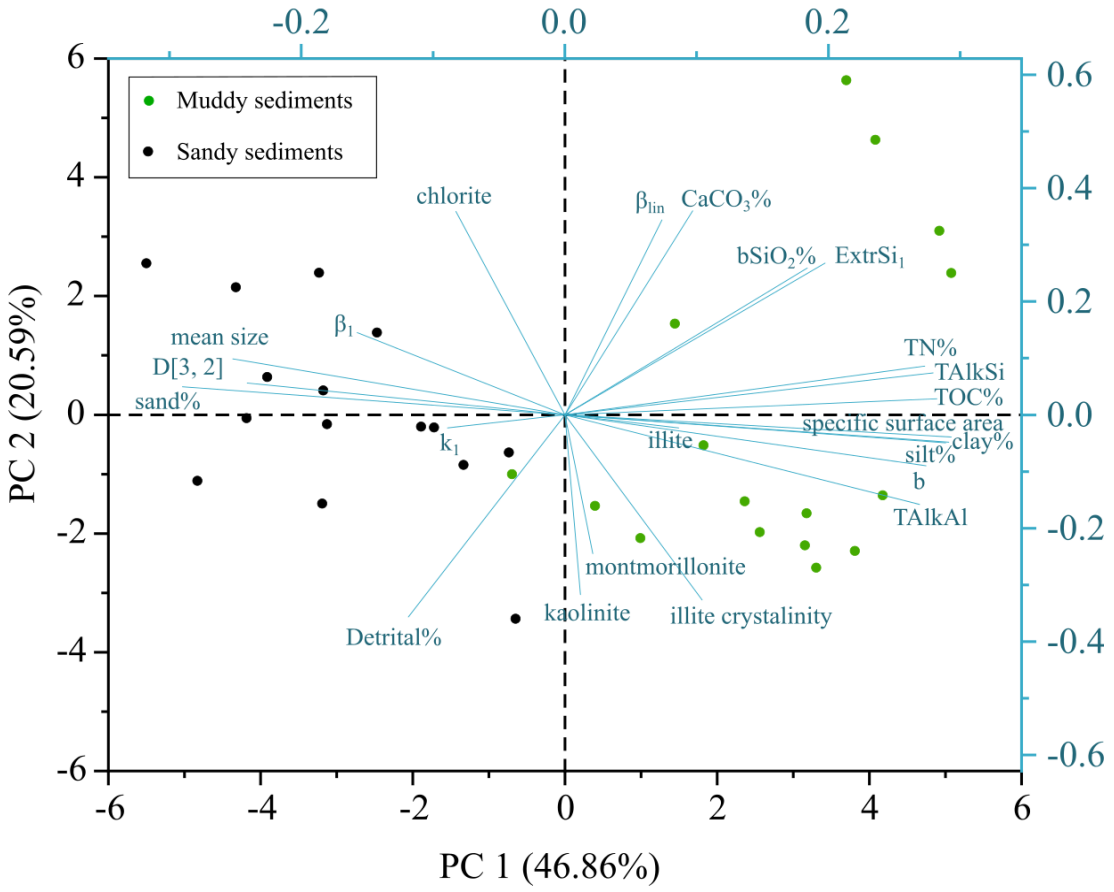

Figure 4.6. Bi-plot of PCA ordination of the determinationed parameters. The symbols in green and black color represent muddy and sandy sediments.

4.4. Discussion

4.4.1. Muddy sediments release more Si and Al than sandy sediments

Sediment samples of this study were grouped as sandy sediment (sand > 50%, SSA < 0.5) and muddy sediment (clay + silt > 70%, SSA > 0.5). The results showed that the alkaline extracted Si and Al from muddy sediments were much higher (> 200%) than the sandy sediments, which indicates muddy sediments as an important Si and Al source to the Chinese marginal Seas. As shown in Figure 4.7, the alkaline extracted TAlkSi, TAlkAl, bSi and silicate minerals from muddy sediments (TAlkSi: 11.85 mg-Si g^{-1}, TAlkAl: 3.62 mg-Al g^{-1}, bSi: 2.63 mg-Si g^{-1} and silicate minerals: 9.22 mg-Si g^{-1}) were 2 to 3 times higher than from sandy sediments (TAlkSi: 2.94 mg-Si g^{-1}, TAlkAl: 1.00 mg-Al g^{-1}, bSi: 0.68 mg-Si g^{-1} and silicate minerals: 2.26 mg-Si g^{-1}). In addition, the alkaline leachable silicate minerals outweigh $bSiO_2$% from both muddy and sandy sediments. A comparison of alkaline leachable Si and Al from different sediment types further confirmed the important role of muddy sediments on Si release. Samples contain more fine-size fractions (< 62.5 µm) released more Si (TAlkSi, bSi and silicate

minerals) and TAlkAl (ANOVA test: $p < 0.001$, Figure 4.8). This positive relationship is due to at least two reasons: 1) high specific surface area (SSA) and 2) species of diatoms in sediments and their cell sizes, and detailed explanations are presented in the following separate paragraphs.

Dissolution of silica (bSi and silicate minerals) in solution is controlled by temperature, pH and surface area of solid particles (Mackenzie et al., 1967; Lerman et al., 1975; Hurd, 1983; Niibori et al., 2000; Dixit and Van Cappellen, 2002; Rickert et al., 2002; Van Cappellen et al., 2002; Cama and Ganor, 2015; Maldonado et al., 2022). Therefore, under a temperature and pH controlled experimental condition, the dissolution kinetics of Si and elements combined with Si (i.e., Al (Gehlen et al., 2002; Koning et al., 2002; Loucaides et al., 2010), Fe (Liao et al., 2023) and Ge (Mortlock and Froelich, 1989; Sutton et al., 2018; Baronas et al., 2019)) are dependent on the SSA of the particles. As shown in Figure 4.6 and Figure S4.2, SSA has a positive relationship with the clay% and silt%, and it is negatively related to the sand% and D [3, 2] surface weighted mean. Therefore, an increased yields of alkaline extracted Si and Al phases from muddy sediments (see Figure 4.7) are due to large SSA.

Another reason that caused an enhanced Si and Al dissolution from muddy sediments is attributed to bSi species and sizes. Several types of bSi (diatom, radiolarian, sponge spicules and phytolith) were found in sediments of the Chinese marginal Sea (Chen et al., 2014; Zhang et al., 2015; Ran et al., 2018; Qu et al., 2020; Zhu et al., 2023). However, phytolith were mainly found in sediments of river estuaries (Ran et al., 2018). Radiolarian tests and sponge spicules were more abundant in sediments of continental slope of the ECS and SCS basin (Chou et al., 2012; Zhang et al., 2015; Zhu et al., 2023). Therefore, diatoms were the major types of bSi in sediments of the continental shelf of the Chinese marginal Seas. Based on the measurement of bSi content in various sediment size fractions and the scanning electron microscopic observations, Wang et al. (2014) found largest $bSiO_2$% in the sediment size fraction of < 16 μm, and the microscopic measurements showed most of the diatoms were nano-diatoms with a diameter smaller than 14 μm (dominant cells diameters: 2 – 14 μm). Thus, we contend that the presence of nano-diatoms in sediment is one of the reasons that caused the positive relationship between $bSiO_2$% vs. muddy sediment. Further, the presence of sponge spicules and radiolarians may affect our interpretations too. There are five samples (filled symbols) characterized by high $bSiO_2$% than other sediments ($bSiO_2$%:TOC% as shown in Figure S4.3 B, slope of TAlkSi vs. TAlkAl as shown in Figure S4.4), indicating better bSi preservation. These samples were located at the continental slope of ECS and NSCS deep water (> 500 m) and contains sponge spicules and radiolarians(Zhang et al., 2015; Zhu et al., 2023). The burial mechanism (accumulation at sediment-water interface) of radiolarian and sponge spicules bSi in different

sediment context and their relationship with OC preservation ($bSiO_2$%: OC%) may be different from diatoms and requires further research.

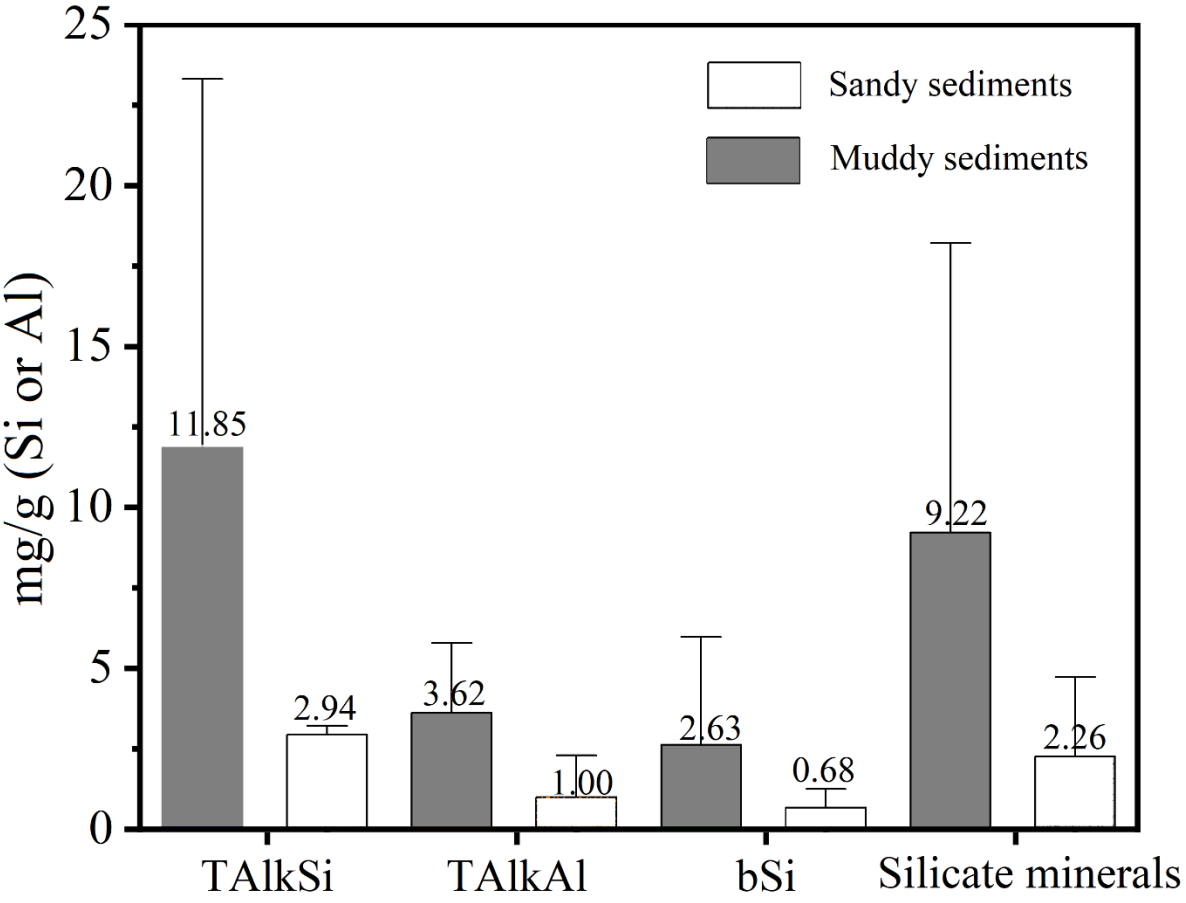

Figure 4.7. Plot of alkaline extracted Si (TAlkSi, bSi, silicate minerals) and Al (TAlkAl) from sandy sediment and muddy sediment. Error bars represent data range with 1.5 IQR (Interquartile Range), and the numbers above bar chart represent mean values.

4.4.2. Al from silicate minerals hindering the dissolution of bSi in sediments

Our results confirm that dissolution (reactivity) of bSi in sediments is hindered by structural incorporation of Al which originate from silicate minerals, and suggest a decreased reactivity of bSi probably cause enhanced opal preservation in muddy sediments of CCMZs. Based on the high-resolution alkaline extraction of Si and Al and the triplicates grain-size measurement data, we found the reactivity (k_1) and Si:Al ratio (β_1) of bSi decrease with the increase of sedimentary SSA (Figure 4.6 and Figure 4.9). The decrease in bSi reactivity in muddy sediments is explained by an increased amount of Al (low Si:Al ratio) incorporated with bSi (Figure 4.9 A, B), because incorporation of Al prevents bSi dissolution (Van Cappellen and Qiu, 1997; Dixit et al., 2001). In addition, previous study used Scanning Electron Microscopy

coupled with an Energy Dispersive Spectrometer (SEM-EDS) to qualitatively measure element distributions at diatom surface and found enriched Al in sedimentary diatom frustules of ECS (Zhu et al., 2023), which further confirms our findings. The decreased bSi reactivity also explains the reason why $bSiO_2$% is higher in muddy sediments than sandy sediments, because lower reactivity assists bSi preservation.

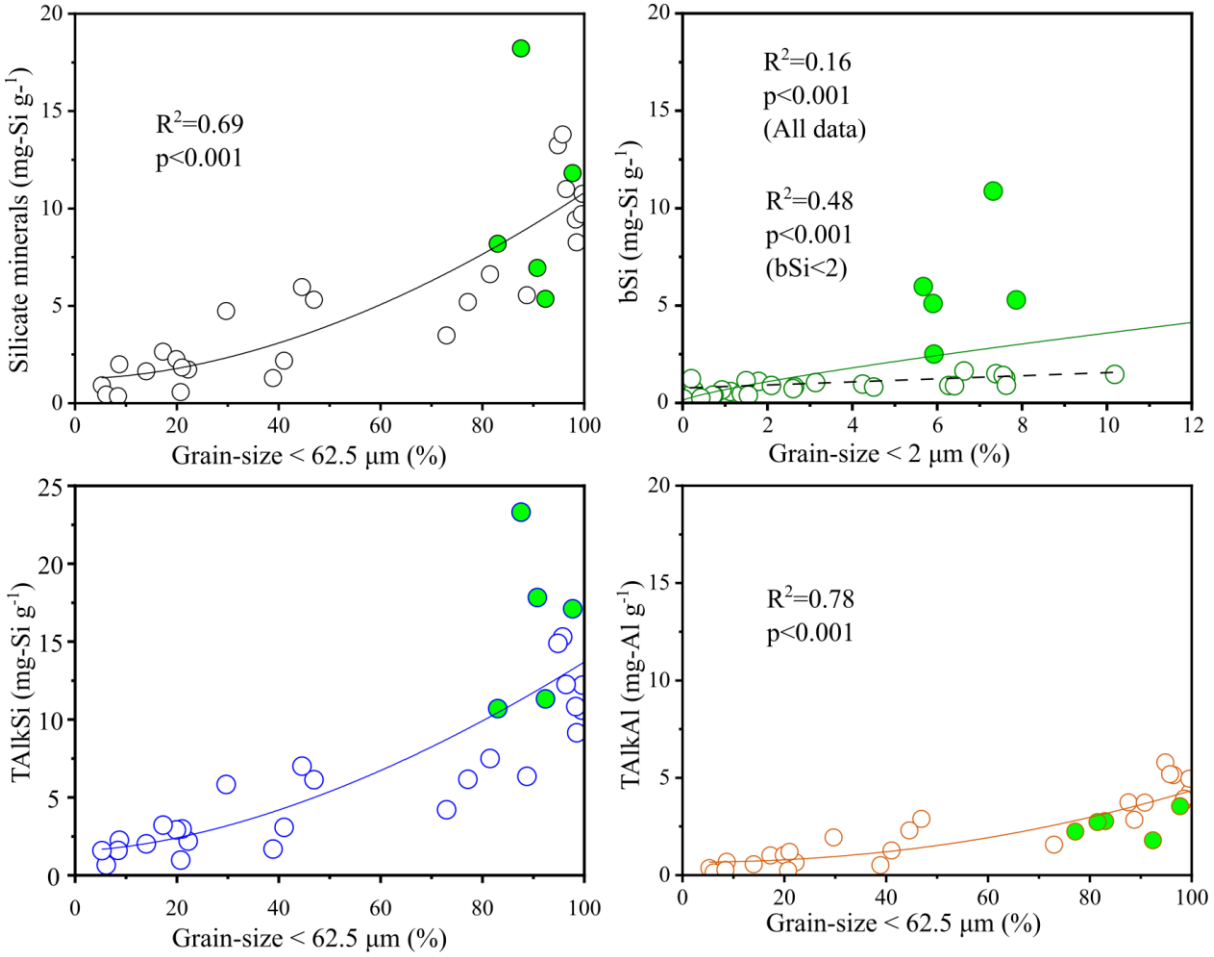

Figure 4.8. Relation of alkaline extracted Si&Al and sediment grain-size content. Samples contain higher percentage of fine grains potentially release more (A) silicate minerals, (B) bSi, (C) TAlkSi and (D) TAlkAl. The dots filled in green color of the plot B are samples from the slope/deep-water depth (see Figure 1: sample C12, D12, DC, F8, NSCS7).

Further, we argue that the Al incorporated with bSi structures mostly originate from silicate minerals of the sediments. Siliceous frustules produced in photic zone contain trace amount of Al (Si:Al > 120 (van Bennekom et al., 1989; Rickert et al., 2002; Koning et al., 2007)), a diagenesis process (such as reverse weathering process, Michalopoulos and Aller, 2004; Ehlert et al., 2012) and diagenetic Al uptake (Ren et al., 2013) starts during the deposition and burial

of bSi which cause elevated Al content of bio-siliceous structures in sediments (Si:Al < 50) (van Bennekom et al., 1989; Van Beusekom et al., 1997; Rickert et al., 2002; Ren et al., 2013). Our results showed high Al (Si:Al < 40, Figure 4.9 B) content in bSi of Chinese marginal Seas' sediments, especially high Al content (Si:Al < 10) of bSi in sediment of high SSA, e.g., muddy sediments (Figure 4.9 B) which is characterized by high dissolution rate of silicate minerals (Figure 4.9 D). Since dAl concentrations in overlying water at sediment-water interface and pore water (> 120 nM (Mackin and Aller, 1984)) are much higher than the in the water column (< 50 nM (Ren et al., 2006; Li et al., 2018; Zhang et al., 2020)) and the residence time of bSi at the seafloor overtake the time of settling from the surface to bottom water (15 – 70 m d^{-1} (Passow, 1991; Ran et al., 2015)). It is, therefore, reasonable to attribute the major source of Al that is incorporated with bSi to silicate minerals dissolution.

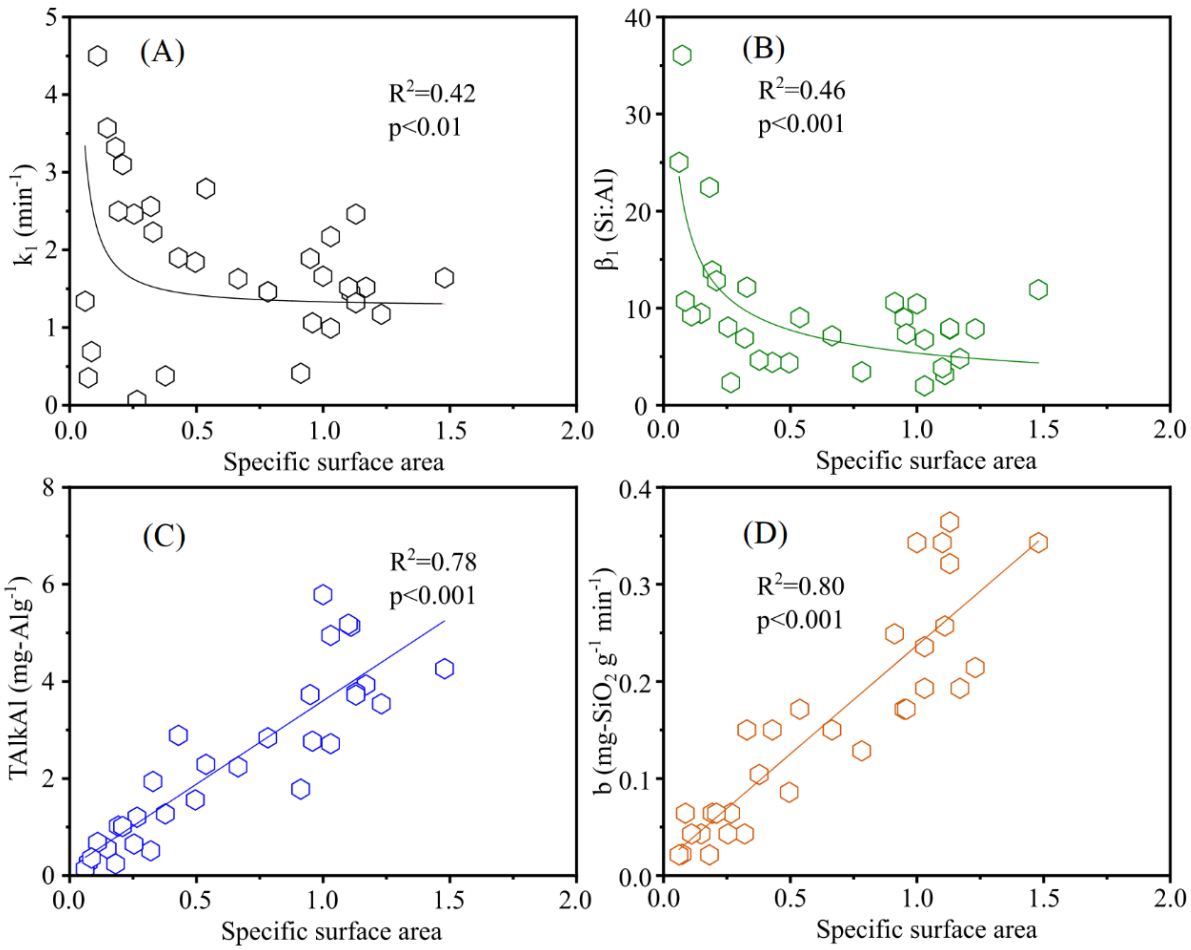

Figure 4.9. Relationship of grain-size specific surface area (SSA) and bSi reactivity constant (A), Si:Al ratio (β_1) of bSi (B), TAlkAl (C), and silicate mineral dissolution rate (b) (D).

4.4.3. Implications of simultaneous alkaline extraction of Si and Al

The simultaneous alkaline extraction of Si and Al proposed by Koning et al. (2002) is widely

applied for differentiating various bio-available Si phases (Barão et al., 2015; Raimonet et al., 2015; Zhu et al., 2023). The definition of the alkaline extracted Si of silicate minerals is based on a slow linear dissolution of clay minerals (illite, kaolinite and montmorillonite), the distinct different Si:Al ratios between bSi (Si:Al > 5) and different clays (Si:Al < 5) allows an accurate measurement of bSi-poor sediments that contain high silicate minerals, e.g., CCMZs of Chinese marginal Seas and the Amazon shelf (Koning et al., 2002).

Previous studies found the Si:Al ratios and the reactivity of bSi is dependent on bSi types, 'ageing' or diagenetic alteration of bSi (Hurd, 1983; Van Cappellen, 1996; Van Cappellen and Qiu, 1997; Dixit et al., 2001; Van Cappellen et al., 2002). Therefore, the reactivity and Si:Al ratio of bSi calculated by non-linear dissolution models cannot be used to compare samples of different depositional environments (Koning et al., 2002). However, the dissolution rate of silicate minerals (b, mg-SiO_2 g^{-1}) in hot alkaline solution is dependent on the SSA of solid particles, and the β_{lin} is dependent on the clay mineral compositions (type and content) of sediments. By comparing with previously published data (Figure 4.10), we found β_{lin} reflects the major types of clay minerals of sediments. For example, the β_{lin} of Congo deep-sea fan sediments (β_{lin} = 1.16 to 1.18, Barão et al. (2015); sediments enriched in kaolinite, Griffin et al. (1968)) are equal to Si:Al ratio of kaolinite (1.10 – 1.18, Kamatani and Oku (2000) and Koning et al. (2002)). The β_{lin} of Angola basin (β_{lin} = 1.90 to 2.15, Koning et al. (2002); sediments enriched in kaolinite and montmorillonite, Griffin et al. (1968)) are within the Si:Al ratio of kaolinite (1.10 – 1.18) and montmorillonite (2.80 – 4.80, Kamatani and Oku (2000) and Koning et al. (2002)). The β_{lin} of Iberian margin sediments (β_{lin} = 2.23 to 2.34, Koning et al. (2002); 80% of illite, Griffin et al. (1968)) are similar to illite (2 – 2.47, Kamatani and Oku (2000) and Koning et al. (2002)). In addition, the clay mineral in sediment of Tokyo Bay is mainly illite (50%) and montmorillonite (40%), which therefore lead to an alkaline extracted Si:Al ration of 2.41 (Kamatani and Oku, 2000), this ratio is calculated from the slope of Si vs. Al plot which may be underestimated. The β_{lin} of the samples from Chinese marginal Seas (β_{lin} = 2 – 3) are within the range of Si:Al ratio illite with exceptions for SCS samples which has higher kaolinite or illite content (Figure 4.10). The reason for this good correlation is because of the high solubility of clay mineral compared with other crystalized silicates (such as quartz and feldspar). Thus, the Si and Al signals of clays can be distinguished even though clay size fraction only represents ~10% of total sample volume. Moreover, the β_{lin} of opal-rich samples (Equatorial Pacific: β_{lin} > 9 (Barão et al., 2015), and particulate bSi sample: β_{lin} = 48 (Koning et al., 2002)) and beach sand sample (Texel, North Sea: β_{lin} = 6.9 (Koning et al., 2002)) are characterized by high Si:Al ratios (> 5) and reasons for the elevated value (normally β_{lin} < 5) was not well

explained. Further studies should check whether it is an artifact caused by inappropriate modeling or due to sediment compositions.

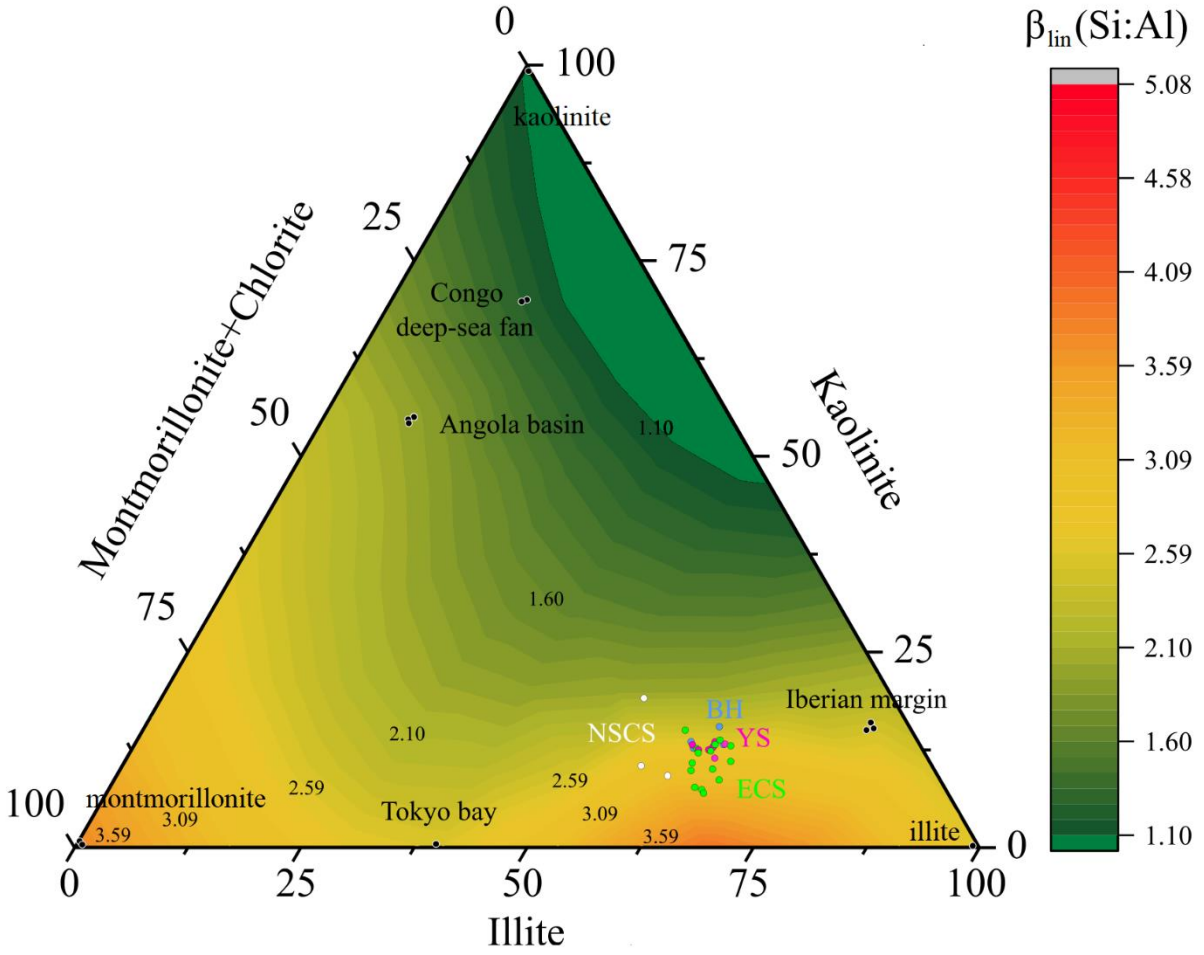

Figure 4.10. Relative clay mineral (illite, kaolinite and montmorillonite+chlorite) content of sediment and the Si:Al ratio of silicate minerals (β_{lin}) calculated from the continuous alkaline extraction of Si and Al. Color bar represents the β_{lin} values. Numbers within the plot are contours claculated based on determined β_{lin}. Data sources of clay mineral composition: 1) Conge seep-sea fan, Angola basin and Ibrtian margin: Griffin et al. (1968); 2) Tokyo Bay: Oinuma and Kobayashi (1966); 2) Clay minerals (illite, kaolinite and montmorillonite): Kamatani and Oku (2000) and Koning et al. (2002). 4) Chinese marginal Seas (BH, YS, ECS, SCS): this study. Data sources of Si:Al ratio of silicate minerals (β_{lin}) from simiutaneous alkaline extraction of Si and Al: 1) Conge seep-sea fan: Barao et al. (2015); 2) Angola basin and Ibrtian margin: Koning et al. (2002); 3) Tokyo Bay: Kamatani and Oku (2000); 4) BH, YS and ECS: Zhu et al. (2023); 5) NSCS: this study. All samples were selected from regions under strong influence of terristrial input and sediments contain high silicate minerals content.

4.5. Conclusion

We conducted simultaneous alkaline extraction of Si and Al in sediments of Chinese marginal Seas and measured the physical and the chemical properties of sediments for understanding the incongruent dissolution of silicate minerals in sediments of CCMZs. Our results demonstrated that more Si (sourced from bSi and silicate minerals) and Al dissolve from muddy sediments than from sandy sediments. Although the dissolution rate of silicate minerals is slower than of bSi, the contribution of silicate mineral to the reactive Si pool overweighs the bSi due to their large quantities, highlighting muddy sediments as an important potential Si source for the CCMZs of Chinese marginal Seas. We found decreased bSi reactivity is correlated with low Si:Al ratios, especially for samples of muddy deposits. The source of Al is likely originating from silicate minerals dissolution. The incorporation of Al into bio-siliceous structures hinders the dissolution of bSi, thus enhances bSi preservation. The preservation efficiency may vary among different types of bSi. Applying continuous alkaline extraction methods can help to understand the differences due to its ability of differentiating Si phases with different rates of dissolution. Further, high-resolution simultaneous extraction of Si and Al combined with non-linear first order dissolution models uncovered dominant clay minerals exists in sediments because of the different chemical characteristics (Si:Al ratios) of various types of clays and will require dedicated studies.

5. Estimating the methodological biases of the global marine biogenic silica burial flux

Abstract

Biogenic silica (bSi), as an important component of marine sediments, is produced mainly by diatoms, radiolarians and siliceous sponges. The burial of bSi on seafloor is corelated to both the surface productivity and carbon storage, thus, it is one of the key processes of the global marine silicon cycle. Accurate evaluation of the global marine bSi burial flux is particularly challenging due to the methodological biases since there is a lack of internationally recognized procedure for measuring the opal content of various sediment types of the world ocean. In order to estimate the methodological biases of the global bSi burial flux, this study examined samples from different marine environments, e.g., sediment of coastal and continental marginal zones (East China Sea, the Congo deep-sea fan and Baffin Bay) and sediments of open oceans (the Southern Ocean, North Atlantic, Equatorial Pacific) using X-ray Diffraction (XRD) method and different wet chemical methods. We also evaluated the Infrared method (IR: including Infrared method and Fourier Transform Infrared Spectrometer method). Our results showed that the $bSiO_2$% determined by XRD method was about 0.5 ($bSiO_2$% > 10%) to 5.5 ($bSiO_2$% < 10%) times higher than that determined by wet chemical method, the $bSiO_2$% determined by IR method was about 10% ($bSiO_2$% > 30%) to 35% ($bSiO_2$% < 30%) lower than the average value that determined by wet chemical methods. The $bSiO_2$% determined following the Mortlock and Froelich (1989) method was significantly higher ($p < 0.05$) than other wet chemical methods, e.g., DeMaster (1981), Koning et al. (2002) and Kamatani and Oku (2000). And the $bSiO_2$% determined following Kamatani and Oku (2000) was significantly lower than that determined by the DeMaster (1981) and Koning et al. (2002). There is no significant difference between the Koning et al. (2002) and DeMaster (1981) method. Based on our results and previously published research, we re-evaluated the global bSi burial flux to 6.7 ± 2.7 Tmol-SiO_2 yr^{-1} which is about 30% lower than previous studies. Our results have important implications for the modern marine Si cycle research because of the large uncertainties of the current marine bSi burial flux which brings out the question of whether the marine Si cycle is at steady state. In addition, our results showed the pretreatment procedure, e.g., grinding and pretreating sediments using HCl and H_2O_2, can cause overestimation of the $bSiO_2$%. Further, a general wet alkaline digestion procedure was proposed for determining the $bSiO_2$% in sediments of various depositional environments.

5.1. Introduction

The marine biogeochemical cycle of silicon (Si) is particularly important due to its intertwined relationship with carbon and nitrogen cycles through the biological pump (Pondaven et al., 2000; Tréguer et al., 2018). Therefore, understanding the marine Si cycle is important for knowing the functioning of the marine biogeochemical cycles. Biogenic silica (bSi) is amorphous silicious structure produced by silicifiers (e.g., diatoms, radiolarians and silicious sponges) that utilize dissolved silicon (dSi) to thrive. Recent studies demonstrate that the exportation of diatoms in future acidified oceans will be enhanced (Tréguer et al., 2018; Taucher et al., 2022), which potentially leads to an imbalanced marine Si steady state. Therefore, as one of the key processes of marine Si cycle, the burial of bSi needs to be accurately evaluated because of its large uncertainties (Tréguer et al., 1995, 2021; DeMaster, 2002, 2019; Tréguer and De La Rocha, 2013; Hayes et al., 2021).

The current estimation of bSi burial flux at open oceans (>1000 m water depth) is based on the bSi content ($bSiO_2$%) determined using several methods, such as wet chemical methods, X-ray diffraction (XRD), Infrared methods (IR, including the frontier transform infrared technique: FTIR) and smear slides method (Hayes et al., 2021). Among the different methods, the wet chemical methods (Eggimann et al., 1980; DeMaster, 1981; Mortlock and Froelich, 1989; Conley and Schelske, 1993; Müller and Schneider, 1993; Landen et al., 1996; Schlüter and Rickert, 1998; Kamatani and Oku, 2000; Koning et al., 2002), XRD (Goldberg, 1958; Eisma and van der Gaast, 1971; Leinen, 1985) and IR (Frohlich, 1989; Vogel et al., 2016; Melucci et al., 2019) are the most well-developed techniques for bSi measurement (Conley, 1998; Vogel et al., 2016; Melucci et al., 2019; Hayes et al., 2021) so far. However, large biases in $bSiO_2$% determined by wet chemical methods, XRD and IR still exist, and these biases were not well evaluated (Hurd and Birdwhistell, 1983; Conley, 1998; Vogel et al., 2016; Melucci et al., 2019). For example, the $bSiO_2$% determined by XRD method outweighs the bSi yields measured by wet chemical methods (Conley, 1998), and comparison of the $bSiO_2$% determined by IR vs. wet chemical method show large offsets (Vogel et al., 2016). In addition, studies that applied the commonly used wet chemical methods adopted varieties of extraction procedures (i.e., types of alkaline solution and alkaline concentrations, sediment/solution ratios and pretreatment procedure) which further generate large standard deviations of $bSiO_2$%, especially for the samples of coastal and continental zones (CCMZs) which contain low opal contents (DeMaster, 1991; Conley, 1998; Liu et al., 2002; Barão et al., 2015; Zhu et al., 2023). Therefore, the methodological biases in $bSiO_2$% can have significant influence on the evaluation of the bSi

burial flux of CCMZs which represents 40% of the global bSi burial (Conley, 1998; DeMaster, 2002; Tréguer et al., 2021).

Several forms of silicates present in marine sediments, including bSi, metal-Si oxides (Si-MeOx), authigenic aluminosilicate (Au-Si: a product of the bSi reverse weathering reaction which includes active and inactive phase) and crystalized silicate minerals (clays, quartz and feldspar) (Michalopoulos and Aller, 2004; Rahman, 2019). Compared with silicate minerals, Au-Si, Si-MeOx and bSi are more soluble and reactive, thus they are defined as reactive Si pool (Michalopoulos and Aller, 2004; Rahman et al., 2016; Pickering et al., 2020). Accurate differentiation of the different Si pools is difficult, because of the physical (X-ray amorphous form) or chemical (Si:Al ratio) properties (Hurd 1983; Pickering et al., 2020; Zhu et al., 2023). Applying the Si/Al wet chemical method (Kamatani and Oku, 2000; Koning et al., 2002) is capable of distinguishing bSi from other reactive Si pool but may underestimate some resistant bSi (radiolarian and sponge spicules) (Zhu et al., 2023). Therefore, a generalized determination procedure for measuring bSi of various sediment types is necessary.

The goals of the present study are to evaluate the methodological biases of the bSi burial flux in the world ocean and to develop a method of broad applicability which can be used to quantify opal content in sediments of various depositional environments. To achieve the objectives, we evaluated multiple methods (XRD, wet alkaline method and IR) by determining the bSi content of different types of sediments (opal-depleted coastal sediments vs. opal-depleted deep-sea sediments, opal-rich deep-sea sediments and sediment contains different types of bSi). The clay mineral interferences and effect of different extraction procedures on bSi measurements were examined. Based on our results and previously published data, we re-estimated the bSi burial flux of the modern ocean.

5.2. Materials and methods

5.2.1. Surface sediments

Figure 5.1 shows the surface sediments (17 samples) collected from various depositional environments of the world ocean. The international calibration sediments (Still Pond and R-64) were collected from Chesapeake Bay (Conley, 1998). D226 is a surface sediment containing mainly calcium carbonate and detrital material (Ragueneau et al., 2001; Gallinari et al., 2002) and was collected from the North Atlantic during the BENGAL research project. ST4 was obtained from Baffin Bay (the Arctic) during the Green Edge Project (Lafond et al., 2019). The sources of clay minerals of Baffin Bay sediments are mainly from the West Greenland shelf and Baffin Island shelves (Andrews, 2019). In addition, diatoms (Lafond et al., 2019) and siliceous

sponges (Baker et al., 2018; Murillo et al., 2018) are dominant bio-siliceous structures in Baffin Bay sediments. Sample MTB-2 was collected by multicores from the Congo deep-sea fan (> 4000 m water depth) in 2011 during the WACS cruise (Rabouille et al., 2016). The Congo deep-sea fan sediments contain high Aluminum (Al) content (van Bennekom et al., 1989) and most of the sediment materials (70%) are delivered by the Congo River (Garzanti et al., 2021). Sample Eq is taken from the central Pacific Ocean during the JGOFS cruise (McManus et al., 1995). Previous studies found abundant radiolarian tests in Equatorial Pacific (Hurd, 1973). Sample B10 was collected from the Bohai Sea where tremendous amounts of sediments were delivered from the Yellow River. Sample A1, F8, DC and C12 were collected from the East China Sea (ECS) which is under the influence of Yangtze River discharge. Information on the samples from the Chinese marginal seas is given in Zhu et al. (2023). Sample H555, F104, 2368G, 2714CQ, MC8B and 3585CQ are surface sediments collected from the Southern Ocean. The ^{14}C age of H555 (surface sediment: < 2 cm core depth) is ca. 8000 yr BP (Cortese and Prebble, 2015). The location (latitude, longitude) and sampling water depth were shown in Table 4.2. The $bSiO_2$% of sample A1, F8, DC and C12 were determined using XRD method, the $bSiO_2$% of sample B10, C12, ST4, Still Pond, R-64, D226, MTB2, H555, F104, Eq, MC8B, 2368G, 2714CQ and 3585CQ were determined by the Si/Al methods (one-hour continuous alkaline extractions, Koning et al. (2002); twenty-four-hour manual extractions, Kamatani and Oku (2000)). Further, kaolinite (chemical formula: $Al_4Si_4O_{10}(OH)_8$) and bentonite (mainly composed of montmorillonite, chemical formula: $H_2Al_2O_6Si$, Sigma-Aldrich) were used to determine the influence of pretreatment (grinding and 1.0 M HCl and 10% H_2O_2) on clay mineral dissolution and bSi determination.

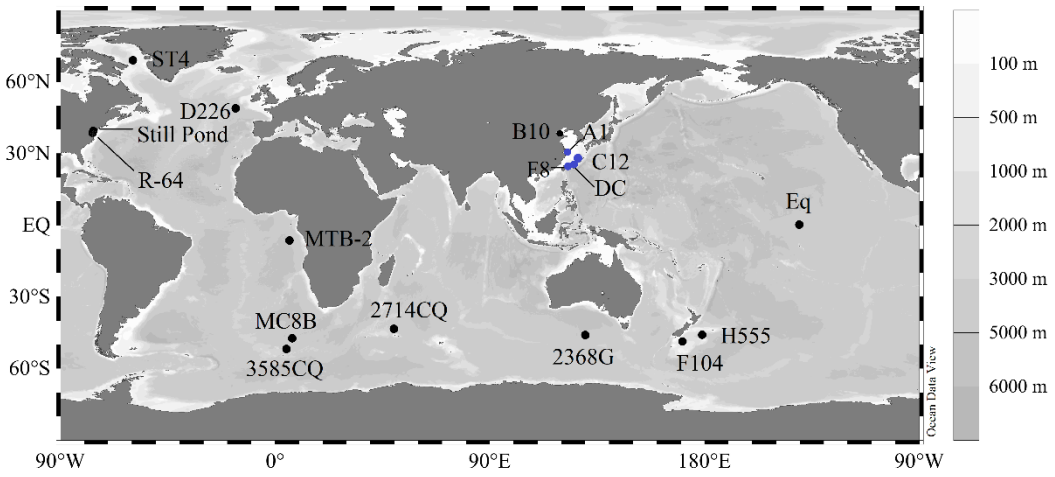

Figure 5.1. Location of surface sediment samples. Figure plotted using the program Ocean Data View (Schlitzer, 2012). The symbol "●" represent samples (A1, F8, DC and C12) determined

using XRD technique, the symbol "●" represent sample determined using wet chemical method. Sample C12 was determined using both methods. The coordinates and water depth of the samples were also present in Table 5.1.

5.2.2. X-ray diffraction measurements

We determined the bSi content ($bSiO_2$%) using the X-ray diffraction method (XRD) following the procedure described by Goldberg (1958) and Leinen (1985). The standard addition method was applied for measuring the $bSiO_2$% in sediments (A1, F8, C12, DC) of the East China Sea, where the opal content is low. The aims of the experiment are to (1) evaluate whether the XRD method can be used for measuring opal-depleted sediment and (2) to test precision of this method. The XRD analysis was carried out at Unité Géosciences Marines, IFREMER, Centre de Brest.

Generally, ~25 g of freeze-dried sediments was pretreated using 1.0 M HCl to remove calcium carbonate ($CaCO_3$), residual sediments were centrifugated at 4000 rpm for 5 min, and the upper clear solution was removed through pipetting carefully. Then residual sediments were washed three times using Mili-Q water (18 MΩ) in order to fully remove HCl from the sediment liquid mixture. Afterwards, the sediments were dried (60 ℃) in an oven overnight. The dried sediments were ground into fine powers (< 2 μm) mechanically. Later, the weighted sediments were mixed with a known amount of decarbonated diatomite (0%, 0.5%, 1.0% and 1.5%SiO_2 dry weight) before combustion (1050 ℃, 4 hours). The area of the resultant 4.04 Å diffraction peak of cristobalite was determined on an X-ray Diffraction Spectrometer (Brucker AXS D8 Advance and Brucker AXS D2 Phaser) at 40 KV and 35 MA, using Cu−Kα radiation over 2θ ranging from 2° to 70° (Goldberg, 1958). The $bSiO_2$% was calculated based on the added $bSiO_2$% (X axis) vs. cristobalite area (Y axis) plot, and the $bSiO_2$% equals to absolute value on X axis where Y is zero.

5.2.3. Wet alkaline extractions

Two Si/Al wet chemical methods, including a one-hour continuous analysis method (Koning et al., 2002; Barão et al., 2015) and a modified twenty-four-hour manual alkaline extraction method (Kamatani and Oku, 2000), were performed. Both digestions were displayed using hot (85℃) 0.5M NaOH solution. The procedures of the continuous analysis method were described in Barão et al. (2015) and Zhu et al. (2023). In general, homogenized sediments were weighed and placed into a preheated stainless-steel vessel filled with 180 mL of 0.5M NaOH solution. A rotating blade connected with a metallic cover was placed in the vessel for homogenizing the sediment-solution mixture and keeping a constant sample to solution ratio (S/L). The S/L is

0.41 (g/L) in average (Table S5.1) and the sampling resolution is 1 second (s). The manual extractions were displayed within a fluorinated ethylene propylene (FEP) centrifuge tube. Homogenized sediments were placed in the tube, then 40 mL of alkaline solution was added and well mixed with the samples. The S/L for the manual extraction is 1.26 (g/L) on average (Table S5.1). Sub-samples were obtained at 1, 2, 3, 4, 5, 6, 7, 8, 20, 24 h. The dissolved Si (dSi) was determined following the molybdate-blue method (Grasshoff et al., 1983) using a spectrophotometer as described in Zhu et al. (2023). The dissolved Aluminum (dAl) was determined following the fluorometric method (Hydes and Liss, 1976). The determination of regent blanks corresponds to the baseline of the measurements. Detailed explanation of dSi and dAl measurements were described previously (Barão et al., 2015; Zhu et al., 2023). To examine the influence of pretreatment procedure (using 1.0 M HCl, 10% H_2O_2) on bSi determination, controlled experiments of pretreated and non-pretreated clay (kaolinite and bentonite) and marine sediments (C12 and B10) were performed. In addition, gently mixed sediment and finely ground sediment (C12) were digested for studying the influence of grinding procedure on Si dissolution.

5.2.4. Analytical procedures for Si and Al data

The alkaline extractions in the continuous analysis procedure and the manual extraction procedure provide dSi and dAl concentrations through time at one-second (s) resolution and one hour (h) resolution, respectively. The unit of parameter t in the model (Eq.4.1) was normalized into minutes (min). The $bSiO_2$% was calculated following the models (model 1: i = 1, model 2: i = 2, model 3: i = 3) as shown in Eq.4.1 using the Origin 2021b software. For comparison, the $bSiO_2$% was also calculated using SiO_2%:Al_2O_3% ratio (Eq. 5.1) according to Kamatani and Oku (2000).

Here, Si_{aq} and Al_{aq} are the concentrations of dSi and dAl in mg L^{-1}, in the reaction vessel at time t (min). $ExtrSi_i$ is the initial extractable silica present in the vessel in mg L^{-1}, k_i is the reactivity constant (min^{-1}) of no-linear dissolving phases and β_i is the atomic ratio of Si and Al released during the dissolution of extractable silica fraction. b (mg-Si g^{-1} min^{-1}) represents the constant dissolution rate of Si from clay minerals and β_{lin} is the Si/Al ratio in the lithogenic fraction. Normally, several alkaline extractable Si ($ExtrSi_i$) phases exist, the biogenic Si phases are distinguished with high Si:Al ratio (Si μM: Al μM > 5) (Koning et al., 2002; Barão et al., 2015). Further, the total amount of alkaline extracted Si (TAlkExSi, mg-Si g^{-1}) and Al (TAlkExAl, mg-Al g^{-1}) equal to the average value determined during the last minute. An optimum model was selected by applying a likelihood statistical analysis (see Eq.2.4)

(Armstrong et al., 2002; Moriceau et al., 2009; Zhu et al., 2023).

The extracted SiO_2% and Al_2O_3% at each one-hour digestion interval was calculated following the equations: Eq.5.1. Where SiO_2% and Al_2O_3% represents extracted silica and aluminum oxide content through time (1 to 24 h), λ is the constant value which represents $bSiO_2$% (Eq.5.1) and α represents the slope of SiO_2 vs. Al_2O_3 plot (Kamatani and Oku, 2000).

$$SiO_2\% = \alpha * Al_2O_3\% + \lambda \quad (5.1)$$

5.2.5. Scanning electron microscope (SEM) and optical microscopy

The siliceous organisms in the sediment samples were imaged using Scanning Electron Microscopy (SEM; JCM-7000 NeoScope™ Benchtop SEM and Hitachi TM4000). Typically, the bio-siliceous tests were handpicked under a stereomicroscope and mounted on an adhesive carbon tab (Leit) using a brush. The carbon tab was pasted on pin stubs and coated with gold (Cheize et al., 2019). Then samples were placed in the equipment and imaged under high vacuum mode. Microscopy observations were applied for determining the bSi types in sediments. In this study, an inverted microscope (Zeiss Axio Observer A1) at 10X magnification was applied (Zhu et al., 2023).

5.2.6. Biogenic silica burial flux

Calculations of the burial flux of bSi is expressed as $F_b = C * w$, where F_b represents the burial flux of bSi, C represents the bSi content (mol g^{-1}), w represent sediment mass accumulation rate (g cm^{-2} yr^{-1}). Sediment mass accumulation rate (SMA, g cm^{-2} ky^{-1}) data were from Hayes et al, (2021) which is based on global data set of ^{230}Th-normalized fluxes, the unit of SMA was normalized as g cm^{-2} yr^{-1} later. The sediment mass accumulation rate of the Chinese marginal seas was based on previously published ^{210}Pb results. To better evaluate the bSi burial flux in the global ocean, we adopted the burial flux calculation approach proposed by Hayes et al, (2021). In general, the $bSiO_2$% data collected from previously published research and the data analyzed in this study were grouped into different marine regions according to biogeochemical provinces (56 provinces) proposed by Longhurst et al. (1995). These biogeochemical provinces were specified from regional oceanography and by examination of the chlorophyll fields. The bSi burial flux (Tmol-Si yr^{-1}) at each province was calculated as: area (km^2) * opal flux (mol-Si km^{-2} yr^{-1}). In order to evaluate the methodological bias of the global bSi burial flux, a new estimate of the bSi burial using the corrected $bSiO_2$% was compared with the recent estimate by Hayes et al. (2021).

5.3. Results

5.3.1. Major types of biogenic silica

The main types of bSi varied among sediments (Table 5.1). Sample B10, D226 and 3585CQ contain mainly diatoms. Sample MC8B, 2714CQ contain mainly diatoms and radiolarians, and the numbers of radiolarian tests are more abundant than diatoms in 2714CQ. Sample ST4, Still Pond, R-64, MTB-2 and 2368G contain mainly diatoms and sponge spicules, and sample C12, H555, F104 and Eq contain diatoms, radiolarians and sponge spicules. As shown in Figure 5.2, the shapes, sizes and numbers of bio-silicious individuals varied among the sample C12, Eq, 3585CQ and R-64. The numbers of bSi structures in sample C12 (from ECS) is rare. The numbers of bSi tests in sample 3585CQ (from Southern Ocean) were abundant and numbers of diatom frustules outweigh the numbers of radiolarians (Figure 5.2). Further, according to the types of bSi observed in sediment, the samples used in this study were grouped as (1) diatom type sediments and (2) other type (diatom and radiolarian; diatom and sponge spicules; diatom, radiolarian and sponge spicules) sediments.

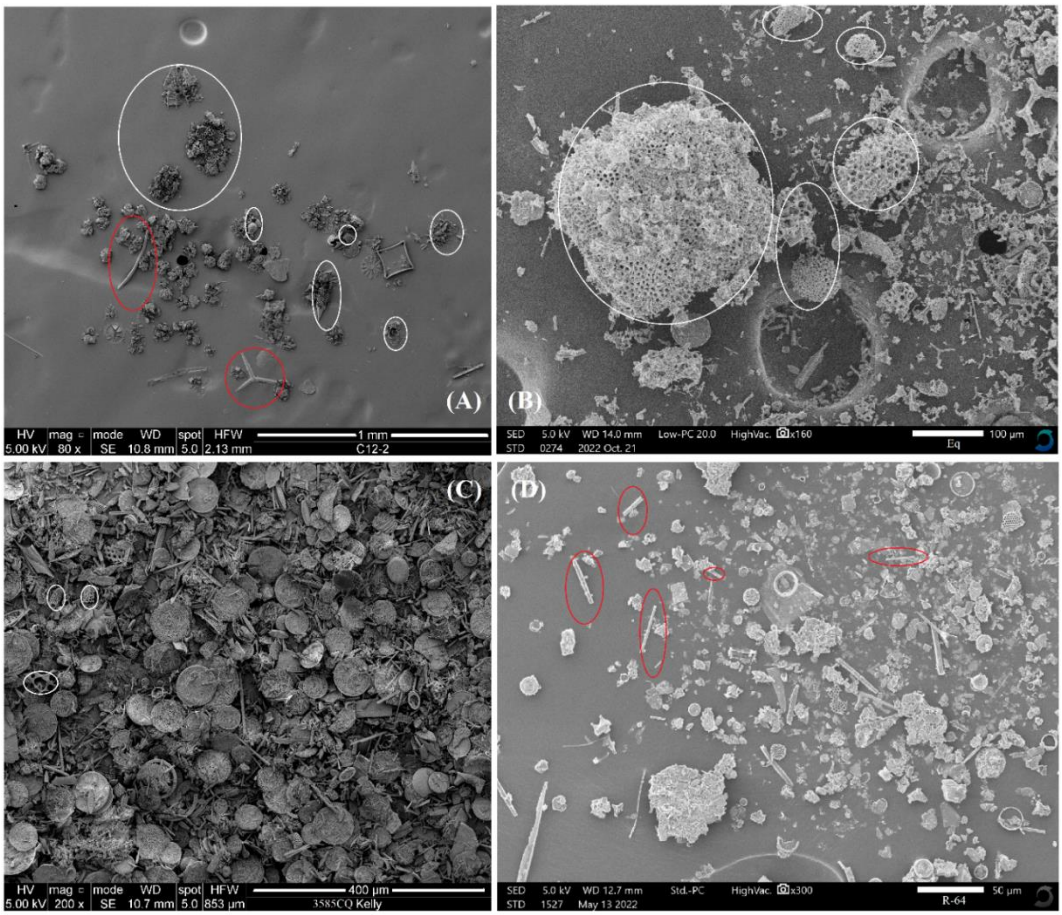

Figure 5.2. SEM images show the bio-siliceous structures in sediments. (A): C12, (B): Eq, (C):

3585CQ and (D): R-64. Red circle: sponge spicules, white circle: radiolarians. Note that phytolith tests were observed in R-64 but they were not marked with the image.

5.3.2. Evaluating the $bSiO_2$% by X-ray diffraction

The $bSiO_2$% (< 3%) of the East China Sea sediments are close to the lower limit of detection for XRD method (Goldberg, 1958) and are lower than the determination limit (< 10%) reported by Eisma and van der Gaast (1971) and Hurd (1983). As shown in Figure 5.3, the area of cristobalite spectra of the sample is small but increases slightly due to the addition of purified diatomite. After calculation, the cristobalite area of the samples used in this study were < 0.1 (Figure 5.4). Triplicate analysis results of sample DC, C12 and A1 has shown large standard deviations (large error bars as shown in Figure 5.4). The $bSiO_2$% was 1.89%, 2.09%, 4.66% and 6.84% of DC, A1, C12 and F8, specifically.

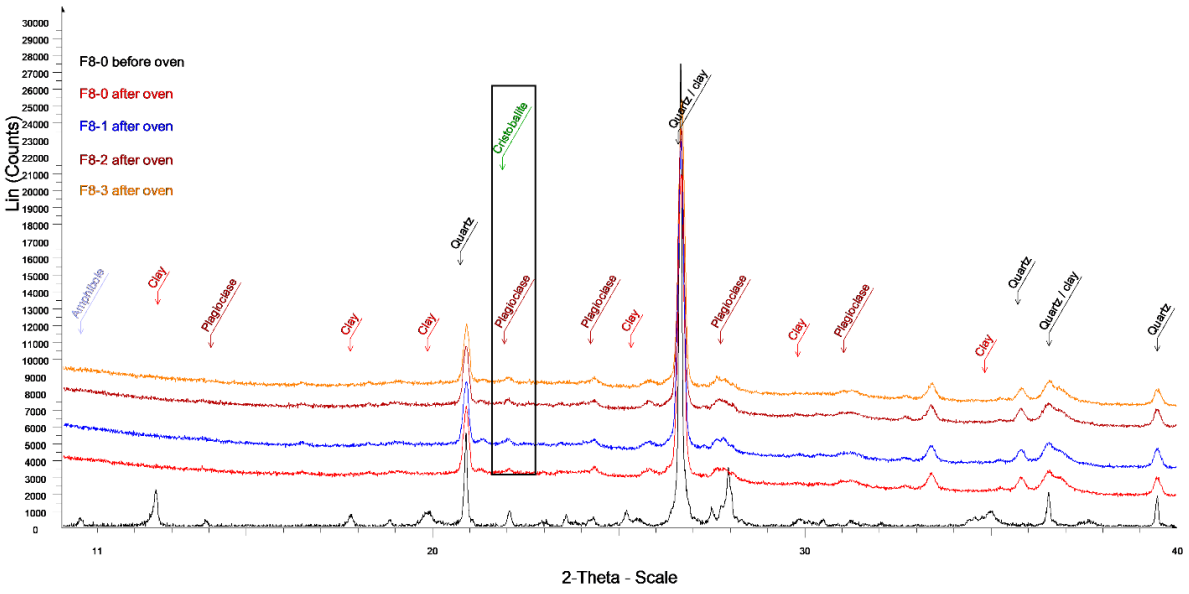

Figure 5.3. Example (sample F8 from the East China Sea) of X-ray diffraction measurement. The area of the cristobalite was calculated for determining the quantity of $bSiO_2$% in sediments. The area of cristobalite is small due to the sediments used in this study.

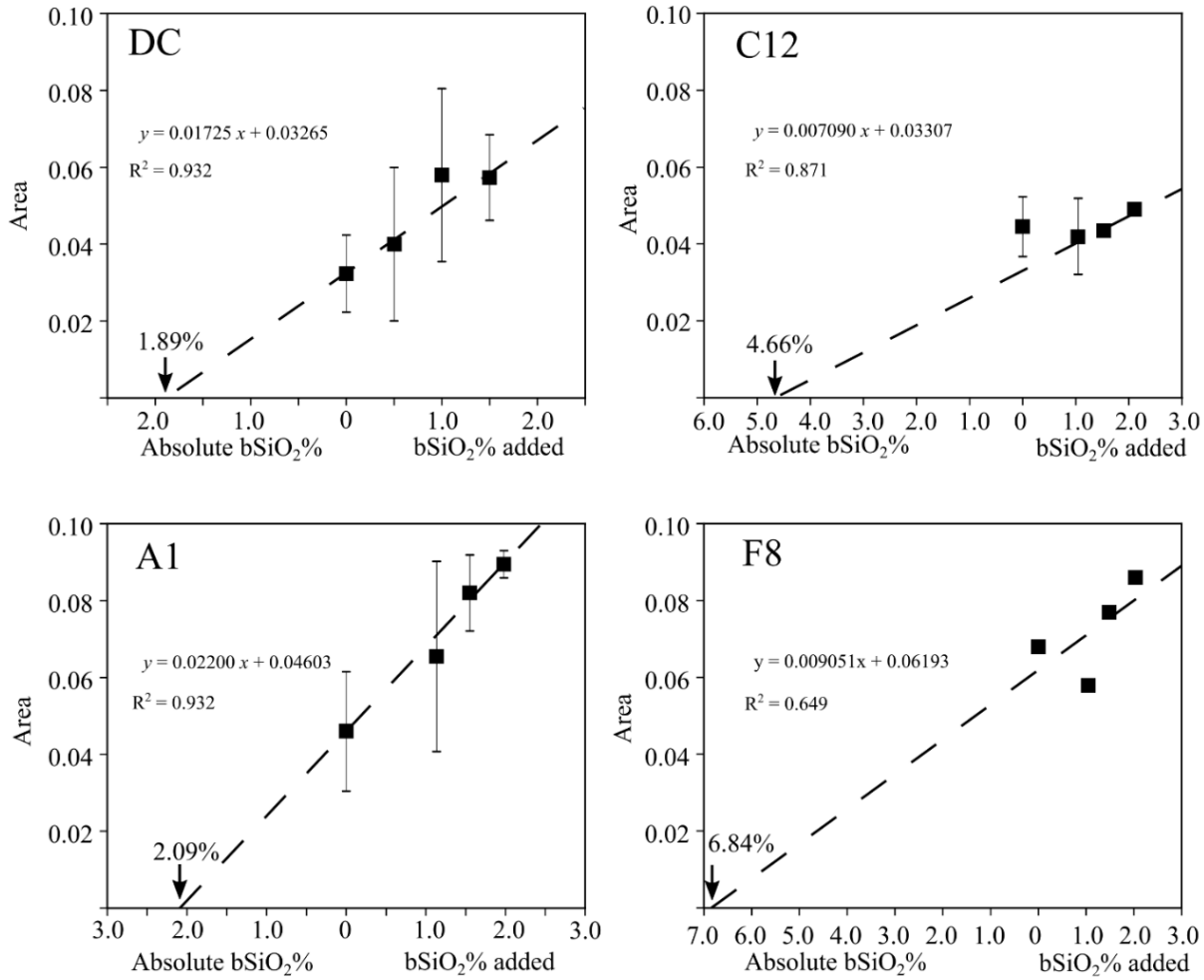

Figure 5.4. Biogenic silica content ($bSiO_2$%) of East China Sea sediments that were determined using XRD method. Error bars represent one standard deviation based on measurement of triplicate samples.

5.3.3. Evaluating the $bSiO_2$% using two Si/Al Methods

The $bSiO_2$% were determined using two Si/Al methods, because the one-hour alkaline extraction using 0.5 M NaOH does not allow complete extraction of silica, so that radiolarians, sponge spicules and even diatoms were noticed in the sediment residuals. An eight-hour digestion is capable of digesting most of the bi-siliceous tests and nearly all bSi were completely digested after 24 h. Results of the extractions and optimal estimation of the $bSiO_2$% are presented below.

5.3.3.1. One-hour continuous extractions

The continuous analysis method is an efficient wet chemical method which extract sediment for short period of time (< 1.5 h, Figure 5.6) (Koning et al., 2002). A relative flat “plateau” of extracted Si and Al dissolution curve was reached for sample MC8B, Eq, R-64 and 3585CQ,

whereas the extracted Si and Al continue to increase through time for other samples (C12, B10, ST4, F104, H555, 2368G, D226, Still Pond, MTB2 and 2714CQ) (Figure 5.5). The extracted SiO_2% was high in sample R-64 (9.87%), MTB2 (9.13%), 2714CQ (19.40%) and 3585CQ (65.29%). Additionally, the extracted Al_2O_3% of sample C12 (0.66%), B10 (0.96%), D226 (0.81%), Eq (0.47%), Still Pond (0.90%), R-64 (1.50%), MTB2 (2.64%) and 3585CQ (0.57%) were high, extremely low extracted Al_2O_3% was found in sample F104 (0.03%), the extracted Al_2O_3% ranged from 0.10% to 0.30% in other samples (Figure 5.5). According to the first order non-linear fit, sample B10, C12, Still Pond and R-64, ST4, MTB2, H555, 2368G were fitted with Model 2. The optimum model for samples D226, F104, Eq, MC8, 2714CQ and 3585CQ is Model 1 (Table 5.2). Non-linear fitting of sample F104, Eq, MC8B, 2714CQ and 3585CQ was difficult due to relative low Al content (TAlkExAl = 0.18−2.91 mg-Al g^{-1}) compared with Si (TAlkExSi = 1.48−314.64 mg-Si g^{-1}). Generally, the first fraction detected ($ExtrSi_1$) was consistently more reactive (k_1 = 0.15−2.24) than the second fraction ($ExtrSi_2$, k_2 = 0.05−0.18) (Table 5.2). The Si:Al ratio (β_i) of first Si fraction is higher than the second fraction and lSi ($\beta_1 > \beta_2 > \beta_{lin}$). In addition, the bSi contribution to the TAlkExSi is low (bSi: TAlkExSi < 31%) for B10, C12 and F104, and is high (bSi: TAlkExSi > 50%) for other samples (Table 5.2). The calculated $bSiO_2$% was shown in table 5.2.

Further, sediment residuals were daubed evenly on a smear slide and observed under microscope for determining whether the digestion of bSi was complete. For most samples, sponge spicules and radiolarian tests were noticed, and diatoms were found in the residual of sample 2714CQ and 3585CQ. Complete digestion of bSi was only noticed for sample B10 and D226 which contain low bSi content and single type of bio-siliceous structure (i.e., diatom) (Table 5.1).

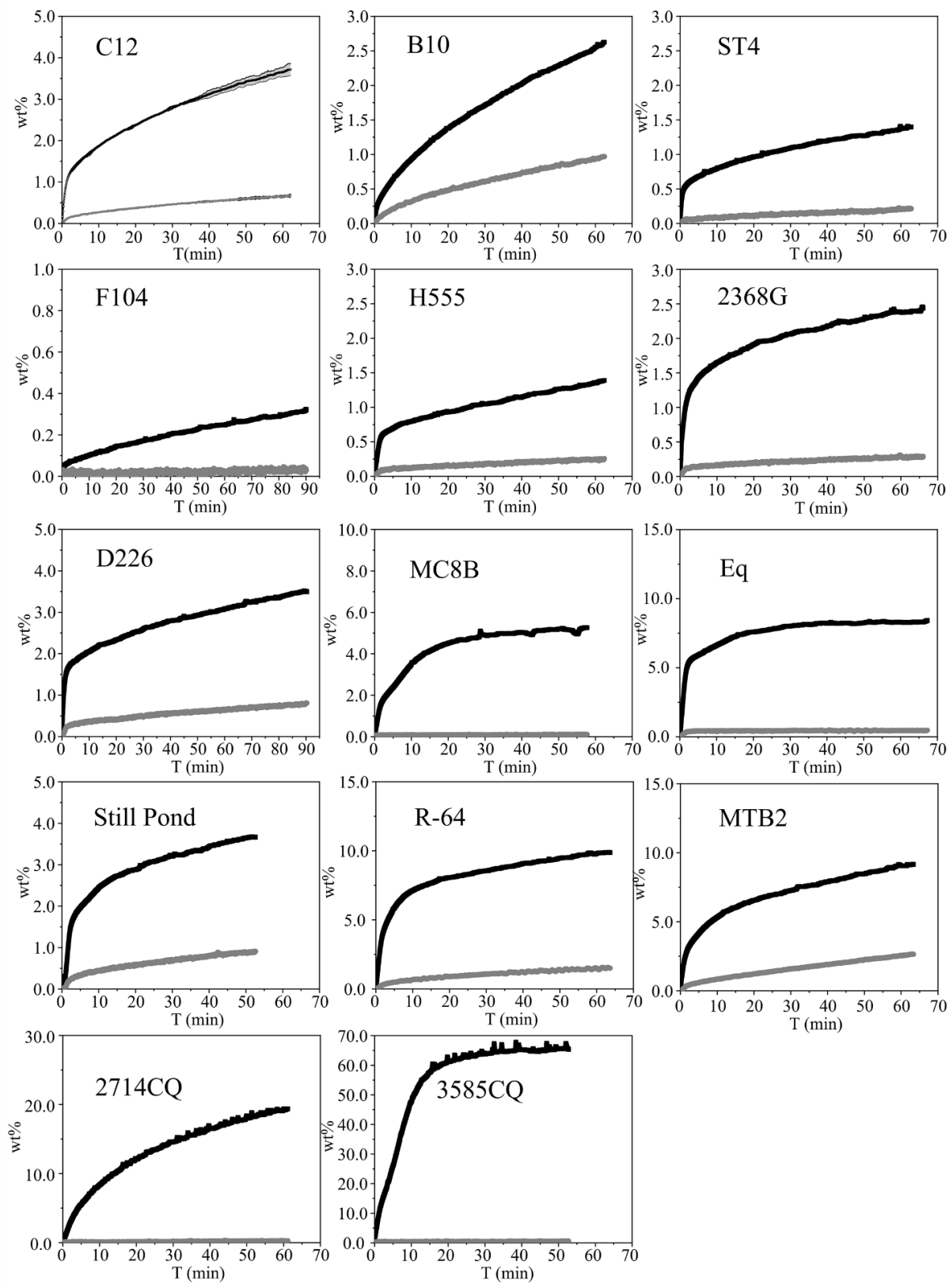

Figure 5.5. Extracted SiO_2% (lines in black color) and Al_2O_3% (lines in grey color) using 0.5 M NaOH solution following the continuous alkaline extraction procedures. The duration of the extraction was about one hour. Note the different scales on the Y axis.

5.3.3.2. Twenty-four-hour manual extractions

The twenty-four hours alkaline digestion aims to completely extract all bSi structures. The extracted SiO_2% and Al_2O_3% continue to increase through time for most samples and only sample 2368G, MC8B, 2714CQ, Eq and 3585CQ reached a relative constant concentration after one-hour digestion (Figure 5.6). High extracted SiO_2% (> 10%) were found for sample R-64, MTB2, 2714CQ and 3585CQ, and high extracted Al_2O_3% (> 2%) were found for sample B10, Still Pond, R-64 and MTB2 (Figure 5.6). According to the first order dissolution model, all samples were fitted with Model 1, representing one non-linear dissolving Si fraction. The reason why only model 1 was fitted successfully is due to the limited data (10 data points for dSi and dAl). Radiolarians and sponge spicules were noticed in the sediment residuals after 8 hours digestion, then 24 hours digestions were applied for extract all bSi (Table 5.1). Therefore, the calculation of the $bSiO_2$% was also based on the fact of whether the complete digestion of bSi was reached. Note that a few pieces of radiolarian fragments were found in sample F104 and 2714CQ (Table 5.1), but quantity is negligible. Details of the dissolution of radiolarian were shown in Figure 5.7.

The parameters of the non-linear fit of the dSi and dAl were shown in Table 5.3. In general, the TAlkExSi (3.52 ± 283.99 mg-Si g^{-1}) content is higher than TAlkExAl (0.85 ± 41.19 mg-Al g^{-1}). The reactivity (k_1 = 0.004−0.006 min^{-1}, excluding sample 3585CQ) of bSi and dissolution rate (b = 0.001−0.030 mg-Si g^{-1} min^{-1}) of lSi from the manual analysis (see Table 5.3) were one to two orders of magnitude lower than the continuous analysis (see Table 5.2). Other parameters, such as TAlkExSi, TAlkExAl, β_1 and $bSiO_2$%, were comparable to the continuous digestions. The calculations of $bSiO_2$% (Eq. 5.2) following Kamatani and Oku (2000) showed that α values are time dependent (Table 5.4) and should be used with caution, because negative $bSiO_2$% were obtained based on the calculations. For example, the $bSiO_2$% calculation is difficult for sample F104, Eq and 3585CQ, because of the negative λ or α values (Table 5.4). Therefore, calculations of the $bSiO_2$% were adapted to different alkaline digestion time (5 h, 8 h and 24 h Table 5.4). And the best estimate of the bSi yield (see Table 5.4) was achieved based on microscopic observations. For a methodological comparison, the $bSiO_2$% was also calculated based on a linear regression of the SiO_2% vs. time plot (DeMaster, 1981) and a single measurement of the $bSiO_2$% at 5 h (Mortlock and Froelich, 1989) which are shown in Table 5.4. Generally, the bSi yields determined following Mortlock and Froelich (1989) were higher than DeMaster (1981) and the Si/Al method (as described by Kamatani and Oku (2000)).

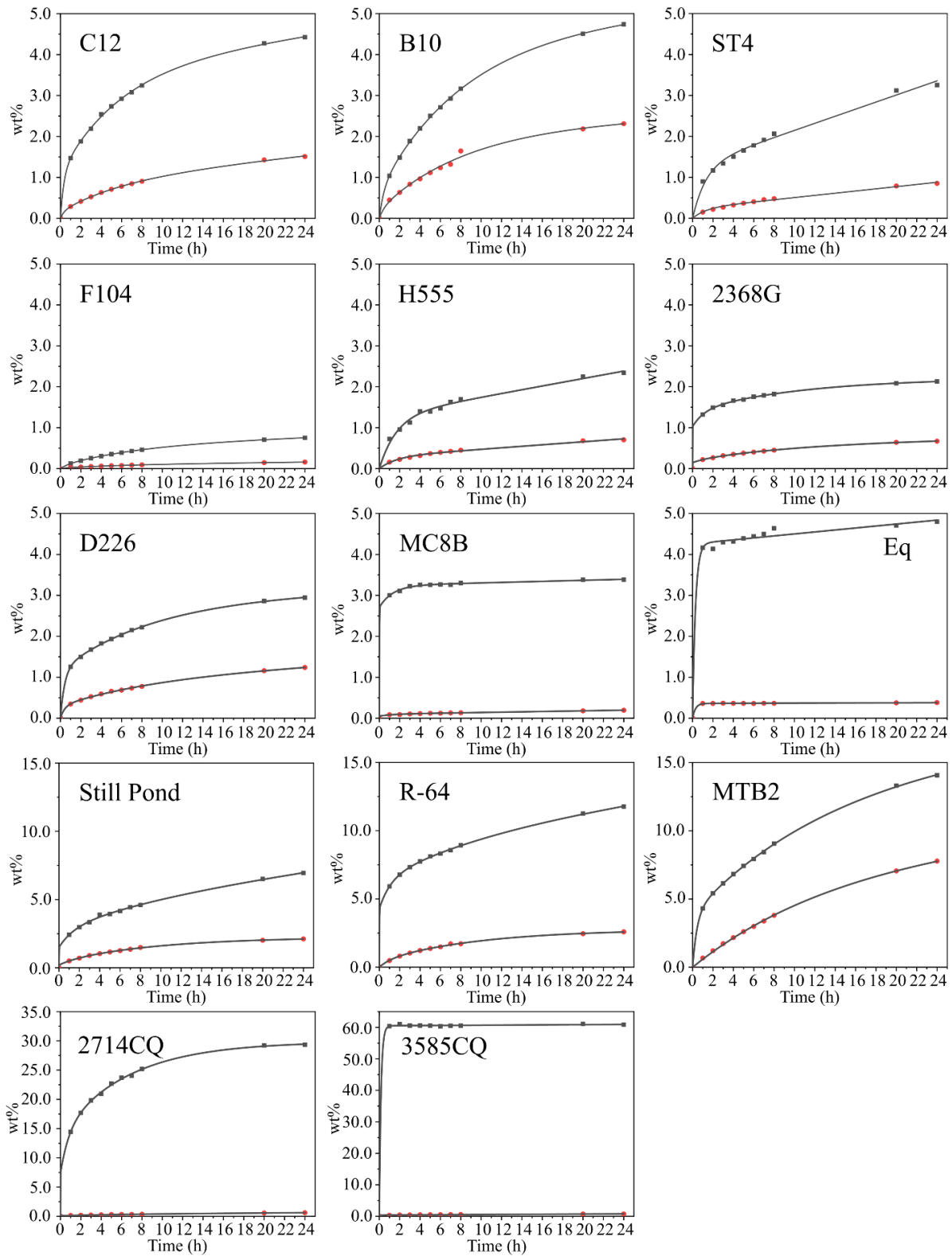

Figure 5.6. Extracted SiO_2% (symbols in black color) and Al_2O_3% (symbols in red color) using 0.5 M NaOH solution following the manual alkaline extraction procedures. The duration of the extraction was 24 h aiming to dissolve bSi completely. Note the different scales on the Y axis.

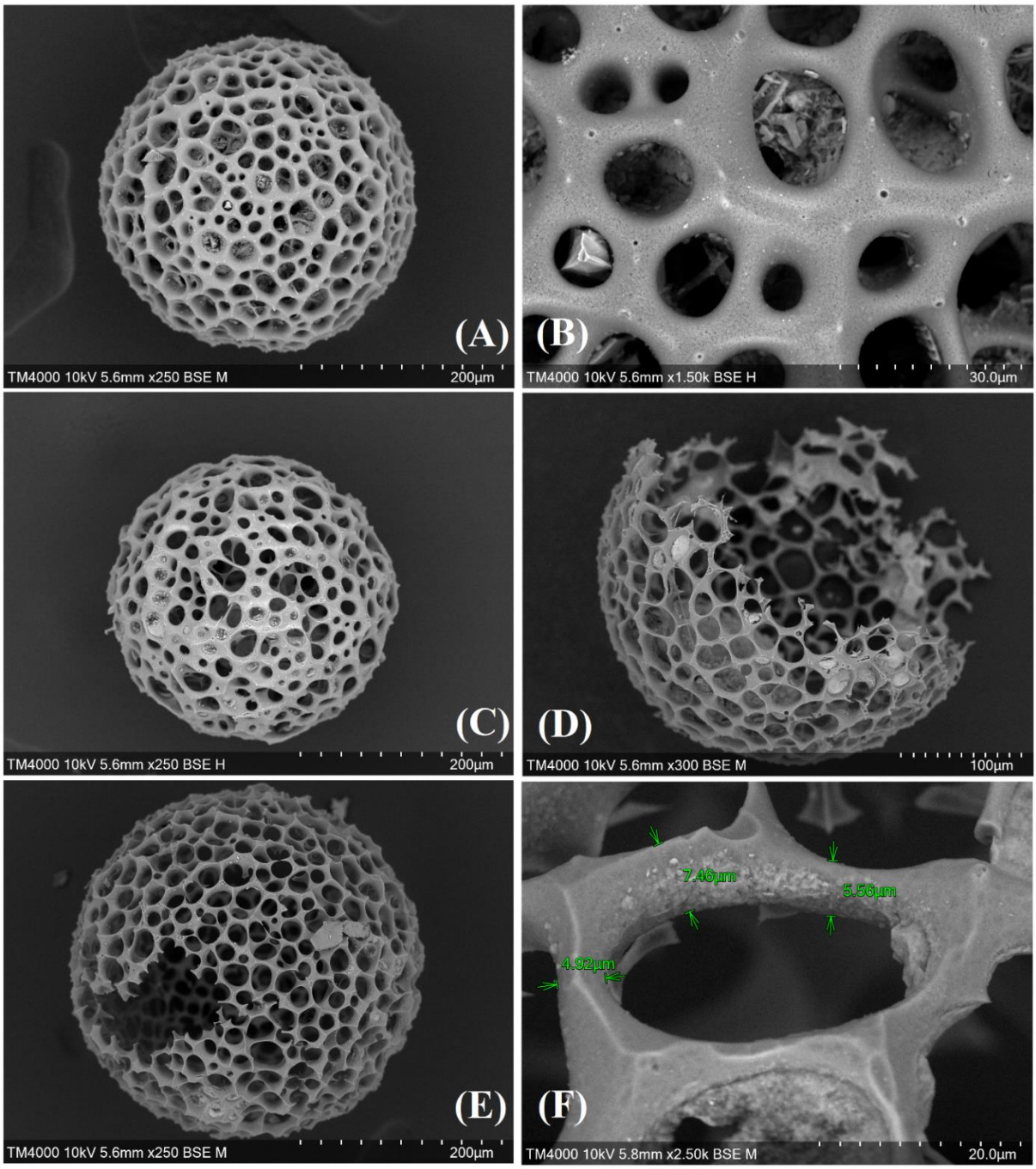

Figure 5.7. Radiolarian tests extracted in 0.5M NaOH for 20 min (A, B), 5 h (C, D) and 10 h (E, F). A and B are the same radiolarian individual showing a partly extraction of both silicious structures and internal filler (diatom frustules); C and D are two radiolarian individuals, the internal fillers were fully extracted after 5 h; E and F are the same radiolarian test, the SEM image shows larger diameter for clay coated structure than the un-coated (F).

5.3.4. Alkaline extractions of pretreated sediments

5.3.4.1. Extracting the HCl and H_2O_2 pretreated samples

The pretreatment using HCl (1.0 M) and H_2O_2 (10%) leached little amount of SiO_2 (<

0.1%SiO_2) and Al_2O_3 (< 0.15% Al_2O_3) from sediments but this process can enhance the solubility of silicate significantly. Alkaline extractions showed enhanced dissolution of SiO_2% and Al_2O_3% from pretreated samples (kaolinite, bentonite and bulk sediments), and both linear regression calculations and modeling parameters confirmed more important influence of pretreatment on sediments than crystalized clays (kaolinite and bentonite).

As shown in Figure 5.8, alkaline extracted SiO_2% and Al_2O_3% of the pretreated kaolinite, bentonite, C12 and B10 were higher than the non-pretreated samples. The increased alkaline extracted SiO_2% and Al_2O_3% were more important for samples C12 and B10 than the clays (bentonite and kaolinite). The slope of SiO_2 vs. Al_2O_3 plot represents the relationship of the two components in alkaline solution. The α value for kaolinite (P: 1.24, NP: 1.22), bentonite (P: 2.64, NP: 2.65) is constant, but the α value increased in the pretreated B10 (P: 3.15, NP: 1.96) and C12 (P: 4.17, NP: 2.36). In addition, α values of non-pretreated B10 and C12 (< 3) are similar to bentonite and kaolinite. Calculations based on SiO_2 vs Al_2O_3 plot showed negative intercept values for kaolinite (P: -1.16%, NP: -0.53%) and the B10 (P: -0.49%), implicit excess Al leached from the samples.

5.3.4.2. Extracting finely ground sediments

To evaluate the effect of grinding on bSi measurement, the pretreated and non-pretreated sediments (both finely ground (FG) and non-ground (NG) sediments) were extracted in 0.5 M NaOH. As shown in Figure 5.9A, the extracted SiO_2 and Al_2O_3 from FG sediment were higher than the NG sediment, but the effect of grinding was less important when compared with the HCl and H_2O_2 pretreatment. In addition, the SiO_2: Al_2O_3 ratio (Figure 5.9 B and C) was not affected by the grinding procedure. Based on the data showed in Figure 5.9 A, the $bSiO_2$% was calculated following Si/Al method (Kamatani and Oku, 2000) and Si/time method (DeMaster, 1981) (Figure 5.9 D). The $bSiO_2$% yields were not affected by grinding. Further, the bSi yields determined by Si/time method were about 100% higher than Si/Al method (Figure 5.9 D), showing the selection of calculation methodology is at priority.

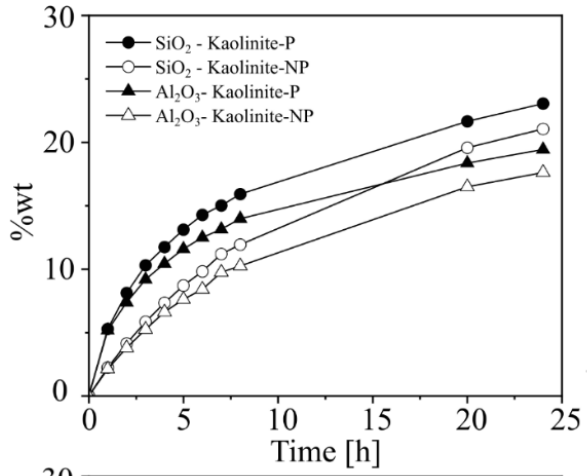
SiO2 - Kaolinite-P
SiO2 - Kaolinite-NP
Al2O3- Kaolinite-P
Al2O3- Kaolinite-NP
%wt
Time [h]

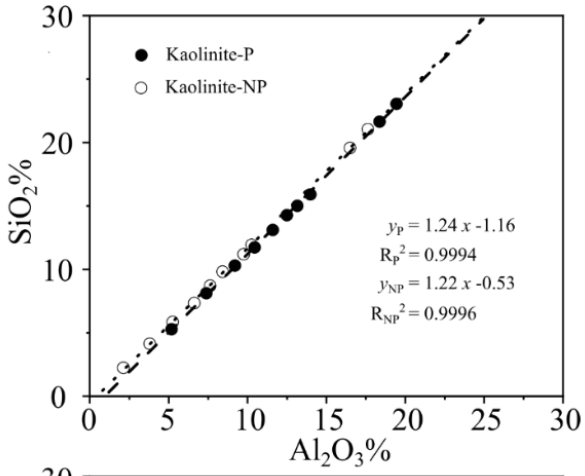
Kaolinite-P
Kaolinite-NP
yP = 1.24 x -1.16
RP2 = 0.9994
yNP = 1.22 x -0.53
RNP2 = 0.9996
SiO2%
Al2O3%

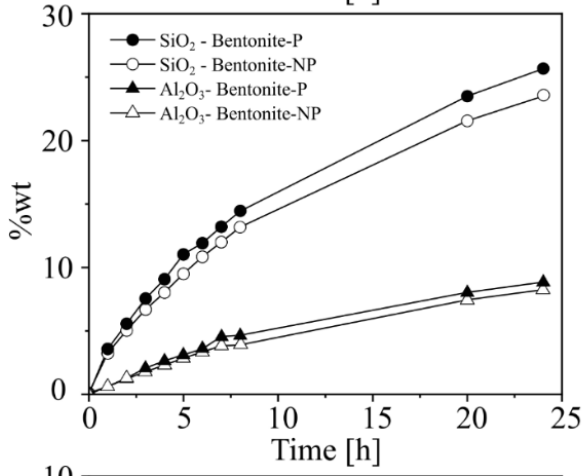
SiO2 - Bentonite-P
SiO2 - Bentonite-NP
Al2O3- Bentonite-P
Al2O3- Bentonite-NP
%wt
Time [h]

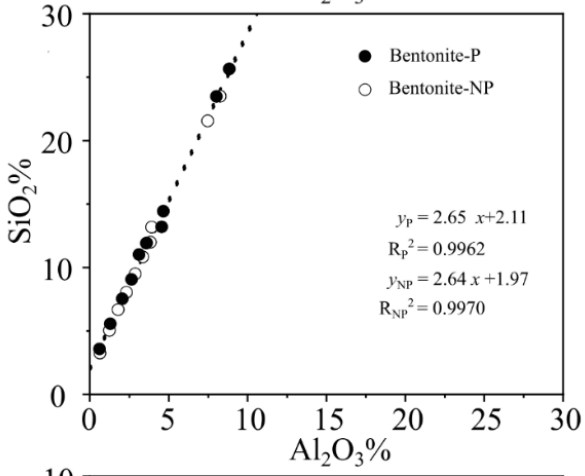
Bentonite-P
Bentonite-NP
yP = 2.65 x+2.11
RP2 = 0.9962
yNP = 2.64 x +1.97
RNP2 = 0.9970
SiO2%
Al2O3%

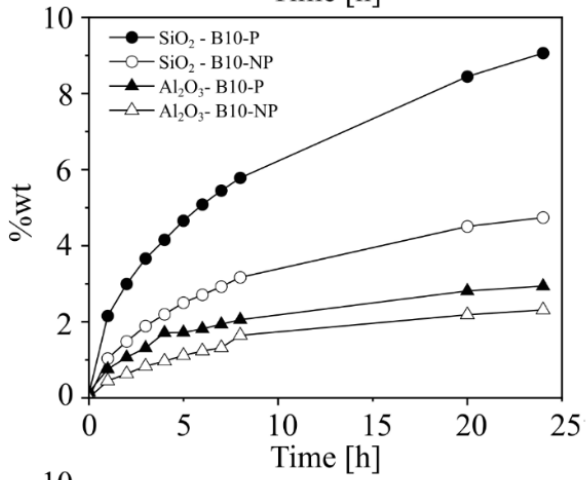
SiO2 - B10-P
SiO2 - B10-NP
Al2O3- B10-P
Al2O3- B10-NP
%wt
Time [h]

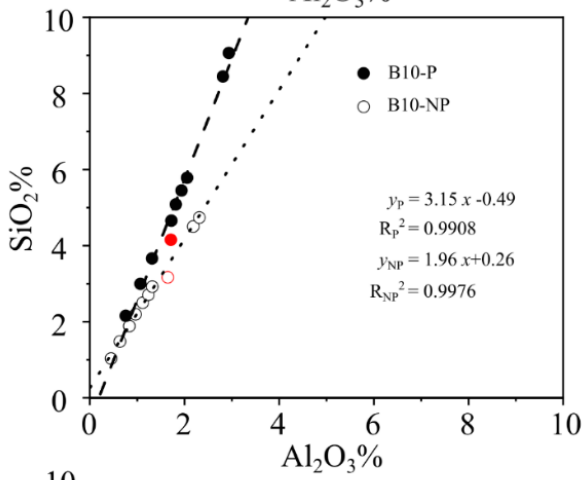
B10-P
B10-NP
yP = 3.15 x -0.49
RP2 = 0.9908
yNP = 1.96 x+0.26
RNP2 = 0.9976
SiO2%
Al2O3%

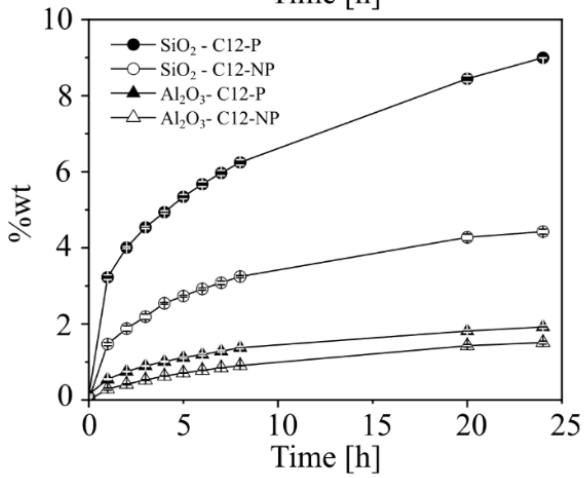
SiO2 - C12-P
SiO2 - C12-NP
Al2O3- C12-P
Al2O3- C12-NP
%wt
Time [h]

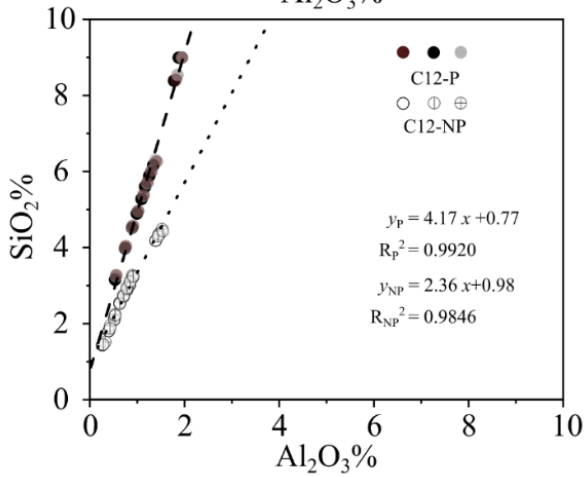
C12-P
C12-NP
yP = 4.17 x +0.77
RP2 = 0.9920
yNP = 2.36 x+0.98
RNP2 = 0.9846
SiO2%
Al2O3%

Figure 5.8. Extraction of the pretreated (P: 1.0 M HCl, 10% H_2O_2) and non-pretreated (NP) samples (kaolinite, bentonite, B10, C12). The abnormal data (B10) marked in red were not used for linear regression calculation. Triplicate extractions for sample C12. The SiO_2% and Al_2O_3% in HCl and H_2O_2 solution was low (Kaolinite: 0.002%SiO_2, 0.022%Al_2O_3; Bentonite: 0.08%SiO_2, 0.10%Al_2O_3; C12: 0.09 ± 0.01%SiO_2, 0.14 ± 0.01%Al_2O_3; B10: 0.09%SiO_2, 0.15% Al_2O_3). The linear relationship of SiO_2 vs. Al_2O_3 (right) agrees with offshore sediment from Tokyo Bay determined by Kamatani and Oku (2000). Red symbols represent abnormal data and they were not used for calculating the quadratic equation.

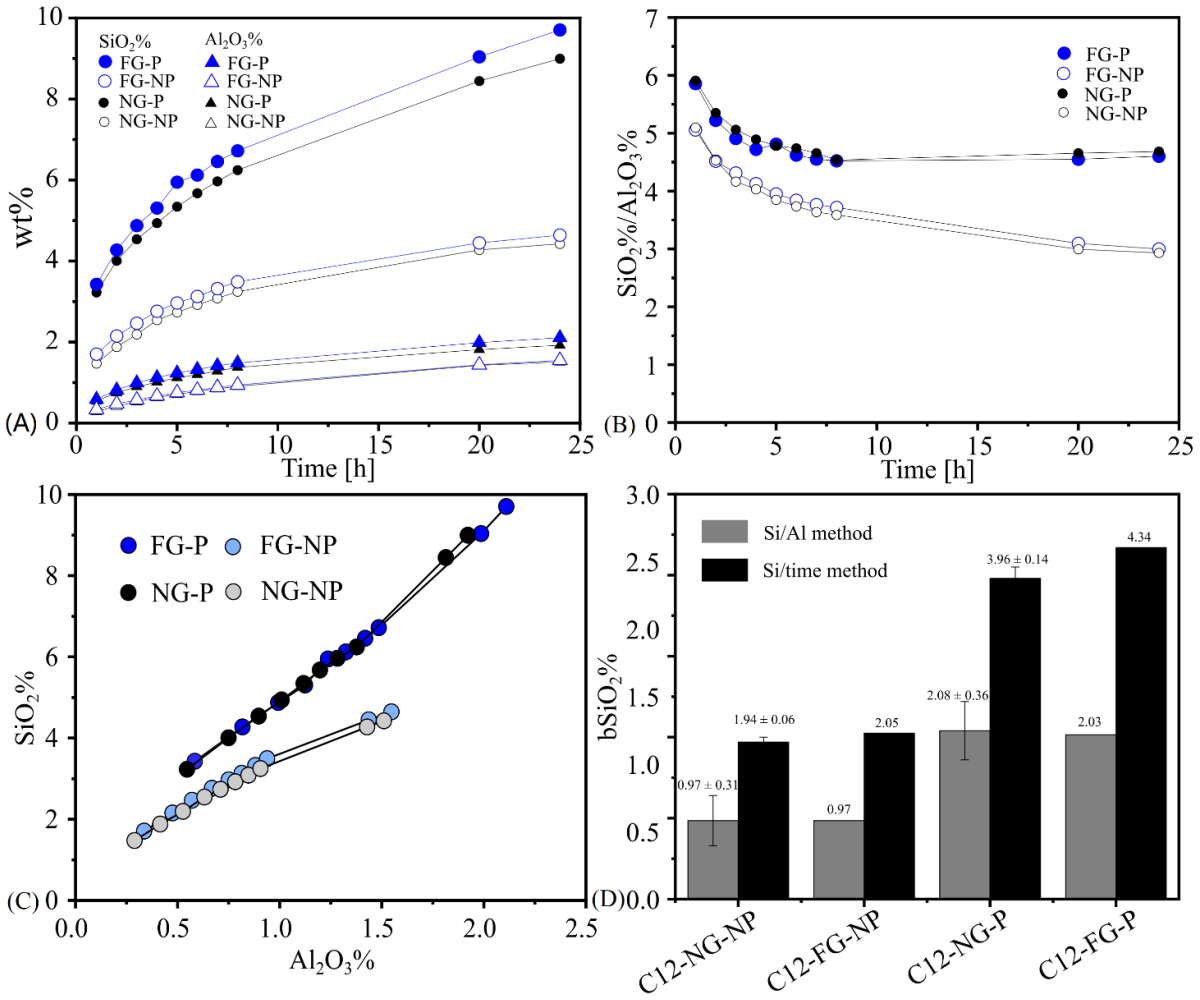

Figure 5.9. Extraction of pretreated (P) and non-pretreated (NP) finely ground (FG) and not ground (NG) sediment (C12). A: extracted SiO_2% and Al_2O_3% through time, B: the SiO_2% /Al_2O_3% ratio through time, C: SiO_2% vs. Al_2O_3% plot and D: bSiO_2% determined by Si/Al (Kamatani and Oku, 2000) and Si/time method (DeMaster, 1981).

5.4. Discussion

5.4.1. Question for wet alkaline digestions: pretreating or not pretreating?

The pretreatment of sediments can have an important effect on bSi determination, however, whether a pretreatment should be used is still under dispute (Mortlock and Froelich, 1989; Conley, 1998; Landen et al., 1996; DeMaster, 2002). Our results confirmed that pretreatment can enhance the dissolution of Si from both bSi and silicate minerals, eventually, causing an overestimation of $bSiO_2$%. Therefore, the pretreatment of sediment using HCl and H_2O_2 as well as powdering of sediments are not recommended. In addition, the Si/Al method is recommended for measuring the $bSiO_2$% in silicate mineral rich sediments, such as sediments of coastal and continental margin zones where are under the influence of terrestrial transported materials.

The grinding of sediment was used in several studies (Muller and Schneider, 1993; Liu et al., 2002). We found an increased dissolution of Si and Al after grinding (Figure 5.9 A), which causes overestimation of $bSiO_2$%. In addition, the $bSiO_2$% determined by Si/time method is about 100% higher than that of the Si/Al method. Since the SiO_2% : Al_2O_3% ratio of silicate minerals was not influenced by grinding (Figure 5.10 B and C), thus, applying the Si/Al mineral correction is more appropriate for minimizing mineral interference. Also, the Si/time correction can overestimate the $bSiO_2$%. Therefore, the Si/Al method is recommended for measuring the $bSiO_2$% in silicate mineral rich sediments. Further, the grinding of sediments may have little influence for measuring the bSi in sediment of opal rich samples, such as the Southern Ocean and the Equatorial Pacific due to the high $bSiO_2$% and low silicate mineral content.

Regarding the pretreatment procedure using HCl and H_2O_2 prior to alkaline digestion recommended by Mortlock and Froelich (1989), note that the effect of the process on bSi determination was found to be negligible and thus was also recommended by Landen et al, (1996). The aim of this procedure is to enhance the digesting efficiency without bringing out mineral interference. However, the significantly enhanced bSi yields (2 to 3 times) after pretreatment was noticed but not well explained (Mortlock and Froelich, 1989; Landen et al., 1996; DeMaster, 2002; Michalopoulos and Aller, 2004; Rahman et al., 2016; Pickering et al., 2020). Through a series of alkaline extractions of the pretreated and non-pretreated sediments and microscopic observation, Zhu et al. (2023) concluded that HCl and H_2O_2 pretreatment can activate silicate minerals (authigenic aluminosilicate and clays) and cause an overestimation of the $bSiO_2$%. However, Zhu et al. (2023) only measured Si concentrations in alkaline solutions and did not measure the Al concentrations. Here, we determined both the alkaline extracted Si

and Al concentrations of the pretreated and non-pretreated sediments and clay minerals (Figure 5.9). The increased amount of alkaline extracted SiO_2% and Al_2O_3% from pretreated clays and sediments (Figure 5.8) indicated that pretreatment can activate both bSi and silicate minerals, therefore, enhancing their solubility. In addition, the modeling data (Table 5.3: kaolinite, B10, C12) also showed an increase of bSi reactivity (k_1) and the dissolution rate of silicate minerals (b). The dissolution of Si from silicate minerals can cause significant $bSiO_2$% overestimation (2-3 times) when calculations of the bSi yields are based on Si/time method which described by DeMaster (1981) and Mortlock and Froelich (1989). However, the overestimation of $bSiO_2$% due to HCl and H_2O_2 pretreatment can be corrected by applying the Si/Al method which proposed by Kamatani and Oku (2000) and Koning et al. (2002).

5.4.2. Evaluating different wet chemical methods on bSi measurements

Here, we evaluated two Si/Al methods (e.g., Kamatani and Oku (2000) and Koning et al. (2002)) and two Si/time methods (e.g., DeMaster (1981) and Mortlock and Froelich (1989)) and found methodological biases (Figure 5.10). These biases can be minimized by selecting an optimal alkaline digestion procedure according to the different sediment types and the types of bSi in sediments.

As shown in Figure 5.10 and Table 5.5, the uncertainties of the $bSiO_2$% determined by Si/time and Si/Al methods ranged from 4% to 116%, the largest uncertainties were found for low $bSiO_2$% sample (B10). A two-way analysis of variance (ANOVA) test (see Table 5.5) showed no significant difference among all methods (Table S5.2). However, after removing the high $bSiO_2$% samples (2714CQ and 3585CQ), the two-way ANOVA test (Table S5.3) indicated a significant difference ($p < 0.05$) of the Koning et al, (2002) vs. the method of Kamatani and Oku (2000), the Mortlock and Froelich (1989), Kamatani and Oku (2000) and DeMaster (1981) method. Note that there is no significant ($p > 0.05$) difference between Koning et al, (2002) and DeMaster (1981) method. The $bSiO_2$% calculated following Kamatani and Oku (2000) were lower than the bSi yields calculated following the models as described by Koning et al, (2002). The reason for this low $bSiO_2$% is due to an underestimation caused by clay minerals, since negative $bSiO_2$% values were found when measuring the clay minerals (Table 5.4). Thus, calculation of the $bSiO_2$% using the first order dissolution models (Eq 5.1) is recommended when using the Si/Al method. It should be noted that the period of extraction time needs to be adjusted according to the types of bSi in sediments (see above), because a complete digestion of radiolarians and sponge spicules requires a strong digestion (i.e., strong alkaline solution or extended period of extraction). For example, more than 18% of the $bSiO_2$% (mainly radiolarian

tests) were not digested from sample 2714CQ when applying a one-hour 0.5 M NaOH digestion, however, all bSi were completely dissolved after the twenty-four-hour extraction in 0.5 M NaOH solution (Table S5.3). In addition, the $bSiO_2$% determined by Si/time method as described by Mortlock and Froelich (1989) was significantly ($p > 0.05$) higher than the $bSiO_2$% method described by DeMaster (1981). Additionally, no significant difference was found in the $bSiO_2$% as measured using the DeMaster (1981) method and the Si/Al methods (Table S5.3). Note that no significant difference was found between the Koning et al. (2002) and DeMaster (1981) methods.

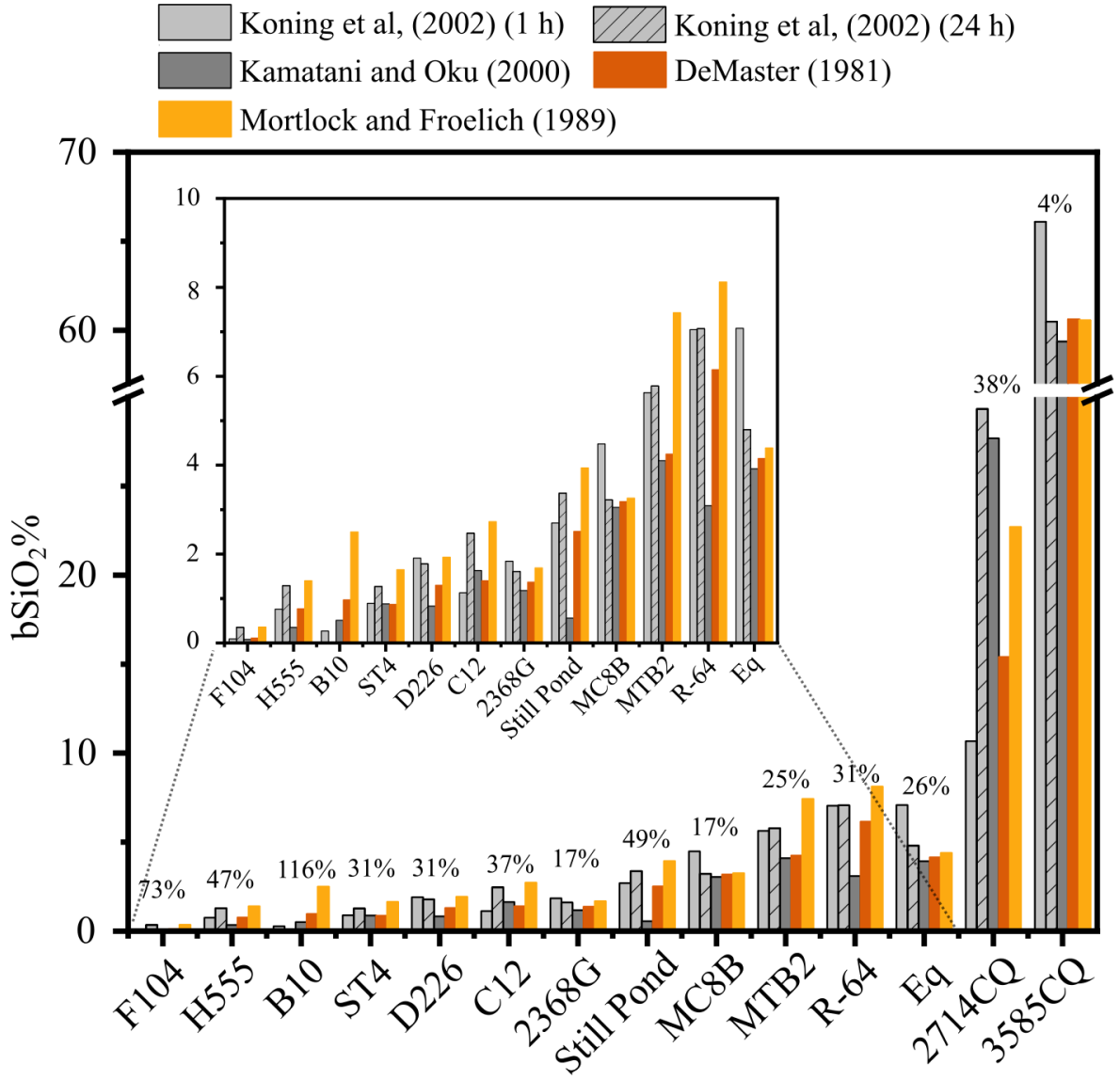

Figure 5.10. The $bSiO_2$% determined by Si/time (Mortlock and Froelich, 1989; DeMaster, 1981) and Si/Al methods (Kamatani and Oku, 2000; Koning et al., 2002) and the uncertainties of the $bSiO_2$%.

By combining our results with the research previously done by DeMaster. (1981), Landen et al. (1996), Mortlock and Froelich (1989), Muller and Schneider. (1993), Gehlen and van Raaphorst (1993), Kamatani and Oku (2000), Koning et al. (2002), Liu et al. (2002), Barão et al. (2015) and Zhu et al. (2023), we recommend to use the Si/Al method to measure bSi in sediment of opal-poor sediments, i.e., the Chinese marginal seas (Bahai Sea, Yellow Sea, East China Sea and Northern South China Sea), Amazon shelf zone, the Congo shelf zone and North Atlantic. DeMaster (1981)'s method is convenient for measuring sediment with > 3%$bSiO_2$ whereas the Mortlock and Froelich (1989) is only appliable for measuring opal-rich sediment that contain little silicate minerals, such as sediment of the Southern Ocean.

5.4.3. Evaluating X-ray diffraction on bSi measurements

XRD analysis is widely used for measuring $bSiO_2$% of sediment cores for understanding the past climatology (Goldberg, 1958; Lippold et al., 2012). We found that the XRD method overestimates the $bSiO_2$%, especially for samples containing low opal content. As shown in Figure 5.11, except data from Leinen (1985), most of the $bSiO_2$% determined by XRD method outweighs that of the wet chemical method. We determined the $bSiO_2$% of East China Sea sediments using XRD method following the protocol described by Leinen (1985). Our results clearly showed that the $bSiO_2$% determined by XRD method were larger than that of wet chemical method. In addition, the methodological difference is more important for samples that contain < 10%$bSiO_2$ ($bSiO_2\%_{XRD}$ = 5.5 $bSiO_2\%_{wet\ chemical\ method}$) as compared to the samples contain > 30%$bSiO_2$ ($bSiO_2\%_{XRD}$ = 1.5 $bSiO_2\%_{wet\ chemical\ method}$). Therefore, XRD method overestimates the $bSiO_2$%, especially for the samples contain < 10%$bSiO_2$.

XRD method is considered as a reasonable empirical approach of measuring the sediments of > 5%$bSiO_2$ (Goldberg, 1958) or > 10%$bSiO_2$ (Eisma and Van Der Gaast, 1971) when the non-biogenic amorphous silica does not react to the temperature treatment (Hurd, 1983). However, determining bSi using XRD method is challenging due to (1) the variation of transformation efficiency of different types of bSi and (2) the interference of non-biogenic amorphous silica in sediments (Hurd and Theyer, 1977; Hurd, 1983). Eisma and Van Der Gaast (1971) determined bSi by measuring the opal "bulge" directly without heating the sediment. However, their measurements have shown large variability on synthetic samples containing clays and quartz, and the detailed description of the corrections of original data was not available in Eisma and Van Der Gaast (1971). The reason why XRD outweighs the bSi yield is probable due to silicate mineral effect. The silicate mineral interference limits the application of XRD method for measuring $bSiO_2$% in sediment of low bSi and high clay mineral contents.

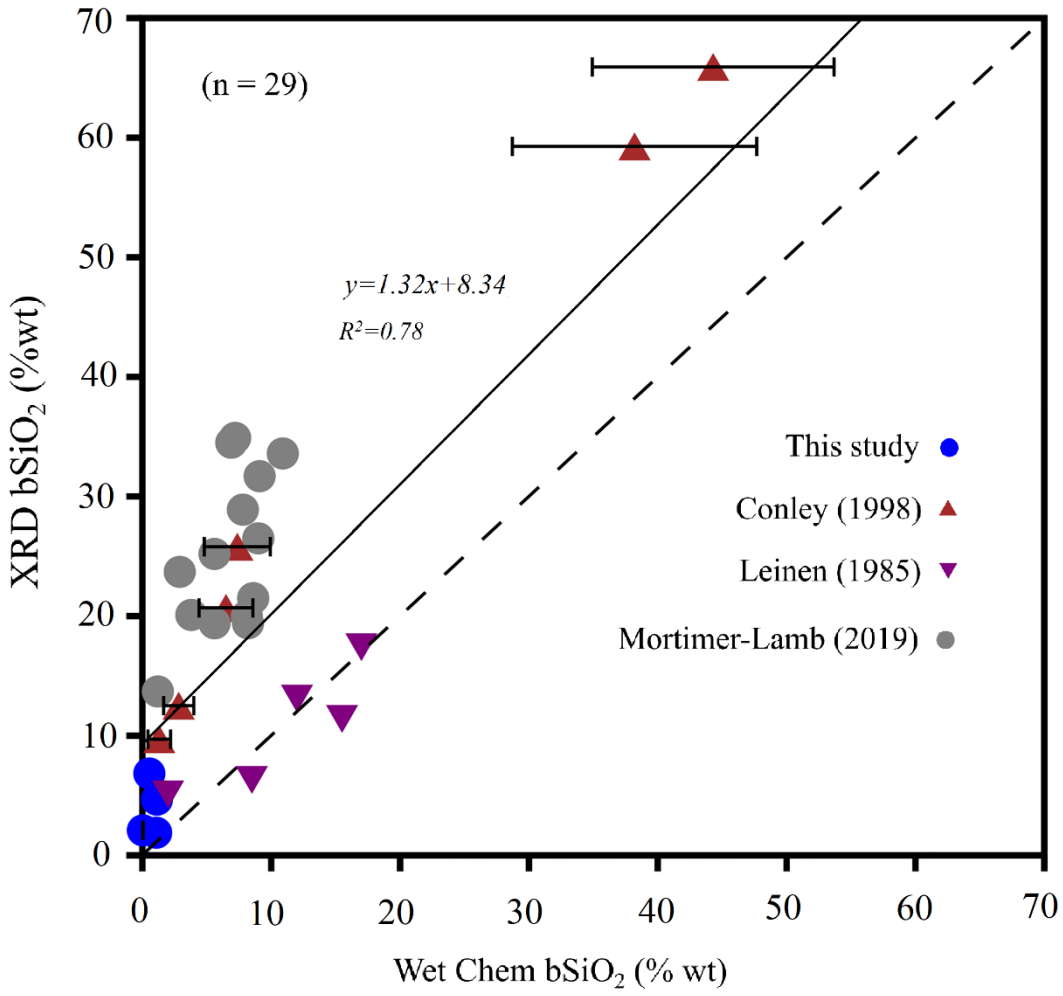

Figure 5.11. Comparation of $bSiO_2$% determined by wet chemical method (x axis) and X-ray diffraction (XRD, y axis) method. The dashed line represents y equals x.

5.4.4. Evaluating infrared method on bSi measurements

The infrared method, including IR analysis and FTIR analysis, is a rapid and efficient technique of determining the $bSiO_2$% in marine sediments (Frohlich, 1989; Meyer-Jacob et al., 2014; Vogel et al., 2016). It is also considered as a promising approach for measuring the $bSiO_2$% in sediments because of the strong correlation ($R^2 = 0.87$) of the IR determined opal content as compared with the wet chemical methods (Vogel et al., 2016). Note that the determined opal content by Vogel et al, (2016) was expressed as $SiO_2 \cdot 0.4H_2O$%, therefore, their bSi yields determined by IR were at least 10% larger than the $bSiO_2$% (expressed as SiO_2%) determined by wet chemical methods. Through comparing the previously published works reported by Vogel et al, (2016) and Melucci et al, (2019), we found the $bSiO_2$% determined by IR method were lower (35% in average) than the $bSiO_2$% determined by wet chemical methods (Figure 5.12). The two-way ANOVA test analysis showed the $bSiO_2$% measured by IR was significantly

($p < 0.05$) lower than wet chemical method. In addition, the differences were more important for samples contain < 30%$bSiO_2$ (the $bSiO_2$% determined by IR method is about 40% smaller than that determined by wet chemical method) as compared to the samples contain > 30%$bSiO_2$ (the $bSiO_2$% determined by IR method is 10% smaller than that determined by wet chemical method) (Figure 5.12).

The larger offset at lower concentrations (Figure 5.12) is explained by a lack of sensitivity of both methods (IR and wet chemical method). For example, the $bSiO_2$% determined by the DeMaster (1981) and Muller and Schneider (1993) methods (both methods are wet chemical methods) were close to the x = y line as shown in Figure 5.12. However, the $bSiO_2$% determined by the Mortlock and Froelich (1989) method were larger than the $bSiO_2$% determined by IR method. The reason why the $bSiO_2$% measured by the Mortlock and Froelich (1989) method was larger than that of IR method is due to a lack of mineral correction. Further, water molecules can be absorbed by dry samples during the IR analysis, which cause an enhanced Si-OH spectra signal and therefore cause a $bSiO_2$% overestimation (Vogel et al., 2016). IR measurement is also influenced by sediment matrix (Melucci et al., 2019). Silica polymorphs absorb at the wavelength of about 800 cm^{-1}, which represents an Si-O-Si stretching mode (Hurd, 1983), the Si-O-Si stretching bond not only present in biogenic silica, but also present in other silicates, such as quartz, opal-CT and opal-A (bSi). The different types of silicates are extremely difficult to separate analytically. Moreover, there are usually several types of bSi (diatoms, radiolarians, sponge spicules, silico-flagellates) in sediments, and their physical properties are not uniform (different water content and degree of silicification), it is not sure how much of the total bSi present in sediments is actually being measured by the IR method (Hurd, 1983).

In conclusion, although the IR method is found to be an efficient and cost-effective technique of determining the $bSiO_2$% in marine sediments (Vogel et al, 2016; Melucci et al., 2019), three challenges still hinder the application of this technique, e.g., (1) water absorption by samples during the analysis (2) silicate mineral interference and (3) the various IR spectra characteristics of different types of bSi. These challenges potentially affect the accurate measurement of bSi and cause methodological biases. The $bSiO_2$% measured by the IR method is about 35% smaller than the conventional wet chemical methods. In order to minimize the methodological biases and to improve the IR analysis method, further research is needed to (1) improve and develop the analytical procedure, (2) quantitatively measure the Si-O-Si stretching bond of different silicate (including different types of bSi and clays) that present in marine sediments for understanding the sediment matrix effect (3) and determined different types of bSi as well as artificial sediments for knowing the actual and the determined bSi content.

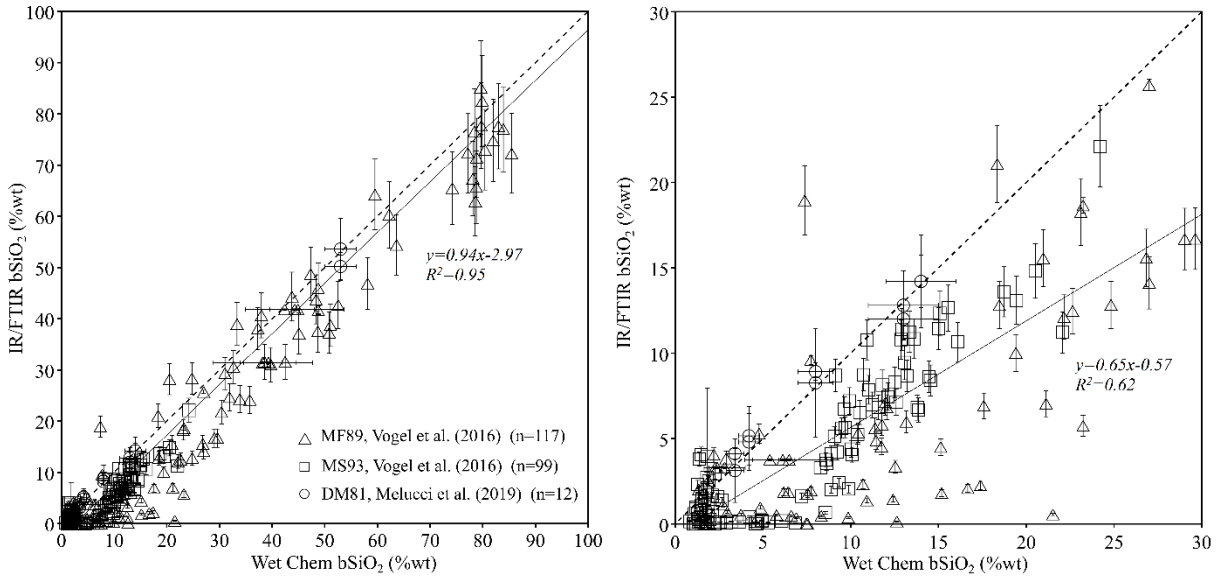

Figure 5.12. Comparation of $bSiO_2$% determined by wet chemical methods (x axis) and Infrared method (IR/FTIR, y axis) method. The wet chemical methods: MF89, MS93 and DM81 represent Mortlock and Froelich (1989), Muller and Schneider (1993) and DeMaster (1981), respectively. The dashed line represents y equals x. Data were obtained from Vogel et al., (2016).

5.4.5. Evaluating the global bSi burial flux

There is a wide range of variability in the measurement of bSi across the community of aquatic scientists (Conley, 1998). As discussed in previous sections, we studied the methodological biases among the wet chemical methods, IR and XRD methods. Compared with IR and XRD method, so far, wet chemical method is more robust in determining the $bSiO_2$% of marine sediments. Therefore, based on the previous published data and our results, we corrected the $bSiO_2$% following the relationship below: $bSiO_2\%_{\text{wet chemical method}} = 0.5\ bSiO_2\%_{XRD}$, $bSiO_2\%_{\text{wet chemical method}} = 1.35\ bSiO_2\%_{IR}$. In addition, the $bSiO_2$% determined by the Mortlock and Froelich (1989) method was reduced by 10% for a mineral correction (based on data of Figure S5.5). Our evaluation of the $bSiO_2$% determined by different methods represents a moderate correction, and may have different influences on the evaluation of the burial flux of CCMZs and open ocean. For example, the $bSiO_2$% determined by XRD method is about 5.5 times larger than that determined by wet chemical method for low bSi (> 10%) sediments, and is 50% larger for high bSi (> 30%) sediments. We divided all $bSiO_2$% measured by XRD method by 2. This correction is moderate for CCMZs samples but may under-evaluate the open ocean samples. Further, an overestimation of silicate mineral rich samples also exists

for sediments of CCMZs which determined by Mortlock and Froelich (1989) method, because our correction maybe not be adequate to remove all mineral interferences. Considering the area of CCMZs and open oceans, our data presented here represents a lower limit of the $bSiO_2$%. The ranges of the $bSiO_2$% of raw data is 0 − 100% and is 0 − 80% after our correction. As shown in Figure 5.13, the $bSiO_2$% in surface sediments of global ocean plotted based on the raw data from Hayes et al, (2021) (Figure 5.13A) and our normalized data (Figure 5.13B) showed similar patterns, of which high $bSiO_2$% in sediments of the Southern Ocean, Equatorial Pacific, Central Indian Ocean and North Pacific, and other regions were characterized by low $bSiO_2$%.

After correcting the previously published $bSiO_2$% data set, we recalculated the bSi mass accumulation rate (g cm^{-2} kyr^{-1}) in different marine regions of the global ocean (see Figure 5.14). Most of the data were based on ^{230}Th normalized mass accumulation rate, except for the CHIN (^{210}Pb data from Qiao et al. (2017)) and REDS (^{210}Pb and ^{14}C, Seeberg-Elverfeldt et al. (2004)). As shown in Figure 5.14, high bSi mass accumulation rate was found at the Southern Ocean (SANT, ANTA, ISSG), Western Pacific (BERS, CHIN) and Western African Coast (GUIN). High bSi mass accumulation rate at the Southern Ocean is mainly due to the high $bSiO_2$% in sediments, whereas the high bSi mass accumulation rate at the coastal regions is due to the high sediment mass accumulation rate. The bSi mass accumulation rate determined using the raw data and corrected data and their differences were shown in Figure 5.14. After multiplying the bSi mass accumulation rate by the surface area of each marine region, the annual bSi burial flux of each marine region as well as the global bSi burial flux were re-evaluated. As shown in Figure 5.15, our calculated bSi burial flux at coastal and continental margin zones were higher than previous estimate, because Hayes et al, (2021) only calculated the bSi burial flux in open ocean. Further, our calculated bSi burial flux in the marine regions of the Southern Hemisphere (see Figure 5.15) was lower than the estimate reported by Hayes et al (2021) which is due to methodological biases. Based on the data set arranged by Hayes et al., (2021), the bSi burial flux in the global ocean is 7.1 ± 3.2 Tmol-Si yr^{-1}, after correcting the methodological biases, our calculated bSi burial flux is 6.2 ± 2.7 Tmol-Si yr^{-1}. Our estimate is close to the bSi burial flux reported by Tréguer and De La Rocha, (2013) (6.3 ± 3.6 Tmol-Si yr^{-1}), but were lower than the recent annual flux evaluated by DeMaster (2019) (7.6 ± 1.8 Tmol-Si yr^{-1}) and Tréguer et al, (2021) (9.2 ± 1.6 Tmol-Si yr^{-1}). Therefore, our estimated global bSi burial flux is about 11%, 18% and 32% lower than the estimate based on raw data, the estimate done by DeMaster (2019) and Tréguer et al., (2021), respectively. In addition, our estimated bSi burial flux at the coastal region and open ocean are 2.5 ± 0.6 Tmol-Si yr^{-1} and 3.7 ± 1.1 Tmol-Si yr^{-1}, respectively. The

lower value of the bSi burial flux at CCMZs (3.7 Tmol-Si yr^{-1}, Tréguer et al., 2021) and open ocean (5.5 Tmol-Si yr^{-1}, Hayes et al., 2021) in this thesis are possibly due to 1) underestimate of bSi burial flux at certain CCMZs, i.e., the Ganges-Brahmaputra system, the Indo-Pacific Archipelago shelves, the mobile mud deposits of the Amazon shelf and the Gulf of Mexico, due to lack of both bSi data and sediment accumulation rate data and 2) underestimate of bSi due to over-corrected bSi data set determined by XRD method. Considering one-third of bSi were buried on seabed and two-thirds of bSi were buried as authigenic clays (1.0 Tmol-Si yr^{-1}) at the proximal zones (Rahman et al., 2017), there is about 0.5 Tmol-Si $yr^{-1}$of bSi added into our bSi burial flux of CCMZs (3.0 Tmol-Si yr^{-1}). Therefore, the burial flux of bSi at the global ocean is 6.7 ± 2.7 Tmol-Si yr^{-1}. The bSi burial flux in the CCMZs represents 45% of the global bSi burial flux, further studies are needed to quantify the bSi burial flux in the CCMZs, especially the proximal zones where sediment mass accumulation rate is high.

Our estimated bSi burial flux (6.7 ± 2.7 Tmol-Si yr^{-1}) revised the total marine Si output flux into 13.1 ± 2.7 Tmol-Si yr^{-1} (bSi burial flux: 6.7 ± 2.7 Tmol-Si yr^{-1}, sponge spicules: 1.7 ± 1.6 Tmol-Si yr^{-1}, reverse weathering: 4.7 ± 2.3 Tmol-Si yr^{-1}), which is higher than the total Si input flux (11.8 ± 2.1 Tmol-Si yr^{-1}) determined by DeMaster (2019) but less than the total Si input flux (14.8 ± 2.6 Tmol-Si yr^{-1}) proposed by Tréguer et al. (2021). We conclude that the contemporary marine Si cycle is at steady state because the Si output flux is not significantly different from the Si input flux. However, further study is still necessary for understanding whether there is a missing Si sink (2.5 Tmol-Si yr^{-1}) or previous study over-evaluated the bSi burial flux, which further verify this research.

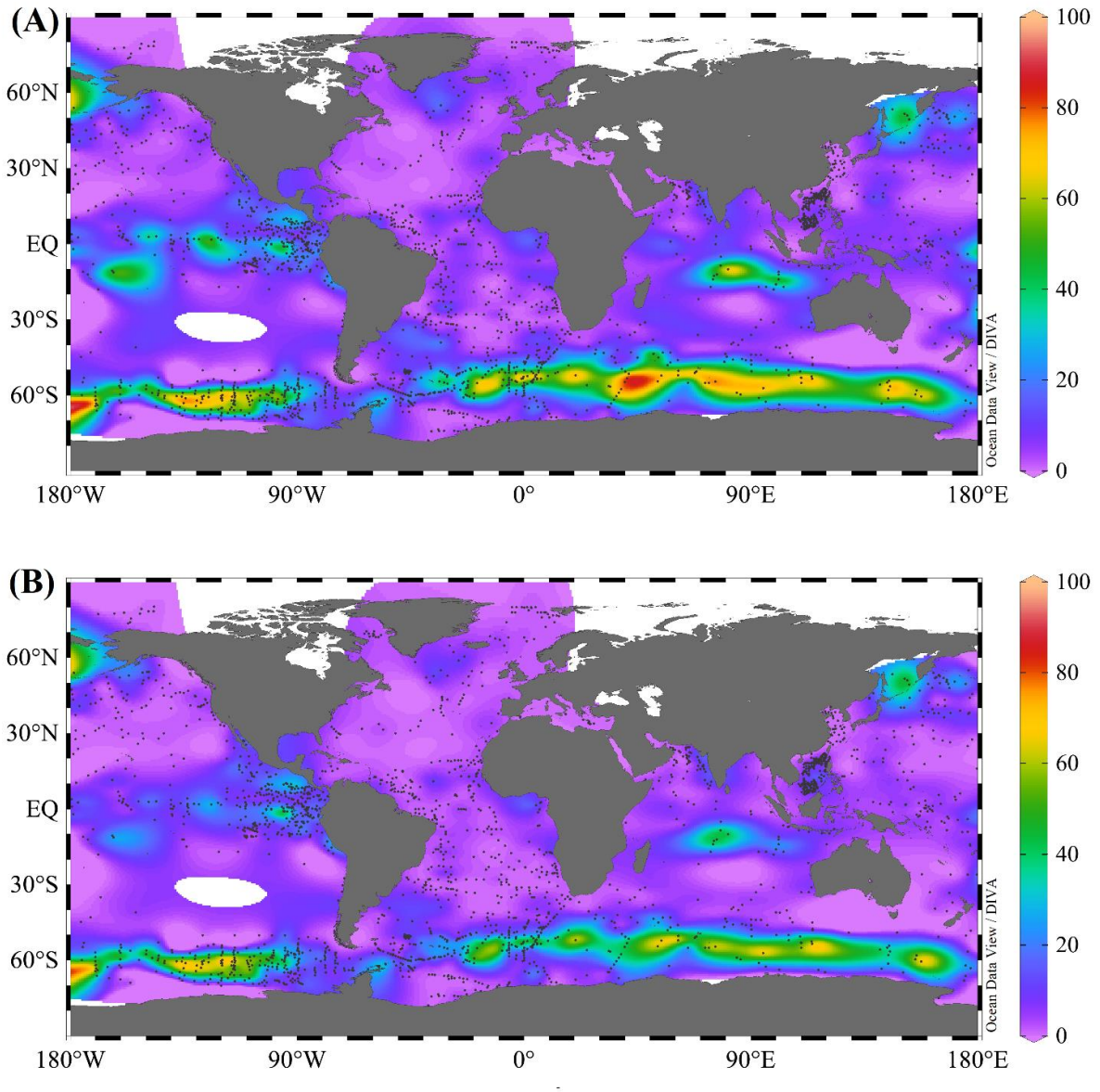

Figure 5.13. The biogenic silica content in surface sediments of the global ocean. A: biogenic silica distribution plotted using raw data from Hayes et al, (2021); B: biogenic silica distribution plotted using corrected biogenic silica data set. White color represents areas that lack data. The corrected data (B) has smaller ranges (0 − 80%) than the ranges (0 − 100%) of raw data set (A). Note that black symbols are sample locations. Certain regions, i.e., the Ganges-Brahmaputra system, the Indo-Pacific Archipelago shelves, the mobile mud deposits of the Amazon shelf and the Gulf of Mexico, are areas which lack of data (both bSi data and sediment accumulation rate data).

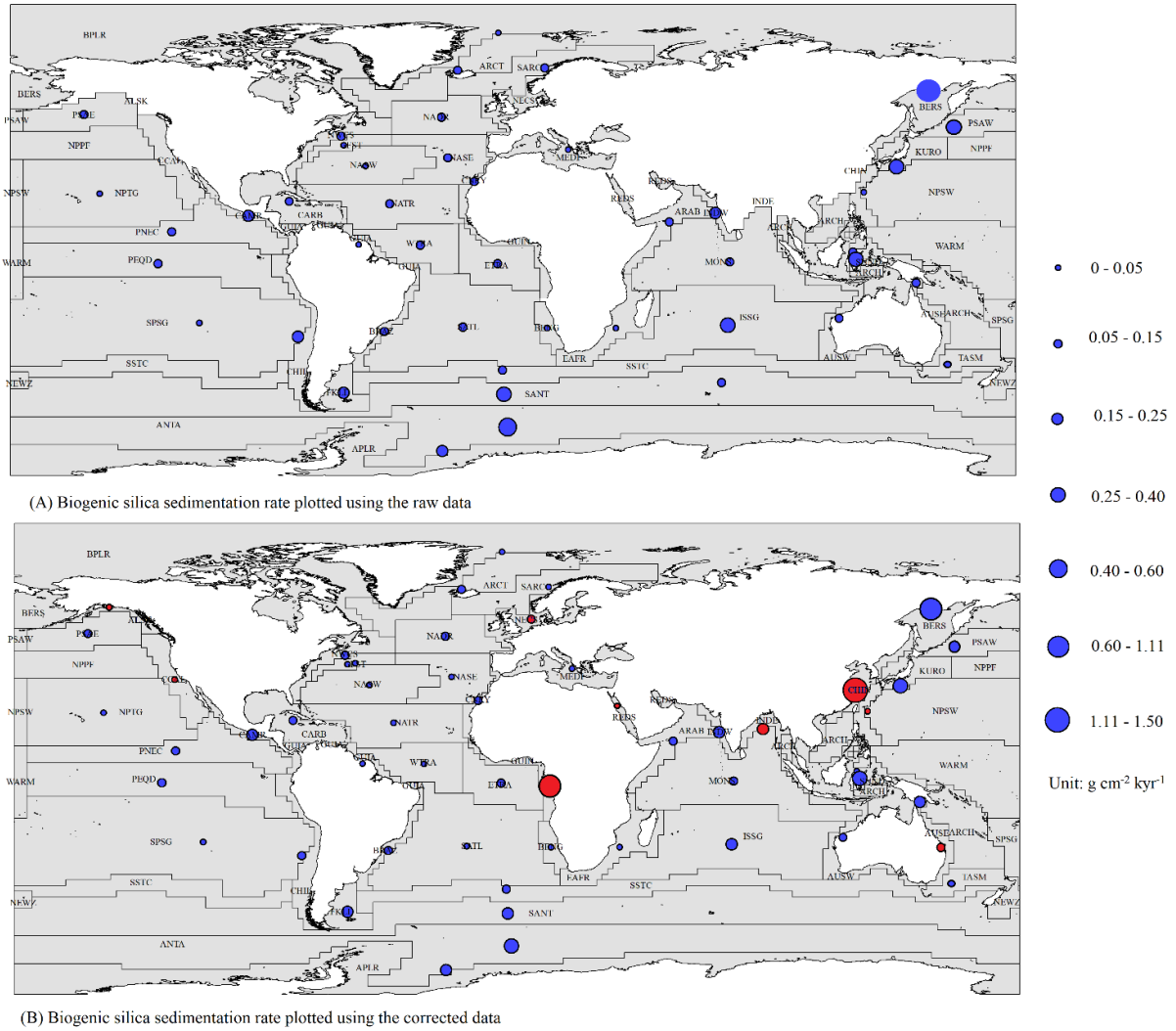

(A) Biogenic silica sedimentation rate plotted using the raw data

(B) Biogenic silica sedimentation rate plotted using the corrected data

Figure 5.14. Biogenic silica mass accumulation rate (g cm^{-2} kyr^{-1}) at different marine regions of the global ocean. A: biogenic silica mass accumulation rate plotted using the raw data from Hayes et al, (2021), B: biogenic silica mass accumulation rate plotted using normalized data of this study. The symbols in red color represent biogenic silica mass accumulation rate that was not included in the raw data set by Hayes et al, (2021).

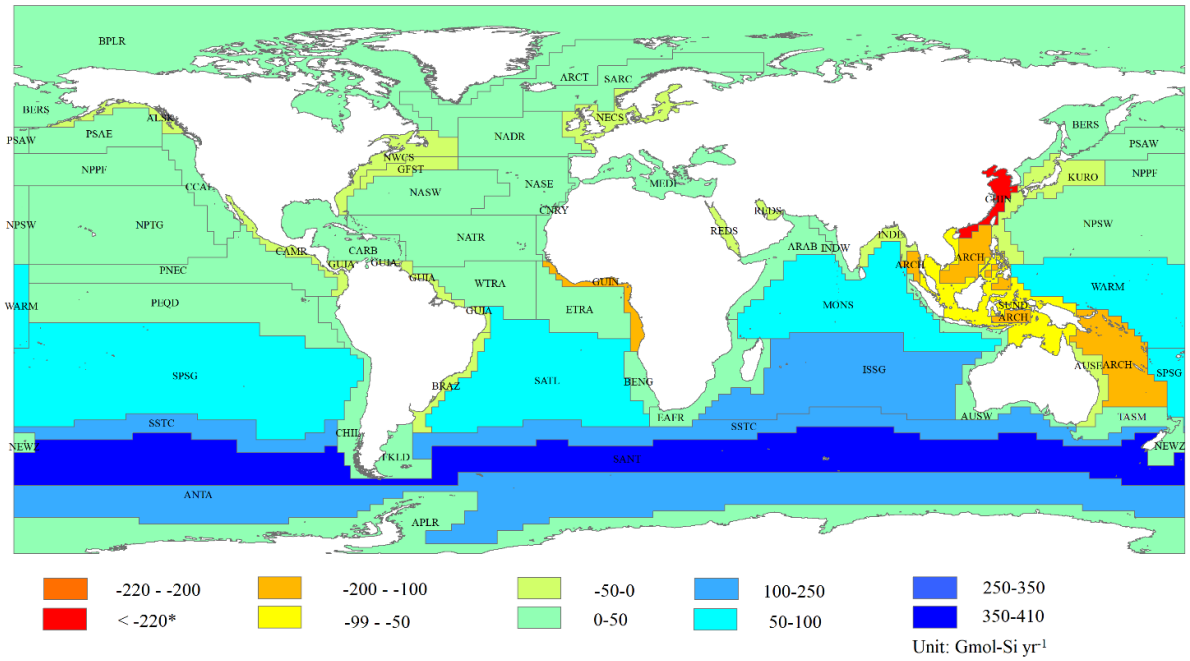

Figure 5.15. Differences of the biogenic silica annual burial flux between Hayes et al, (2021) and this study (bSi burial flux calculated using the raw data from Hayes et al, (2021) – corrected bSi burial flux). Note that Hayes et al, (2021) calculated the bSi burial flux of open ocean (> 1000 m), thus, the bSi burial flux at coastal and continental margin zones of CHIN, NECS, GUIN, REDS, INDE, ALSK, AUSE, GFST, NPSE and OCAL were lower than the burial flux calculated based on corrected data (warm color in this study).

5.4.6. Optimized protocol for determining the $bSiO_2$% in sediments of various depositional environments

In order to minimize the large variability of the determined $bSiO_2$% by different methods, we proposed an optimized wet chemical protocol for determining the $bSiO_2$% in sediments of various depositional environments of the world ocean. This protocol was based on the generalized wet chemical procedure for measuring the bSi in sediment of coastal and continental margin zones (see Chapter 3 and Zhu et al. (2023)) and data from this study. Thus, it can be applied for measuring bSi in sediment of both coastal and open oceans. The wet chemical procedures were listed below:

(1) Check the coordinates/sample location for understanding the depositional environment.

(2) Microscopic observation: check the major types of bSi in sediments.

(3) Select the alkaline extraction technique according to the information of sample location and types of bSi following the decision chart shown in Figure 5.16.

(4) Sample preparation. Gently mix the freeze-dried sediment using agate pestle and mortar.

Weighing the sediments in a plastic tube (sediment of coastal ocean: 40 to 200 mg, solid to liquid ratio: 1 to 5 g/L; sediment of open oceans: 15 to 30 mg, solid to liquid ratio: 0.375 to 0.75 g/L).

(5) Fill in the plastic tube with 40 mL of alkaline solution and mix the sediments with alkaline solution using a vortex mixer. Soak the plastic tubes into a shaking water bath pre-heated to 85℃. Take the alkaline solution samples for dSi and/or dAl analysis.

(6) After the extraction, check the residual sediments using a microscope. Continuing to digest the sediments when bSi was observed.

In this protocol, the extraction solution, period of digestion and method of bSi calculation are adjusted based on the types of bSi and types of sediments, thus, the interference of silicate minerals on bSi determination and the issue of incomplete digestion are resolved. In addition, the pretreatment proceude (grinding, HCl and H_2O_2 pretreatment) are avioded for minimizing the influence of silicate minerals ddissolution.

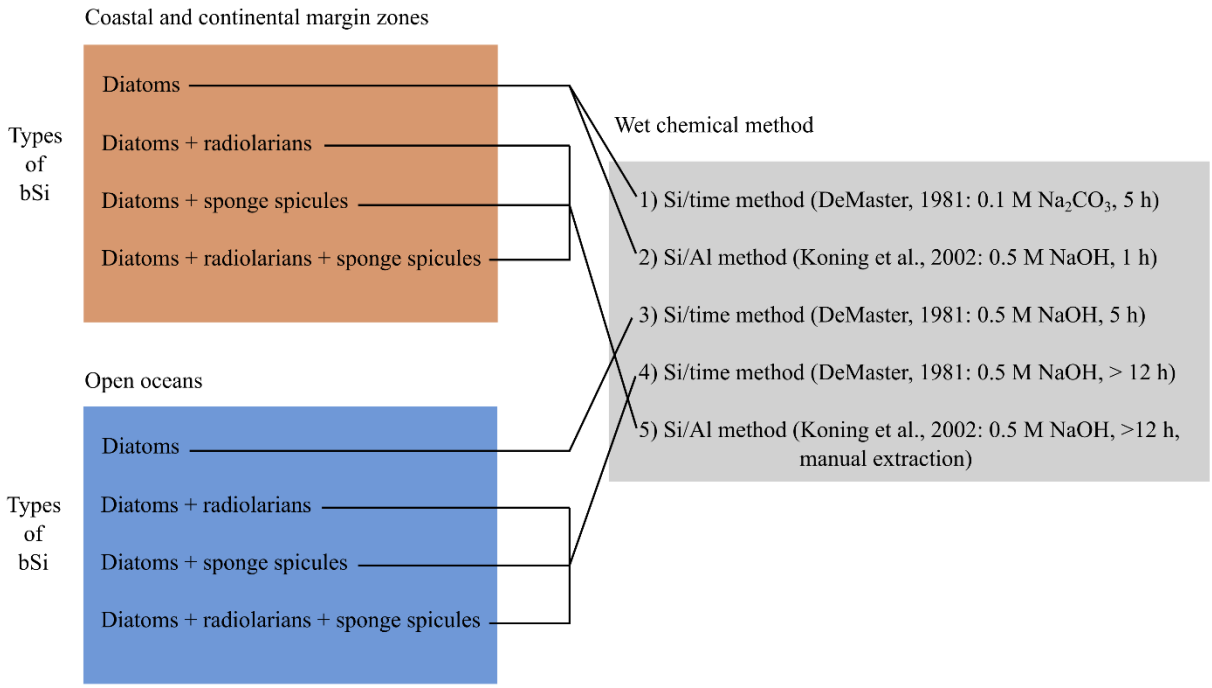

Figure 5.16. A decision chart for selecting an appropriate wet chemical method of measuring the bSiO2% in different marine sediments (sediments of coastal and continental margin zones and open oceans).

5.4.7. Importance of redefining the bSi burial flux for understanding the global marine silicon cycle

The contemporary marine silicon cycle is found to be at a relative steady state, e.g., the

marine Si input flux equals to the output flux (DeMaster, 2019; Tréguer et al, 2021). However, from the marine Si output perspective, this study found large methodological biases caused large uncertainties in the determined bSi burial flux. Therefore, bringing out the concerns of whether the modern marine Si budget is at balance. The results showed that previous studies over-estimated the global bSi burial flux by 10% to 30%, this overestimation is even larger (200%) for CCMZs where opal content is low and terrestrial lithogenic material content is high. Reasons for the overestimation are due to 1) an extraction of lithogenic silica (i.e., clays, authigenic aluminosilicates) in CCMZs sediments which include the lithogenic silica into the bSi pool and 2) minerals interferences on XRD analysis of the open ocean sediments. Although, previous studies also utilized IR method to determine the bSi content, due to the selection of samples (open ocean sediments which contain little amount of clay minerals), the methodological difference is not significant (30%) compared to the conventional wet alkaline method (Vogel et al., 2016).

The re-evaluated bSi burial flux implies a Si residence time of the modern ocean at the range of 8 ka to 10 ka, which is not significantly different as compared to the previous calculation (7.7 ka) reported by Tréguer et al, (2021). However, the new estimate of the bSi burial flux of CCMZs indicated 1) the burial rate of the bSi in sediment was overestimated and 2) the Si input (from rivers, submarine ground water, atmosphere deposition) may overweight the bSi burial unless there is an un-defined and/or underestimated pool (such as radiolarian and sponge spicules pool, and the reverse weathering of bSi). Through the measurement of Si and Al concentrations of the alkaline extracted sediments (pretreated and un-pretreated), it is more likely that the previous studies defined the authigenic aluminosilicates as bSi, thus overestimated the bSi burial flux/bSi burial rate. Therefore, further research utilizing the different geochemical tools (Ge/Al, Si/Al and Si isotopes) to quantify the Si burial due to reverse weathering is needed.

The optimum method for determining bSi content in marine sediments is the wet chemical method which utilize alkaline solution to extract bio-siliceous structures. Through applying the general wet chemical procedures proposed in this study, the methodological biases of the determined bSi content can be minimized, which subsequently minimize the uncertainties of the estimated bSi burial flux. This is particularly important for understanding the Si cycle of the modern ocean, because biases of the determined bSi content can lead to misunderstanding of marine Si cycle, especially considering that natural climate change (i.e., global warming, ocean acidification and sea-level rise) would cause a decreased Si input from rivers (Phillipps, 2020) and enhanced Si exportation from seawater (Taucher et al., 2022).

5.5. Conclusion

Based on a thorough measurement of bSi in sediments of various depositional environments using multiple methods, we found the XRD method overestimates the $bSiO_2$% and the IR method underestimates the $bSiO_2$%. Therefore, although there is variability in the determined $bSiO_2$% among different wet chemical methods, the wet chemical methods are more appropriate for measuring the bSi in marine sediments so far. Among the several alkaline extraction techniques, e.g., the Si/time method and the Si/Al method, the Si/Al method is recommended for measuring the $bSiO_2$% in sediment of coastal and continental margin zones where silicate mineral content is high, whereas the Si/time method is recommended for measuring the $bSiO_2$% in sediments of open oceans where silicate mineral contents are low. To minimize the large uncertainties of the determined $bSiO_2$%, the pretreatment procedures (i.e., grinding, HCl and H_2O_2 pretreatment) are not recommended since they enhance the dissolution of silicate minerals and subsequently cause an over-estimation. In addition, we proposed a general wet alkaline extraction procedure for determining the $bSiO_2$% in sediments of different types of bSi. Based on our results and the previously published data, we re-calculated the global bSi burial flux. We found bSi burial flux at the coastal regions is 3.0 ± 0.6 Tmol-Si yr^{-1}, which represents about 45% of the global bSi burial flux (6.7 ± 2.7 Tmol-Si yr^{-1}). Our estimation of the global bSi burial flux was about 30% lower than previous studies, showing the needs of a better understanding the bSi burial flux determinations in order to know either there is an overestimation by previous study or there is a missing Si sink.

Table 5.1 Sample name, latitude, longitude, water depth and main types of bSi in sediments before and after alkaline digestions. “D”, “S” and “R” represent diatoms, sponge spicules and radiolarians respectively. “Y” and “-” represent items were present and absent in sediment/ residual.

Sample	Latitude	Longitude	Depth [m]	No-extraction			0.5 M NaOH (~1h)			0.5 M NaOH (8h)			0.5 M NaOH (24h)		
				D	S	R	D	S	R	D	S	R	D	S	R
C12	28.07	127.02	1027	Y	Y	Y	-	Y	-	-	Y	-	-	-	-
B10	38.45	118.41	16	Y	-	-	-	-	-	-	-	-	-	-	-
ST4	68.98	-59.60	309	Y	Y	-	-	Y	-	-	Y	-	-	-	-
Still Pond	39.35	-76.18	10	Y	Y	-	-	Y	-	-	-	-	-	-	-
R-64	38.56	-76.43	17	Y	Y	-	-	Y	-	-	Y	-	-	-	-
D226	48.82	-16.50	4850	Y	-	-	-	-	-	-	-	-	-	-	-
MTB-2	-6.46	6.03	4759	Y	Y	-	-	Y	-	-	-	-	-	-	-
H555	-45.92	178.98	2738	Y	Y	Y	-	Y	Y	-	Y	Y	-	-	-
F104	-48.67	170.81	801	Y	Y	Y	-	Y	Y	-	Y	Y	-	-	Few pieces
Eq	0.20	-140.23	4358	Y	Y	Y	-	Y	Y	-	Y	Y	-	-	-
MC8B	-47.33	7.19	1878	Y	-	Y	-	-	Y	-	-	Y	-	-	-
2368G	-45.96	130.01	4506	Y	Y	-	-	Y	-	-	Y	-	-	-	-
2714CQ	-43.40	49.89	2290	Y	-	Y	Y	-	Y	-	-	Y	-	-	Few pieces
3585CQ	-51.83	4.81	3746	Y	-	Y	Y	-	Y	-	-	-	-	-	-

Table 5.2 Parameters from the Si and Al continuous dissolution with one-hour 0.5 M NaOH digestion. The unit for *ExtrSi*, TAlkSi, TAlkAl, k is mg-Si g^{-1}, mg-Si g^{-1} , mg-Al g^{-1} and min^{-1}, respectively.

Sample	Model	$ExtrSi_1$	$ExtrSi_2$	TAlkExSi	TAlkExAl	k_1	k_2	β_1	β_2	b	β_{lin}	bSi: TAlkExSi [%]	$bSiO_2$%
C12	2	5.29	5.67	17.10	3.54	1.17	0.06	7.86	4.79	0.10	3.8	30.9	1.13
B10	2	1.26	3.73	12.25	5.14	1.45	0.07	3.16	2.53	0.12	1.95	10.3	0.27
ST4	2	2.44	1.73	6.47	1.12	2.24	0.07	9.98	8.66	0.04	3.63	64.4	0.89
Still Pond	2	7.44	5.18	17.11	4.81	0.5	0.05	5.88	5.18	0.09	1.79	73.8	2.70
R-64	2	15.16	17.76	43.65	11.26	1.26	0.18	22.06	11	0.18	2.96	75.4	7.05
D226	1	8.89		15.70	4.05	0.69		5.49		0.08	2.91	56.6	1.91
MTB2	2	10.08	16.21	42.65	14.02	1.45	0.14	7.61	8.62	0.27	1.54	61.7	5.63
H555	2	2.80	0.73	6.44	1.30	1.02	0.10	6.11	5.34	0.05	3.93	54.8	0.76
F104	1	0.44		1.48	0.18	0.26		10.50		0.01	4.00	29.7	0.09
Eq	1	33.04		38.99	2.39	0.44		29.06		0.10	2.49	84.7	7.08
MC8B	1	20.93		24.54	0.57	0.15		37.97		0.06	2.59	85.3	4.48
2368G	2	5.29	3.29	11.29	1.50	1.10	0.09	8.51	13.11	0.04	4.15	75.9	1.84
2714CQ	1	49.80		89.76	1.41	0.11		>1000		0.68	2.30	55.5	10.67
3585CQ	1	308.40		314.64	2.91	0.12		112.54		<0.001	2.07	98.0	66.09

Table 5.3 Parameters from the Si and Al dissolution with 24-hour 0.5 M NaOH digestion. NP and P represent non-pretreated and pretreated (using 1.0M HCl and 10% H_2O_2) sediments, FG represents finely ground sediments, NG represents non-ground sediments. The units for $ExtrSi_i$, TAlkSi, TAlkAl, k and b are mg-Si g^{-1}, mg-Si g^{-1} , mg-Al g^{-1} and min^{-1} , mg-Si g^{-1} min^{-1}, respectively.

Sample	Model	$ExtrSi_1$	TAlkExSi	TAlkExAl	k_1	β_1	b	β_{lin}	bSi: TAlkExSi [%]	$bSiO_2$%
Kaolinite (NP)	1	57.82	98.25	93.30	0.003	0.96	0.029	1.22	0	0
Kaolinite (P)	1	58.78	107.61	102.91	0.008	1.02	0.034	1.02	0	0
Bentonite (NP)	1	48.18	109.68	43.63	0.004	3.84	0.043	1.97	0	0
Bentonite (P)	1	52.56	119.75	46.82	0.004	3.50	0.047	2.08	0	0
C12 (NG-NP)	1	11.52±0.09	20.65±0.31	7.99±0.20	0.010±0.001	4.19±0.06	0.007±0.001	1.74±0.03	55.8	2.47±0.02
C12 (NG-P)	1	20.77±0.31	41.98±0.01	10.17±0.21	0.016±0.001	4.44±0.02	0.015±0.001	3.75±0.12	49.5	4.45±0.07
C12 (FG-NP)	1	12.33	21.66	8.19	0.012	4.27	0.007	1.77	56.9	2.64
C12 (FG-P)	1	22.79	45.29	11.17	0.015	4.35	0.016	3.68	50.3	4.88
B10 (NP)	1	14.20	22.12	5.93	0.004	2.01	0.006	1.50	0	0.00
B10 (P)	1	18.83	42.28	15.55	0.009	2.27	0.016	3.11	0	0.00
ST4	1	5.94	15.18	4.51	0.013	4.72	0.007	2.86	39.2	1.27

Still Pond	1	15.74	32.40	11.18	0.012	3.31	0.012	2.46	48.6	3.37
R-64	1	32.97	54.90	13.71	0.024	6.93	0.016	2.32	60.1	7.07
D226	1	8.32	13.75	6.56	0.012	3.10	0.004	1.42	60.5	1.78
MTB2	1	26.98	65.62	41.19	0.015	4.56	0.028	1.10	41.1	5.78
H555	1	6.01	10.92	3.73	0.010	3.92	0.004	2.20	55.1	1.29
F104	1	1.64	3.52	0.85	0.005	4.54	0.001	3.89	46.4	0.35
Eq	1	19.83	22.39	2.02	0.058	10.71	0.002	10.71	100	4.80
MC8B	1	15.02	15.79	1.03	0.034	30.44	0.001	1.52	95.1	3.22
2368G	1	7.52	9.94	3.55	0.018	4.92	0.002	1.17	75.7	1.61
2714CQ	1	97.90	136.94	3.27	0.016	94.50	0.030	18.45	100	29.34
3585CQ	1	282.25	283.99	3.93	39445.60	132.24	0.002	1.10	99.4	60.48

Table 5.4 The λ (bSiO$_2$%) and α (slope) calculated from the Si and Al dissolution with 0.5M NaOH (see Eq.5.2, modified after Kamatani and Oku. (2000). For comparation, the calculated bSiO$_2$% following DeMaster (1981) is also presented. Both methods show variations of bSiO$_2$% due to different calculations.

Sample	Kamatani and Oku (2000)								DeMaster (1981)	Mortlock and Froelich (1989)
	5 h		8 h		24 h		Best estimate			
	α	λ	α	λ	α	λ	α	λ	bSiO$_2$%	bSiO$_2$%
Kaolinite (NP)	-0.27	1.17	1.20	0.39	1.22	0.53	1.23	-0.56	3.58	8.71
Kaolinite (P)	-0.94	1.22	1.21	-0.86	1.24	-1.16	1.20	-0.21	9.32	13.11
Bentonite (NP)	1.61	2.79	2.85	1.52	2.64	1.97	2.97	-0.58	3.81	11.03
Bentonite (P)	1.77	2.88	2.58	2.28	2.65	2.11	2.97	-0.67	4.35	9.50
C12 (NP)	0.61±0.05	3.02±0.12	2.86±0.08	0.68±0.04	2.36±0.03	0.98±0.03	2.29±0.24	0.97±0.31	1.94±0.06	2.73±0.03
C12 (P)	1.23±0.05	3.69±0.07	3.67±0.09	1.24±0.07	4.17±0.11	0.77±0.08	3.60±0.19	2.08±0.36	3.96±0.14	5.34±0.06
C12 (NP-FG)	0.68	3.08	2.93	0.76	2.37	1.11	2.37	0.97	2.05	2.97

C12 (P-FG)	1.20	3.74	3.68	1.26	4.10	0.82	3.63	2.03	4.34	5.95
B10 (NP)	0.07	2.19	1.87	0.33	1.92	0.27	1.83	0.51	1.33	2.50
B10 (P)	0.49	2.31	2.71	0.05	3.17	-0.6	3.56		3.00	4.65
ST4	0.40	3.43	3.39	0.41	3.38	0.41	2.79	0.88	0.93	1.65
Still Pond	1.24	2.41	2.22	1.38	2.73	0.90	3.02	0.56	2.87	3.94
R-64	4.75	2.46	2.29	4.90	2.73	4.42	3.35	3.09	6.47	8.12
D226	0.52	2.19	2.22	0.50	1.87	0.70	1.71	0.83	1.47	1.93
MTB2	3.36	1.59	1.47	3.53	1.35	3.80	1.28	4.10	4.51	7.43
H555	0.18	3.49	3.27	0.23	2.86	0.35	2.82	0.35	0.81	1.40
F104	-0.02	5.26	5.28	-0.02	4.74	0.01	4.19	0.08	0.19	0.36
Eq	-6.34	29.24	19.35	-2.65	22.99	-3.97	2.30	3.92	3.83	4.39
MC8B	2.44	7.11	5.21	2.63	2.84	2.88	1.71	3.05	3.15	3.26
2368G	0.84	2.30	2.10	0.90	1.68	1.04	1.42	1.18	1.56	1.69
2714CQ	7.45	53.16	47.68	8.55	28.77	12.34	2.68	27.69	19.07	22.71
3585CQ	60.29	0.75	-0.45	60.76	1.06	60.08	2.00	59.37	59.74	60.55

Table 5.5 Comparation of the bSiO2% determined and/or calculated by different methods. The values in the brackets represent: 100%*(standard deviation/average bSiO2%).

Sample	Modeling (1 h)	Modeling (24 h)	Kamatani and Oku (2000)	DeMaster (1981)	Mortlock and Froelich (1989)	Average
C12	1.13	2.47 ± 0.02	1.63 ± 0.03	1.40 ± 0.14	2.73 ± 0.03	1.87 ± 0.69 (37%)
B10	0.27	0	0.51	0.97	2.50	0.85 ± 0.99 (116%)
ST4	0.89	1.27	0.88	0.87	1.65	1.11 ± 0.35 (31%)
Still Pond	2.70	3.37	0.56	2.51	3.94	2.62 ± 1.28 (49%)
R-64	7.05	7.07	3.09	6.15	8.12	6.30 ± 1.92 (31%)
D226	1.91	1.78	0.83	1.30	1.93	1.55 ± 0.48 (31%)
MTB2	5.63	5.78	4.10	4.25	7.43	5.44 ± 1.35 (25%)
H555	0.76	1.29	0.35	0.77	1.40	0.91 ± 0.43 (47%)
F104	0.09	0.35	0.08	0.11	0.36	0.20 ± 0.14 (73%)
Eq	7.08	4.8	3.92	4.15	4.39	4.87 ± 1.28 (26%)
MC8B	4.48	3.22	3.05	3.18	3.26	3.44 ± 0.59 (17%)
2368G	1.84	1.61	1.18	1.37	1.69	1.54 ± 0.26 (17%)
2714CQ	10.67	29.34	27.69	15.41	22.71	21.16 ± 7.98 (38%)
3585CQ	66.09	60.48	59.37	60.62	60.55	61.42 ± 2.66 (4%)

Table 5.6 List of biogenic silica accumulation rate (g cm^{-2} ky^{-1}) and annual biogenic silica burial flux (Tmol-Si yr^{-1}) of different marine regions. The 56 different marine regions were grouped following the biogeochemical provinces defined by Longhurst et al, (1995). The area of each province is referred to Longhurst et al, (1995).

Code	Marion regions	Area (10^6 km^2)	Accumulation rate (g cm^{-2} ky^{-1})		Annual burial Flux (Tmol-Si-yr^{-1})	
			Raw data	This study	Raw data	This study
BPLR	Polar - Boreal Polar Province (POLR)	1.66	0.014	0.013	0.004	0.004
ARCT	Polar - Atlantic Arctic Province	2.10	0.124	0.087	0.043	0.030
SARC	Polar - Atlantic Subarctic Province	2.33	0.060	0.031	0.023	0.012
NADR	Westerlies - N. Atlantic Drift Province (WWDR)	3.50	0.119	0.074	0.069	0.043
NASW	Westerlies - N. Atlantic Subtropical Gyral Province (West) (STGW)	2.80	0.035	0.031	0.034	0.030
NATR	Trades - N. Atlantic Tropical Gyral Province (TRPG)	8.27	0.055	0.043	0.076	0.059
WTRA	Trades - Western Tropical Atlantic Province	5.36	0.071	0.048	0.064	0.043
ETRA	Trades - Eastern Tropical Atlantic Province	2.34	0.081	0.057	0.072	0.051
SATL	Trades - South Atlantic Gyral Province (SATG)	17.77	0.052	0.027	0.153	0.081
CNRY	Coastal - Canary Coastal Province (EACB)	0.81	0.087	0.056	0.012	0.008
GUIA	Coastal - Guianas Coastal Province	1.23	0.043	0.043	0.009	0.009

NWCS	Coastal - NW Atlantic Shelves Province	2.00	0.105	0.105	0.035	0.035
MEDI	Westerlies - Mediterranean Sea, Black Sea Province	3.08	0.004	0.004	0.002	0.002
CARB	Trades - Caribbean Province	4.48	0.118	0.062	0.088	0.046
NASE	Westerlies - N. Atlantic Subtropical Gyral Province (East) (STGE)	4.45	0.077	0.048	0.057	0.036
BRAZ	Coastal - Brazil Current Coastal Province	1.20	0.082	0.082	0.016	0.016
FKLD	Coastal - SW Atlantic Shelves Province	1.42	0.231	0.151	0.055	0.036
BENG	Coastal - Benguela Current Coastal Province	1.13	0.043	0.038	0.008	0.007
MONS	Trades - Indian Monsoon Gyres Province	14.21	0.092	0.058	0.219	0.138
ISSG	Trades - Indian S. Subtropical Gyre Province	19.25	0.301	0.225	0.964	0.723
EAFR	Coastal - E. Africa Coastal Province	3.72	0.036	0.018	0.022	0.011
ARAB	Coastal - NW Arabian Upwelling Province	2.93	0.108	0.093	0.053	0.046
INDW	Coastal - W. India Coastal Province	0.80	0.249	0.236	0.033	0.031
AUSW	Coastal - Australia-Indonesia Coastal Province	2.94	0.111	0.086	0.054	0.042
BERS	Polar - N. Pacific Epicontinental Province	3.89	1.111	1.091	0.720	0.707
PSAE	Westerlies - Pacific Subarctic Gyres Province (East)	3.20	0.106	0.096	0.057	0.051
PSAW	Westerlies - Pacific Subarctic Gyres Province (West)	2.90	0.254	0.230	0.123	0.111
KURO	Westerlies - Kuroshio Current Province	3.70	0.311	0.323	0.192	0.199

NPPF	Westerlies - N. Pacific Polar Front Province	3.02	0.028	0.022	0.014	0.011
NPSW	Westerlies - N. Pacific Subtropical Gyre Province (West)	3.93	0.026	0.013	0.017	0.009
TASW	Westerlies - Tasman Sea Province	1.65	0.013	0.007	0.013	0.007
SPSG	Westerlies - S. Pacific Subtropical Gyre Province	37.29	0.037	0.026	0.232	0.161
NPTG	Trades - N. Pacific Tropical Gyre Province	21.09	0.006	0.003	0.020	0.012
PNEC	Trades - N. Pacific Equatorial Countercurrent Province	8.17	0.101	0.095	0.137	0.129
PEQD	Trades - Pacific Equatorial Divergence Province	10.34	0.149	0.127	0.258	0.218
WARM	Trades - W. Pacific Warm Pool Province	16.78	0.072	0.041	0.201	0.114
ARCH	Trades - Archipelagic Deep Basins Province	8.84	0.121	0.195	0.178	0.287
CCAL	Coastal - California Upwelling Coastal Province	0.96	0.045	0.028	0.007	0.004
CAMR	Coastal - Central American Coastal Province	1.26	0.247	0.247	0.052	0.052
CHIL	Coastal - Chile-Peru Current Coastal Province	2.61	0.236	0.133	0.103	0.058
CHIN	Coastal - China Sea Coastal Province	0.97	−	1.357	−	0.219
SUND	Coastal - Sunda-Arafura Shelves Province	6.33	0.250	0.303	0.264	0.319
NEWZ	Coastal - New Zealand Coastal Province	1.04	0.078	0.042	0.013	0.007
SSTC	Westerlies - S. Subtropical Convergence Province	16.84	0.102	0.061	0.287	0.170
SANT	Westerlies - Subantarctic Province	30.25	0.267	0.187	1.344	0.941
ANTA	Polar - Antarctic Province	8.87	0.407	0.326	0.601	0.482
APLR	Polar - Austral Polar Province	1.93	0.190	0.160	0.061	0.052

NECS	Coastal - NE Atlantic Shelves Province	1.36	−	0.075	−	0.017
GUIN	Coastal - Guinea Current Coastal Province	1.42	−	0.800	−	0.189
REDS	Coastal - Red Sea, Persian Gulf Province	0.56	−	0.003	−	0.000.560
INDE	Coastal - E. India Coastal Province	0.97	−	0.236	−	0.0380.97
ALSK	Coastal - Alaska Downwelling Coastal Province	0.59	−	0.028	−	0.0030.59
AUSE	Coastal-Pacific	1.14	−	0.087	−	0.017
GFST	Westerlies - Gulf Stream Province	1.10	−	0.031	−	0.006
NPSE	Westerlies-Pacific	6.83	−	0.022	−	0.025
OCAL	Westerlies-Pacific	2.39	−	0.028	−	0.011

6. Summary and general conclusions

This thesis aims to redefine the burial flux of bSi in the world ocean and its role in the global marine silicon cycle. To achieve the research aims, a thorough evaluation of the physical and chemical properties of sediments obtained from different marine depositional environments (CCMZs: the Chinese marginal seas, Congo deep-sea fan, Baffin Bay; open ocean: the Atlantic, Pacific and Indian Ocean sector of the Southern Ocean, Equatorial Pacific, North Atlantic) were examined using multiple methods (e.g., different wet chemical methods, XRD and IR). Knowing the sediment physical (grain size, specific surface area) and chemical (organic carbon, inorganic carbon, total nitrogen, clay mineral content) properties assisted a better understanding the factors that influence the measurement of bSi in sediments. Through this thesis, a comprehensive understanding of the bSi determinations and the methodological biases of the bSi burial flux at both CCMZs (Chinese marginal seas as a case study) and open oceans has been achieved. Further, detailed descriptions of the Si vs. Al modeling parameters and their relationships with silicate mineral contents were established. The main conclusions are presented below:

(1) Based on the extraction of sediments of CCMZs of the East China Seas using different concentrations of alkaline solutions (0.1 M, 0.2 M, 2.0 M of Na_2CO_3 and 0.5 M NaOH), pretreatment procedures and different wet chemical methods (Si/time and Si/Al method), we found that alkaline extractions using 2.0 M Na_2CO_3 solution resulted in an overestimation of the $bSiO_2$% owing to silica being digested from clay minerals. Applying a 0.1 M Na_2CO_3 digestion (20 h) can minimize the silicate minerals interference on bSi determination but can cause at least 20% underestimation of the $bSiO_2$% owing to incomplete digestion of sponge spicules. Ensuring a complete extraction of sponge spicules remains a challenge and microscopic observation is recommended when determining the $bSiO_2$% since spicules are widely spread on seafloor.

(2) Measurement of alkaline extracted Si and Al of pretreated sediments (i.e., grinding, HCl and H_2O_2 pretreatment) showed enhanced dissolution of both bSi and silicate minerals. Based on the first order non-linear dissolution models, we conclude that the increased $bSiO_2$% after pretreatment is due to the digestion of the authigenic silicate phases and clays, and subsequently overestimate the bSi burial flux. Thus, we argue that the pre-treatment process applied in previous estimates is the main reason that bSi burial flux was previously over-estimated, and pretreatment procedure is not suggested for studies aiming to measure bSi in

sediments. For studies aiming to quantify authigenic alumino-silicates, combination of both Si and Al as well as Si isotopes in sequential alkaline extractions are necessary.

(3) Based on a thorough measurement of types of bSi and the $bSiO_2$% in sediments of various depositional environments using multiple methods, we found the XRD method overestimates the $bSiO_2$% by 50% to 550% and the IR method underestimates the $bSiO_2$% by 10% to 35%. Therefore, the wet chemical methods are more appropriate of measuring the bSi in marine sediments so far, although there is variability in the determined $bSiO_2$% among different wet chemical techniques. Among the several alkaline extraction techniques (e.g., the Si/time method and the Si/Al method), the Si/Al method is recommended for measuring the $bSiO_2$% in sediment of CCMZs where silicate mineral content is high, whereas the Si/time method is recommended for measuring the $bSiO_2$% in sediments of open oceans where silicate mineral content is low. Further, the proposed general procedure for determining bSi in sediment of CCMZs and open oceans is recommended for future studies that measure the $bSiO_2$%. In order to ensure the accurate determination of bSi from different depositional settings in the future, we strongly suggest the development of an international intercalibration exercise.

(4) Based on the application of the Si/Al method in order to produce accurate $bSiO_2$% results, the bSi burial flux of the east China seas was revised to 253 ± 286 Gmol-SiO_2 yr^{-1}, which is one third of the previously reported (924 ± 693 Gmol-SiO_2 yr^{-1}). This estimate still underestimates bSi burial flux of the east China seas, and further works on examining the resistant bSi (i.e., phytolith, radiolarian and sponge spicule) content are still required.

(5) Through evaluating the methodological biases of bSi, the global bSi burial flux was re-evaluated. The bSi burial flux at the coastal regions is 3.0 ± 0.6 Tmol-Si yr^{-1}, which represents about 45% of the global bSi burial flux (6.7 ± 2.7 Tmol-Si yr^{-1}). The global bSi burial flux determined by this thesis is about 30% lower than the previous studies, which addressed the importance of selecting an appropriate bSi determining method, and the needs of a better understanding the bSi burial flux determinations in order to know either there is an overestimation by previous study or there is a missing Si sink.

(6) The simultaneous alkaline extractions of Si and Al in sediments of Chinese marginal Seas and the determined physical as well as the chemical properties of sediments indicated an incongruent dissolution of Si from different types of sediments of CCMZs. Our results demonstrated that more Si (sourced from bSi and silicate minerals) and Al dissolve from muddy sediments than sandy sediments. Although the dissolution rate of silicate minerals is slower than bSi, the contribution of silicate mineral to the reactive Si pool overweighs the bSi due to their large quantities, highlighting muddy sediments as an important potential Si

source for the CCMZs of Chinese marginal Seas. We found decreased bSi reactivity corelate with low Si: Al ratios, especially for samples of muddy deposits. The source of Al is likely originating from silicate minerals dissolution. The incorporation of Al into bio-siliceous structures hinders the dissolution of bSi, thus enhances bSi preservation. The preservation efficiency may vary among different types of bSi, applying continuous alkaline extraction can help to understand the differences due to its advantage of differentiating Si phases with different rates of dissolution. Further, high-resolution simultaneous extraction of Si and Al combined with non-linear first order dissolution models uncover major clay minerals exists in sediments because of the different chemical characteristics (Si:Al ratios) of various types of clays and will require dedicated studies.

The main innovative points of the thesis: (1) This thesis evaluated the methodological biases of bSi through measuring opal content in different regions of the world oceans using wet chemical methods, XRD and IR method. Through a thorough evaluation of factors (i.e., pretreatment of sediment, sediment matrices) that affect the bSi measurements, this thesis proposed a general wet alkaline extraction procedure that is suitable for measuring bSi in sediments of marginal seas and open oceans. The new general wet chemical procedure will minimize the uncertainty of the determined bSi content which is important for marine Si research. (2) This thesis re-evaluated the bSi burial flux of the east China seas CCMZs and the global ocean. The new estimates showed previous estimations over-assessed the bSi burial flux. The results addressed the importance of appropriate determination of bSi content in sediments and the development of an international intercalibration exercise in further studies (3) Through the measurement of sediment mineral compositions, grain-size analysis, chemical composition of sediment (IC, OC, bSi and TN) and the simultaneous measurement of Si and Al from wet alkaline extraction experiments, this study provides a theoretical basis for the first-order dissolution kinetic models of Si.

References:

[1] Amann, T., Hartmann, J., Struyf, E., De Oliveira Garcia, W., Fischer, E. K., Janssens, I., et al. (2020). Enhanced Weathering and related element fluxes - A cropland mesocosm approach. *Biogeosciences* 17, 103–119.

[2] Andrews, J. T. (2019). Baffin bay/nares strait surface (Seafloor) sediment mineralogy: Further investigations and methods to elucidate spatial variations in provenance. *Can. J. Earth Sci.* 56, 814–828.

[3] Armstrong, H. A., and Brasier, M. D. (2013). "Radiozoa (Acantharia, Phaeodaria and Radiolaria) And Heliozoa," in *Microfossils*, eds. H. A. Armstrong and M. D. Brasier (Hoboken: Blackwell Publishing Ltd), 188–199.

[4] Armstrong, R. A., Lee, C., Hedges, J. I., Honjo, S., and Wakeham, S. G. (2002). A new, mechanistic model for organic carbon fluxes in the ocean based on the quantitative association of POC with ballast minerals. *Deep. Res. Part II Top. Stud. Oceanogr.* 49, 219–236.

[5] Baker, E., Odenthal, B., Walkusz, W., Siferd, T., Rios, P., Tompkins, G., et al. (2018). Sponges from the 2010-2014 Paamiut Multispecies Trawl Surveys, Eastern Arctic and Subarctic: Class Demospongiae, Subclass Heteroscleromorpha, Order Poecilosclerida, Families Dendoricellidae and Tedaniidae.

[6] Barão, L., Clymans, W., Vandevenne, F., Meire, P., Conley, D. J., and Struyf, E. (2014). Pedogenic and biogenic alkaline-extracted silicon distributions along a temperate land-use gradient. *Eur. J. Soil Sci.* 65, 693–705.

[7] Barão, L., Vandevenne, F., Clymans, W., Frings, P., Ragueneau, O., Meire, P., et al. (2015). Alkaline-extractable silicon from land to ocean: A challenge for biogenic silicon determination. *Limnol. Oceanogr. Methods* 13, 329–344.

[8] Baronas, J. J., Hammond, D. E., McManus, J., Wheat, C. G., and Siebert, C. (2017). A global Ge isotope budget. *Geochim. Cosmochim. Acta* 203, 265–283.

[9] Baronas, J. J., Hammond, D. E., Rouxel, O. J., and Monteverde, D. R. (2019). A first look at dissolved ge isotopes in marine sediments. *Front. Earth Sci.* 7:162.

[10] Barron, J. A., Bukry, D., and Hendy, I. L. (2015). High-resolution paleoclimatology of the Santa Barbara Basin during the Medieval Climate Anomaly and early Little Ice Age based on diatom and silicoflagellate assemblages in Kasten core SPR0901-02KC. *Quat. Int.* 387, 13–22.

[11] Biard, T. (2022). Diversity and ecology of Radiolaria in modern oceans. *Environ.*

Microbiol. 24, 2179–2200.

[12] Biard, T., Bigeard, E., Audic, S., Poulain, J., Gutierrez-Rodriguez, A., Pesant, S., et al. (2017). Biogeography and diversity of Collodaria (Radiolaria) in the global ocean. *ISME J.* 11, 1331–1344.

[13]Biscaye, P. E. (1965). Geological Society of America Bulletin Mineralogy and Sedimentation of Recent Deep-Sea Clay in the Atlantic Ocean and Adjacent Seas and Oceans. *Geol. Soc. Am. Bulletim* 76, 803–832.

[14] Blattmann, T. M., Liu, Z., Zhang, Y., Zhao, Y., Haghipour, N., Montluçon, D. B., et al. (2019). Mineralogical control on the fate of continentally derived organic matter in the ocean. *Science (80-.).* 366, 742–745.

[15] Blott, S. J., and Pye, K. (2001). Gradistat: A grain size distribution and statistics package for the analysis of unconsolidated sediments. *Earth Surf. Process. Landforms* 26, 1237–1248.

[16] Boltovskoy, D. (2017). Vertical distribution patterns of Radiolaria Polycystina (Protista) in the World Ocean: Living ranges, isothermal submersion and settling shells. *J. Plankton Res.* 39, 330–349.

[17] Boltovskoy, D., Anderson, O. R., and Correa, N. M. (2017). "Radiolaria and Phaeodaria," in *Handbook of the Protists*, 731–763.

[18] Boltovskoy, D., and Correa, N. (2016). Biogeography of Radiolaria Polycystina (Protista) in the World Ocean. *Prog. Oceanogr.* 149, 82–105.

[19] Boltovskoy, D., Kling, S. A., Takahashi, K., and Kjell, B. (2010). World atlas of distribution of recent polycystina (radiolaria). *Palaeontol. Electron.* 13.

[20] Bostrom, K., Joensuu, O., Valdi, S. S., and Riera, M. (1972). Geochemical history of South Atlantic Ocean sediments since Late Cretaceous. *Mar. Geol.* 12, 85–121.

[21] Boury-Esnault, N., and Rutzler, K. (1997). *Thesaurus of Sponge Morphology*. , eds. N. Boury-Esnault and K. Rutzler Washington, D.c.: Smithsonian Institution Press.

[22] Bracher, A., Vountas, M., Dinter, T., Burrows, J. P., Rottgers, R., and Peeken, I. (2009). Quantitative observation of cyanobacteria and diatoms from space using PhytoDOAS on SCIAMACHY data. *Biogeosciences* 6, 751–764.

[23] Brzezinski, M. A., Krause, J. W., Baines, S. B., Collier, J. L., Ohnemus, D. C., and Twining, B. S. (2017). Patterns and regulation of silicon accumulation in Synechococcus spp. *J. Phycol.* 53, 746–761.

[24] Cael, B. B., Dutkiewicz, S., and Henson, S. A. (2021). Abrupt shifts in 21st-century plankton communities. *Sci. Adv.*

[25] Cama, J., and Ganor, J. (2015). *Dissolution Kinetics of Clay Minerals*. Elsevier.

[26] Cheize, M., Planquette, H. F., Fitzsimmons, J. N., Pelleter, E., Sherrell, R. M., Lambert, C., et al. (2019). Contribution of resuspended sedimentary particles to dissolved iron and manganese in the ocean: An experimental study. *Chem. Geol.* 511, 389–415.

[27] Chen, C., Zhao, G., Chen, M., Lan, D., and Lan, B. (2014). Diatom distribution in surface sediments from Chinese inshore waters and the relationship to modern environmental variables. *Chinese J. Oceanol. Limnol.* 32, 828–844.

[28] Chen, M. H., Zhang, Q., Zhang, L. L., Zarikian, C. A., and Wang, R. J. (2014). Stratigraphic distribution of the radiolarian Spongodiscus biconcavus Haeckel at IODP Site U1340 in the Bering Sea and its paleoceanographic significance. *Palaeoworld* 23, 90–104.

[29] Chen, M., and Tan, Z. (1997). Radiolarian distribution in surface sediments of the northern and central South China Sea. *Mar. Micropaleontol.* 32, 173–194.

[30] Cho, H. M., Kim, G., Kwon, E. Y., Moosdorf, N., Garcia-Orellana, J., and Santos, I. R. (2018). Radium tracing nutrient inputs through submarine groundwater discharge in the global ocean. *Sci. Rep.* 8, 4–10.

[31] Chou, Y., Lou, J. Y., Chen, C. T. A., and Liu, L. L. (2012). Spatial distribution of sponge spicules in sediments around Taiwan and the Sunda Shelf. *J. Oceanogr.* 68, 905–912.

[32] Chu, J. W. F., Maldonado, M., Yahel, G., and Leys, S. P. (2011). Glass sponge reefs as a silicon sink. *Mar. Ecol. Prog. Ser.* 441, 1–14.

[33] Conley, D. J. (1998). An interlaboratory comparison for the measurement of biogenic silica in sediments. *Mar. Chem.* 63, 39–48.

[34] Conley, D. J., Frings, P. J., Fontorbe, G., Clymans, W., Stadmark, J., Hendry, K. R., et al. (2017). Biosilicification drives a decline of dissolved si in the oceans through geologic time. *Front. Mar. Sci.* 4.

[35] Conley, D. J., and Schelske, C. L. (1993). Potential Role of Sponge Spicules in Influencing the Silicon Biogeochemistry of Florida Lakes. *Can. J. Fish. Aquat. Sci.* 50, 296–302.

[36] Conley, D. J., and Schelske, C. L. (2001). "Biogenic Silica," in *Biogenic silica. In Tracking Environmental Change Using Lake Sediments,* ed. L. W. Smol JP, Birks HJB (KluwerAcademic Publishers, Dordrecht,The Netherlands.), 281–293.

[37] Cortese, G., and Prebble, J. (2015). A radiolarian-based modern analogue dataset for palaeoenvironmental reconstructions in the southwest Pacific. *Mar. Micropaleontol.* 118, 34–49.

[38] Costello, M. J., Cheung, A., and De Hauwere, N. (2010). Surface area and the seabed area,

volume, depth, slope, and topographic variation for the world's seas, oceans, and countries. *Environ. Sci. Technol.* 44, 8821–8828.

[39] Dai, Z., Xue, Y., Zhang, H., Tu, C., and Luo, Y. (2017). Biogenic silica in the surface sediment of the Bohai Sea. *Mar. Sci.* 41, 42–49.

[40] DeMaster, D. J. (1981). The supply and accumulation of silica in the marine environment. *Geochim. Cosmochim. Acta* 45, 1715–1732.

[41] DeMaster, D. J. (1991). "Measuring biogenic silica in marine sediments and suspended matter," in *Marine Particles: Analysis and Characterization,* ed. D. W. S. David C. Hurd (American Geophysical Union), 363–367.

[42] DeMaster, D. J. (2002). The accumulation and cycling of biogenic silica in the Southern Ocean: Revisiting the marine silica budget. *Deep. Res. Part II Top. Stud. Oceanogr.* 49, 3155–3167.

[43] DeMaster, D. J. (2019). *The global marine silica budget: Sources and sinks*. 3rd ed. Elsevier Inc.

[44] Dixit, S., and Van Cappellen, P. (2002). Surface chemistry and reactivity of biogenic silica. *Geochim. Cosmochim. Acta* 66, 2559–2568.

[45] Dixit, S., and Van Cappellen, P. (2003). Predicting benthic fluxes of silicic acid from deep-sea sediments. *J. Geophys. Res. Ocean.* 108, 1–10.

[46] Dixit, S., Van Cappellen, P., and Van Bennekom, A. J. (2001). Processes controlling solubility of biogenic silica and pore water build-up of silicic acid in marine sediments. *Mar. Chem.* 73, 333–352.

[47] Dodd, J. P., Wiedenheft, W., and Schwartz, J. M. (2017). Dehydroxylation and diagenetic variations in diatom oxygen isotope values. *Geochim. Cosmochim. Acta* 199, 185–195.

[48] Dutkiewicz, A., Müller, R. D., O'Callaghan, S., and Jónasson, H. (2015). Census of seafloor sediments in the world's ocean. *Geology* 43, 795–798.

[49] Dutkiewicz, S., Cermeno, P., Jahn, O., Follows, M. J., Hickman, A. A., Taniguchi, D. A. A., et al. (2020). Dimensions of marine phytoplankton diversity. *Biogeosciences* 17, 609–634.

[50] Eggimann, D. W., Manheim, F. T., and Betzer, P. R. (1980). Dissolution and analysis of amorphous silica in marine sediments. *J. Sediment. Petrol.* 50, 215–225.

[51] Ehlert, C., Doering, K., Wallmann, K., Scholz, F., Sommer, S., Grasse, P., et al. (2016). Stable silicon isotope signatures of marine pore waters – Biogenic opal dissolution versus authigenic clay mineral formation. *Geochim. Cosmochim. Acta* 191, 102–117.

[52] Ehlert, C., Grasse, P., Mollier-Vogel, E., Böschen, T., Franz, J., F.de Souza, G., et al.

(2012). Factors controlling the silicon isotope distribution in waters and surface sediments of the Peruvian coastal upwelling. *Geochim. Cosmochim. Acta* 99, 128–145.

[53] Eisma, D., and van der Gaast, S. J. . (1971). Determination of opal in marine sediments by X-Ray diffraction. *Netherlands J. Sea Res.* 5, 382–389.

[54] Fabre, S., Jeandel, C., Zambardi, T., Roustan, M., and Almar, R. (2019). An Overlooked Silica Source of the Modern Oceans: Are Sandy Beaches the Key? *Front. Earth Sci.* 7, 1–13.

[55] Finkel, Z. V., Matheson, K. A., Regan, K. S., and Irwin, A. J. (2010). Genotypic and phenotypic variation in diatom silicification under paleo-oceanographic conditions. *Geobiology* 8, 433–445.

[56] Fontorbe, G., De La Rocha, C. L., Chapman, H. J., and Bickle, M. J. (2013). The silicon isotopic composition of the Ganges and its tributaries. *Earth Planet. Sci. Lett.* 381, 21–30.

[57] Fontorbe, G., Frings, P. J., De La Rocha, C. L., Hendry, K. R., Carstensen, J., and Conley, D. J. (2017). Enrichment of dissolved silica in the deep equatorial Pacific during the Eocene-Oligocene. *Paleoceanography* 32, 848–863.

[58] Flemming, B. W. (2000). A revised textural classification of gravel-free muddy sediments on the basis of ternary diagrams. Cont. Shelf Res. 20, 1125–1137.

[59] Frings, P. (2017). Revisiting the dissolution of biogenic Si in marine sediments: a key term in the ocean Si budget. *Acta Geochim.* 36, 429–432.

[60] Frings, P. J., De La Rocha, C., Struyf, E., van Pelt, D., Schoelynck, J., Hudson, M. M., et al. (2014). Tracing silicon cycling in the Okavango Delta, a sub-tropical flood-pulse wetland using silicon isotopes. *Geochim. Cosmochim. Acta* 142, 132–148.

[61] Frings, P. J., Oelze, M., Schubring, F., Frick, D. A., and von Blanckenburg, F. (2021a). Interpreting silicon isotopes in the Critical Zone. *Am. J. Sci.* 321, 1164–1203.

[62] Frings, P. J., Schubring, F., Oelze, M., and von Blanckenburg, F. (2021b). Quantifying biotic and abiotic Si fluxes in the Critical Zone with Ge/Si ratios along a gradient of erosion rates. *Am. J. Sci.* 321, 1204–1245.

[63] Frohlich, F. (1989). Deep-sea biogenic silica: new structural and analytical data from infrared analysis- geological implications. *Terra Res.* 1, 267–273.

[64] Gallinari, M., Ragueneau, O., Corrin, L., DeMaster, D. J., and Tréguer, P. (2002). The importance of water column processes on the dissolution properties of biogenic silica in deep-sea sediments I. Solubility. *Geochim. Cosmochim. Acta* 66, 2701–2717.

[65] Gallinari, M., Ragueneau, O., DeMaster, D. J., Hartnett, H., Rickert, D., and Thomas, C. (2008). Influence of seasonal phytodetritus deposition on biogenic silica dissolution in

marine sediments-Potential effects on preservation. *Deep. Res. Part II Top. Stud. Oceanogr.* 55, 2451–2464.

[66] Garzanti, E., Bayon, G., Dennielou, B., Barbarano, M., Limonta, M., and Vezzoli, G. (2021). The Congo deep-sea fan: Mineralogical, REE, and ND-isotope variability in Quartzose passive-margin sand. *J. Sediment. Res.* 91, 433–450.

[67] Gehlen, M., Beck, L., Calas, G., Flank, A. M., Van Bennekom, A. J., and Van Beusekom, J. E. E. (2002). Unraveling the atomic structure of biogenic silica: Evidence of the structural association of Al and Si in diatom frustules. *Geochim. Cosmochim. Acta* 66, 1601–1609.

[68] Gehlen, M., and van Raaphorst, W. (1993). Early diagenesis of silica in sandy North sea sediments: quantification of the solid phase. *Mar. Chem.* 42, 71–83.

[69] Geilert, S., Grasse, P., Doering, K., Wallmann, K., Ehlert, C., Scholz, F., et al. (2020). Impact of ambient conditions on the Si isotope fractionation in marine pore fluids during early diagenesis. *Biogeosciences* 17, 1745–1763.

[70] Goldberg, E. D. (1958). Determination of opal in marine sediments. *J. Mar. Res.*, 178–182.

[71] Golubev, S. V, Bauer, A., and Pokrovsky, O. S. (2006). Effect of pH and organic ligands on the kinetics of smectite dissolution at 25 ° C. *Geochim. Cosmochim. Acta* 70, 4436–4451.

[72] Griffin, J. J., Windom, H., and Goldberg, E. D. (1968). The distribution of clay minerals in the World Ocean. *Deep. Res. Oceanogr. Abstr.* 15, 433–459.

[73] García, Hernán E.; Locarnini, Ricardo A.; Zweng, Melissa M.; Mishonov, Alexey V.; Reagan, James R.; Weathers, Katharine A.; Baranova, Olga K.; Paver, Christopher R.; Seidov, Dan; Smolyar, Igor V. (2018). World Ocean Atlas 2018.

[74] García, H. E., K. Weathers, C. R. Paver, I. Smolyar, T. P. Boyer, R. A. Locarnini, M. M. Zweng, A. V. Mishonov, O. K. Baranova, D. Seidov, and J. R. Reagan, 2019. World Ocean Atlas 2018, Volume 4: Dissolved Inorganic Nutrients (phosphate, nitrate and nitrate+nitrite, silicate). A. Mishonov Technical Ed.; NOAA Atlas NESDIS 84, 35 pp.

[75] Grasshoff, K., Ehrhardt, M., and Kremling, K. (1983). Methods of seawater analysis. 2nd Edition Vol. 419 (Weinheim: WILEY-VCH Verlag Chemie GmbH).

[76] Gutt, J., Böhmer, A., and Dimmler, W. (2013). Antarctic sponge spicule mats shape macrobenthic diversity and act as a silicon trap. *Mar. Ecol. Prog. Ser.* 480, 57–71.

[77] Hamm, C. E., Merkel, R., Springer, O., Jurkojc, P., Maler, C., Prechtel, K., et al. (2003). Architecture and material properties of diatom shells provide effective mechanical protection. *Nature*, 841–843.

[78] Harrison, K. G. (2000). Role of increased marine silica input on paleo-pCO2 levels. *Paleoceanography* 15, 292–298.

[79] Hatton, J. R., Hendry, J. E., de Souza, K. R., Wadham, G. F., Ivanovic, J. L.,, R., et al. (2018). The silicon cycle impacted by past ice sheets. *Nat. Commun.* 9, 1–10.

[80] Hawkings, J. R., Wadham, J. L., Benning, L. G., Hendry, K. R., Tranter, M., Tedstone, A., et al. (2017). Ice sheets as a missing source of silica to the polar oceans. *Nat. Commun.* 8.

[81] Hayes, C. T., Costa, K. M., Anderson, R. F., Calvo, E., Chase, Z., Demina, L. L., et al. (2021). Global Ocean Sediment Composition and Burial Flux in the Deep Sea. *Global Biogeochem. Cycles* 35, 1–25.

[82] Hendry, K. R., Marron, A. O., Vincent, F., Conley, D. J., Gehlen, M., Ibarbalz, F. M., et al. (2018). Competition between silicifiers and non-silicifiers in the past and present ocean and its evolutionary impacts. *Front. Mar. Sci.* 5, 1–21.

[83] Hilborn, R., and Mangel, M. (1997). "The ecological detective: confrontingmodels with data," in Monographs in population biology no. 28. Eds. S. A. Levin andH. S. Horn (NJ, USA: Princeton University Press), 315.

[84] Hori, R. S., Shinki, T., Iwakiri, A., Matsuoka, A., Suzuki, N., Ogane, K., et al. (2021). Growth pattern of the siliceous skeletons of living Spumellaria (Radiolaria) from the Kuroshio Current, offshore southwestern Shikoku Island, Japan. *Rev. Micropaleontol.* 71, 100504.

[85] Hu, B., Zhang, C., and Zhang, X. (2022). The Effects of Hydrochloric Acid Pretreatment on Different Types of Clay Minerals. *Minerals* 12.

[86] Hurd, D. C. (1973). Interactions of biogenic opal, sediment and seawater in the Central Equatorial Pacific. *Geochim. Cosmochim. Acta* 37.

[87] Hurd, D. C. (1983). "Hurd 1983 Physical adn chemical properties of ciliceous skeletons.pdf," in *Silicon Geochemistry and Biogeochemistry*, ed. S. R. Aston (London: Academic Press), 187–245.

[88] Hurd, D. C., and Birdwhistell, S. (1983). On producing a more general model for biogenic silica dissolution. *Am. J. Sci.* 283, 1–28.

[89] Hurd, D. C., and Theyer, F. (1977). Changes in the physical and chemical properties of biogenic silica from the Central Equatorial Pacific: Part II. Refractive Index, Density, and Water Content of Acid-Cleaned Samples. *Am. J. Sci.* 277, 1168–1202.

[90] Hydes, D. J., and Liss, P. S. (1976). Fluorimetric method for the determination of low concentrations of dissolved aluminium in natural waters. *Analyst* 101, 922–931.

[91] Ingall, E., and Jahnke, R. (1994). Evidence for enhanced phosphorus regeneration from

marine sediments overlain by oxygen depleted waters. *Geochim. Cosmochim. Acta* 58, 2571–2575.

[92] Isson, T. T., and Planavsky, N. J. (2018). Reverse weathering as a long-term stabilizer of marine pH and planetary climate. *Nature* 560, 471–475.

[93] Jaijel, R., Goodman Tchernov, B. N., Biton, E., Weinstein, Y., and Katz, T. (2021). Optimizing a standard preparation procedure for grain size analysis of marine sediments by laser diffraction (MS-PT4SD: Marine sediments-pretreatment for size distribution). *Deep. Res. Part I Oceanogr. Res. Pap.* 167.

[94] Jeandel, C. (2016). Overview of the mechanisms that could explain the "Boundary Exchange" at the land-ocean contact. *Philos. Trans. R. Soc. A Math. Phys. Eng. Sci.* 374.

[95] Jeandel, C., and Oelkers, E. H. (2015). The influence of terrigenous particulate material dissolution on ocean chemistry and global element cycles. *Chem. Geol.* 395, 50–66.

[96] Jeandel, C., Peucker-Ehrenbrink, B., Jones, M. T., Pearce, C. R., Oelkers, E. H., Godderis, Y., et al. (2011). Ocean margins: The missing term in oceanic element budgets? *Eos (Washington. DC).* 92, 217–218.

[97] Kamatani, A. (1971). Physical and chemical characteristics of biogenous silica. *Mar. Biol.* 8, 89–95.

[98] Kamatani, A. (1982). Dissolution rates of silica from diatoms decomposing at various temperatures. *Mar. Biol.* 68, 91–96.

[99] Kamatani, A., and Oku, O. (2000). Measuring biogenic silica in marine sediments. *Mar. Chem.* 68, 219–229.

[100]Kamatani, A., Riley, J. P., and Skirrow, G. (1980). The dissolution of opaline silica of diatom tests in sea water. *J. Oceanogr. Soc. Japan* 36, 201–208.

[101] Köhler, S. J., Bosbach, D., and Oelkers, E. H. (2005). Do clay mineral dissolution rates reach steady state? *Geochim. Cosmochim. Acta* 69, 1997–2006.

[102] Komadel, P., and Madejová, J. (2006). Chapter 7.1 Acid Activation of Clay Minerals. *Dev. Clay Sci.* 1, 263–287.

[103]Koning, E., Brummer, G. J., Van Raaphorst, W., Van Bennekom, J., Helder, W., and Van Iperen, J. (1997). Settling, dissolution and burial of biogenic silica in the sediments off Somalia (northwestern Indian Ocean). *Deep. Res. Part II Top. Stud. Oceanogr.* 44, 1341–1360.

[104]Koning, E., Epping, E., and Van Raaphorst, W. (2002). Determining biogenic silica in marine samples by tracking silicate and aluminium concentrations in alkaline leaching solutions. *Aquat. Geochemistry* 8, 37–67.

[105]Koning, E., Gehlen, M., Flank, A. M., Calas, G., and Epping, E. (2007). Rapid post-mortem incorporation of aluminum in diatom frustules: Evidence from chemical and structural analyses. *Mar. Chem.* 103, 97–111.

[106]Kou, Q., Gong, L., and Li, X. (2018). A new species of the deep-sea spongicolid genus Spongicoloides (Crustacea, Decapoda, Stenopodidea) and a new species of the glass sponge genus Corbitella (Hexactinellida, Lyssacinosida, Euplectellidae) from a seamount near the Mariana Trench, with a novel. *Deep. Res. Part I Oceanogr. Res. Pap.* 135, 88–107.

[107]Lafond, A., Leblanc, K., Queguiner, B., Moriceau, B., Leynaert, A., Cornet, V., et al. (2019). Late spring bloom development of pelagic diatoms in Baffin Bay. *Elem. Sci. Anthr.* 7, 1–24.

[108]Landen, A., Holby, O., and Hall, O. J. (1996). Determination of biogenic silcia in marine sediments-selection of pretreatment method and effect of sample size. *Vatten* 52, 85–92.

[109]Leinen, M. (1977). A normative calculation technique for determining opal in deep-sea sediments. *Geochim. Cosmochim. Acta* 41, 671–676.

[110]Leinen, M. (1985). Techniques for determining opal in deep-sea sediments: A comparison of radiolarian counts and x-ray diffraction data. *Mar. Micropaleontol.* 9, 375–383.

[111]Lerman, A. ., Mackenzie, F. T. ., and Bricker, O. P. (1975). Rate of Dissoution of Aluminosilicates in Seawater. *Earth Planet. Sci. Lett.* 25, 82–88.

[112]Levi, C., Barton, J. L., Guillemet, C., Le Bras, E., and Lehuede, P. (1989). A remarkably strong natural glassy rod: the anchoring spicule of the Monorhaphis sponge. *J. Mater. Sci. Lett.* 8, 337–339.

[113]Leynaert, A., Fardel, C., Beker, B., Soler, C., Delebecq, G., Lemercier, A., et al. (2018). Diatom Frustules Nanostructure in Pelagic and Benthic Environments. *Silicon* 10, 2701–2709.

[114]Leynaert, A., Longphuirt, S. N., An, S., Lim, J. H., Claquin, P., Grall, J., et al. (2011). Tidal variability in benthic silicic acid fluxes and microphytobenthos uptake in intertidal sediment. *Estuar. Coast. Shelf Sci.* 95, 59–66.

[115]Leynaert, A., Nelson, D. M., Queguiner, B., and Treguer, P. (1993). The silica cycle in the Antarctic Ocean: is the Weddell Sea atypical? *Mar. Ecol. Prog. Ser.* 96, 1–15.

[116]Li, L., Li, F. M., Wang, Z. W., Zhao, M. X., Zhang, J., and Ren, J. L. (2018a). Factors influencing the use of dissolved aluminum as a source tracer in the East China Sea and adjacent waters. *Mar. Chem.* 204, 133–143.

[117]Li, X., Kou, Q., Wang, J., Gan, Z., Yang, M., Gong, L., et al. (2020a). Advances and

perspectives of researches on taxonomy and phylogeny of marine invertebrates in China. *Mar. Sci.* 44, 26–70.

[118]Li, Y., Fang, J., Tian, L. Z., Wang, F., and Chen, Y. S. (2020b). Diatom assemblages in surface sediments and their reflection on the water migration pathway from the inshore waters of western bohai bay, china. *Appl. Ecol. Environ. Res.* 18, 2179–2196.

[119]Li, Y., Wang, L., Fan, D., Chen, M., and Lin, Y. (2018b). Distribution of biogenic silica in seafloor sediments on the East China Sea inner shelf: Seasonal variations and typhoon impact. *Estuar. Coast. Shelf Sci.* 212, 353–364.

[120]Liang, Y., Ran, L., and Zhang, L. (2021). The spatial distribution of biogenic silica content and diatom abundance in the surface sediment of the China seas. *Acta Micropaleontol. Sin.* 38, 112–130.

[121]Liao, W. H., Planquette, H., Moriceau, B., Lambert, C., Desprez de Gesincourt, F., Laurenceau-Cornec, E., et al. (2023). The effect of temperature on the release of silicon, iron and manganese into seawater from resuspended sediment particles. *Geochim. Cosmochim. Acta* 351, 1–13.

[122]Lippold, J., Luo, Y., Francois, R., Allen, S. E., Gherardi, J., Pichat, S., et al. (2012). Strength and geometry of the glacial Atlantic Meridional Overturning Circulation. *Nat. Geosci.* 5, 813–816.

[123]Liu, D., Liu, L., Di, B., Wang, Y., and Wang, Y. (2015). Paleoenvironmental analyses of surface sediments from the Bohai Sea, China, using diatoms and silicoflagellates. *Mar. Micropaleontol.* 114, 46–54.

[124]Liu, J., Zang, J., Bouwman, L., Liu, S., Yu, Z., and Ran, X. (2016). Distribution and budget of dissolved and biogenic silica in the Bohai Sea and Yellow Sea. *Biogeochemistry* 130, 85–101.

[125]Liu, L., Zhang, Q., Chen, M. H., Zhang, L. L., and Xiang, R. (2017). Radiolarian biogeography in surface sediments of the Northwest Pacific marginal seas. *Sci. China Earth Sci.* 60, 517–530.

[126]Liu, S. M., Hong, G. H., Zhang, J., Ye, X. W., and Jiang, X. L. (2009). Nutrient budgets for large Chinese estuaries. *Biogeosciences* 6, 2245–2263. doi: 10.5194/bg-6-2245-2009.

[127]Liu, S. M., Li, L. W., and Zhang, Z. (2011). Inventory of nutrients in the Bohai. *Cont. Shelf Res.* 31, 1790–1797.

[128]Liu, S. M., Ye, X. W., Zhang, J., and Zhao, Y. F. (2002). Problems with biogenic silica measurement in marginal seas. *Mar. Geol.* 192, 383–392.

[129]Liu, S. M., Zhang, J., Chen, S. Z., Chen, H. T., Hong, G. H., Wei, H., et al. (2003).

Inventory of nutrient compounds in the Yellow Sea. *Cont. Shelf Res.* 23, 1161–1174.

[130]Liu, S. M., Zhang, J., and Li, R. X. (2005). Ecological significance of biogenic silica in the East China Sea. *Mar. Ecol. Prog. Ser.* 290, 15–26.

[131]Lipps, J.H. (1979). Silicoflagellates . In: Paleontology. Encyclopedia of Earth Science. Springer, Berlin, Heidelberg.

[132]Llopis Monferrer, N., Boltovskoy, D., Tréguer, P., Sandin, M. M., Not, F., and Leynaert, A. (2020). Estimating Biogenic Silica Production of Rhizaria in the Global Ocean. *Global Biogeochem. Cycles* 34.

[133]Llopis Monferrer, N., Leynaert, A., Tréguer, P., Gutiérrez-Rodríguez, A., Moriceau, B., Gallinari, M., et al. (2021). Role of small Rhizaria and diatoms in the pelagic silica production of the Southern Ocean. *Limnol. Oceanogr.* 66, 2187–2202.

[134]Longhurst, A., Sathyendranath, S., Platt, T., and Caverhill, C. (1995). An estimate of global primary production in the ocean from satellite radiometer data. *J. Plankton Res.* 17, 1245–1271.

[135]Locarnini, R. A., A. V. Mishonov, O. K. Baranova, T. P. Boyer, M. M. Zweng, H. E. García, J. R. Reagan, D. Seidov, K. Weathers, C. R. Paver, and I. Smolyar, 2019. World Ocean Atlas 2018, Volume 1: Temperature. A. Mishonov Technical Ed.; NOAA Atlas NESDIS 81, 52 pp.

[136]López-Acosta, M., Maldonado, M., Grall, J., Ehrhold, A., Sitjà, C., Galobart, C., et al. (2022). Sponge contribution to the silicon cycle of a diatom-rich shallow bay. *Limnol. Oceanogr.* 67, 2431–2447.

[137]Loucaides, S., Michalopoulos, P., Presti, M., Koning, E., Behrends, T., and Van Cappellen, P. (2010). Seawater-mediated interactions between diatomaceous silica and terrigenous sediments: Results from long-term incubation experiments. *Chem. Geol.* 270, 68–79.

[138]Lyle, A. O., and Lyle, M. W. (2002). Determination of Biogenic Opal in Pelagic Marine Sediments: A Simple Method Revisited. *Proc. Ocean Drill. Program, 199 Initial Reports* 199.

[139]Ma, Y., Yang, B., Zhou, N., Huang, J., Liu, S. M., Zhu, D., et al. (2023). Distribution and dissolution kinetics of biogenic silica in sediments of the northern South China Sea. *Front. Mar. Sci.* 10, 1–15.

[140]Ma, Y., Zhang, L., Liu, S., and Zhu, D. (2022). Silicon balance in the South China Sea. *Biogeochemistry* 157, 327–353.

[141]Mackenzie, F. T., Garrels, R. M., Bricker, O. P., and Bickley, F. (1967). Silica in sea water: Control by silica minerals. *Science (80-.).* 155, 1404–1405.

[142]Mackin, J. E. (1989). Relationships between Si, Al, and Fe deposited on filter-covered glass substrates in marine sediments and in suspensions of sediments and standard clays. *Mar. Chem.* 26, 101–117.

[143]Mackin, J. E., and Aller, R. C. (1984). Dissolved Al in sediments and waters of the East China Sea: Implications for authigenic mineral formation. *Geochim. Cosmochim. Acta* 48, 281–297.

[144]Maldonado, M., López-Acosta, M., Abalde, S., Martos, I., Ehrlich, H., and Leynaert, A. (2022). On the dissolution of sponge silica: Assessing variability and biogeochemical implications. *Front. Mar. Sci.* 9, 1–16.

[145]Maldonado, M., López-Acosta, M., Sitjà, C., García-Puig, M., Galobart, C., Ercilla, G., et al. (2019). Sponge skeletons as an important sink of silicon in the global oceans. *Nat. Geosci.* 12, 815–822.

[146]Maldonado, M., Navarro, L., Grasa, A., Gonzalez, A., and Vaquerizo, I. (2011). Silicon uptake by sponges: A twist to understanding nutrient cycling on continental margins. *Sci. Rep.* 1.

[147]Maldonado, M., Ribes, M., and van Duyl, F. C. (2012). *Nutrient Fluxes Through Sponges. Biology, Budgets, and Ecological Implications*. 1st ed. Elsevier Ltd.

[148]Malinverno, E., Cerino, F., Karatsolis, B. T., Ravani, A., Dimiza, M., Psarra, S., et al. (2019). Silicoflagellates in the eastern mediterranean and Black Seas: Seasonality, distribution and sedimentary record. *Deep. Res. Part II Top. Stud. Oceanogr.* 164, 122–134.

[149]Maliva, R. G., Knoll, A. H., and Siever, R. (1989). Secular change in chert distribution: a reflection of evolving biological participation in the silica cycle. *Palaios* 4, 519–532.

[150]McManus, J., Hammond, D. E., Berelson, W. M., Kilgore, T. E., Demaster, D. J., Ragueneau, O. G., et al. (1995). Early diagenesis of biogenic opal: Dissolution rates, kinetics, and paleoceanographic implications. *Deep. Res. Part II* 42, 871–903.

[151]Measures, C. I., and Hatta, M. (2021). On Using Si to Unravel Potential Sources of Dissolved Al to the Deep Arctic. *J. Geophys. Res. Ocean.* 126, 1–17.

[152]Mei, X., Li, X., Mi, B., Zhao, L., Wang, Z., Zhong, H., et al. (2020). Distribution regularity and sedimentary differentiation patterns of China seas surface sediments. *Geol. CHINA* 47, 1447–1462.

[153]Melucci, D., Zappi, A., Poggioli, F., Morozzi, P., Giglio, F., and Tositti, L. (2019). ATR-FTIR spectroscopy, a new non-destructive approach for the quantitative determination of biogenic silica in marine sediments. *Molecules* 24.

[154]Meunier, J. D., Keller, C., Guntzer, F., Riotte, J., Braun, J. J., and Anupama, K. (2014). Assessment of the 1% Na2CO3 technique to quantify the phytolith pool. *Geoderma* 216, 30–35.

[155]Meyer-Jacob, C., Vogel, H., Gebhardt, A. C., Wennrich, V., Melles, M., and Rosen, P. (2014). Biogeochemical variability during the past 3.6 million years recorded by FTIR spectroscopy in the sediment record of Lake El'gygytgyn, Far East Russian Arctic. *Clim. Past* 10, 209–220.

[156]Michalopoulos, P., and Aller, R. C. (1995). Rapid clay mineral formation in Amazon delta sediments: Reverse weathering and oceanic elemental cycles. *Science (80-.).* 270, 614–617.

[157]Michalopoulos, P., and Aller, R. C. (2004). Early diagenesis of biogenic silica in the Amazon delta: Alteration, authigenic clay formation, and storage. *Geochim. Cosmochim. Acta* 68, 1061–1085.

[158]Michalopoulos, P., Aller, R. C., and Reeder, R. J. (2000). Conversion of diatoms to clays during early diagenesis in tropical, continental shell muds. *Geology* 28, 1095–1098.

[159]Milliman, J. D., and Meade, R. H. (1983). World wide delivery of river sediments to oceans. *J. Geol.* 91, 1–21.

[160]Morganti, T. M., Slaby, B. M., Kluijver, A. de, Busch, K., Hentschel, U., Middelburg, J. J., et al. (2022). Giant sponge grounds of Central Arctic seamounts are associated with extinct seep life. *Nat. Commun.* 13.

[161]Moriceau, B., Goutx, M., Guigue, C., Lee, C., Armstrong, R., Duflos, M., et al. (2009). Si-C interactions during degradation of the diatom Skeletonema marinoi. *Deep. Res. Part II Top. Stud. Oceanogr.* 56, 1381–1395.

[162]Mortlock, R. A., and Froelich, P. N. (1989). A simple method for the rapid determination of biogenic opal in pelagic marine sediments. *Deep Sea Res. Part A, Oceanogr. Res. Pap.* 36, 1415–1426.

[163]Müller, P. J., and Schneider, R. (1993). An automated leaching method for the determination of opal in sediments and particulate matter. *Deep. Res. Part I* 40, 425–444.

[164]Müller, W. E. G., Belikov, S. I., Tremel, W., Perry, C. C., Gieskes, W. W. C., Boreiko, A., et al. (2006). Siliceous spicules in marine demosponges (example Suberites domuncula). *Micron* 37, 107–120.

[165]Murillo, F. J., Kenchington, E., Tompkins, G., Beazley, L., Baker, E., Knudby, A., et al. (2018). Sponge assemblages and predicted archetypes in the eastern Canadian Arctic. *Mar. Ecol. Prog. Ser.* 597, 115–135.

[166]Nelson, D. M., Tréguer, P., Brzezinski, M. A., Leynaert, A., and Quéguiner, B. (1995). Production and dissolution of biogenic silica in the ocean: Revised global estimates, comparison with regional data and relationship to biogenic sedimentation. *Global Biogeochem. Cycles* 9, 359–372.

[167]Niibori, Y., Chida, T., and Tochiyama, O. (2000). Journal of Nuclear Science and Technology, Vol. 37, No. 4, 2000: Pp. 349–357. *J. Nucl. Sci. Technol.* 37, 349–357.

[168]Ng, H. C., Cassarino, L., Pickering, R. A., Woodward, E. M. S., Hammond, S. J., and Hendry, K. R. (2020). Sediment efflux of silicon on the Greenland margin and implications for the marine silicon cycle. Earth Planet. Sci. Lett. 529, 115877.

[169]Ng, H. C., Hawkings, J. R., Bertrand, S., Summers, B. A., Sieber, M., Conway, T. M., et al. (2022). Benthic Dissolved Silicon and Iron Cycling at Glaciated Patagonian Fjord Heads. Global Biogeochem. Cycles 36, 1–22.

[170]Oehler, T., Schlüter, M., and Schückel, U. (2015). Seasonal dynamics of the biogenic silica cycle in surface sediments of the Helgoland Mud Area (southern North Sea). *Cont. Shelf Res.* 107, 103–114.

[171]Ohlendorf, C., and Sturm, M. (2008). A modified method for biogenic silica determination. *J. Paleolimnol.* 39, 137–142.

[172]Oinuma, K., and Kobayashi, K. (1966). Quantitative Study of Clay Minerals in Some Recent Marine Sediments and Sedimentary Rocks from Japan. *Clays Clay Miner.* 14, 209–219.

[173]Passow, U. (1991). Species-specific sedimentation and sinking velocities of diatoms. *Mar. Biol.* 108, 449–455.

[174]Petschick, R. (2002). MacDiff 4.2.6. Available at: http://servermac.geologie.uni-frankfurt.de/Rainer.html.

[175]Phillips, A. K. (2020). Modelling riverine dissolved silica on different spatial and temporal scales using statistical and machine learning methods.

[176]Pickering, R. A., Cassarino, L., Hendry, K. R., Wang, X. L., Maiti, K., and Krause, J. W. (2020a). Using Stable Isotopes to Disentangle Marine Sedimentary Signals in Reactive Silicon Pools. *Geophys. Res. Lett.* 47, 1–11.

[177]Pokras, E. M., and Molfino, B. (1986). Oceanographic control of diatom abundances and species distributions in surface sediments of the tropical and southeast Atlantic. *Mar. Micropaleontol.* 10, 165–188.

[178]Pondaven, P., Ragueneau, O., Tréguer, P., Hauvespre, A., Dezileau, L., and Reyss, J. L. (2000). Resolving the “opal paradox” in the Southern Ocean. *Nature* 405, 168–172.

[179]Pudsey, C. J. (1993a). Calibration of a point-counting technique for estimation of biogenic silica in marine sediments. *J. Sediment. Petrol.* 63, 760–762.

[180]Qiao, S., Shi, X., Wang, G., Zhou, L., Hu, B., Hu, L., et al. (2017). Sediment accumulation and budget in the Bohai Sea, Yellow Sea and East China Sea. *Mar. Geol.* 390, 270–281.

[181]Qu, H., Wang, J., Xu, Y., and Li, X. (2020a). Radiolarian assemblage as an indicator of environmental conditions in the marginal seas of the Western North Pacific. *Mar. Micropaleontol.* 157, 101859.

[182]Qu, H., Xu, Y., Wang, J., and Li, X. Z. (2020b). Radiolarian assemblages in the shelf area of the East China Sea and Yellow Sea and their ecological indication of the Kuroshio Current derivative branches. *PeerJ* 8, 1–19.

[183]Rabouille, C., Olu, K., Baudin, F., Khripounoff, A., Dennielou, B., Arnaud-Haond, S., et al. (2016). The Congolobe project, a multidisciplinary study of Congo deep-sea fan lobe complex: Overview of methods, strategies, observations and sampling. *Deep. Res. Part II Top. Stud. Oceanogr.* 142, 7–24.

[184]Racki, G., and Cordey, F. (2000). Radiolarian palaeoecology and radiolarites: Is the present the key to the past? *Earth Sci. Rev.* 52, 83–120.

[185]Ragueneau, O., Chauvaud, L., Leynaert, A., Thouzeau, G., Paulet, Y. M., Bonnet, S., et al. (2002). Direct evidence of a biologically active coastal silicate pump: Ecological implications. *Limnol. Oceanogr.* 47, 1849–1854.

[186]Ragueneau, O., Gallinari, M., Corrin, L., Grandel, S., Hall, P., Hauvespre, A., et al. (2001). The benthic silica cycle in the Northeast Atlantic: Annual mass balance, seasonality, and importance of non-steady-state processes for the early diagenesis of biogenic opal in deep-sea sediments. *Prog. Oceanogr.* 50, 171–200.

[187]Ragueneau, O., Savoye, N., Del Amo, Y., Cotten, J., Tardiveau, B., and Leynaert, A. (2005). A new method for the measurement of biogenic silica in suspended matter of coastal waters: Using Si:Al ratios to correct for the mineral interference. *Cont. Shelf Res.* 25, 697–710.

[188]Ragueneau, O., Schultes, S., Bidle, K., Claquin, P., and Moriceau, B. (2006). Si and C interactions in the world ocean: Importance of ecological processes and implications for the role of diatoms in the biological pump. *Global Biogeochem. Cycles* 20, 1–15.

[189]Ragueneau, O., and Tréguer, P. (1994). Determination of biogenic silica in coastal waters: applicability and limits of the alkaline digestion method. *Mar. Chem.* 45, 43–51.

[190]Rahman, S. (2019). *Reverse weathering reactions in marine sediments*. 3rd ed. Elsevier Ltd.

[191]Rahman, S., Aller, R. C., and Cochran, J. K. (2016). Cosmogenic 32Si as a tracer of biogenic silica burial and diagenesis: Major deltaic sinks in the silica cycle. *Geophys. Res. Lett.* 43, 7124–7132.

[192]Rahman, S., Aller, R. C., and Cochran, J. K. (2017). The Missing Silica Sink: Revisiting the Marine Sedimentary Si Cycle Using Cosmogenic 32Si. *Global Biogeochem. Cycles* 31, 1559–1578.

[193]Rahman, S., Tamborski, J. J., Charette, M. A., and Cochran, J. K. (2019). Dissolved silica in the subterranean estuary and the impact of submarine groundwater discharge on the global marine silica budget. *Mar. Chem.* 208, 29–42.

[194]Raimonet, M., Ragueneau, O., Jacques, V., Corvaisier, R., Moriceau, B., Khripounoff, A., et al. (2015). Rapid transport and high accumulation of amorphous silica in the Congo deep-sea fan: A preliminary budget. *J. Mar. Syst.* 141, 71–79.

[195]Ran, L., Chen, J., Wiesner, M. G., Ling, Z., Lahajnar, N., Yang, Z., et al. (2015). Variability in the abundance and species composition of diatoms in sinking particles in the northern South China Sea: Results from time-series moored sediment traps. *Deep. Res. Part II Top. Stud. Oceanogr.* 122, 15–24.

[196]Ran, X., Liu, J., Liu, S., Zang, J., Wang, B., and Zhao, J. (2018). The biogenic silica composition, behavior and budget in the Changjiang Estuary. *Acta Oceanol. Sin.* 37, 60–72.

[197]Ran, X., Xu, B., Liu, J., Zhao, C., Liu, S., and Zang, J. (2017). Biogenic silica composition and δ13C abundance in the Changjiang (Yangtze) and Huanghe (Yellow) Rivers with implications for the silicon cycle. *Sci. Total Environ.* 579, 1541–1549.

[198]Randelhoff, A., Oziel, L., Massicotte, P., Bécu, G., Lacour, L., Dumont, D., et al. (2019). The evolution of light and vertical mixing across a phytoplankton ice-edge bloom. *Elem. Sci. Anthr.* 7.

[199]Ren, H., Brunelle, B. G., Sigman, D. M., and Robinson, R. S. (2013). Diagenetic aluminum uptake into diatom frustules and the preservation of diatom-bound organic nitrogen. *Mar. Chem.* 155, 92–101.

[200]Ren, J. L., Zhang, J., Li, J. B., Yu, X. Y., Liu, S. M., and Zhang, E. R. (2006). Dissolved aluminum in the Yellow Sea and East China Sea - Al as a tracer of Changjiang (Yangtze River) discharge and Kuroshio incursion. *Estuar. Coast. Shelf Sci.* 68, 165–174.

[201]Ren, J. L., Zhang, J., Luo, J. Q., Pei, X. K., and Jiang, Z. X. (2001). Improved fluorimetric determination of dissolved aluminium by micelle-enhanced lumogallion complex in natural waters. *Analyst* 126, 698–702.

[202]Rickert, D. (2000). Dissolution kinetics of biogenic silica in marine environments= Lösungskinetik von biogenem Opal in marinen Systemen.

[203]Rickert, D., Schlüter, M., and Wallmann, K. (2002). Dissolution kinetics of biogenic silica from the water column to the sediments. *Geochim. Cosmochim. Acta* 66, 439–455.

[204]Rogers, J., and De Deckker, P. (2007). Radiolaria as a reflection of environmental conditions in the eastern and southern sectors of the Indian Ocean: A new statistical approach. *Mar. Micropaleontol.* 65, 137–162.

[205]Rosén, P., Vogel, H., Cunningham, L., Reuss, N., Conley, D. J., and Persson, P. (2010). Fourier transform infrared spectroscopy, a new method for rapid determination of total organic and inorganic carbon and biogenic silica concentration in lake sediments. *J. Paleolimnol.* 43, 247–259.

[206]Sandford, F. (2003). Physical and chemical analysis of the siliceous skeletons in six sponges of two groups (demospongiae and hexactinellida). *Microsc. Res. Tech.* 62, 336–355.

[207]Schlüter, M., and Rickert, D. (1998). Effect of pH on the measurement of biogenic silica. *Mar. Chem.* 63, 81–92.

[208]Schwab, D. W., and Shore, R. E. (1971). Mechanism of internal stratification of siliceous sponge spicules [30]. *Nature* 232, 501–502.

[209]Shemesh, A., Mortlock, R. A., Smith, R. J., and Froelich, P. N. (1988). Determination of Ge/Si in marine siliceous microfossils: Separation, cleaning and dissolution of diatoms and radiolaria. *Mar. Chem.* 25, 305–323.

[210]Schlitzer, Reiner, Ocean Data View, odv.awi.de, 2023

[211]Shi. X.F. (2021). Sediment Type Map of the Bohai Sea, Yellow Sea and East China Sea. Science Press. Beijing.

[212]Siever, R. (1968). Establishment of equilibrium between clays and sea water. *Earth Planet. Sci. Lett.* 5, 106–110.

[213]Siever, R. (1991). “Silica in the oceans: Biological-Geochemical Interplay,” in *Scientists on Gaia*, eds. S. Boston and S. and P. (Cambridge, MA: MIT Press), 287–295.

[214]Siever, R. (1992). The silica cycle in the Precambrian. *Geochim. Cosmochim. Acta* 56, 3266–3272.

[215]Smith, C. R., Mincks, S., and Demaster, D. J. (2006). A synthesis of bentho-pelagic coupling on the Antarctic shelf :Food banks, ecosystem inertia and global climate change. 53, 875–894.

[216]Struyf, E., Dausse, A., Van Damme, S., Bal, K., Gribsholt, B., Boschker, H. T. S., et al.

(2006). Tidal marshes and biogenic silica recycling at the land-sea interface. *Limnol. Oceanogr.* 51, 838–846.

[217]Struyf, E., Van Damme, S., Gribsholt, B., Middelburg, J. J., and Meire, P. (2005). Biogenic silica in tidal freshwater marsh sediments and vegetation (Schelde estuary, Belgium). *Mar. Ecol. Prog. Ser.* 303, 51–60.

[218]Sutton, J. N., André, L., Cardinal, D., Conley, D. J., De Souza, G. F., Dean, J., et al. (2018). A review of the stable isotope bio-geochemistry of the global silicon cycle and its associated trace elements. *Front. Earth Sci.* 5.

[219]Swann, G. E. A. (2010). A comparison of the Si/Al and Si/time wet-alkaline digestion methods for measurement of biogenic silica in lake sediments. *J. Paleolimnol.* 44, 375–385.

[220]Taucher, J., Bach, L. T., Prowe, A. E. F., Boxhammer, T., Kvale, K., and Riebesell, U. (2022). Enhanced silica export in a future ocean triggers global diatom decline. *Nature* 605, 696–700.

[221]Tréguer, P., Bowler, C., Moriceau, B., Dutkiewicz, S., Gehlen, M., Aumont, O., et al. (2018). Influence of diatom diversity on the ocean biological carbon pump. *Nat. Geosci.* 11, 27–37.

[222]Tréguer, P. J., and De La Rocha, C. L. (2013). The world ocean silica cycle. *Ann. Rev. Mar. Sci.* 5, 477–501.

[223]Tréguer, P., Nelson, D. M., Van Bennekom, A. J., Demaster, D. J., Leynaert, A., and Quéguiner, B. (1995). The silica balance in the world ocean: A reestimate. *Science (80-.).* 268, 375–379.

[224]Tréguer, P., Sutton, J., Brzezinski, M., Charette, M., Devries, T., Dutkiewicz, S., et al. (2021). Reviews and syntheses: The biogeochemical cycle of silicon in the modern ocean. *Biogeosciences Discuss.* 18, 1269–1289.

[225]Uriz, A., Turon, X., and Becerro, M. A. (2003). Siliceous Spicules and Skeleton Frameworks in Sponges : Origin , Diversity , Ultrastructural Patterns , and Biological Functions. 299, 279–299.

[226]van Bennekom, A. J., Fred Jansen, J. H., van der Gaast, S. J., van Iperen, J. M., and Pieters, J. (1989). Aluminium-rich opal: an intermediate in the preservation of biogenic silica in the Zaire (Congo) deep-sea fan. *Deep Sea Res. Part A, Oceanogr. Res. Pap.* 36, 173–190.

[227]Van Beusekom, J. E. E., Van Bennekom, A. J., Tréguer, P., and Morvan, J. (1997). Aluminium and silicic acid in water and sediments of the Enderby and Crozet Basins. *Deep. Res. Part II Top. Stud. Oceanogr.* 44, 987–1003.

[228]Van Cappellen, P. (1996). Reactive surface area control of the dissolution kinetics of biogenic silica in deep-sea sediments. *Chem. Geol.* 132, 125–130.

[229]Van Cappellen, P., Dixit, S., and van Beusekom, J. (2002a). Biogenic silica dissolution in the oceans: Reconciling experimental and field-based dissolution rates. *Global Biogeochem. Cycles* 16, 23-1-23–10.

[230]Van Cappellen, P., Dixit, S., and van Beusekom, J. (2002b). Biogenic silica dissolution in the oceans: Reconciling experimental and field-based dissolution rates. *Global Biogeochem. Cycles* 16, 23-1-23–10.

[231]Van Cappellen, P., and Qiu, L. (1997). Biogenic silica dissolution in sediments of the Southern Ocean. I. Solubility. *Deep. Res. Part II Top. Stud. Oceanogr.* 44, 1109–1128.

[232]Van Soest, R. W. M., Boury-esnault, N., Vacelet, J., Dohrmann, M., Erpenbeck, D., Voogd, N. J. De, et al. (2012). Global Diversity of Sponges (Porifera). *PLoS One* 7.

[233]van Tol, H. M., Irwin, A. J., and Finkel, Z. V. (2012). Macroevolutionary trends in silicoflagellate skeletal morphology: the costs and benefits of silicification. *Paleobiology* 38, 391–402.

[234]Varkouhi, S., Cartwright, J. A., and Tosca, N. J. (2020a). Anomalous compaction due to silica diagenesis — Textural and mineralogical evidence from hemipelagic deep-sea sediments of the Japan Sea. *Mar. Geol.* 426, 106204.

[235]Varkouhi, S., Tosca, N. J., and Cartwright, J. A. (2020b). Pore-water chemistry: A proxy for tracking the signature of ongoing silica diagenesis.

[236]Varkouhi, S., and Wells, J. (2020). The relation between temperature and silica benthic exchange rates and implications for near-seabed formation of diagenetic opal. *Results Geophys. Sci.* 1–4, 100002.

[237]Vogel, H., Meyer-Jacob, C., Thöle, L., Lippold, J. A., and Jaccard, S. L. (2016). Quantification of biogenic silica by means of Fourier transform infrared spectroscopy (FTIRS) in marine sediments. *Limnol. Oceanogr. Methods* 14, 828–838.

[238]Vogel, H., Rosén, P., Wagner, B., Melles, M., and Persson, P. (2008). Fourier transform infrared spectroscopy, a new cost-effective tool for quantitative analysis of biogeochemical properties in long sediment records. *J. Paleolimnol.* 40, 689–702.

[239]Vogel, H., Wagner, B., Zanchetta, G., Sulpizio, R., and Rosén, P. (2010). A paleoclimate record with tephrochronological age control for the last glacial-interglacial cycle from Lake Ohrid, Albania and Macedonia. *J. Paleolimnol.* 44, 295–310.

[240]Wang, C.-H., and Yeh, H.-W. (1985). Oxygen isotopic compositions of DSDP Site 480 diatoms: Implications and applications. *Geochim. Cosmochim. Acta* 49, 1469–1478.

[241]Wang, L., Fan, D., Li, W., Liao, Y., Zhang, X., Liu, M., et al. (2014). Grain-size effect of biogenic silica in the surface sediments of the East China Sea. *Cont. Shelf Res.* 81, 29–37.

[242]Wang, Y., Liu, D., Di, B., Shi, Y., and Wang, Y. (2016). Distribution of diatoms and silicoflagellates in surface sediments of the Yellow Sea and offshore from the Changjiang River, China. *Chinese J. Oceanol. Limnol.* 34, 44–58.

[243]Warr, L. N. (2018). A new collection of clay mineral 'Crystallinity' Index Standards and revised guidelines for the calibration of Kübler and Árkai indices. *Clay Miner.* 53, 339–350.

[244]Ward, J. P. J., Hendry, K. R., Arndt, S., Faust, J. C., Freitas, F. S., Henley, S. F., et al. (2022). Stable silicon isotopes uncover a mineralogical control on the benthic silicon cycle in the Arctic Barents Sea. *Geochim. Cosmochim. Acta* 329, 206–230.

[245]Wentworth, C. K. (1922). A Scale of Grade and Class Terms for Clastic Sediments. *J. Geol.* 30, 377–392.

[246]Wever, D. P., Dumitrica, P., Caulet, J. P., Nigrini, C., and Caridroit, M. (2002). *Radiolarians in the Sedimentary Record*. Boca Raton: CRC Press.

[247]Williams, L. A., Parks, G. A., and Crerar, D. A. (1985). Silica diagenesis: I. Solubility controls. *J. Sediment. Petrol.* 55, 301–311.

[248]Wu, B., and Liu, S. (2020). Dissolution kinetics of biogenic silica and the recalculated silicon balance of the East China Sea. *Sci. Total Environ.* 743, 140552.

[249]Wu, B., Liu, S. M., and Ren, J. L. (2017). Dissolution kinetics of biogenic silica and tentative silicon balance in the Yellow Sea. *Limnol. Oceanogr.* 62, 1512–1525.

[250]Wu, B., Lu, C., and Liu, S. M. (2015). Dynamics of biogenic silica dissolution in Jiaozhou Bay, western Yellow Sea. *Mar. Chem.* 174, 58–66.

[251]Wu, Z.Y. (2019). Geology Map of the East China Seas. Science Press. Beijing.

[252]Zang, J., Liu, S., Liu, Y., Ma, Y., and Ran, X. (2016). Contribution of phytoliths to total biogenic silica volumes in the tropical rivers of Malaysia and associated implications for the marine biogeochemical cycle. *Chinese J. Oceanol. Limnol.* 34, 1076–1084.

[253]Zhang, L., Wang, R., Chen, M., Liu, J., Zeng, L., Xiang, R., et al. (2015). Biogenic silica in surface sediments of the South China Sea: Controlling factors and paleoenvironmental implications. *Deep. Res. Part II Top. Stud. Oceanogr.* 122, 142–152.

[254]Zhang, W., Xue, S., Zhao, Q., Zhang, X., Li, J., Jin, M., et al. (2003). Biopotentials of marine sponges from China oceans: Past and future. *Biomol. Eng.* 20, 413–419.

[255]Zhang, X., Ren, J., Guo, Y., Lei, L., and Zhang, R. (2020). Distributions and influencing factors of dissolved aluminum in the Zhujiang River Estuary,con- tinental slope of the

northern South China Sea in autumn and summer. *Haiyang Xuebao* 42, 10–20.

[256]Zhang, Z., Sun, X., Dai, M., Cao, Z., Fontorbe, G., and Conley, D. J. (2020). Impact of human disturbance on the biogeochemical silicon cycle in a coastal sea revealed by silicon isotopes. Limnol. Oceanogr. 65, 515–528.

[257]Zhao, B., Yao, P., Bianchi, T. S., Xu, Y., Liu, H., Mi, T., et al. (2017). Early diagenesis and authigenic mineral formation in mobile muds of the Changjiang Estuary and adjacent shelf. *J. Mar. Syst.* 172, 64–74.

[258]Zhu, D., Sutton, N., J., Leynaert, A., Treguer, P., and Liu, S. M. (2022). The global marine silicon cycle and its major challenges. *Earth Sci. Front.* 29, 47–58.

[259]Zhu, D., Sutton, J. N., Leynaert, A., Tréguer, P. J., Schoelynck, J., Gallinari, M., et al. (2023). Revisiting the biogenic silica burial flux determinations: A case study for the East China seas. *Front. Mar. Sci.* 9, 1–22.

Supplementary materials

S1. Supplementary material of chapter 3

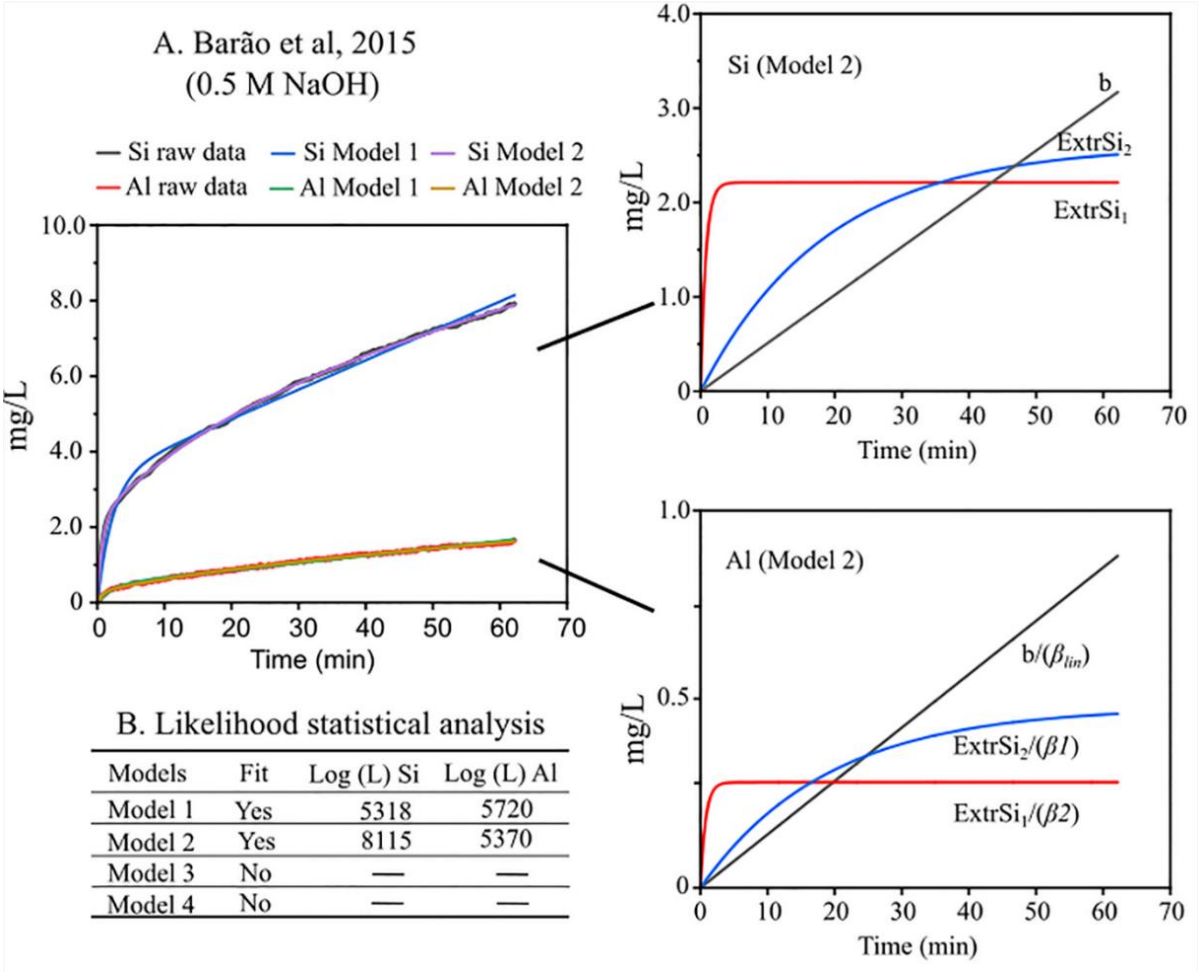

Figure S3.1. Schematic diagram showing the dissolution of Si and Al during the wet alkaline digestion in 0.5 M NaOH (85 °C). (A) shows the actual measure Si and Al concentration (mg L^{-1}) and fitted data using Model 1 (Eq. 3.1) and Model 2 (Eq. 3.2), the figure is plotted following Barão et al, (2015). After the likelihood statistical analysis (B), Model 2 is recognized as a better-fitted model. Different Si and Al fractions (right) were isolated based on the parameters fitted by using Model 2. $AlkExSi_1$ and $AlkExSi_2$ are two nonlinearly alkaline extracted Si fractions and b is the Si minerals interfering with the continuous wet chemical analysis. $ExtrSi_1/(\beta_1)$, $ExtrSi_2/(\beta_2)$, and $b/(\beta_{lin})$ are the corresponding Al content of diffraction fractions. The plot is based on the analysis of sample C12 (randomly chosen), Model 3 and Model 4 cannot successfully fit the measured dSi and dAl concentration of this sample.

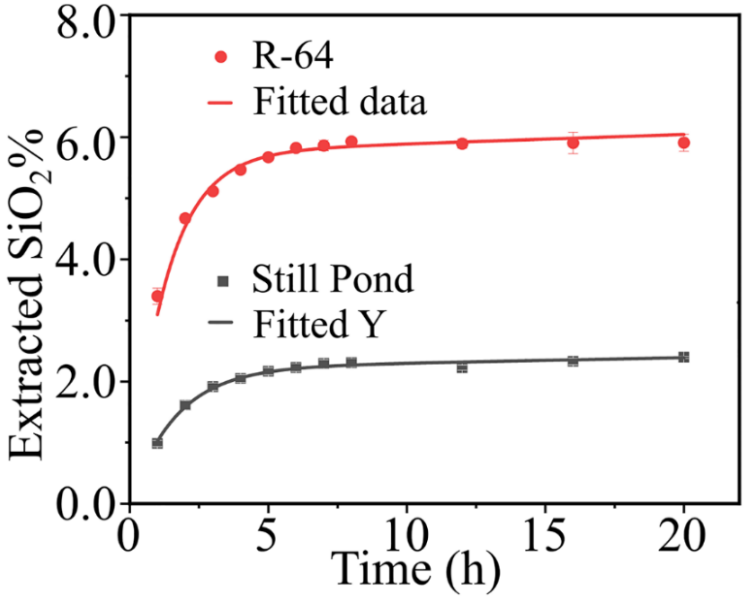

Figure S3.2. Digestion of sediment (Still Pond, R-64) using 0.1 M Na_2CO_3 (NP). The errors are based on triplicate digestions. The redline (fitted Y of sample R-64) and greyline (fitted Y of sample Still Pond) represent nonlinear model fitted data using Model 1 (Eq.1). Subsamples were taken at 1, 2, 3, 4, 5, 6, 7, 8, 12, 16 and 20 h. The asymptotic Si vs. time line reached a "flat plateau" after 8 h-alkaline extraction indicating a complete digestion of bSi.

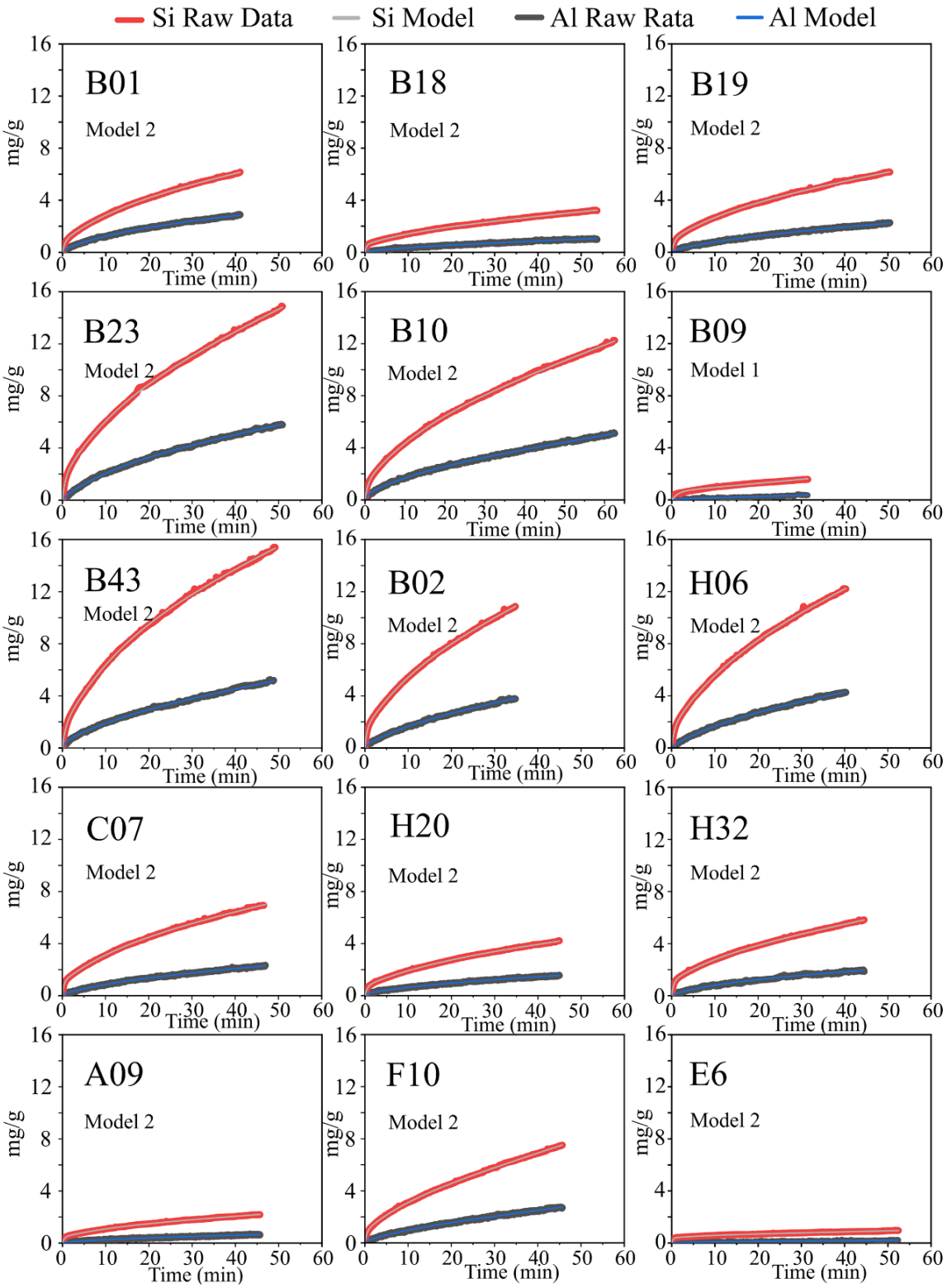

Figure S3.3. Extracted Si (mg/g) and Al (mg/g) in 0.5 M NaOH solution following the Si/Al alkaline digestion method (Koning et al., 2002, Barão et al., 2015). Both the raw data (actual measured) and the best-fitted model data are presented. Model 2 (Eq. 2) was the best-fitted model for most of the samples (27/30). Interlaboratory comparison samples (Still Pond, R-64) were also displayed. Note that the values on the scale bar (X axis and Y axis) can be different.

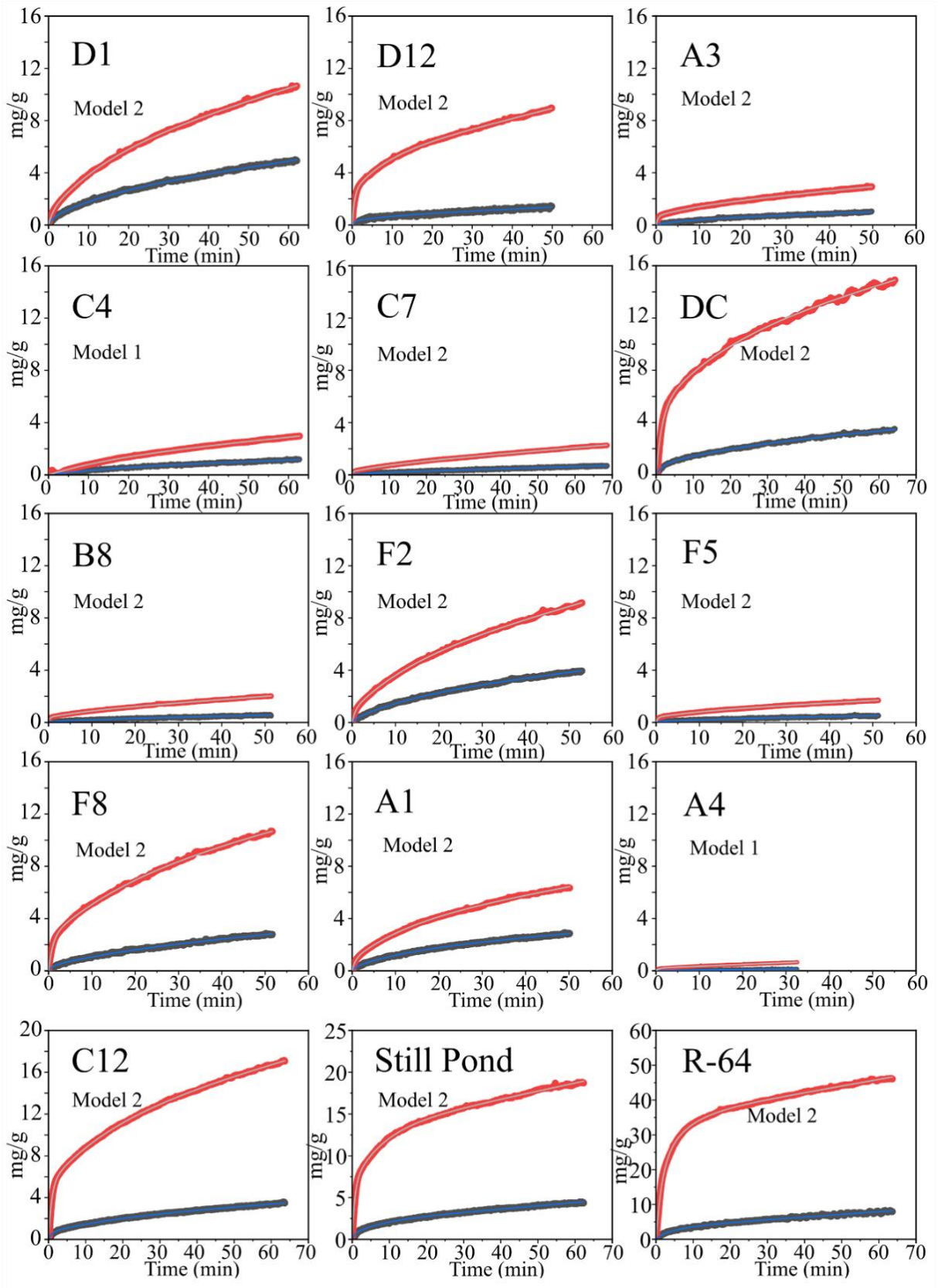

Figure S3.3. Continued.

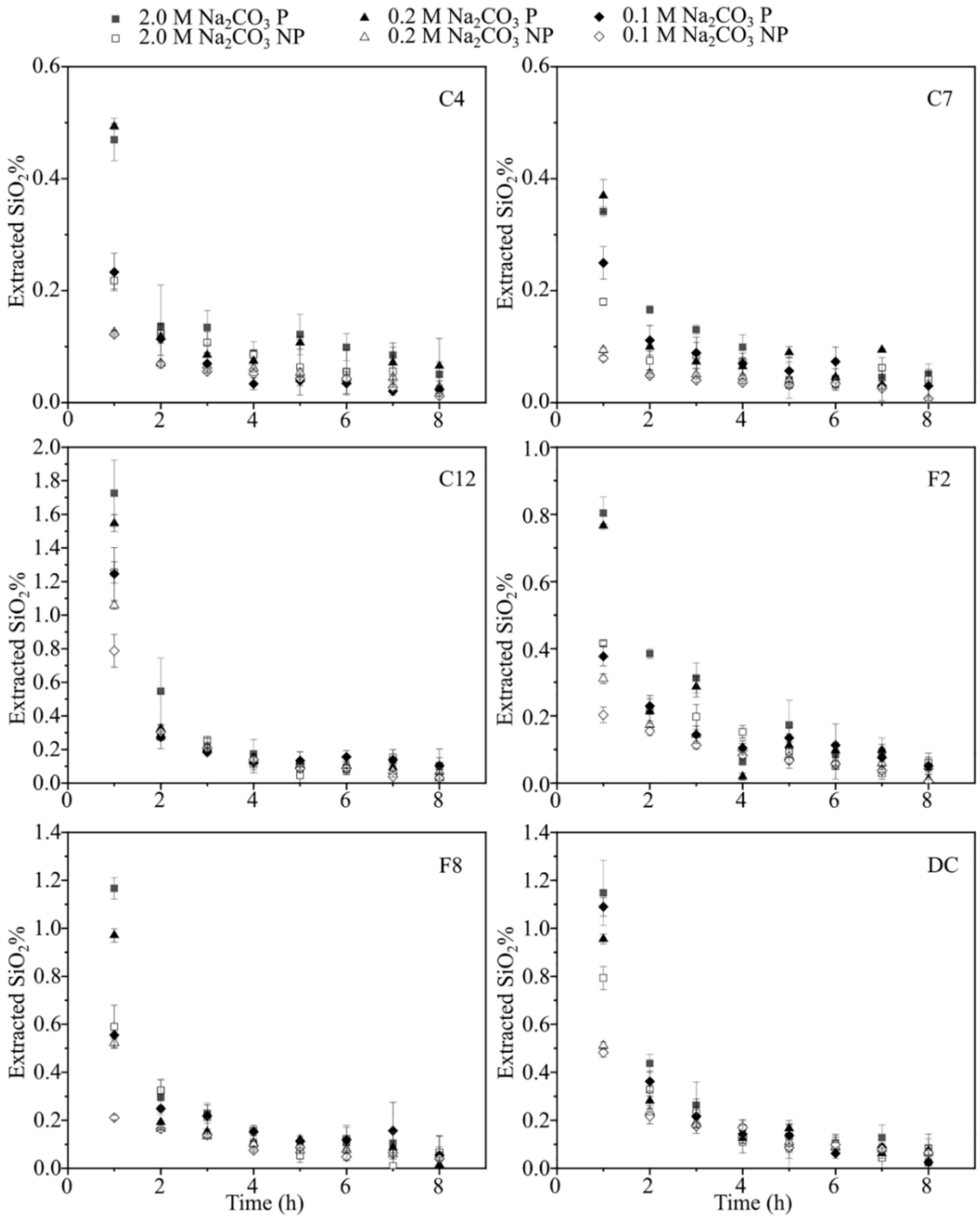

Figure S3.4. The alkaline extracted SiO_2% during each 1 h digestion in Na_2CO_3 (0.1 M, 0.2 M, 2.0 M; P vs. NP). The alkaline extracted SiO_2% at each 1-h digestion interval was calculated from the results presented in Figure 3. The SiO_2% at time 1 to 8 (h) equals to $SiO_2\%_{(n)\,h} - SiO_2\%_{(n-1)\,h}$, the $SiO_2\%_{(0)\,h}$ was not measured and assumed to be 0%. The figure shows more SiO_2% were extracted (meaning relatively rapid extraction of Si) during the first 3 h digestion and less SiO_2% (meaning relatively slow extraction of Si) were extracted afterward. The amount of SiO_2% extracted by different concentrations of Na_2CO_3 (0.1 M, 0.2 M, 2.0 M; P vs. NP) after 4 h was approximately the same.

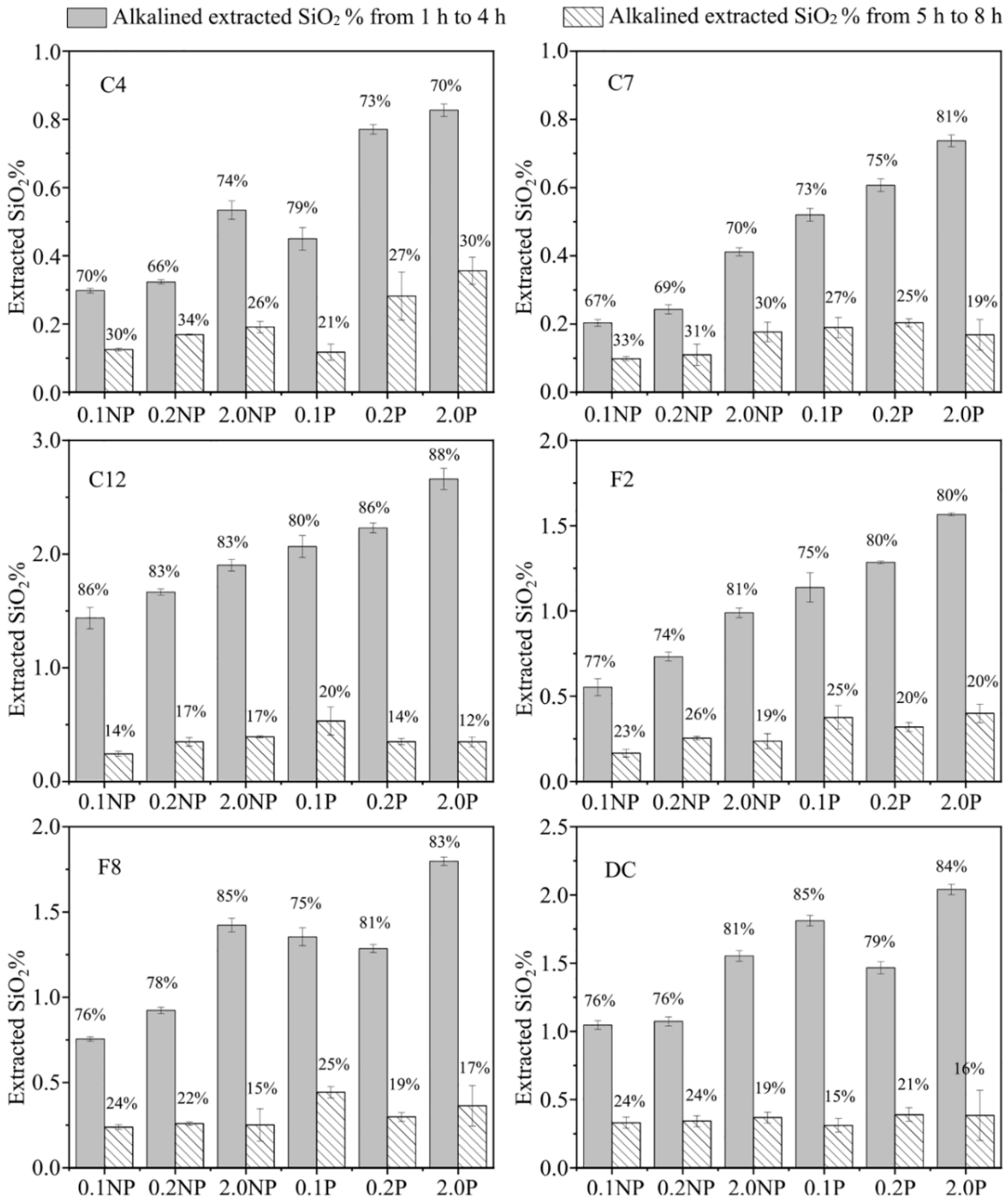

Figure S3.5. The amount of SiO2% extracted during the 1 h to 4 h digestion ($AlkExSi_{(1-4)}$) and 5 h to 8 h digestion ($AlkExSi_{(5-8)}$). Through 8 h alkaline digestion ($AlkExSi_{total}$; $AlkExSi_{total}$ = $AlkExSi_{(1-4)}$ + $AlkExSi_{(5-8)}$), ca. 66% – 86 % of the SiO_2% was extracted during the first 4 h (1 h – 4 h) alkaline digestion and 15% - 34% of the SiO_2% was extracted during the last 4 h (5 h – 8 h) alkaline digestion, the percentage of the SiO_2% extracted at the two time intervals (($AlkExSi_{(1-4)}$), ($AlkExSi_{(5-8)}$)) are showed within the plot. P represents the pretreatment of sediments using HCl (1.0 M) and H_2O_2 (10%), and NP represents the non-pretreatment process. The numbers (0.1, 0.2, 2.0) on x-axis represent the concentration of Na_2CO_3 (0.1 M, 0.2 M, 2.0 M).

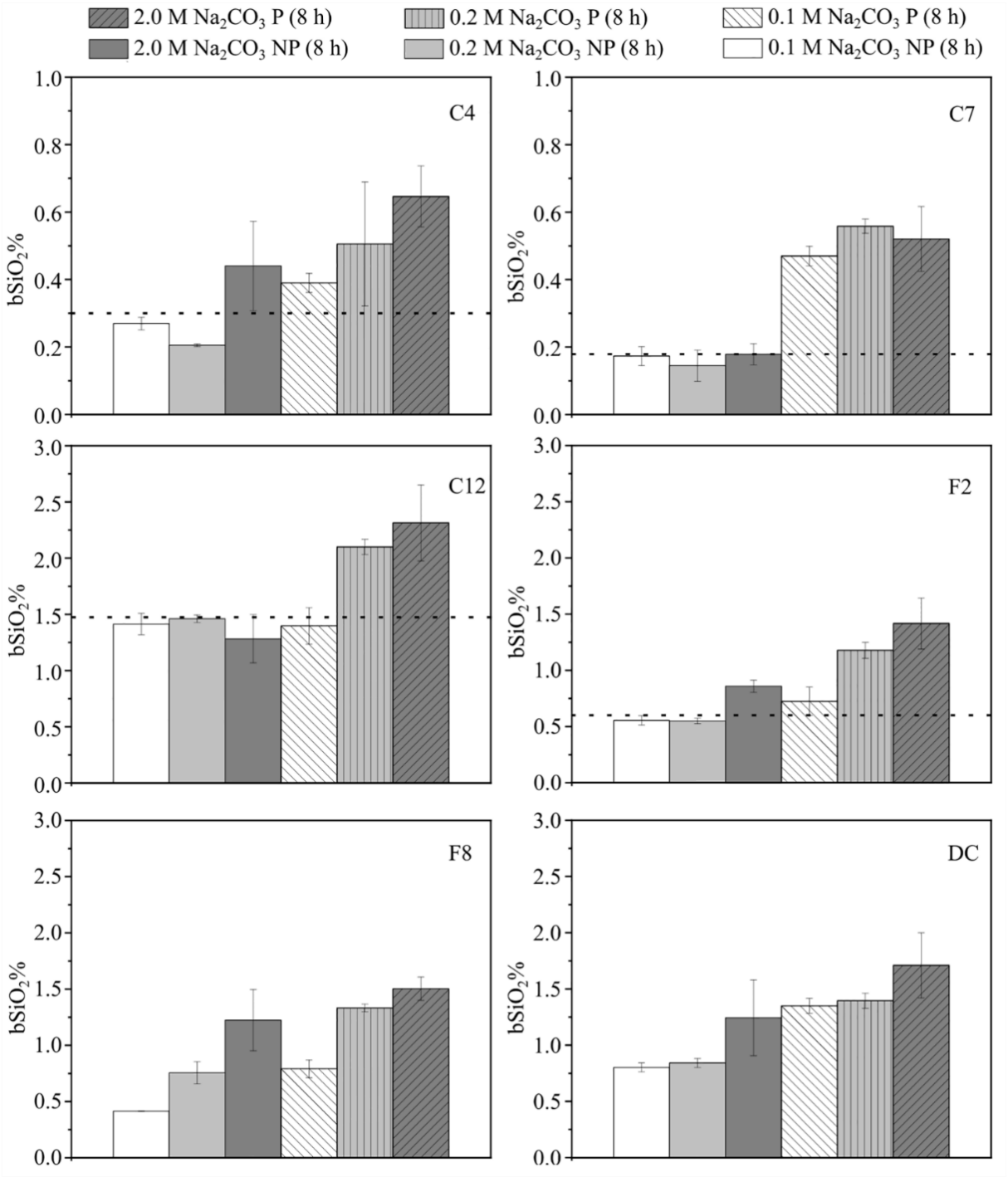

Figure S3.6. The $bSiO_2$% of sample C4, C7, C12, F2, F8 and DC determined using different concentrations of Na_2CO_3 (0.1 M, 0.2 M, 2.0 M; P vs. NP). The duration of the alkaline extraction was 8 h. The dash line for sample C4 (0.31 ± 0.01%), C7 (0.18 ± 0.01%), C12 (1.49 ± 0.09%) and F2 (0.58 ± 0.05%) represent total $bSiO_2$% determined using 0.1 M Na_2CO_3 (NP) after 20 h digestion.

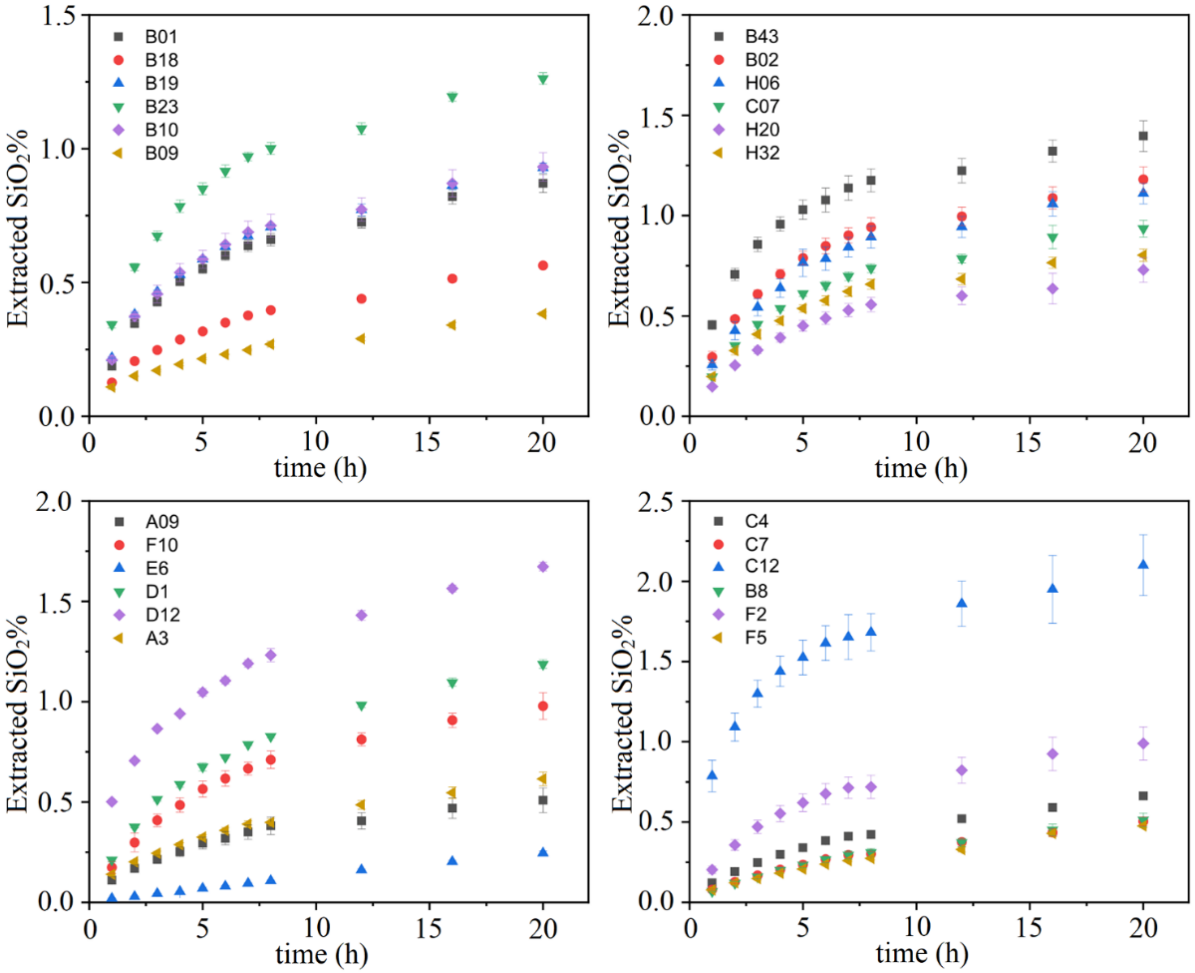

Figure S3.7. Extraction of SiO_2% in 0.1 M Na_2CO_3 solution (NP) at 85 ℃ for 20 h. Subsamples were removed at 1, 2, 3, 4, 5, 6, 7, 8, 12, 16 and 20 h for the analysis of alkaline extracted silicic acid (dSi). The Si vs. time plot showed an asymptotic increase of alkaline extracted SiO_2% through time, but no plateau was reached during the 20 h alkaline digestion (and even 60 h-digestion in 0.1 M Na_2CO_3, Figure S11). The error bars were averaged from triplicate alkaline digestion. The extraction aims to determine the diatom bSi, radiolarian and sponge bSi content in sediments.

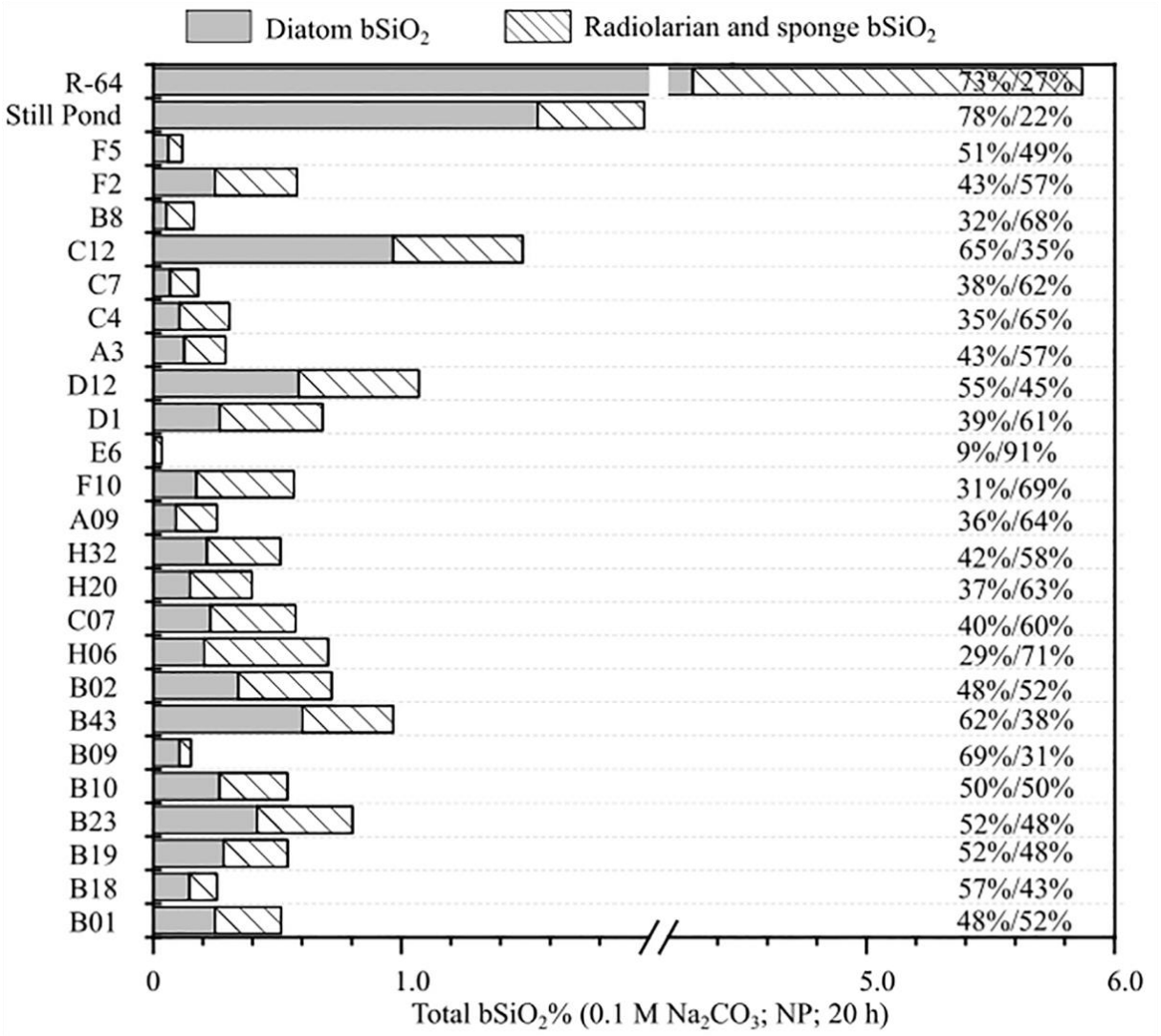

Figure S3.8. The diatom $bSiO_2$%, radiolarian and sponge $bSiO_2$% were determined by a 20 h alkaline digestion using 0.1 M Na_2CO_3 (NP). The values in percentage are the proportions of diatom bSi and radiolarian and sponge bSi.

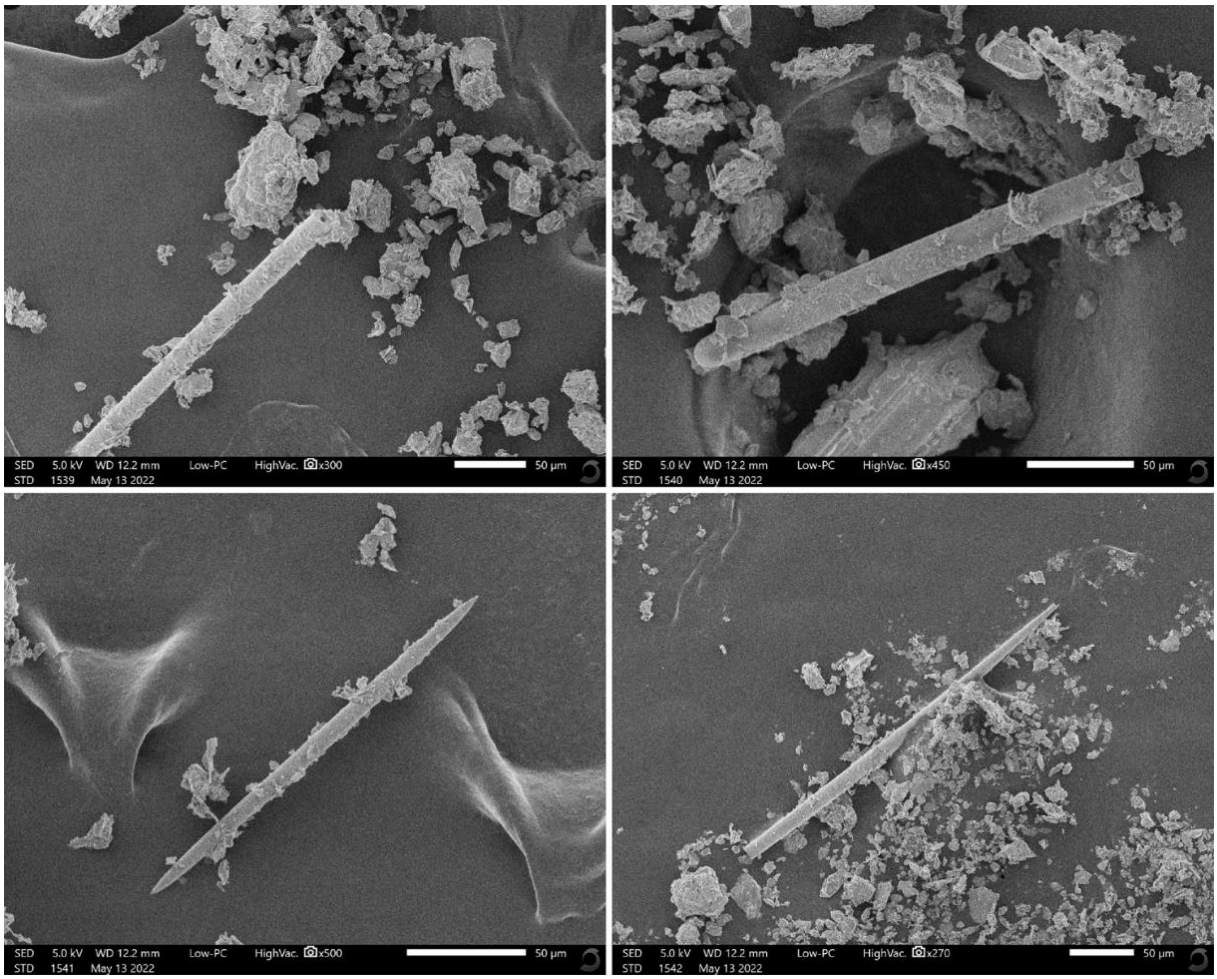

Figure S3.9. SEM images show sponge spicules observed in the residual sediment of sample C12 after 1 h digestion in 0.5 M NaOH (Si/Al method). Diatoms and radiolarian tests were not observed.

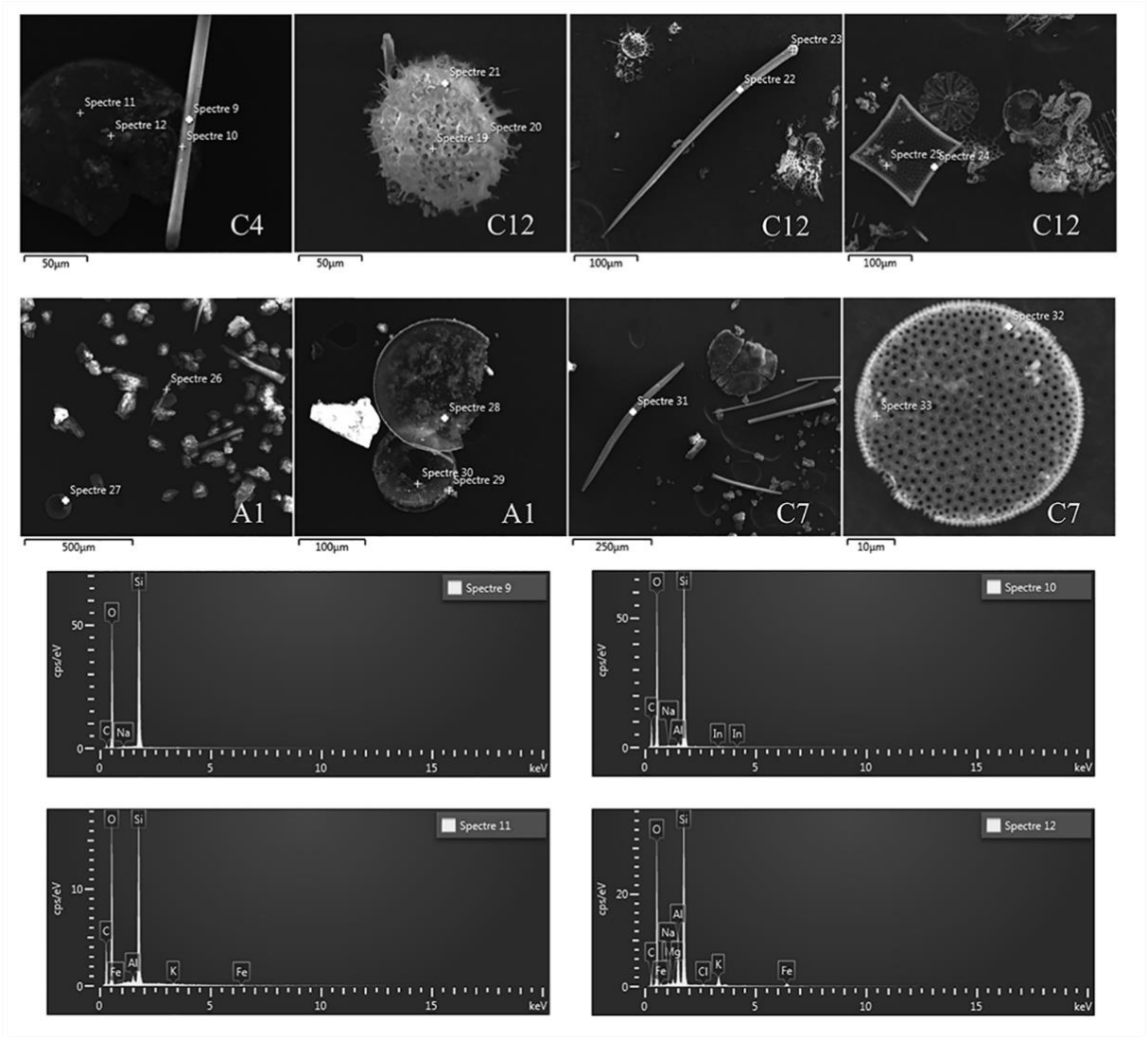

Figure S3.10. Scanning Electron Microscopy (SEM) coupled with Energy Dispersive Spectrometer (SEM-EDS) analysis shows the cation (K, Al, Mg) and Fe – rich neoformed aluminosilicate phase on the surface of biogenic siliceous tests. The detected C (carbon) signals are mainly from the Leit adhesive carbon tab. Note that sample A1 was pretreated using HCl (1.0 M) and H_2O_2 (10%) following the method described by Mortlock and Froelich (1989), sample C4, C7, and C12 were not pretreated using HCl and H_2O_2 nor digested in alkaline solution. Altered diatoms (C4, C7, C12, A1) and radiolarians (C12) were displayed in the SEM photo.

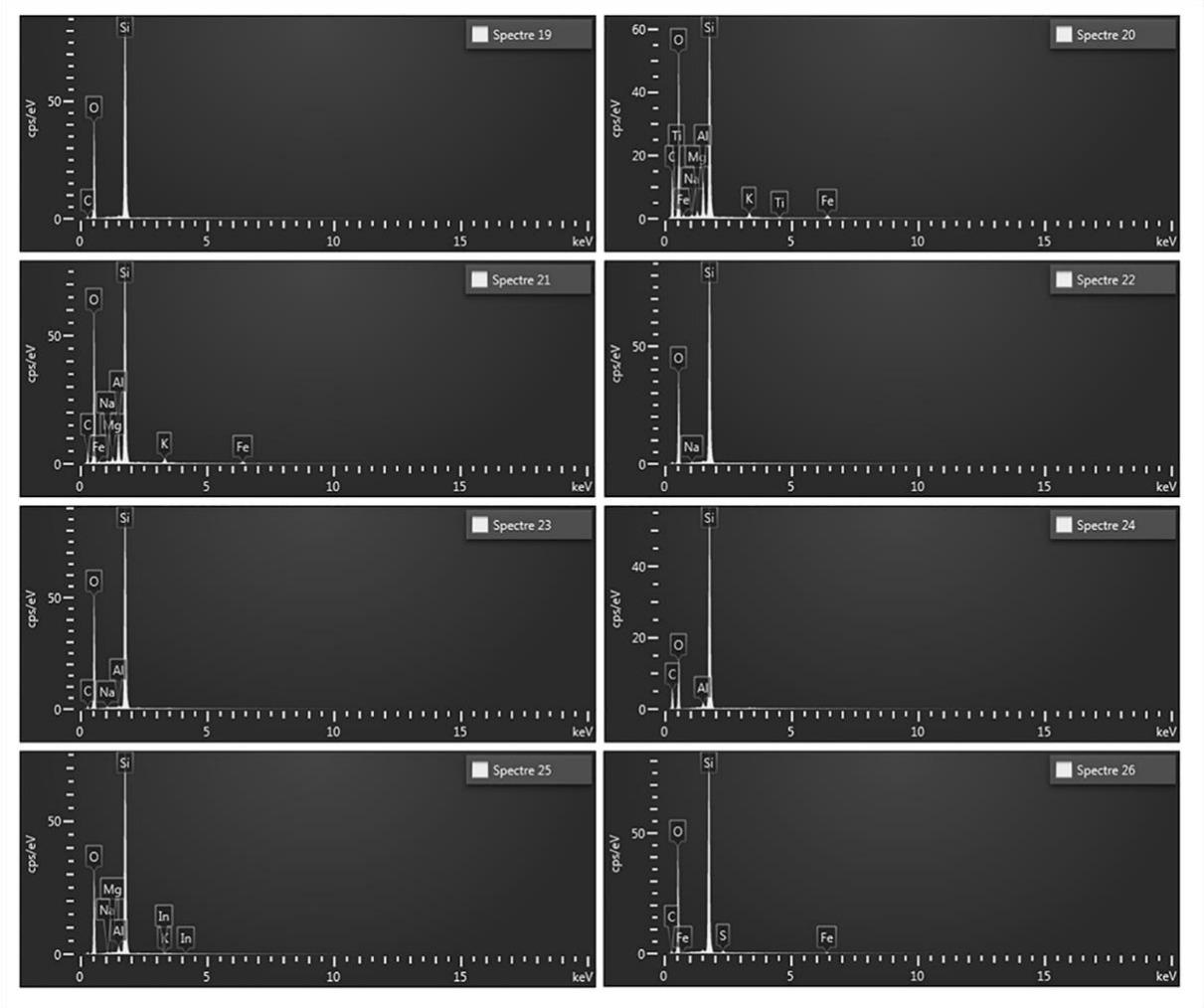

Figure S3.10. Continued.

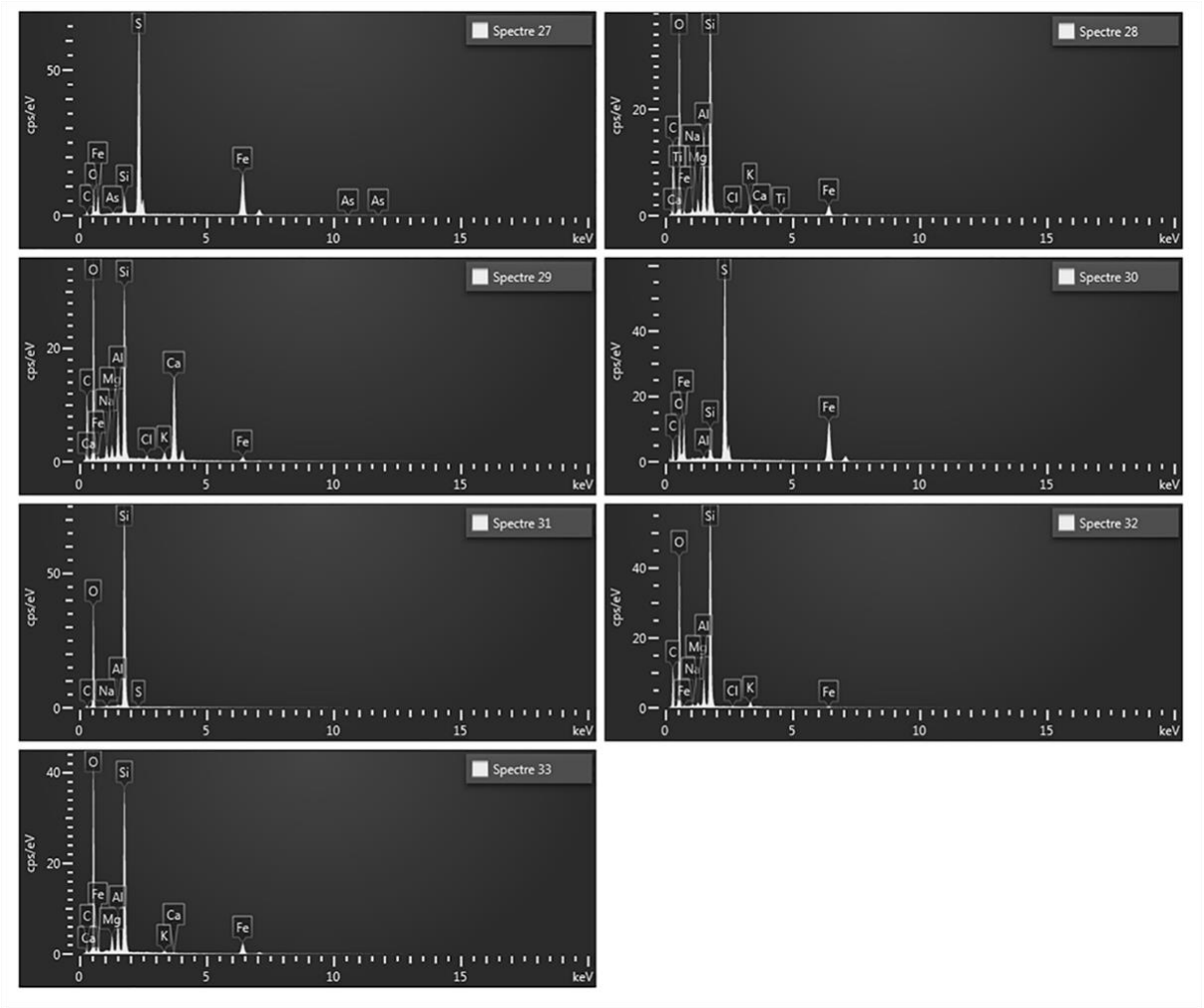

Figure S3.10. Continued.

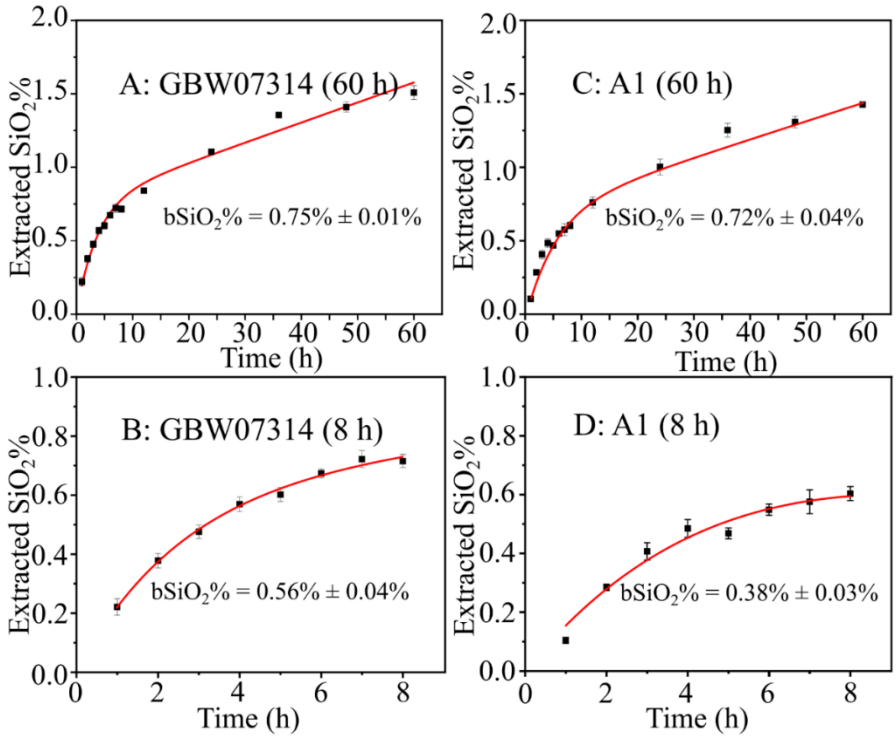

Figure S3.11. The alkaline extracted SiO_2% and the calculated $bSiO_2$% of sample GBW07314 (A, B) and sample A1 (C, D). Samples were extracted in 0.1 M NaCO3 for 60 h with a subsampling at 1, 2, 3, 4, 5, 6, 7, 8, 12, 24, 36, 48 and 60 h. Sample GBW07314 is national offshore reference sediment with bulk SiO_2% of 61.91 ± 0.54%wt. The redline represents nonlinear model fitted data using Model 1 (Eq.1). The $bSiO_2$% contents of sample GBW07314 are 0.75 ± 0.01% (60 h digestion) and 0.56 ± 0.04% (8 h digestion; showed in thumbnail plot), the $bSiO_2$% of sample A1 are 0.72 ± 0.04% (60 h digestion) and 0.36 ± 0.03% (8 h digestion; showed in thumbnail plot), the errors are based on triplicate alkaline digestions. The asymptotic Si vs. time line showed that the alkaline extracted SiO_2% continues to increase slowly without reaching a "flat plateau" as shown in Figure S2.

Table S3.1. The non-parametric Aligned Ranks Transformation (ART) Analysis of Variance (ANOVA) was determined using the $bSiO_2$% of samples C4, C7, C12, F2, F8, and DC (see Figure 3 for each alkaline digestion) determined using different methods. A p. value lower than 0.001 is considered a significant difference between the two methods. The different alkaline methods (concentration of alkaline solution, P vs. NP, or different alkaline solution): M1, M2, M3, M4, M5, M6, M7, M8 represents $bSiO_2$% determined using the 0.1 M Na_2CO_3 (NP, 8 h), 0.1 M Na_2CO_3 (P, 8 h), 0.2 M Na_2CO_3 (NP, 8 h), 0.2 M Na_2CO_3 (P, 8 h), 2.0 M Na_2CO_3 (NP, 8 h), 2.0 M Na_2CO_3 (P, 8 h), 0.5 M NaOH (NP, 1 h) and 2.0 M Na_2CO_3 (P, 5 h).

Methods	M1	M2	M3	M4	M5	M6	M7	M8
M1		<0.0001	<0.0001	<0.0001	<0.0001	<0.0001	0.0527	<0.0001
M2	<0.0001		<0.0001	<0.0001	0.4823	<0.0001	<0.0001	<0.0001
M3	<0.0001	<0.0001		<0.0001	<0.0001	<0.0001	<0.0001	<0.0001
M4	<0.0001	<0.0001	<0.0001		<0.0001	0.0726	<0.0001	<0.0001
M5	<0.0001	0.4823	<0.0001	<0.0001		<0.0001	<0.0001	<0.0001
M6	<0.0001	<0.0001	<0.0001	0.0726	<0.0001		<0.0001	<0.0001
M7	0.0527	<0.0001	<.0001	<0.0001	<0.0001	<0.0001		<0.0001
M8	<0.0001	<0.0001	<.0001	<0.0001	<0.0001	<0.0001	<0.0001	

Table S3.2. The percentage (%) of non-linear Si fractions (*ExtrSi*$_1$, *ExtrSi*$_1$), linear fraction, bSi and lSi to the total alkaline extracted Si (TAlkExSi) according to Si/Al method. The calculation of different fractions was based on the results shown in Table 5. Note that the TAlkExSi is the amount of Si leached in alkaline.

Station	*ExtrSi*$_1$	*ExtrSi*$_2$	Linear fraction	bSi	lSi
B01	13.4	38.2	48.4	13.4	86.6
B10	10.3	30.4	59.3	10.3	89.7
B19	15.6	32.0	52.5	15.6	84.4
B23	11.0	33.0	56.0	11.0	89.0
B18	18.0	25.8	56.2	18.0	82.0
B43	9.7	39.3	50.9	9.7	90.3
H20	17.3	37.0	45.6	17.3	82.7
B09	41.9	0.0	58.1	41.9	58.1
B02	12.9	35.1	52.0	48.0	52.0
H06	12.0	36.9	51.2	12.0	88.0
H32	18.9	29.0	52.1	18.9	81.1
C07	14.9	35.5	49.7	14.9	85.1
A09	21.0	31.1	47.9	21.0	79.0
F10	11.7	23.2	65.1	34.9	65.1
A3	22.6	21.9	55.4	44.6	55.4
D1	8.4	38.5	53.1	8.4	91.6
D12	10.6	11.3	78.1	21.9	78.1
E6	28.0	33.0	39.0	61.0	39.0
B8	41.3	16.5	42.2	57.8	42.2
C4	19.3	19.3	61.4	38.6	61.4
C7	38.3	0.0	61.7	38.3	61.7
C12	11.1	17.4	71.5	11.1	88.9
F2	30.9	33.2	35.9	30.9	69.1
F5	9.8	38.5	51.7	9.8	90.2
F8	23.2	26.1	50.7	23.2	76.8
A1	23.4	43.2	33.4	23.4	76.6
A4	12.8	42.8	44.4	12.8	87.2
Ave	19.3	27.4	53.3	25.0	75.0

Std	9.9	12.6	10.1	15.3	15.3.
SP-1	34.9	34.4	30.7	69.3	30.7
SP-2	43.5	30.3	26.2	73.8	26.2
R-64-1	41.7	33.2	25.1	74.9	25.1
R-64-2	34.7	40.7	24.6	75.4	24.6

S2. Supplementary material of chapter 4

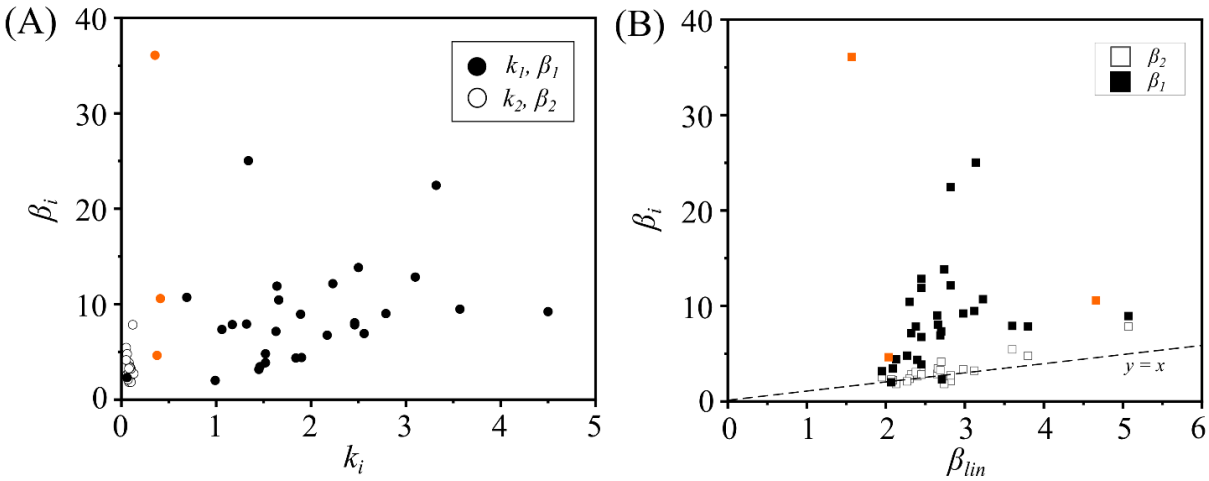

Figure S4.1. Relationsip of A): reactivity (k_i) of non-linear dissolving Si fraction and Si:Al ratios (β_i) and B) the Si:Al ratio of lSi (β_{lin}) and non-linear dissolving Si fractions (β_i). The symbols in organe represents samples of SCS which contain one non-linear dissolving Si fraction.

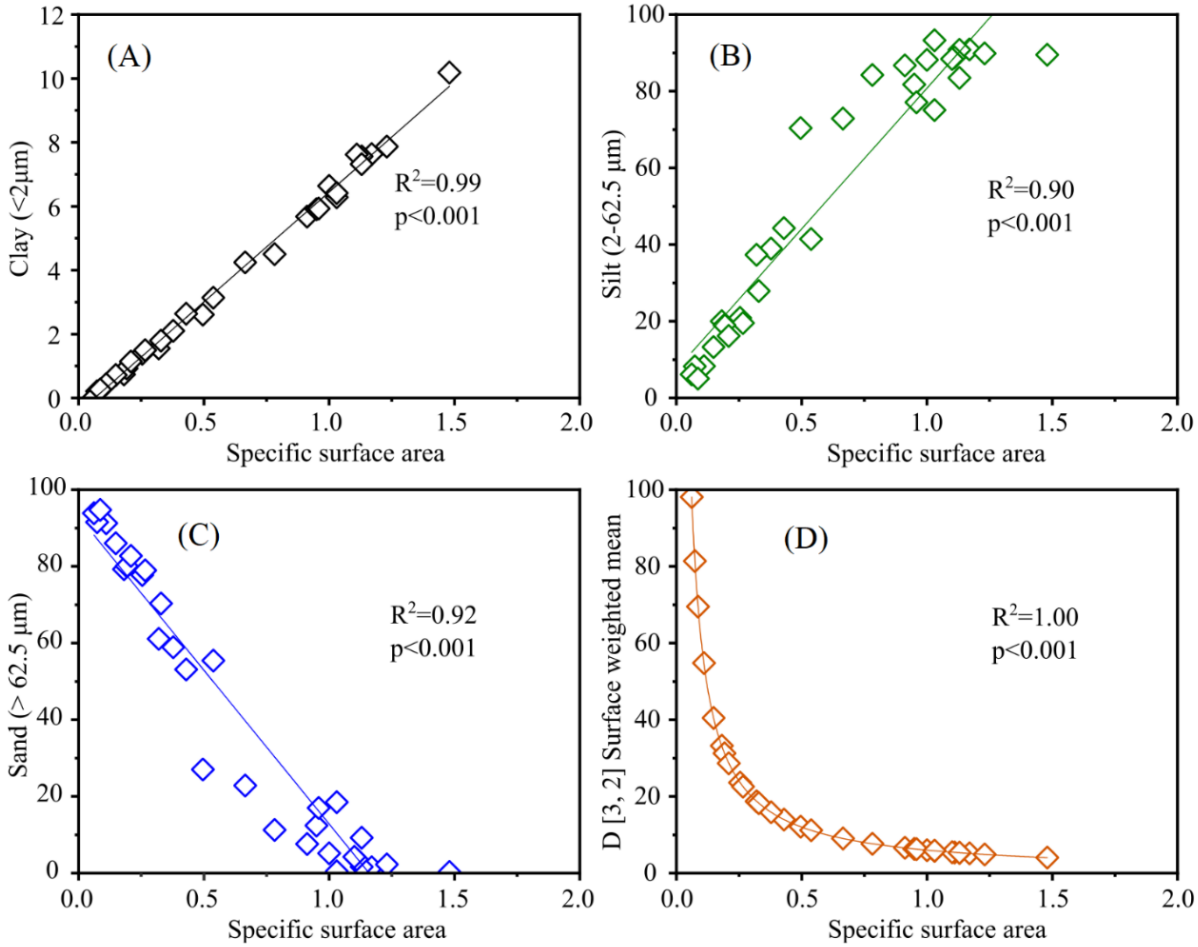

Figure S4.2. Plot of calculated specific surface area (SSA) of sediment and grain-size. (A) SSA vs. Clay%, (B) SSA vs. Silt%, (C) SSA vs. Sand%, and (D) SSA vs. D [3, 2] surface weighted mean.

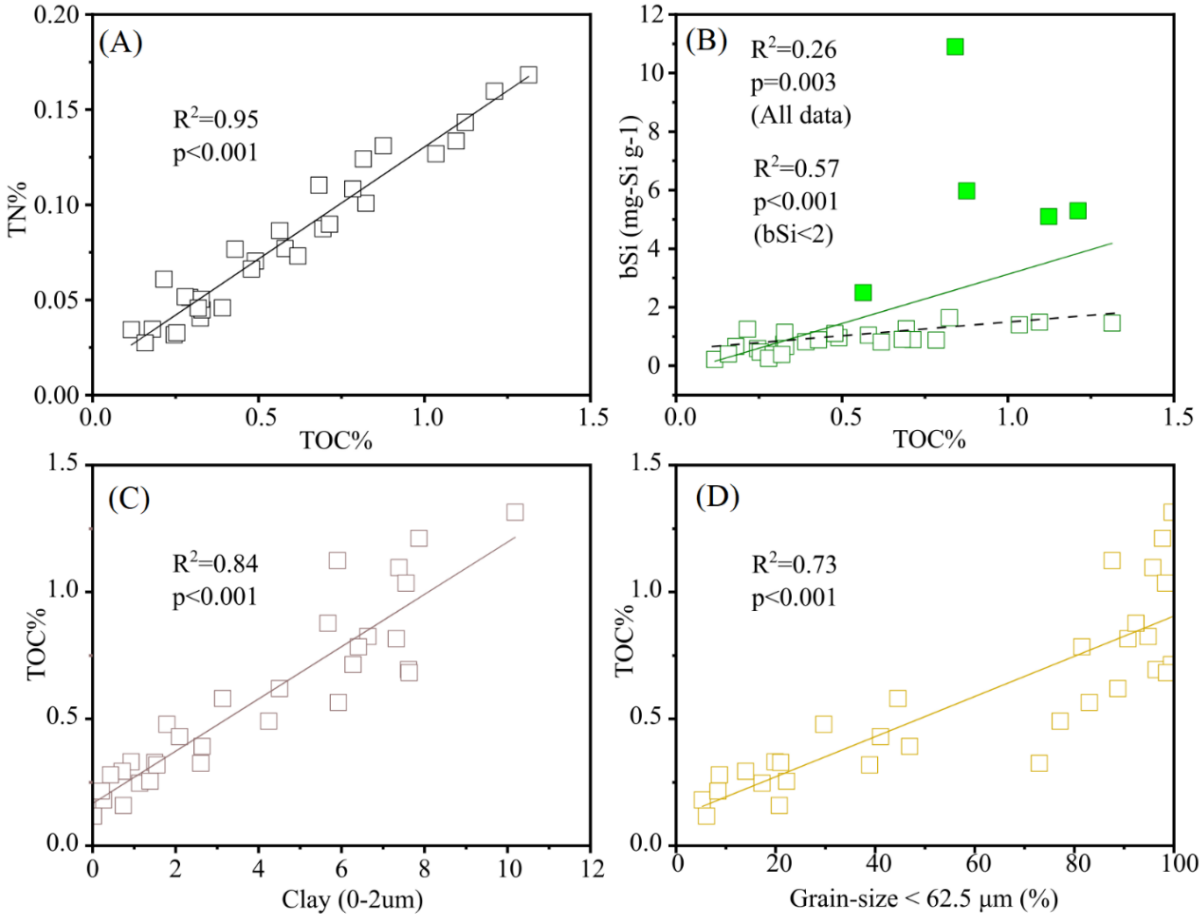

Figure S4.3. Different sediment chemical compositions and their relationship with grain-size.

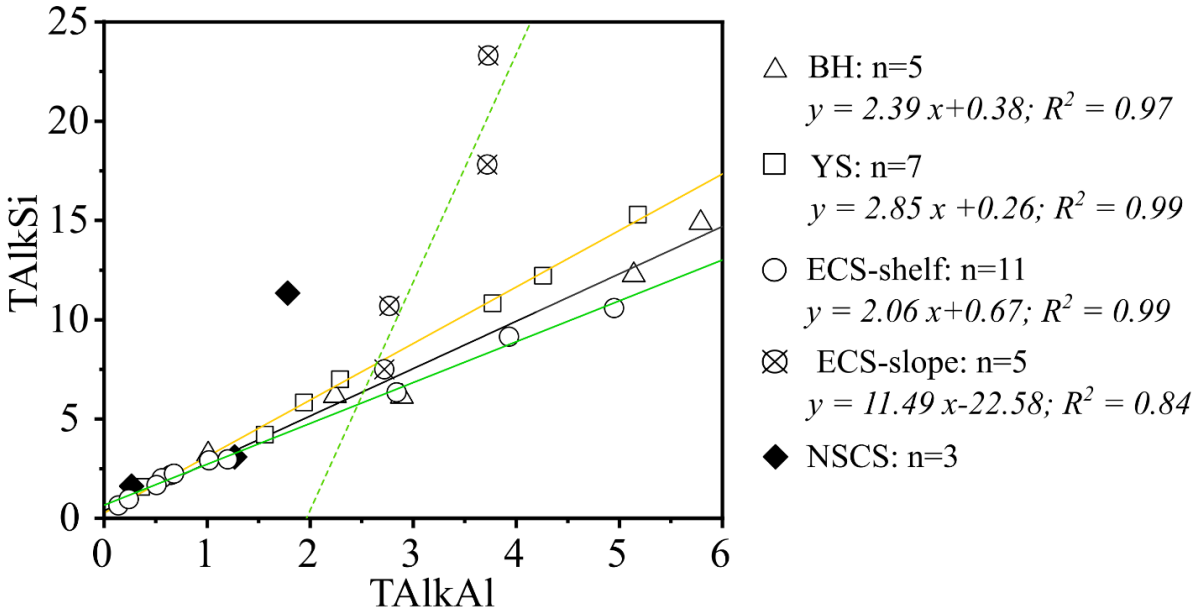

Figure S4.4. Total amount of alkaline extracted Si (TAlkSi, mg-Si g^{-1})and Al (TAlkAl, mg-Al g^{-1}). The lines in black, yellow, green color are linear fitted data of samples from BH, YS and ECS. The dash line represent fitted data of samples from ECS slope. Filled symbles represent NSCS samples. Distinct difference of the slope of fitted data.

S3. Supplementary material of chapter 5

S3.1. Insights of the different wet alkaline digestion techniques

As described in "chapter 1- Introduction and research background", wet alkaline digestion techniques can be grouped into Si/time methods (DeMaster, 1981; Mortlock and Froelich, 1989; Muller and Schneider, 1993; Landen et al., 1996; Liu et al., 2002; Lyle and Lyle, 2002;) and Si/Al methods (Kamatani and Oku, 2000; Koning et al., 2002). These techniques utilize different alkaline solutions, e.g., Na_2CO_3 (DeMaster, 1981; Mortlock and Froelich, 1989; Landen et al., 1996; Liu et al., 2002), NaOH (Muller and Schneider, 1993; Kamatani and Oku, 2000; Koning et al., 2002; Schluter and Rickert, 1998;) and KOH (Lyle and Lyle, 2002). Strong alkaline digests the radiolarians and sponge spicules more efficiently. Schluter and Rickert (1998) considered that extraction of bSi is pH dependent. We found that the buffer effect of alkaline is even more important than alkaline pH.

As shown in Table S5.4, the pH of alkaline solution decreases when the temperature increases. At 70 °C, the pH of Na_2CO_3 (0.1 M to 2.0 M) and NaOH (0.032 M to 0.5 M) are not significantly different (± 0.5), however, high alkaline concentrations are capable of extracting more Si from silicates (bSi and silicate minerals) than less concentrated alkaline. Although, Na_2CO_3 and NaOH are the mostly used regents, Lyle and Lyle (2002) choose to 2.0 M KOH to extract Eocene and Miocene samples (enriched with radiolarian tests) instead of 2.0 M Na_2CO_3, they found 2.0 M KOH can completely digest radiolarians whereas 2.0 M Na_2CO_3 was not. This thesis utilized 0.5 M NaOH to digest radiolarian ooze sediment (2714CQ) and found all radiolarians were completely dissolved after 24 hours. Thus, it is likely that there is no difference in extraction capability between the same concentration of NaOH and KOH.

Two methods were used to calculate the bSi content using Si and Al data, (1) calculate the intercept value of the Si vs Al plot as shown by Kamatani and Oku (2000) and (2) run the first order dissolution models as shown by Koning et al. (2000). Based on results presented in chapter 5, the calculation using the intercept on Y axis mostly underestimate $bSiO_2$% of coastal sediments because of silicate mineral interference (due to negative $bSiO_2$% values of the clay minerals). Thus, first order dissolution models proposed by Koning et al. (2002) are recommended for processing the Si and Al data.

The Si/time method calculates the $bSiO_2$% based on dissolution kinetics of bSi and silicate minerals (DeMaster, 1981). The complexity of dissolution rate of diatoms, radiolarians, sponge spicules as well as different clays were not considered (see Figure 1.7). Under a hot alkaline extraction, 1% to 50% clay mineral and 20% to 100% of bSi dissolve within 5 h. Therefore, the

differences in dissolution rate of the various types of bSi and clays should be taken into account in bSi determination. Thus, information of the types and distributions (see Chapter 1) of bSi in sediments is important prior to alkaline extraction. Generally, diatoms are distributed in all sediment types of world ocean and are enriched in the Southern Ocean; radiolarians are enriched in sediment of Equatorial Pacific, some regions of the Southern Ocean, Central South China Sea; sponge spicules are likely to be found in all types of sediments that contain different abundances of spicules. By re-analyzing the data of mass (mg-Si/g) and abundances (10^4 g) of sponge spicules reported by Maldonado et al. (2019). We found the mass of spicules in sediments is positively related to the length of spicules (Figure S5.1) for low abundance samples, but not for high spicule content samples (Figure S5.2). Thus, further research aims to quantify sponge bSi of low spicule content (< 10 × 10^4 g) sediments can determine the abundance of spicules.

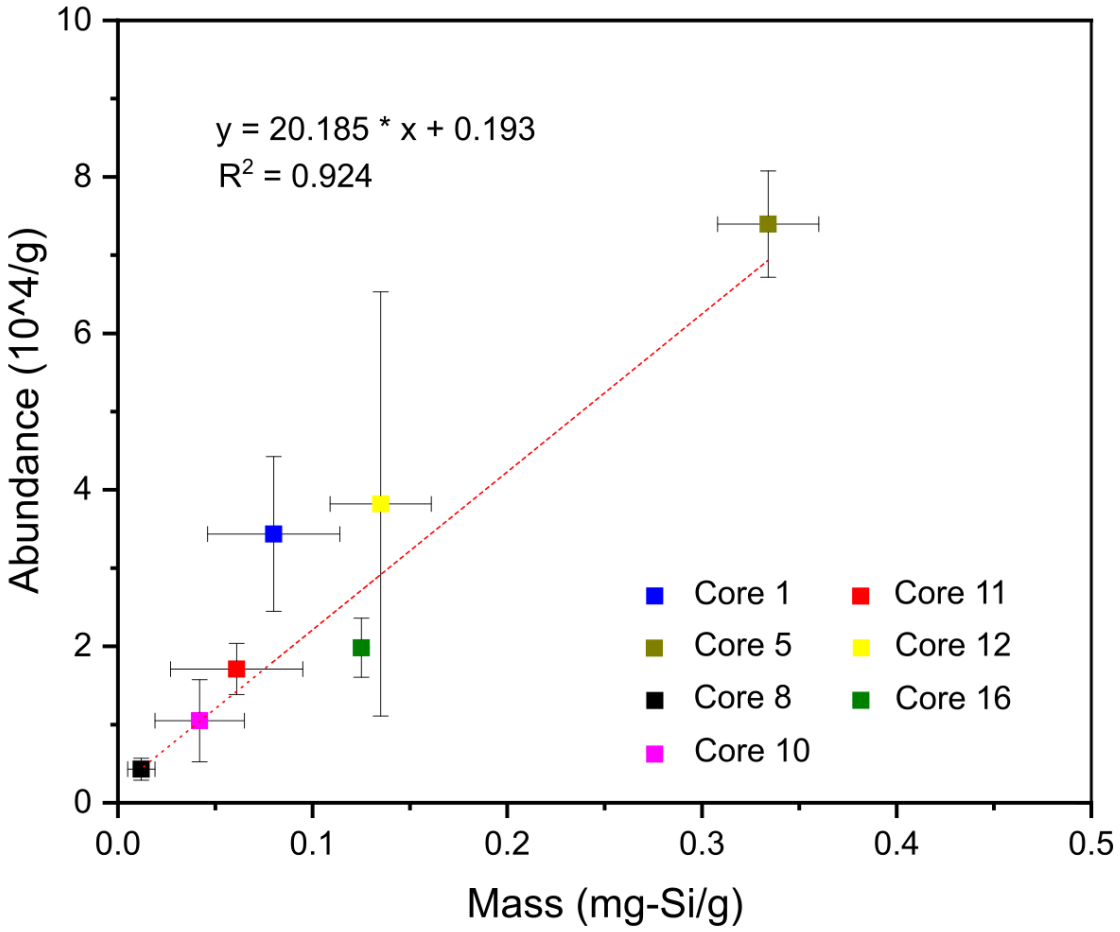

Figure S5.1. Relationship of spicules abundance and spicules mass in sediments of low spicules content samples. The data and core numbers are referred to Maldonado et al. (2019). A positive relationship between spicules and their mass was observed.

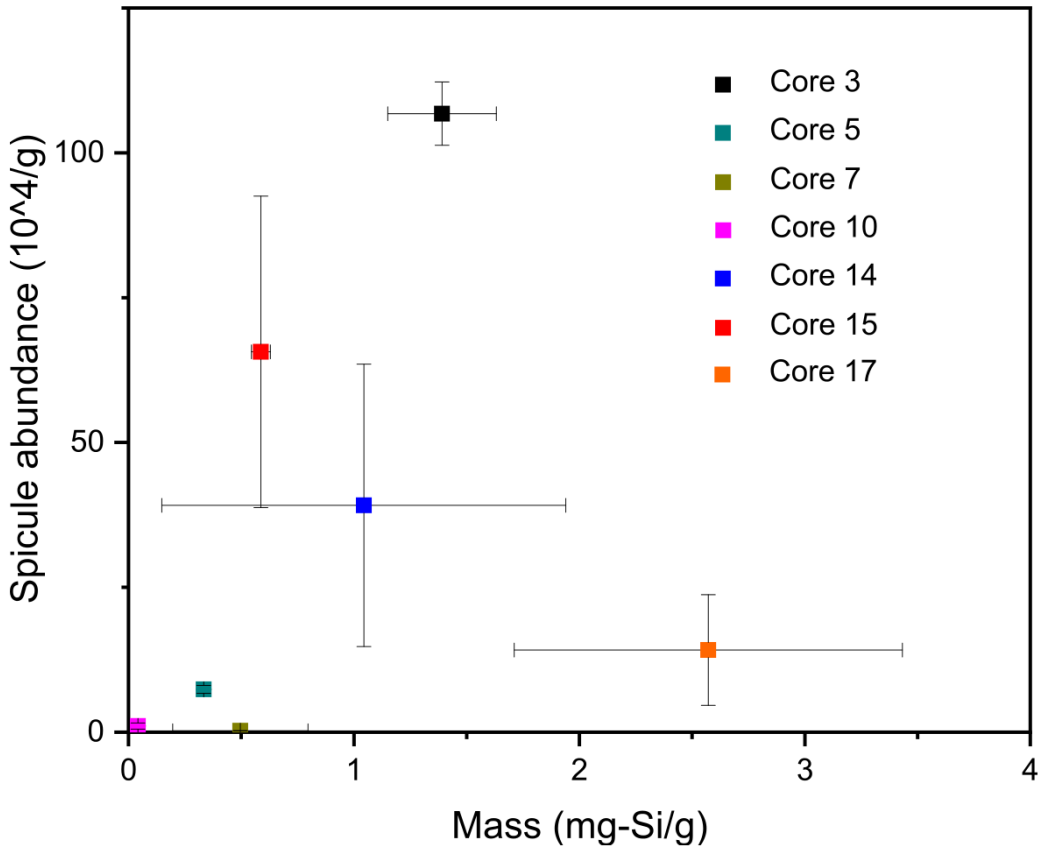

Figure S5.2. Relationship of spicules abundance and spicules mass in sediments of high spicules content samples. The data and core numbers are referred to Maldonado et al. (2019).

S3.2. Flow-Cam: A rapid method to determine types and abundance of bSi

To examine the types and abundance of bSi in sediments, this thesis applied a Flow-Cam technique which can efficiently record particles (image and measure the size of solid material) in sediments. We found that the use of Flow-Cam to measure bSi abundances in sediments is difficult, mainly due to the broad size distributions of different types of bSi and other particles (i.e., sand, clays). Therefore, an optimum protocol to homogenize the sediment sizes (such as sieving) is necessary in future studies. The procedures, results and discussions are presented below:

Procedures: (1) Weighing about 1 mg of homogenized dry sediments, remove organic matter and carbonates using HCl and H_2O_2. (2) Remove the liquid after centrifugate the solution and add 10 mL of Mili-Q water. (3) Add flow-cell and adjust the Flow-Cam system using standard samples. (4) add the solution into the tube connected with flow-cell (width: 100 μM) to measure the particles.

Results: The abundances of diatoms, sponge spicules and radiolarians determined by Flow-Cam method were 6.0×10^4 g, 13.8×10^4 g and 2.3×10^4 g, respectively. The abundances of

diatoms, sponge spicules and radiolarians determined by microscope were 1.5×10^4 g, 23.2×10^4 g and 1.2×10^4 g respectively. Although, the abundance of bSi measured were at the same by two methods (optically and by Flow-Cam) were at the same order of magnitude. There are still large variabilities in the determined bSi abundances.

Discussions: Comparing with the microscope method, Flow-Cam technique is capable of measuring the bSi abundances within 20 min. However, the large variability (± 100%) of the determined bSi abundances between two methods indicated poor accuracy of Flow-Cam method. To improve reliability of Flow-Cam method, the following procedures are recommended to be used: (1) remove the large grains (such as sand and wood fractions), carbonates (such as foraminifera), organic matters, (2) sieve the sediments into several size fractions (such as: >150 µM, 45 – 150 µM, 45 – 5 µM, < 5 µM) and select an appropriate flow-cell, (3) build a representative bSi library to select different bSi structures automatically.

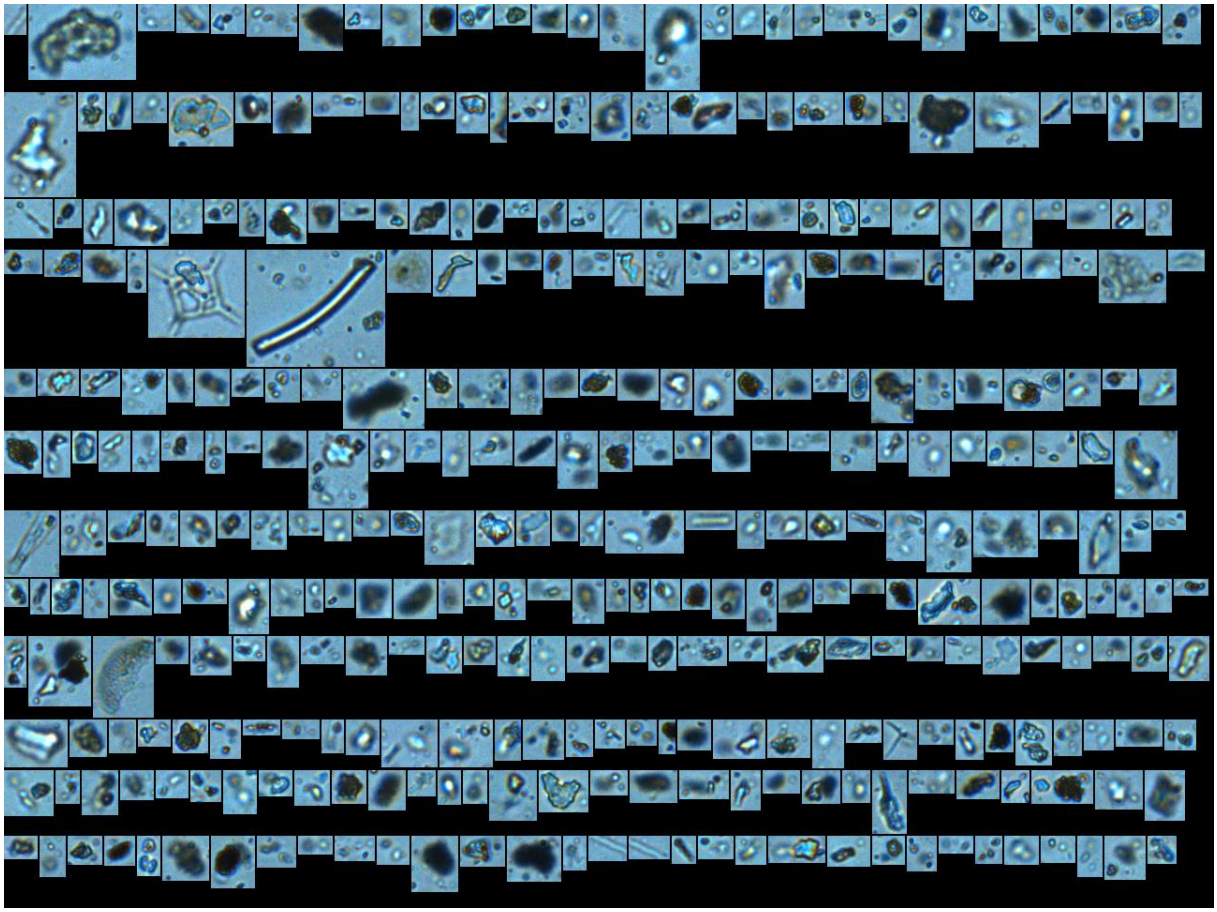

Figure S5.3. Flow-Cam images of particles observed in sample C12. Diatoms, sponge spicules, silico-flagellate and other structures (sand grains, clay and foraminifera fractions) were observed within the figure. Note that a sediment flotation method was not applied prior to the Flow-Cam analysis.

S3.3. Application of benchtop micro-XRF to define bSi

The benchtop micro-XRF produces micrometer to centimeter scale measurement of major and trace-element analysis with minimal sample preparation. Therefore, micro-XRF can be applied to define bSi structures (based on the characteristics of bSi structures and the element content) in sediment, theoretically. To curry out the measurements, one layer of freeze-dried sediments were gently mixed and put on a plastic film surface. Then the samples were put into the benchtop micro-XRF at vacuum mode, the major and trace elements were determined based on machine settings (one hour analysis for sample area: 3 × 3 mm). Figure S5.4 shows the Si, Al, Fe, Mn and Ca distributions in sediments. At the millimeter scale, the distributions of elements and enriched elements (Si, Fe Ca) surrounding larger grains were distinguished (Figure S5.4). However, bio-siliceous structures were not observed due to their relatively small sizes (20 μm to 200 μm). Thus, micro-XRF analysis is not applicable of finding bSi in sediments (e.g., semi-quantification of bSi or examine bSi diagenesis).

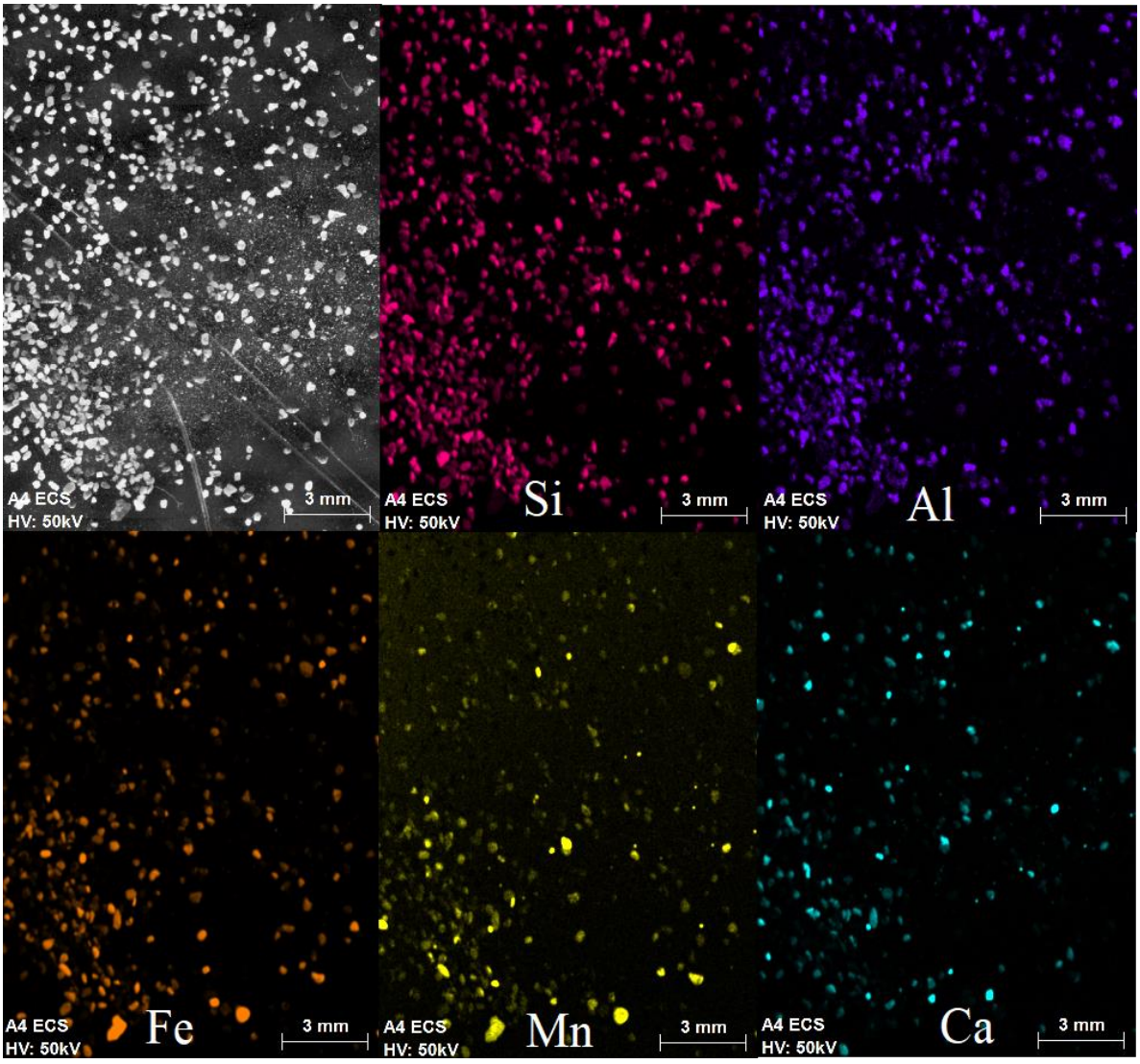

Figure S5.4. Micro-XRF image shows the elements (Si, Al, Fe, Mn, Ca) distributions on the surface of sediments. The sample (A1) was obtained from the Yangtze River estuary.

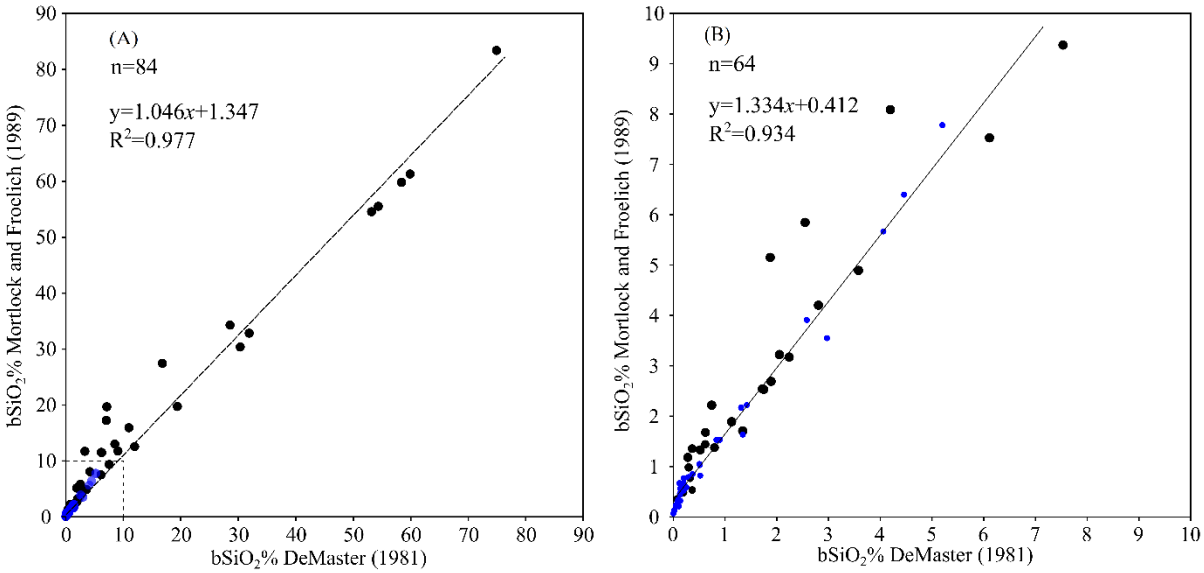

Figure S5.5. Comparison of the $bSiO_2$% determined by wet chemical methods. The DeMaster (1981) refers to calculation of bSi with mineral corrections, and Mortlock and Froelich (1989) refers to calculation of bSi without mineral corrections. (A) $bSiO_2\% < 90\%$; (B) $bSiO_2\% < 10\%$. The differences between the two calculations are more important for low bSi samples as compared to all data plotted. Averaged Note that all data listed in the graph does not include measurements which applied pretreatment using HCl and H_2O_2, experiments described in chapter 3 discussed methodological differences of the $bSiO_2$% determined by DeMaster (1981), Mortlock and Froelich (1989) and Koning et al. (2002) of coastal sediments. The samples used in this figure were shown in Figure 2.1.

Table S5.1. Parameters of wet alkaline extraction: mass of sediment (mg), volume of alkaline solution (mL) and sediment to liquid ratio (S/L, unit: g/L).

Sample	Manual extraction (24 h)			Continuous digestion(~1 h)		
	Weight [mg]	$V_{0.5M\ NaOH}$ [mL]	S/L ratio [g/L]	Weight [mg]	$V_{0.5M\ NaOH}$ [mL]	S/L ratio [g/L]
Kaolinite-NP	19.7	40	0.49	-	-	-
Kaolinite-P	19.9	40	0.50	-	-	-
Bentonte-NP	21.0	40	0.54	-	-	-
Bentonte-P	21.4	40	0.53	-	-	-
C12-NP-NG	65.0	40	1.63	109.9	180	0.61
C12-NP-NG	62.5	40	1.56	81.4	180	0.45
C12-NP-NG	64.8	40	1.62	79.8	180	0.44
C12-P-NG	65.1	40	1.63	-	180	-
C12-P-NG	61.8	40	1.55	-	180	-
C12-P-NG	64.0	40	1.60	-	180	-
C12-NP-FG	54.3	40	1.36	-	180	-
C12-P-FG	54.0	40	1.35	-	180	-
B10-NP	59.2	40	1.48	100.8	180	0.56
B10-P	59.9	40	1.50	-	180	-
ST4	62.6	40	1.57	94.5	180	0.53
Still Pond	59.3	40	1.48	66.4	180	0.37
R-64	55.7	40	1.39	66.2	180	0.37
D226	55.2	40	1.38	55.8	180	0.31
MTB-2	50.0	40	1.25	70.3	180	0.39
H555	63.2	40	1.58	94.4	180	0.52
F104	71.5	40	1.79	99.4	180	0.55
Eq	41.8	40	1.05	56.5	180	0.31
MC8B	47.2	40	1.18	81	180	0.45
2368G	61.6	40	1.54	92.3	180	0.51
2714CQ	33.2	40	0.83	30.5	180	0.17
3585CQ	20.3	40	0.51	15.2	180	0.08

Table S5.2. Probability (p) value determined by two-way analysis of variance (ANOVA) test using the Holm-Bonferroni method. A significant p-value ($p < 0.05$) suggests that at least one group mean is significantly different from the others. Data from table 5.5.

	Koning et al. (2002) (1h)	Koning et al. (2002) (24h)	Kamatani and Oku (2000)	DeMaster (1981)	Mortlock and Froelich (1989)
Koning et al. (2002) (1h)	-	0.344	0.795	0.559	0.351
Koning et al. (2002) (24h)	0.344	-	0.229	0.129	0.989
Kamatani and Oku (2000)	0.795	0.229	-	0.746	0.234
DeMaster (1981)	0.559	0.129	0.746	-	0.132
Mortlock and Froelich (1989)	0.351	0.989	0.234	0.132	-

Table S5.3. Probability (p) value determined by two-way analysis of variance (ANOVA) test using the Holm-Bonferroni method. Data from table 5.5 which does not include sample 2714CQ and 3585CQ.

	Koning et al. (2002) (1 h)	Koning et al. (2002) (24 h)	Kamatani and Oku (2000)	DeMaster (1981)	Mortlock and Froelich (1989)
Koning et al. (2002) (1 h)	-	0.832	< 0.001	0.083	0.154
Koning et al. (2002) (24 h)	0.832	-	0.002	0.126	0.103
Kamatani and Oku (2000)	< 0.001	0.002	-	0.081	< 0.001
DeMaster (1981)	0.083	0.126	0.081	-	0.002
Mortlock and Froelich (1989)	0.154	0.103	< 0.001	0.002	-

Table S5.4. The pH of alkaline solutions at room temperature (~20℃) and high temperature (70℃). The pH value decreases when the temperature of alkaline solution increases.

Alkaline solution	pH (room temperature)	pH (70℃)
0.1M Na_2CO_3	11.2[1]	10.60
0.2M Na_2CO_3	11.35	10.86
0.5M Na_2CO_3	11.5[1]	10.96
1.0M Na_2CO_3	11.35	10.95
2.0M Na_2CO_3	11.6[2]	10.89
0.032M NaOH	12.5[3]	11.01
0.1M NaOH	12.8[1]	11.50
0.2M NaOH	13.1[1]	11.49
0.5M NaOH	13.7[4]	11.73

1: Kamatani and Oku (2000); 2: Eggimann et al. (1980); 3: Schluter and Rickert (1998); 4: Koning et al. (2002).

Table S5.5. Sample code, station name, coordinates and water depth.

Code	Station	Region	Latitude N	Longitude E	Depth [m]
B01	B01	Bohai Sea	40.42	121.51	14
B10	B10	Bohai Sea	38.45	118.41	16
B18	B18	Bohai Sea	38.43	120.78	38
B19	B19	Bohai Sea	37.94	119.67	18
B23	B23	Bohai Sea	38.75	119.50	25
B43	B43	Yellow Sea	38.10	121.98	52
H20	H20	Yellow Sea	34.51	120.62	14
B09	B09	Yellow Sea	38.47	123.47	62
B02	B02	Yellow Sea	36.83	122.58	34
H06	H06	Yellow Sea	35.97	122.65	63
H32	H32	Yellow Sea	33.01	123.50	39
C07	C07	Yellow Sea	35.00	124.52	90
A09	A09	East China Sea	32.86	125.53	95
F10	F10	East China Sea	31.75	126.11	76
A1	A1	East China Sea	31.61	122.40	22
A3	A3	East China Sea	31.69	122.98	38
A4	A4	East China Sea	31.82	123.60	37
A8	A8	East China Sea	32.40	127.02	120
C4	C4	East China Sea	30.41	123.18	60
C7	C7	East China Sea	29.40	124.93	79
C12	C12	East China Sea	28.07	127.02	1027
D1	D1	East China Sea	29.24	122.24	17
D12	D12	East China Sea	26.69	125.50	780
B8	B8	East China Sea	30.09	126.89	102
E6	E6	East China Sea	26.79	124.07	122
F2	F2	East China Sea	26.83	120.73	42
F4	F4	East China Sea	26.53	121.16	73
F5	F5	East China Sea	26.26	121.55	76
F8	F8	East China Sea	25.53	122.60	595
DC	DC	East China Sea	27.47	126.61	1588

NSCS1	NSCS1	North South China Sea	21.82	114.01	39
NSCS7	NSCS7	North South China Sea	19.96	115.00	855
NSCS10	NSCS10	North South China Sea	20.35	113.91	111
ST1	G115	Baffin Bay (Arctic)	68.38	-61.27	1720
ST2	G201	Baffin Bay (Arctic)	68.58	-59.92	1322
ST3	G300	Baffin Bay (Arctic)	69.00	-56.78	198.08
ST4	G306b	Baffin Bay (Arctic)	68.98	-59.60	308.99
ST5	G312	Baffin Bay (Arctic)	69.33	-59.62	1452
ST6	G413	Baffin Bay (Arctic)	68.13	-59.00	276
ST7	G418	Baffin Bay (Arctic)	68.11	-57.76	385
ST8	G605	Baffin Bay (Arctic)	70.44	-62.49	2017
ST9	G615	Baffin Bay (Arctic)	70.49	-59.47	602.57
ST10	G707	Baffin Bay (Arctic)	69.51	-59.81	1428
ST11	G713	Baffin Bay (Arctic)	69.50	-61.58	1895
ST12	G719	Baffin Bay (Arctic)	69.50	-63.28	1950
2100G	EM1 MD97-2100G	Southern Ocean-Indian Ocean Sector	-35.974	80.937	2510
2101G	EM2 MD97-2101G	Southern Ocean-Indian Ocean Sector	-43.501	79.843	3145
2115G	EM3 MD97-2115G	Southern Ocean-Indian Ocean Sector	-43.193	-171.801	2160
2118G	EM4 MD97-2118G	Southern Ocean-Indian Ocean Sector	-45.117	179.187	2690
2362G	EM5 MD00-2362G	Southern Ocean-Indian Ocean Sector	-45.450	123.450	4750
2366G	EM6 MD00-2366G	Southern Ocean-Indian Ocean Sector	-44.950	125.433	4430
2368G	EM7 MD00-2368G	Southern Ocean-Indian Ocean Sector	-45.967	130.017	4506
2370G	EM8 MD00-2370G	Southern Ocean-	-45.383	119.867	4230

		Indian Ocean Sector			
2371G	EM9 MD00-2371G	Southern Ocean-Indian Ocean Sector	-45.400	113.500	4103
2373G	EM11 MD00-2373G	Southern Ocean-Indian Ocean Sector	-43.500	99.983	3764
2714CQ	EM13 MD04-2714CQ	Southern Ocean-Indian Ocean Sector	-43.400	49.890	2290
2716CQ	EM14 MD04-2716CQ	Southern Ocean-Indian Ocean Sector	-46.160	52.930	3320
2719G	EM15 MD04-2719G	Southern Ocean-Indian Ocean Sector	-49.740	72.180	640
3352CQ	EM17 MD11-3352CQ	Southern Ocean-Indian Ocean Sector	-50.560	68.390	1560
3396CQ	EM18 MD12-3396CQ	Southern Ocean-Indian Ocean Sector	-47.730	87.700	3615
3401CQ	EM19 MD12-3401CQ	Southern Ocean-Indian Ocean Sector	-44.680	80.390	3400
3405CQ	EM20 MD12-3405CQ	Southern Ocean-Indian Ocean Sector	-46.680	72.150	2600
MC8	KL20 MD225_ACC2_MC8	Southern Ocean-Atlantic Sector	-47.33	7.19	1878
MC5	KL14 MD225_ACC2_MC5	Southern Ocean-Atlantic Sector	-51.83	4.81	3746
3585Q	KL15 MD30-3585Q	Southern Ocean-Atlantic Sector	-51.83	4.81	3746
MC7	KL16 MD225_ACC2_MC7	Southern Ocean-Atlantic Sector	-50.48	-5.94	2594
MC4	KL18 MD225_ACC2_MC4	Southern Ocean-Atlantic Sector	-46.61	7.55	2594
A466	NIWA 1 A466	Southern Ocean-Pacific Sector	-78.433	185.167	NA
A532	NIWA 2 A532	Southern Ocean-Pacific Sector	-77.742	166.335	452

A459	NIWA 3 A459	Southern Ocean-Pacific Sector	-75.283	172.333	535
B32	NIWA 4 B32	Southern Ocean-Pacific Sector	–53.63	169.87	799
D216	NIWA 5 D216	Southern Ocean-Pacific Sector	-67.243	164.075	1837
F104	NIWA 6 F104	Southern Ocean-Pacific Sector	-48.67	170.81	801
F150	NIWA 7 F150	Southern Ocean-Pacific Sector	-49.47	174.47	501
G820	NIWA 8 G820	Southern Ocean-Pacific Sector	-33.15	162.6	793
G837	NIWA 9 G837	Southern Ocean-Pacific Sector	-67.7	175.333	3455
G855	NIWA 10 G855	Southern Ocean-Pacific Sector	-77.322	181.145	NA
G863	NIWA 11 G863	Southern Ocean-Pacific Sector	-77.517	164.7	254
G944	NIWA 12 G944	Southern Ocean-Pacific Sector	-40.12	179.99	2890
G977	NIWA 13 G977	Southern Ocean-Pacific Sector	-33.86	185.93	5883
H555	NIWA 14 H555	Southern Ocean-Pacific Sector	-45.92	178.98	2738
I168	NIWA 15 I168	Southern Ocean-Pacific Sector	-18.26	188.98	4833
I171	NIWA 16 I171	Southern Ocean-Pacific Sector	-22.66	185.01	3496
J1049	NIWA 17 J1049	Southern Ocean-Pacific Sector	-44.5	178.73	1339
J39	NIWA 18 J39	Southern Ocean-Pacific Sector	-37.00	170.00	2096
J50	NIWA 19 J50	Southern Ocean-	-36.67	170.65	2112

		Pacific Sector			
J51	NIWA 20 J51	Southern Ocean-Pacific Sector	-36.39	170.7	2000
P937	NIWA 21 P937	Southern Ocean-Pacific Sector	-41.32	166.46	3253
Q633	NIWA 22 Q633	Southern Ocean-Pacific Sector	-38.46	148.89	2350
Q636	NIWA 23 Q636	Southern Ocean-Pacific Sector	-38.82	149.01	2450
S631	NIWA 24 S631	Southern Ocean-Pacific Sector	-45.33	172.11	1329
X250	NIWA 25 X250	Southern Ocean-Pacific Sector	-36.67	177.19	2835
D226	PAP(B) D226	North Attlantic	48.82	-16.50	4850
9N	9N	Equatorial Pacific	9.53	-140.38	5100
0	0	Equatorial Pacific	0.20	-140.23	4358
12S	12S	Equatorial Pacific	-12.00	-135.58	4294
MTB2	Congo A MTB2	Congo deep-sea fan	-6.46	6.03	4759
MTB3	Congo A MTB3	Congo deep-sea fan	-6.47	6.04	4774
MTB6	Congo C MTB6	Congo deep-sea fan	-6.67	5.47	4951
WAP	WAP-FB-I	Southern Ocean - WAP Antarctic	-65.13	-64.83	550
5S	5S	Equatorial Pacific	-5.63	-140.23	4198
2S	2S	Equatorial Pacific	-3.48	-140.38	4293
2N	2N	Equatorial Pacific	2.10	-140.23	4397
5N	5N	Equatorial Pacific	5.11	-140.07	4493
K1	K1	East China Sea	32.87	122.37	25
M0	M0	East China Sea	32.65	122.11	21
M1	M1	East China Sea	32.72	122.35	28
M2	M2	East China Sea	32.76	122.50	26
M3	M3	East China Sea	32.86	122.80	33
M5	M5	East China Sea	32.95	123.12	34
M6	M6	East China Sea	33.10	123.56	36

M7	M7	East China Sea	33.24	124.03	66
N1	N1	East China Sea	32.00	122.29	19
N2	N2	East China Sea	32.04	122.51	28
N3	N3	East China Sea	32.17	122.95	34
N4	N4	East China Sea	32.28	123.33	35
N5	N5	East China Sea	32.43	123.86	40
N6	N6	East China Sea	32.73	124.74	64
A2	A2	East China Sea	31.65	122.64	33
A5	A5	East China Sea	31.94	124.25	41
A6	A6	East China Sea	32.01	124.75	45
A7	A7	East China Sea	32.15	125.61	72
A8	A8	East China Sea	32.40	127.02	120
B1	B1	East China Sea	31.27	122.44	19
B3	B3	East China Sea	31.19	123.33	42
B5	B5	East China Sea	31.12	124.66	55
B6	B6	East China Sea	31.03	125.77	63
B7	B7	East China Sea	30.94	127.04	103
O8	O8	East China Sea	31.78	120.95	18
O7	O7	East China Sea	31.75	121.07	13
O6	O6	East China Sea	31.59	121.31	25
O5	O5	East China Sea	31.50	121.43	17
O4	O4	East China Sea	31.38	121.61	16
O2	O2	East China Sea	31.13	121.93	9
O1	O1	East China Sea	31.00	122.23	11
C1	C1	East China Sea	30.91	122.35	13
C2	C2	East China Sea	30.77	122.57	19
C3	C3	East China Sea	30.59	122.82	38
C6	C6	East China Sea	29.73	124.36	73
C8	C8	East China Sea	28.97	125.65	109
C9	C9	East China Sea	28.60	126.37	120
C10	C10	East China Sea	28.31	126.78	208
D2	D2	East China Sea	29.15	122.49	49
D3	D3	East China Sea	29.08	122.60	55

D4	D4	East China Sea	28.67	123.31	65
D5	D5	East China Sea	28.36	123.87	80
D8	D8	East China Sea	27.21	125.83	190
E1	E1	East China Sea	28.20	121.77	22
E2	E2	East China Sea	28.05	122.08	58
E3	E3	East China Sea	27.80	122.46	80
E4	E4	East China Sea	27.57	122.92	97
F1	F1	East China Sea	26.95	120.57	26
F3	F3	East China Sea	26.73	120.86	55

Acknowledgements:

I would like to thank my supervisors Prof. Su Mei Liu, Associate Prof. Jill N. Sutton, Dr. Aude Leynaert, not only for their scientific advice but especially for their confidence in me and the liberty they gave me during my studies and for the fruitful discussions and critical comments during this thesis. Without their guidance, I could not fulfill my studies at the Ocean University of China and the Université de Bretagne Occidentale.

I am very grateful to Prof. Paul Tréguer who offered me guidance in marine silicon cycle research throughout my doctoral studies. Prof. Paul Tréguer not only provided me with constructive comments and suggestions on my research topic, but also introduced me to several research scientists (for example, Prof. Dave DeMaster and Prof. Robert Aller) who answered my questions related to biogenic silica diagenesis in marine environments.

I thank my doctoral committee members, Prof. Jingling Ren, Dr. Stefan Lalonde and Prof. Zuosheng Yang, for their helpful suggestions during my doctoral study.

I have benefited from the fruitful discussions with many research experts, and I especially thank Prof. Daniel Conley, Dr. Morgane Gallinari, Dr. Brivaëla Moriceau, Prof. Philippe Pondaven, Dr. Gaspard Delebecq, Prof. Dave DeMaster, Dr. Rebecca Pickering, Dr. Shaily Rahman, Prof. Guiling Zhang and Dr. Yuwei Ma.

Many thanks to Prof. Jonas Schoelynck who hosted me to carry out the continuous analysis experiment at the University of Antwerp. I also thank Dr. Eric Struyf for the discussions about the continuous analysis system. Special thanks to Mrs. Anne Cools, Mrs. Anke De Boeck and Mr. Tom Van der Spiet for their help and assistance during the alkaline digestion experiment, and to Dr. Lucia Barao who helped me to resolve the problems related to silica dissolution models.

I also want to thank many people who helped me during my studies, including Prof. Guiling Zhang, Associate Prof. Guodong Song, Associate Prof. Xianbiao Lin, Mrs. Nian Wu, Mr. Wen Liang, Dr. Wen-Hsuan Liao, Dr. Hong Chin Ng, Dr. Lucie Cassarino, Dr. Min Jin, Dr. Jie Lv, Dr. Wei Lu, Dr. Xiao Wang, Dr. Maria Lopez-Acosta, Dr. Natalia Llopis Monferrer, Dr. Helene Planquette, Dr. Floriane Desprez de Gesincourt, Dr. Geraldine Sarthou, Mrs. Elisabeth Bondu, Mrs. Aurelie Claude.

This thesis was funded by the Natural Sciences Foundation of China (NSFC: U1806211, 42176040), the Taishan Scholars Program of Shandong Province, Aoshan Talents Program Supported by the Qingdao National Laboratory for Marine Science and Technology (No. 2015ASTP-OS08).

This thesis was supported by the French National Research Agency (18-CEO1-0011-01) and the ISblue project, Interdisciplinary graduate school for the blue planet (ANR-17-EURE-0015) and co-funded by a grant from the French government under the program "Investissements d'Avenir" embedded in France 2030. Special thanks to the mobility grants from the ISblue project and the Université de Bretagne Occidentale.

I deeply thank my thesis jury members (Prof. Paul Tréguer, Dr. Shaily Rahman, Dr. Wei- Li Hong, Dr. Xiangbin Ran, Prof. Dejiang Fan, Prof. Qingzhen Yao, Prof. Jingling Ren) and also three thesis reviewers for their constructive comments and helpful suggestions. Many thanks to Dr. Shaily Rahman and Dr. Wei- Li Hong who are also my external thesis reviewers.

I would like to thank my wife who takes care of our son and encourages me to fulfill the dual doctoral degree, I would not finish my study successfully without her support. I thank my parents, grandparents, my sister and all other family members for their support during my studies.

Resume

Born on 17/08/1990 at Ningyang, Taian City, Shandong Province, China.

Studied at Shenyang University of Chemical Technology, College of Materials Science and Engineering from September 2010 to July 2014, majoring in Materials Physics, and graduated with a Bachelor of Science degree.

From August 2014 to March 2016, worked in Beijing EMK Technology Development Co., Ltd. as an R&D engineer.

From April 2016 to October 2016, worked at Beijing United Coating Technology Co., Ltd. as a manager of the quality management department.

From October 2016 to June 2019, studied at the University of Haifa, Faculty of Natural Sciences, Leon H. Charney School of Marine Sciences, Israel, where he graduated with a Master of Science degree.

From August 2019 to present, study at the School of Chemistry and Chemical Engineering, Ocean University of China and the European Marine Environment Laboratory (Institut Universitaire Européen de la Mer), Université de Bretagne Occidentale, France.

Publications:

1. **Dongdong Zhu**, Jill N. Sutton*, Aude Leynaert, Paul Tréguer, Jonas Schoelynck, Morgane Gallinari, Yuwei Ma, Su Mei Liu*. Revisiting the biogenic silica burial flux determinations: A case study for the east China seas. (2023). Frontier in Marine Science, 9, 1058730, doi: 10.3389/fmars.2022.1058730, (SCI).
2. **Dongdong Zhu**, Jill N. Sutton, Aude Leynaert, Tréguer J. Paul, Su Mei Liu*, The global marine silicon cycle and its major challenges, (2022) [J/OL]. Earth Science Frontiers, 29, 47-57, doi:10.13745/j.esf.sf.2021.8.6, (EI).
3. **Dongdong Zhu**, Su Mei Liu*, Aude Leynaert, Paul Tréguer, Jonas Schoelynck, Yuwei Ma, Jill N. Sutton*. Are muddy sediments an important potential silicon source of Coastal and Continental Margin Zones? Marine Chemistry, (under review), (SCI).
4. **Dongdong Zhu**, Su Mei Liu*, Aude Leynaert, Paul Tréguer, Jill N. Sutton*. Revisiting the methodological biases of biogenic silica burial flux in the world ocean. Biogeochemistry, (under submission).
5. Yuwei Ma, Lanlan Zhang, Su Mei Liu, **Dongdong Zhu**. Silicon balance in the South China Sea. (2022), Biogeochemistry, 157, 327-353, doi: 10.1007/s10533-021-00879-4, (SCI).
6. Yuwei Ma, Bin Yang, Nan Zhou, Jin Huang, Sumei Liu, **Dongdong Zhu**, Wen Liang. Distribution and dissolution kinetics of biogenic silica in sediments of the northern South China Sea. (2023). Frontier in Marine Science, 10, 1083233, doi: 10.3389/fmars.2023.1083233, (SCI).
7. Mengxue Wang, Xiaokun Ding, Xing Hou, Wu Nian, Yun Wang, Nan Zhou, Lingyan Wang, Xiaotong Zhang, **Dongdong Zhu**, Chongcong Liu, Su Mei Liu, Temporal and spatial variations of chlorophyll α and their corresponding influencing factors in the Bohai Sea. (2023). Journal of Ocean University of China, 53(9), 123-131, doi: 101.6441/jc.nkih.dxb2.0220262, (EI).
8. Shuai Ding, Solomon Felix Dan, Yan Liu, Jia He, **Dongdong Zhu**, Lixin Jiao. Importance of ammonia nitrogen potentially released from sediments to the development of eutrophication in a plateau lake. (2022), Environmental Pollution, 305, 119-275, doi:10.1016/j. envpol.2022.119275, (SCI).
9. Wen Liang, Yun Wang, Sumei Liu, Mengxue Wang, Liang Zhao, Chongcong Liu, Xiaotong Zhang, Nian Wu, Lingyan Wang, **Dongdong Zhu**, Yuwei Ma, Chang Luo. Nutrient dynamics and coupling with biological processes and physical conditions in the Bohai Sea. (2022), Frontier in Marine Science, 9,1025502, doi: 10.3389/fmars.2022.1025502, (SCI).

Conferences and invited talks:

1. Revisiting the methods for biogenic silica determinations in marine sediments. SILICAMICS (hybrid) workshop, IUEM, Brest, 15 May 2023.
2. Revisiting the biogenic silica burial flux determinations: A case study for the east China seas. Invited talk at Lund University. March 2023.
3. Alkaline extractable silicon fractions in marine sediments and its association with clay mineral content. 6th Nereis Park Conference and Thematic School- Bioturbation in the past and present : from terrestrial to marine ecosystems. August 2022, Logonna Daoulas-France, CNRS.
4. Determination of biogenic silica in marine sediment: problems of conventional alkaline digestion method and an optimized protocol. IBiS 2022 conference. June 2022, Lund University.
5. Methodological biases in the estimation of the global biogenic silica burial flux. SILICAMICS3, October 2021, Second Institute of Oceanography, China.
6. Bias in the Estimation of the Global Burial Flux of Biogenic Silica due to Incomplete Digestion Using Conventional Alkaline Methods. Goldschmidt 2021. June 2021, online.

Titre: Redéfinir le flux d'enfouissement de la silice biogène et son rôle dans le cycle global du silicium marin

Mots clés: Silice biogénique, Flux d'enfouissement, Océan mondial, Cycle du silicium, Méthode analytique

Résumé: L'enfouissement de la silice biogène (bSi) dans les sédiments est important pour étudier et reconstruire la productivité actuelle et passée des océans et pour comprendre le cycle du silicium marin (Si). Cependant, en raison de l'absence de procédures normalisées et reconnues au niveau international, les grandes variabilités de la teneur en bSi déterminée (bSi%) faussent l'évaluation du flux global d'enfouissement de bSi. Pour redéfinir le flux global d'enfouissement du bSi, cette thèse a évalué les facteurs qui affectent la détermination précise du bSi en déterminant la teneur en opale de sédiments provenant de différents environnements de dépôt en utilisant des méthodes variables (méthodes chimiques par voie humide, diffraction des rayons X et méthode infrarouge). Les résultats ont montré que les types et l'abondance de bSi dans les sédiments et les étapes de prétraitement des sédiments affectent la mesure du bSi. Les résultats de l'extraction alcaline ont montré que l'utilisation de la méthode Si/Al corrige avec précision la fraction de silice lithogénique dans les sédiments marins, et améliore ainsi les déterminations de bSi% dans les sédiments. Pour souligner l'influence de ces différences méthodologiques, la thèse a révisé le flux d'enfouissement du bSi dans les mers de Chine orientale et a fourni une nouvelle estimation de 253 (± 286) Gmol-SiO^2 an^{-1}, ce qui représente un tiers des estimations précédentes qui appliquaient une procédure de prétraitement avant les extractions alcalines. Sur la base des résultats et des données publiées précédemment, le flux d'enfouissement du Si marin global réévalué est de 6.7 ± 2.7 Tmol-Si par an, ce qui est inférieur d'environ 10 à 30 % aux études précédentes. Cependant, le cycle marin moderne du Si est toujours dans un état relativement stable. En outre, la dissolution des minéraux silicatés agit comme une importante source potentielle de Si marin et des recherches supplémentaires sont nécessaires pour comprendre la cinétique de dissolution de la silice dans les sédiments marins.

Title: Redefining the burial flux of biogenic silica and its role in the global marine silicon cycle

Keywords: Biogenic Silica, Burial Flux, Global Ocean, Silicon Cycle, Analytical Method

Abstract: The burial of biogenic silica (bSi) in sediments is important for investigating and reconstructing the present and past ocean productivity and for understanding the marine silicon (Si) cycle. However, due to the lack of internationally recognized and standardized procedures, large variabilities of the determined bSi content (bSi%) bias the evaluation of the global bSi burial flux. To redefine the global bSi burial flux, this thesis assessed the factors that affect the accurate determination of bSi by determining the opal content of sediments from different depositional environments using variable methods (wet chemical methods, X-ray diffraction and Infrared method). The results showed the types and abundance of bSi in sediments and sediments' pretreatment steps affect the measurement of bSi. Alkaline extraction results showed that the use of the Si/Al method accurately corrects for the lithogenic silica fraction in marine sediments, and thereby improves the determinations of bSi% in the sediments. To emphasize the influence of these methodological differences, the thesis revised the bSi burial flux in the East China Seas and provided a new estimate of 253 (± 286) Gmol-SiO_2 yr^{-1}, which is one-third of the previous estimates that applied a pretreatment procedure before alkaline extractions. Based on the results and previously published data, the re-evaluated global marine bSi burial flux is 6.7 ± 2.7 Tmol-Si yr^{-1} which is about 10% to 30% lower than previous studies. However, the modern marine Si cycle is still in a relatively steady state. In addition, silicate minerals dissolution acts as an important potential marine Si source and further research is required for understanding the dissolution kinetics of silica of marine sediments.